8-1-2015

Hydrothermal Routes to Technetium Cluster Compounds

William M. Kerlin
University of Nevada, Las Vegas, bwkerlin1@msn.com

HYDROTHERMAL ROUTES TO TECHNETIUM CLUSTER COMPOUNDS

By

William Michael Kerlin

Bachelor of Science in Chemistry

California State University of Sacramento

2004

A dissertation submitted in partial fulfillment of the requirements for the

Doctor of Philosophy - Radiochemistry

Department of Chemistry

College of Sciences

The Graduate College

University of Nevada, Las Vegas

August 2015

UNLV | GRADUATE COLLEGE

Dissertation Approval

The Graduate College
The University of Nevada, Las Vegas

July 2, 2015

This dissertation prepared by

William M. Kerlin

entitled

Hydrothermal Routes to Technetium Cluster Compounds

is approved in partial fulfillment of the requirements for the degree of

Doctor of Philosophy – Radiochemistry
Department of Chemistry and Biochemistry

Kenneth R. Czerwinski, Ph.D.
Examination Committee Co-Chair

Kathryn Hausbeck Korgan, Ph.D.
Graduate College Interim Dean

Paul M. Forster, Ph.D.
Examination Committee Member

Frederic Poineau, Ph.D.
Examination Committee Member

Alfred P. Sattelberger, Ph.D.
Examination Committee Member

Ralf Sudowe, Ph.D.
Graduate College Faculty Representative

ABSTRACT

Hydrothermal Routes to Technetium Cluster Compounds

By

William M. Kerlin

Dr. Kenneth Czerwinski, Advisory Committee Chair

Professor of Chemistry

University of Nevada, Las Vegas

Transition metals of groups six through nine exhibit unique direct multiple metal-metal bonding cores. Technetium is a group seven transition metal and is the lightest radioelement in the periodic table. Technetium exhibits nine oxidation states (from -I to VII) and an extensive set of mixed oxidation states due to bi- or poly- nuclear complex formation. Technetium has no stable isotopes and thirty four technetium isotopes have been discovered. Two main isotopes are of great importance ^{99}Tc and its metastable nuclear isomer ^{99m}Tc. The isotope ^{99m}Tc ($T_{1/2}$ = 6.01 hours, γ = 140.5 keV) is used in diagnostic nuclear medicine while ^{99}Tc ($T_{1/2}$ = 2.13x10^5 years, β = 294 keV) is a prominent fission product and is mainly used in fundamental technetium chemistry research due to its long half-life. The isotope ^{99}Tc is a concern in nuclear waste management due to its high production rate, mobility in the environment, long half-life and radiotoxicity. The rapid use of technetium in various diagnostic procedures extended its coordination chemistry but the fundamental chemistry of low valent

technetium is not as well explored compared to the surrounding elements Mo, Re, and Ru. Currently over 200 compounds containing the Re_2^{+n} (n = 4, 5, 6) cores are known, whereas less than 30 compounds with Tc_2^{+n} (n = 4, 5, 6) cores exist. One example of a Tc_2^{+6} core is $Tc_2(O_2CCH_3)_4Cl_2$ which has been shown to be a useful starting compound for the synthesis of technetium binary halides. Hydro/solvo-thermal synthesis methods are used to reduce pertechnetate species, Tc(VII), to low-valent stable Tc-Tc dimers by changing the temperature and pressure of the system under constant volume and with different salts and acids. Results of these hydro/solvo-thermal reactions have yielded various new ditechnetium compounds that show interesting structures and properties. This study will focus on the synthesis of molecular metal-metal bonded technetium compounds like $Tc_2(\mu\text{-}O_2CCH_3)_4X_2$, (X = Cl, Br), polymeric metal-metal bonded technetium compounds or chains as $[Tc_2(\mu\text{-}X)_4(\eta\text{-}Y)]_n$, (X = carboxylate; Y = carboxylate, I) and technetium cluster chemistry involving iodide as polynuclear species for $K[Tc_8(\mu\text{-}I)_8I_4]I$, and $Tc_5I_5(\mu\text{-}I)_4(\mu_3\text{-}I)_4$.

As a result, these studies related to the synthesis of technetium dimers/clusters will permit acquisition of new information on technetium metal-metal bond chemistry and thus extend the fundamental knowledge of this element as well as its potential applications in the nuclear fuel cycle or nuclear medicine.

ACKNOWLEDGMENTS

I would like to thank first my advisor, Pr. Kenneth Ronald Czerwinski, for selecting me to be part of his research program and to allow me to express myself in the laboratory by doing synthesis with transition metals (technetium-99) as well transuranic compounds.

The work presented in this thesis would not have been possible either without the presence, help and advice given by my committee. Their inputs and suggestions made me grown in technetium chemistry as well as in characterization techniques. Pr. Paul Foster was a significant help during my research method development and crystallographic studies. Dr. Frederic Poineau and Dr. Alfred Sattelberger were key contributors and source of information about technetium chemistry during this study. Dr. Sattelberger has an infectious desire to do synthesis and research daily; without his enthusiasm much of this work described below may have gone without notice to the scientific community. I shall always include him in my future endeavors of science.

I appreciated being part of the radiochemistry group at UNLV and participating to various projects. I would like to thank Tom O'Dou, Julie Bertoia and Trevor Low for making the laboratory work efficiently. And thank you to my labmates for their advice and help.

The support of my friends and family throughout the last five years was what pushed me through to the end. My parents, Mary P. Kerlin and Brent W. Kerlin have

always supported me in my adventures which helped tremendously. I would like to especially thank Maryline Ferrier for her extensive support and being around when I needed to vent. Without you, I would have never imagined completing this work, I would have stayed in the laboratory working on various new syntheses. Many thanks to a great professor of Physical Chemistry, as well as my mentor, supporter and friend Dr. Jeffery Mack of California State University of Sacramento with whom I have shared many great times.

TABLE OF CONTENTS

LIST OF TABLES

LIST OF FIGURES

CHAPTER 1: INTRODUCTION

1.1 Background

Technetium (element 43) was discovered by Perrier and Segrè in 1936 and was the first element to be produced artificially.[1,2] Technetium occupies a central position amongst the transition elements. Because it bears a close electronic relationship to its heavier congener rhenium, the occurrence of analogous compounds is expected, but the radioactive nature of technetium has served to limit the development of its chemistry relative to that of rhenium.[3] Technetium exhibits nine oxidation states (from -1 to +7) and an extensive set of mixed oxidation states due to bi- or poly- nuclear complex formations.[1] These variable oxidation states profoundly influence technetium coordination and redox chemistry, impacting its possible applications.

Technetium has thirty four known isotopes and none are stable.[3] Two main isotopes are of great importance, viz., ^{99}Tc and its metastable nuclear isomer ^{99m}Tc. The isotope ^{99m}Tc ($t_{1/2}$ = 6.01 hours, γ = 140.5 keV) is used in diagnostic nuclear medicine, while ^{99}Tc ($t_{1/2}$ = 2.13x10^5 years, β = 294 keV) is a prominent fission product and is used in research for fundamental technetium chemistry evaluation due to its longer half-life.[4] Technetium-99 accounts for ~6% by mass of the products from the fission of nuclear fuel containing ^{235}U and ^{239}Pu.[5] The prominent forms of technetium in the used nuclear fuel cycle are metallic, alloyed with Mo, Ru, Rh, Pd often called the “epsilon phase”,[4,6,7] and oxides TcO_2 and TcO_4^-[8]. Due to its half-long life and the mobility of the pertechnetate ion under non-reducing environmental conditions,[9] new studies have

been motivated to increase the scientific knowledge of fundamental technetium chemistry. Recent progress in this field is motivated by the extensive use of ^{99m}Tc in nuclear medicine.[10] The extensive use of technetium in various diagnostic procedures has expanded research on its coordination chemistry. A number of simple coordination compounds have been tested *in vivo* and are still in use today. This first generation of compounds where technetium was considered part of the "bioactive" molecule found a niche in radiopharmaceutical applications but the active compounds are not always fully characterized. One of the key compounds in technetium chemistry for radiopharmaceutical use was the preparation of ^{99m}Tc-hexakis-2-methoxy-2-isobutylisonitrile (^{99m}Tc-MIBI). This compound was the first organometallic prepared from TcO_4^- through very simple chemical procedure in aqueous media and was the first organometallic approved for clinical use in 1986 to obtain myocardial imaging.[11] Since 1990, a second generation has emerged and is more focused on the targeting capability of the biomolecule to which the Tc is ligated. In this regard, technetium coordination and fundamental chemistry are of continued interest.[12] For radiopharmaceuticals use, the key starting material is usually the pertechnetate ion which is obtained from a ^{99}Mo generator. The molybdate ion, MoO_4^{2-} is bound to alumina column. In the column the parent ^{99}Mo ($t_{1/2}$ = 67 hours) decays to ^{99m}Tc. The chemical form of technetium, pertechnetate, is not bound to the column and can be eluted with a saline solution (0.9% NaCl).[13] Pertechnetate is then subsequently reduced by an appropriate reducing agent and coordinated to a ligand. This ligand is specially designed to keep the metal centre in its reduced form and to assure the desired biological distribution.[10] For

example a well-established compound is technetium +4 methylene diphosphonate (^{99m}Tc-MDP called Osteolite, DuPont) that is used for skeletal imaging. Technetium can also be reacted with a large variety of ligands to obtain the desired functionality, but the vast majority of these compounds are mononuclear.[11,14]

With respect to coordination chemistry, the discovery of multiple metal-metal bonds between technetium centres is one of the more important advances in its inorganic chemistry. The synthesis and characterization of single and multiple bonds between metal centres started with the preparation of technetium compounds having low oxidation states or even mixed oxidation states. These dinuclear compounds can be used as starting compounds for the synthesis of related complexes or more complex chelated species that may find a use in nuclear medicine.[15]

Published strategies for the synthesis of binuclear (and polynuclear) technetium compounds containing multiple metal-metal bonds typically fall into one of three categories: (1) moderate temperature (100-300 °C) reduction of higher-valent mononuclear technetium precursors in aqueous hydrohalic acid solutions using molecular hydrogen (30-50 atm) as the reductant; (2) reduction of higher-valent mononuclear precursors using chemical reductants other than H_2, either in aqueous acid or non-aqueous solvents; (3) substitution and/or redox reactions involving pre-formed dinuclear complexes. Resvov and coworkers have been advocates for the first approach, while the rest of the community has traditionally opted for the latter two strategies.[16] The hydrogen reductions require the use of high-pressure stainless steel autoclaves. The use of glass test tubes and vessels inside the autoclave (*vide infra*) minimizes corrosion

of the stainless steel. Alternatively, more corrosion resistant alloys, such as Hastelloy, can be used in place of stainless steel.[17] Kryuchkov, and others have isolated a wide variety of dinuclear and polynuclear technetium compounds by systematically varying the experimental parameters (e.g., time, pertechnetate and acid concentrations, nature of the cation, temperature, hydrogen pressure, cool-down rate, etc.), but it is fair to say that serendipity ("thermodynamic self-assembly" in some quarters) plays a role in the outcome of these procedures as it does in many exploratory hydrothermal syntheses.[18]

As a result, acquisition of new knowledge on technetium metal-metal bond chemistry could extend the fundamental knowledge of this element as well as its potential applications in nuclear fuel cycle or nuclear medicine. This work will focus on revisiting the 1980's Russian approach relevant to metal-metal bond preparation. The synthesis and characterization of new technetium species was explored to provide details and insight into technetium fundamental chemistry and potential applications.

Chapter 1 is a bibliographic study on the fundamental and applied chemistry of technetium. In this chapter, metal-metal bond chemistry for other transition metals is compared to technetium. Chapter 2 outlines the materials and methods used in this work, i.e., starting compound synthesis, hydro/solvothermal methods and the characterization techniques employed. Chapter 3 focuses on molecular metal-metal bonded technetium compounds synthesized. This chapter will describe a high yield preparation of $Tc_2(O_2CCH_3)_4X_2$, (X = Cl, Br) as a one-step reduction from pertechnetate ion and compared to traditional synthesis of these molecular dimers**.** Chapter 4 presents synthesis of polymeric metal-metal bonded technetium compounds or chains. These

classes of repeating units; $[Tc_2(O_2CCH_3)_4X]_n$, (X = Cl, Br, I) and $[Tc_2(O_2CR)_4(\mu\text{-}O_2CR)]_n$ (R = CH_3, CH_2CH_3, C6H5, alkyls), are compared to both rhenium and ruthenium homologues. Chapter 5 examines the technetium synthetic and coordination chemistry of the new polynuclear species; $K[Tc_8(\mu\text{-}I)_8I_4]I$, and $Tc_5(\mu\text{-}I)_4(\mu_3\text{-}I)_4I_5$. Chapter 6 summarizes the extent of the synthesis of these hydro-solvothermal reactions from the pertechnetate ion forming a variety of multinuclear metal-metal bonded technetium compounds. In this chapter, conclusions and future work are presented in detail with emphasis and suggestions for continuing the synthesis of these technetium polynuclear compounds.

1.2 **Metal-metal bonded compounds**

1.2.1 ***Transition metals***

The studies of transition metal compounds with metal-metal bonds and their molecular and electronic structures are essential to understand the nature of the metal-metal interactions as well as their catalytic and biological properties.[19-25] In general, transition metals can form single to quintuple bonds with other atoms but bond orders greater than 3 are only formed between two transition metal atoms. Some dinuclear and extended-structure compounds and heteroatomic clusters are found with multiple Tc-Tc bonds but the technetium metal-metal bond chemistry remains underdeveloped compared to its neighboring elements - molybdenum, ruthenium and rhenium.[16,26-29]

Prior to 1963, very little effort was focused on metal-metal bonded compounds. In mid-1963, extensive studies on $[Re_3Cl_{12}]^{3-}$ demonstrated the existence of Re-Re double bonds in this trinuclear cluster anion. Pursuing various rhenium chemistry researchers

questioned the bond order of different compounds. The discovery and structure of $[Re_2Cl_8]^{2-}$, the first quadruply metal-metal bonded dimer,[19] triggered a revolution of sorts and the correlation of metal-metal distances with bond orders ranging from <1 to 4 was discussed and debated, and the concept of metal-metal bond orders was introduced. The quadrupole bond chemistry for rhenium was rapidly investigated and even a metal-metal triple bond was proposed in $Re_2Cl_5(CH_3SCH_2CH_2SCH_3)_2$ compound.[19] During the next 20 years, the field of metal-metal bond grew rapidly, before slowing down to a steady level of research. Nowadays the concept of quadruple bond is well accepted and characterized for about 1500 compounds.[19,30]

It has been suggested that metal-metal bonding interactions exist for almost every transition element, with the possible except of scandium. This type of bonding seems to exist even in higher oxidation states while for later transition metals it is observed primarily in the lower oxidation states. The middle of the transition series and especially the second and third row elements of the Periodic Table seem to have a high tendency to form metal-metal bonds in various oxidation states.[31]

The covalent bonding between two metals is usually found when the compounds need to achieve the 18-electron configuration. Most of the time, a metal-metal bond is found when no other bonding partners or no structural constraints are available. It is known that when two fragments need one electron to complete the inert gas configuration, single bonds are formed. Bond orders of 2, 3 and 4 between metal atoms are now frequently encountered throughout the group 5, 6, 7, 8, and 9 transition metals on the periodic table. Specifically multiple bonds are mostly formed for chromium,

molybdenum, tungsten, technetium, rhenium, ruthenium, and rhodium compounds. The other transition metal elements that exhibit multiple M-M bonding but not as prolifically are those in group 5 (Nb and Ta), plus iron, osmium, cobalt and iridium. Bridging ligands protecting the metals seems to make these compounds more stable and accessible.[32,33]

The main experimental techniques used to detect the presence of metal-metal bond in a compound are: X-ray diffraction analysis, magnetic measurements and Infra-red, Raman, Ultra-Violet and visible spectroscopies.[31]

Bond lengths are reasonable indicator of the presence of a metal-metal bond when the metal atom distances are of the same order as in the metal. Usually when comparing two compounds of similar stereochemistry, the change of bond length shows the presence or absence of metal-metal bond.[32] Normally within most inorganic and organic structures bond order (single, double, and triple bonds) correlate with decreasing bond length. But within the metal-metal bonded realm of second and third row transition metals, specifically group 6-8, it should be noted that bond length and bond order are not strictly a simple inverse relationship.[34]

Magnetic properties differ highly when paramagnetic transition metal ions do or do not interact with each other. The presence of metal-metal bond and their interactions can thus be studied by bulk magnetic susceptibility. The behavior of the compound in a magnetic field will give information about its electronic structure, the presence of unpaired electron or not but also in some case detect the presence of metal-metal bond. A combination of multiple characterization techniques results, such as bulk

magnetic properties, electron spin resonance, UV-Vis spectra and theoretical calculations, can give information about the ordering of the energy levels and the character of the highest filled orbital.[35]

Spectroscopic techniques can be used to explore the metal-metal bond σ-σ*, π-π*, π-δ* and δ-δ*, type transitions and ligand-to-metal charge transfer transitions (LMCT). Of these transition types, δ-δ* are the most thoroughly examined for M_2^{n+} complexes using electronic absorption techniques at low temperature, i.e., 80 to 5 K.[34]

1.2.2 ***Technetium***

Today the number of laboratories worldwide that are equipped to pursue synthetic chemistry with the most readily available isotope, *viz.*, ^{99}Tc, is severely limited. For the past several years, the radiochemistry program at UNLV have been exploring the fundamental chemistry of technetium, including that associated with metal-metal bonded dimers with bonds of order 4, 3.5 and 3.[36] We have found many similarities between the dinuclear chemistry of Tc and Re, but also subtle and sometimes frustrating differences in the synthetic chemistry that are likely a manifestation of the redox properties of the respective elements in equivalent oxidation states. In the literature it has been found that thirteen binary halides exist for rhenium, while only three technetium halides were fully characterized (TcF_6, TcF_5 and $TcCl_4$) prior to 2008. Many new technetium compounds can be then foreseen to be discovered and characterized. For technetium, as of the year 2005, 25 dinuclear species, 4 hexanuclear, 6 octanuclear halide clusters and 3 extended metal-atom chain (EMAC) compounds had

been structurally characterized, but no binary halides beyond those mentioned above.[16]

As part of an effort to expand our knowledge of technetium chemistry, our group investigated the chemistry of the binary halides and prepared seven new phases ($TcBr_4$, $TcBr_3$, α/β-$TcCl_3$, α/β-$TcCl_2$, and TcI_3).[3,37] In these phases, the electronic configuration of the Tc atom has a bearing on the extent of Tc-Tc interaction: in the tetrahalide, there is no appreciable metal-metal interaction, a Tc=Tc double bond is observed in α/β-$TcCl_3$ and a Tc≡Tc triple bond in α/β-$TcCl_2$. Two main routes have proven fruitful for the synthesis of technetium binary halides: reaction between the elements in a sealed evacuated tube,[38,39] and reaction between $Tc_2(O_2CCH_3)_4Cl_2$ and flowing HX gas (X = Cl, Br, I) at elevated temperatures. Technetium trihalides ($TcBr_3$, TcI_3 and α-$TcCl_3$) have been obtained from the reaction of $Tc_2(O_2CCH_3)_4Cl_2$ with HX gas (X = Cl or Br) at 300 °C.[40,41] One compound that we have found to be a very useful starting material for investigations of both dinuclear technetium(III) chemistry and as a precursor to α-$TcCl_3$ (Tc_3Cl_9) is the acetate bridged dimer, $Tc_2(O_2CCH_3)_4Cl_2$.[40] Its rhenium analog, $Re_2(O_2CCH_3)_4Cl_2$, first prepared by Taha and Wilkinson [42], played a key role at the beginning of the multiple metal-metal bond field and was an early example of a d^4-d^4 dimer with a quadruple metal-metal bond. Thus, new technetium metal-metal bonded dimers with carboxylate ligands are of particular interest as precursors for the preparation of new technetium binary halides, TcX_y (X = F, Cl, Br, I; y = 2, 3, 4).[3,43] The study of $Tc_2(O_2CCH_3)_2Cl_4$ also permitted to better understand the influence of acetate ligand on the Tc-Tc bonding.[44] Currently, only five compounds containing a Tc_2^{n+} (n = 5,

6) unit coordinated to acetate and halogen ligands are structurally characterized: $Tc_2(O_2CCH_3)_4X$ [45,46], $K[Tc_2(O_2CCH_3)_4Cl_2]$ and $Tc_2(O_2CCH_3)_4X_2$ (X = Cl, Br),[47,48] and no complexes with multiple metal-metal bonds coordinated to iodide ligands have been reported yet.

Another part of our work effort was to investigate cluster chemistry with technetium. In general, it is known that multiple metal-metal bounds are found with trigonal or tetragonal prismatic geometries in hexanuclear and octanuclear clusters respectively. The first hexanuclear species were obtained after reduction in an autoclave at 140-180 °C of $(Me_4N)_2TcCl_6$ or $(Me_4N)TcO_4$ in concentrated HCl or HBr by H_2 (30-50 atm). The obtained $\{[Tc_6Cl_6(\mu\text{-}Cl)_6]Cl_2\}^{3-}$ and $[Tc_6Cl_6(\mu\text{-}Cl)_6]^{2-}$ clusters contain Tc_6^{11+} and Tc_6^{10+} cores with 31- and 32-electron counts, respectively. The $\{[Tc_6(\mu\text{-}Br)_6Br_6]Br_2\}$ 31-electron cluster is similar to its chloride congener. The structures contain short Tc-Tc distances for the rectangular edges corresponding to the three electron-rich Tc≡Tc bonds, while the distances along the triangular faces are longer indicative of the six Tc single bonds.[49,50,51] Other cluster compounds having higher nuclearity were characterized. For example, the $[Tc_8(\mu\text{-}Br)_8Br_4]^+$ cluster contains four types of Tc–Tc bonds with different distances suggesting the presence of Tc–Tc bonds of high multiplicity. The shorter distances, perpendicular to the rhomboidal faces, are characteristic of triple bonds, while the longer distances along the edge of the faces are described as single bonds.[16] More details are given in Chapter 5, a figure of these clusters are shown in Figure **5.1**. A selected list of structurally characterized technetium compounds with Tc-Tc multiple bonds is shown in Table **1.1** and Table **1.2** separated into

four classes of compounds; molecular species, salts, polymeric chains and polynuclear clusters. Synthesis of these dinuclear compounds, Tc_2^{+5} and Tc_2^{+6} cores, and clusters are prepared by 3 different methods within the literature: (1) hydrogen reduction (30-70 atm) from pertechnetate species in concentrated hydrohalic acid solutions at temperatures between 100 – 250 °C; (2) classic chemical reductions other than hydrogen on pertechnetate or higher valent mononuclear species in a variety of aqueous or organic solvents; (3) using dinuclear species prepared by method (1) by redox reactions or substitutions.[16]

Table 1.1. Selected group of Tc-Tc multiple bonded compounds separated by class of species: molecular and ionic salts.[16] Part A.

Compound	Tc-Tc (Å)	Bond order	Ref.
	Molecular		
$Tc_2(O_2CCH_3)_4Cl_2$	2.1758(3)	4	[48]
$Tc_2(O_2CCMe_3)_4Cl_2$	2.192 (1)	4	[52]
$[Tc_2(O_2CCH_3)_4](TcO_4)_2$	2.149(1)	4	[53,54]
$[Tc_2(O_2CCH_3)_2Cl_4(dma)_2]$	2.1835(7)	4	[55]
$Tc_2Cl_5(PMe_2Ph)_3$	2.109(1)	3.5	[56]
$Tc_2(DTolF)_3Cl_2$	2.094(1)	3.5	[57]
$Tc_2Cl_4(PEt_3)_4$ 2.133(3)	2.133(3)	3	[58]
$Tc_2Cl_4(PMe_2Ph)_4$	2.127(1)	3	[58]
α-$Tc_2Cl_4(Ph_2P(CH_2)_2PPh_2)_2$	2.15(1)	3	[59]
β-$Tc_2Cl_4(Ph_2P(CH_2)_2PPh_2)_2$	2.117(1)	3	[59]
β-$Tc_2Cl_4(Ph_2PCH_2PPh_2)_2$	2.1126(7)	3	[60]
	Salts		
$(Bu_4N)_2Tc_2Cl_8$	2.147(4)	4	[61]
$K_2[Tc_2(SO_4)_4]\cdot 2H_2O$	2.155(1)	4	[62]
$K_3Tc_2Cl_8\cdot nH_2O$	2.117(2)	3.5	[63,64]
$(NH_4)_3Tc_2Cl_8\cdot 2H_2O$	2.13(1)	3.5	[65,66]
$Y[Tc_2Cl_8]\cdot 9H_2O$	2.105(2)	3.5	[67]
$(C_5H_5NH)_3Tc_2Cl_8$	2.1185(5)	3.5	[68]
$K[Tc_2(O_2CCH_3)_4Cl_2]$	2.1260(5)	3.5	[69]
$[Tc_2Cl_4(PMe_2Ph)_4]PF_6$	2.106(1)	3.5	[56]
$K_2[Tc_2Cl_6]$	2.044(1), 2.047(1), 2.042(1)	3	[70,71]
$[Tc_2(NCCH_3)_8(CF_3SO_3)_2](BF_4)_4\cdot CH_3CN$	2.122(1)	3	[72]

dma = N,N'-dimethylacetamide, DTolF = N,N'-di-p-tolylformamidinate

Table 1.2. Selected group of Tc-Tc multiple bonded compounds separated by class of species: polymeric chains and polynuclear clusters.[16] Part B.

Compound	Tc-Tc (Å)	Bond order	Ref.
Polymeric chains			
$Tc_2(hp)_4Cl$	2.095(1)	3.5	[73]
$Tc_2(O_2CCH_3)_4Cl$	2.117(1)	3.5	[45]
$Tc_2(O_2CCH_3)_4Br$	2.112(1)	3.5	[46]
Polynuclear clusters			
<u>Hexanuclear</u>			
$[(CH_3)_4N]_3\{[Tc_6(\mu\text{-}Cl)_6Cl_6]Cl_2\}$	2.16(1), 2.69(1)		[74]
$[(CH_3)_4N]_2[Tc_6(\mu\text{-}Cl)_6Cl_6]$	2.22(1), 2.57(1)		[75]
$[(C_2H_5)_4N]_2\{[Tc_6(\mu\text{-}Br)_6Br_6]Br_2\}$	2.188(5), 2.66(2)		[51]
$[(CH_3)_4N]_3\{[Tc_6(\mu\text{-}Br)_6Br_6]Br_2\}$	2.154(5), 2.702(2)		[51]
<u>Octanuclear</u>			
$\{[Tc_8(\mu\text{-}Br)_8Br_4]Br\}\cdot 2H_2O$	2.146(2), 2.521(2), 2.687(23)		[76]
$[H(H_2O)_2]\{[Tc_8((\mu\text{-}Br)_8Br_4]Br\}$	2.155(3), 2.531(2), 2.70(2)		[77]
$[H(H_2O)_2]_2\{[Tc_8((\mu\text{-}Br)_8Br_4]Br_2\}$	2.152(9), 2.520(9), 2.69(1)		[78]
$[(C_4H_9)_4N]_2\{[Tc_6(\mu\text{-}Br)_4(\mu\text{-}I)_4Br_2I_2]I_2\}$	2.162(9), 2.507(2), 2.704(10)		[51]
$[Fe(C_5H_5)_2]_3\{Tc_6(\mu\text{-}I)_6I_6]I_2\}$	2.17(1), 2.67(1)		[54]

hp = 2-hydroxypyridine

1.2.3 ***Comparison of technetium and surrounding elements***

1.2.3.1 Classic starting materials

The availability of starting materials for the surrounding elements are vast compared to that of technetium. Commonly the oxides of these elements are reduced to lower valent compounds for starting materials. Generally starting materials for the synthesis of dinuclear and clusters compounds are shown in Table **1**.**3**, vary depending on element group. For general purposes the elements manganese and iron will not be discussed due to lack of multiple metal-metal bonding chemistry and has little or no comparison to ditechnetium, Tc_2^{+n}, complexes.

The vast majority of technetium syntheses start from pertechnetate salts, $MTcO_4$ (M = alkali metals, NH_4^+, NR_4^+) and reduced to starting compounds or direct reduction to product, by molecular hydrogen or reducing agents such as trimethylsilyl chloride or zinc. Lower valent salts of $TcCl_6^{2-}$, such as $(NH_4)_2TcCl_6$ are reacted with Zn in concentrated hydrochloric acid to produce the octachloroditechnetate(II,III) anion, $(NH_4)_3Tc_2Cl_8$, with its Tc_2^{+5} core, which can be used as a starting material to many of the 25 known Tc_2^{+n} dinuclear compounds listed in Table **1**.**1** and Table **1**.**2**.[79]

Table 1.3. Common starting material for synthesis of dinuclear and clusters by element.

Element	Starting Materials (X = Cl, Br)
Chromium	$Cr(CO)_6$, $[Cr_2(CO_3)_4]^{4-}$, $Cr_2(O_2CCH_3)_4(H_2O)_2$
Molybdenum	$Mo(CO)_6$, $MoCl_3$, $Mo_2(O_2CCH_3)_4$
Tungsten	WCl_4, $W(CO)_6$, $[W_2Cl_8]^{2-}$, $W_2(O_2CY)_4$ (Y = CH_3,CF_3)
Technetium	TcO_4^-, $TcCl_6^{2-}$, $[Tc_2X_8]^{n-}$ (n = 2, 3)
Rhenium	ReO_4^-, $ReCl_6^{2-}$, $[Re_2X_8]^2$, Re_3Cl_9 $Re_2(O_2CR)_4X_2$ (R = Alkyl)
Ruthenium	$RuCl_3{\cdot}nH_2O$, $Ru_2(O_2CR)_4Cl$ (R= Alkyl) $Ru_2(O_2CCH_3)_4(THF)_2$
Osmium	$OsCl_3$, OsX_6^{2-}, $Os_2(O_2CMe)_4X_2$

Similar to technetium, at the infancy of rhenium dinuclear chemistry the method of choice was high pressure H_2 reduction from potassium or ammonium perrhenate salts, $MReO_4$. This method was chosen but was unpopular because of the corrosive nature of the reactants on the reaction vessel and competition $[ReCl_6]^{2-}$ formation providing low yields of the $[Re_2Cl_8]^{2-}$ anion.[80] It was not until 1982 when the synthesis of the tetra-n-butylammonium salt, $(Bu_4N)_2Re_2Cl_8$, was reported from the reaction of $(Bu_4N)ReO_4$ with reflexing benzoyl chloride followed by addition of gaseous saturated solution of hydrogen chloride in ethanol to give a straightforward quick simple one-pot synthesis in high yield (<90%).[81] The organic salt, $(Bu_4N)_2Re_2Cl_8$, became the starting material for

preparation of most dinuclear rhenium compounds known to date, approximately 150.[82] A simple substitution reaction with RCO_2H, R= alkyl groups and accompanying anhydride with $(Bu_4N)_2Re_2Cl_8$ yields Re_2^{+6} dihalotetracarboxylate compounds.[83,84] These $Re_2(O_2CR)_4X_2$ starting materials lead to a plethora of over 40 dirhenium Re_2^{+6} compounds.

Group 6 elements; chromium, molybdenum and tungsten have very different chemistry when forming metal-metal bonded compounds. Most Cr_2^{n+}, compounds are formed from chromium (II) acetate, chromium (II)/(III) chlorides and tetracarbonato anion, $[Cr_2(CO_3)_4]^{4-}$, and chromium hexacarbonyl. Examination into the reactions that form dinuclear chromium compounds will be summed up to substitution reaction with $Cr_2(O_2CCH_3)_4$, $[Cr_2(CO_3)_4]^{4-}$ and organo-lithium chemistry with $Cr(CO)_6$.[85] For molybdenum, classically $Mo(CO)_6$ is heated in with a carboxylic acid and its anhydride with in diglyme or 1,2-dichlorobenzene affords $Mo_2(O_2CR)_4$ compounds to which the majority of dinuclear Mo_2^{+n} compounds are synthesized.[86,87] The compound most used in formation of well over 500 Mo_2^{+n} complexes is tetraacetato dimolybdate(II), $Mo_2(O_2CCH_3)_4$, by simple substitution reactions.[88] Tungsten unfortunately is more complicated than molybdenum with reference to easy direct formation of W_2^{n+} carboxylates.[89] For example attempts in early 1970's to react $W(CO)_6$ with acetic acid and acetic anhydride was unsuccessful in yielding $W_2(O_2CCH_3)_4$, as does $Mo(CO)_6$ to $Mo_2(O_2CCH_3)_4$.[90,91,92] A breakthrough in tungsten quadruple dimer chemistry came with the first structural characterization of $W_2(O_2CCF_3)_4 \cdot 0.67$(diglyme) via the reaction of Na/Hg reduction of $NaW_2Cl_7(THF)_5$ with addition of sodium triflouroacetate (originally

reported as $W_2Cl_6(THF)_4$ but later characterized as $NaW_2Cl_7(THF)_5$).[93,94] Ultimately in 1985, a route to $W_2(O_2CCH_3)_4$ was synthesized through $W_2(O_2CCF_3)_4$ with tetrabutylammonium acetate in toluene, providing the basis for synthesis of other W_2^{+4} tetracarboxylates.[93,95,96,97,98] Additional routes to W_2^{n+} compounds involves reduction of WCl_4 with a variety of reducing agents; i.e. Na/Hg, $NaBEt_3H$ with alkyl carboxylates and phosphine ligands to form $W_2(O_2CR)_4$ and $W_2Cl_4(PR_3)_4$ compounds, where R = alkyl group.[89]

Ruthenium and osmium exhibit very similar synthetic routes to M_2^{+n}, (M = Ru, Os) carboxylate compounds and dinuclear species. Diruthenium compounds with Ru_2^{5+} cores are highly abundant, and readily obtained from reaction of $RuCl_3 \cdot nH_2O$ refluxing with a carboxylic acid and the corresponding anhydride or preferred bridging ligand in ethanol under inert atmosphere leading to $Ru_2(O_2CR)_4Cl$, (R = H, Me, Et, Pr^n).[99,100,101,102,103] The building material for the majority of Ru_2^{n+} compounds comes from $Ru_2(O_2CPr^n)_4Cl$, by substitution reactions in both aqueous and organic solvents as well as molten amides. Compounds of $Ru_2^{+4,6}$ are synthesized via oxidation or reduction of $Ru_2(O_2CPr^n)_4Cl$.[104] What separates ruthenium and osmium dinuclear chemistry is the $OsCl_3$ reaction with carboxylic acid and anhydride will not produce $Os_2(O_2CPr^n)_4Cl$, as does ruthenium, but addition of 2-hydroxypyridine(hp) will afford, Os_2^{6+} core, $Os_2(hp)_4Cl_2$.[105] In order to obtain a carboxylate compound $OsCl_6^{2-}$ in hydrochloric acid solution is reacted with acetic acid/anhydride producing $Os_2(O_2CCH_3)_4Cl_2$, then with simple carboxylate exchange, structures of the type $Os_2(O_2CR)_4Cl_2$ are generated.[106,107,108,109]

The chemistry of technetium polynuclear clusters greater than binuclear can be summed to one type of general reaction. The reduction of pertechnetate ion in concentrated HCl, HBr, HI under pressure (3 - 8 MPa) with molecular hydrogen at 140-220 °C produces hexanuclear and octanuclear halides with counter cations, or hydration species.[52,54,74-79] As for the chemistry Mo and W polynuclear cluster are formed by metal-hexacarbonyl with iodide or disproporation and reduction reactions from metal chlorides of varying oxidation states. Rhenium(III) chloride is naturally a trinuclear species and is a great starting compound for synthesis of rhenium clusters.[21]

1.2.3.2 Molecular carboxylate structures, $M_2(O_2CR)_nX_z$

Only 6 structurally characterized molecular carboxylate structures of technetium, Tc_2^{+6} quadruple bond, shown in Table 1.1 and Table 1.2, and those presented in Chapter 3 are known today. For the elements surrounding technetium with structure motif, $M_2(O_2CR)_nX_z$ (M = Tc, Re, Mo, W, Ru, Os; R = Alkyl; X = singly charged anionic ligand; n = 2-4; z = 1-4) exhibit a wider known group of compounds. This can be attributed to the lack of laboratories worldwide working with technetium especially investigations of metal-metal bonded chemistry. Molecular carboxylate dimers of rhenium have been synthesized and characterized on the order of 30 compounds a 5 fold increase over those of technetium. Besides halogen, dirhenium carboxylate dimers coordinated with water, solvents (i.e., CH_2Cl_2, DMF, DMSO, THF), ReO_4^-, and large organic molecules are known.

Similar to rhenium, osmium exhibits about ten, Os_2^{+6}, molecular carboxylates with halide and solvent coordinated structures. On the other hand, diruthenium complexes prefer Ru_2^{+4} molecular carboxylate orientation numbering some fifteen characterized compounds compared to zero Ru_2^{+6} molecular carboxylates. As for molybdenum and tungsten a plethora of Mo_2^{+4} and W_2^{+4} carboxylate structures are known but no evidence for $Mo_2(O_2CCH_3)_4Cl_2$ or $W_2(O_2CCH_3)_4Cl_2$. Although tungsten, exhibits metal-metal triple bonds with W_2^{+6} paddelwheel type structure have been reported in literature, ie, $W_2(hpp)_4Cl_2$, (hpp = 1,3,4,6,7,8-hexahydro-2H-pyrimido[1,2-a]pyrimidine).[110,111]

1.2.3.3 Polymeric carboxylate chain structures, $M_2(O_2CR)_nX$

Technetium and ruthenium seem to share a unique class of M_2^{+5} core structures to which the core is linked by one atom or unit, $M_2(O_2CR)_4X$ (M = Tc, Ru; R = alkyl; X = ligand). These compounds are paramagnetic units with Tc-Tc dimer sharing one unpaired electron, and Ru-Ru dimers with 3 unpaired electrons within the paddlewheel structure. Further exploration of this class of dinuclear carboxylate dimer is described in chapter 4.

It should be noted that technetium, ruthenium and osmium form polymeric paddlewheel chains with O,N- or N,N- bridging ligands, i.e., $M_2(hp)_4Cl$, (hp = 2-hydroxypyridine) where polymeric linkage is formed through the chlorine atom.[19]

1.2.3.4 Known polynuclear cluster compounds

A hypothesis within the cluster community is that these polynuclear species, $[Tc_8Br_{14}]^{2-}$ form from the binuclear ions $[Tc_2X_8]^{4-}$ and $[Tc_2X_8]^{5-}$ by cycloaddition, (Figure **1.1**), and believed to mechanistically form $[Tc_6X_{14}]^{2-}$ in the same manner.[62,112] Molybdenum and tungsten form hexa-nuclear chloride species $[M_6Cl_{14}]^{3-}$ as well as other bromides and iodides. Recently interesting results for penta-nuclear W iodide, $[W_5I_{13}]^{n-}$, (n = 1, 2) clusters in which analogues $[Mo_5Cl_{13}]^{2-}$ but no iodide structure of Mo penta-nuclear cluster is known.[113,114] Chapter 5 will focus on technetium polynuclear iodide synthesis and characterization.

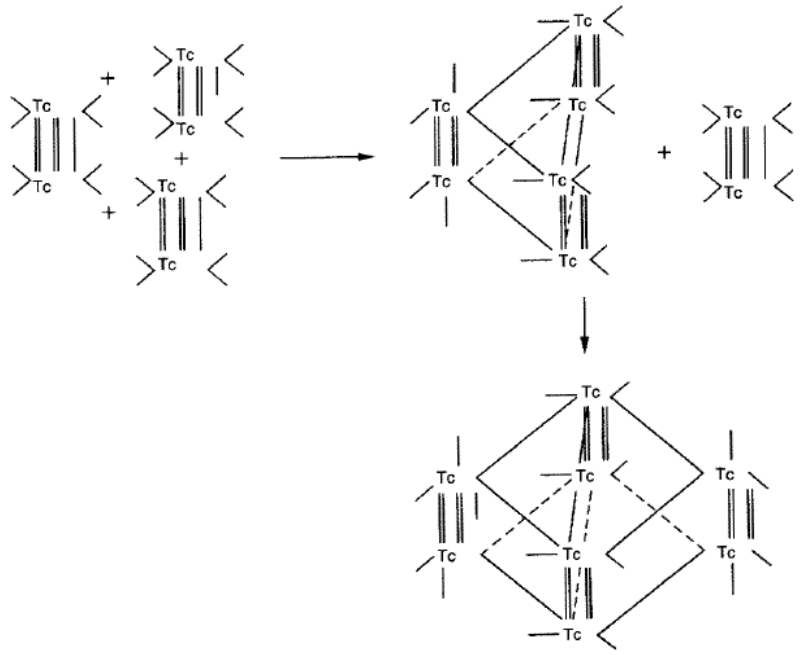

Figure 1.1. A scheme of $[Tc_2X_8]^{n-}$ units (n = 4,5) assembling via cycloaddition to form octanuclear technetium clusters. [62]

CHAPTER 2: Materials and Methods

This chapter will describe the preparation of the starting technetium compound, $KTcO_4$, the different types of hydrothermal methods, and the various characterization techniques used in this work.

2.1 Materials and methods used

Caution. Due to the radioactivity of ^{99}Tc (beta E_{max} = 292 keV), all manipulations were performed in a specially designed laboratory that can handle chemical synthesis with radionuclides and is equipped with HEPA-filtered fume hoods. Local procedures and regulations were followed for safe radioisotope handling.

All chemicals were purchased and used as received from suppliers. Using a Milli-Q system, the water was purified to > 18 MΩ cm. The synthesis of the primary technetium starting compound is described below.

2.1.1 *Synthesis and characterization of $KTcO_4$*

The synthesis of this starting compound was following a slightly modified procedure described in literature.[115] In an Erlenmeyer flask, 500 mg of NH_4TcO_4 purchased from Oak Ridge National Laboratory was dissolved in about 5 mL of DI H_2O. To assure complete dissolution and purification of the compound, the solution was heated boiling (reflux) and 40 µL of 30% H_2O_2 was added which oxidizes any black TcO_2 impurity to TcO_4^-. To precipitate the desired white solid 150 mg of KOH was added to the boiling

solution. The white suspension was cooled to room temperature and the supernate was removed by glass pipet. The white solid was washed with isopropanol and diethyl ether, three times each with 3 mL. The solid was then thoroughly dried in the oven 90 °C overnight (492 mg, yield = 90%). See Figure **2.1** for pictures of the various steps of the synthesis. The solid was analyzed by UV-Visible after dilution in water and attenuated total reflectance IR spectroscopy; see Figure **2.2** and Figure **2.3**. The UV-Visible spectrum of the compound dissolved in water displayed two major peaks at 244 nm and 287 nm which confirmed the presence of pertechnetate at the concentration of 2.25 x 10^{-4} mol·L^{-1}. The concentration of the solution was determined using the Beer Lambert Law described in Equation 2.4 in section 2.2.2.2 and a molar absorptivity value at 244 nm of 5690 L·mol^{-1}·cm^{-1}.[3] The IR spectrum showed a strong peak at 904 cm^{-1} which is characteristic of Tc=O vibrations present in pertechnetate. Another feature of the IR spectrum is the absence of a water signature, confirming the purity of the dehydrated compound and thus the molecular weight of the white precipitate to be 202 g·mol^{-1}.

Figure 2.1. NH_4TcO_4 from Oak Ridge (left), dissolution and purification of bought pertechnetate (middle) and white precipitate $KTcO_4$ (right).

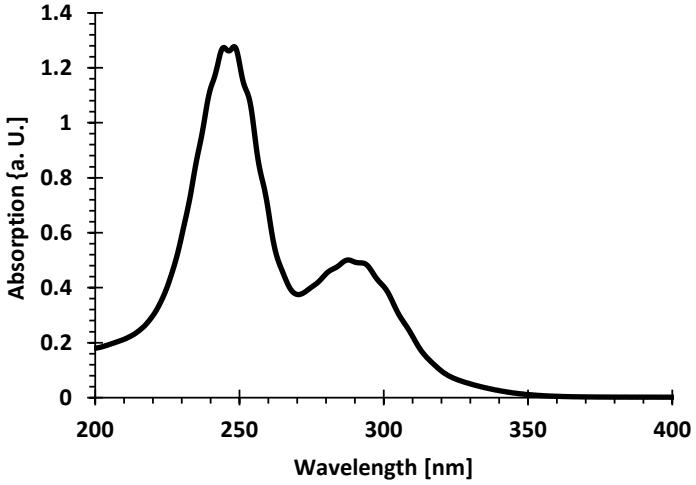

Figure 2.2. UV-Visible spectrum of $KTcO_4$ in H_2O.

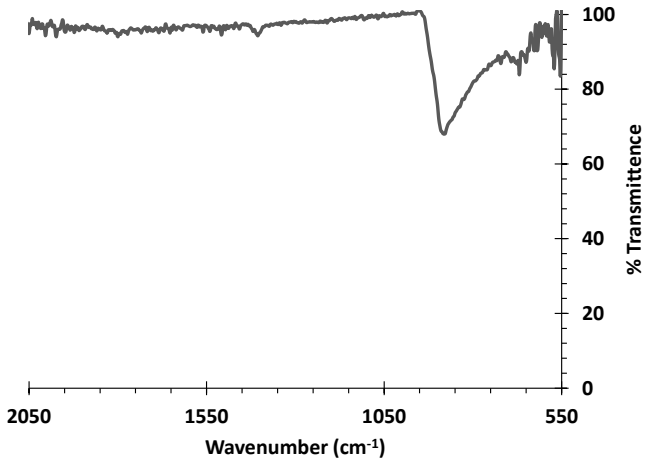

Figure 2.3. Infra-red spectrum of $KTcO_4$ solid.

2.1.2 ***Hydro/Solvo-thermal reaction techniques***

Important branches of synthetic inorganic chemistry are hydrothermal and solvothermal syntheses. Hydrothermal and solvothermal reactions refer to syntheses in a sealed and heated apparatus containing an aqueous solution and/or organic solution,

respectively, at appropriate temperature (100 °C – 1000 °C) and pressure (1 MPa – 100 MPa) to dissolve or recrystallize materials that are relatively insoluble under ordinary conditions. The origin of these techniques was focused on the synthesis of minerals and extraction of elements from minerals. Recently their application has involved, *inter alia*, inorganic syntheses of conventional and advanced compounds like zeolites, microporous or nano materials, growth of large single crystals like quartz, treatment of wastes, and mimicking of geothermal and bio-hydrothermal processes. The operability and tunable-ness of hydro/solvo-thermal chemistry enables bridges between synthetic chemistry and physical properties of as-made materials. [116]

The definition of a hydro/solvo-thermal reaction varies from author to author and depends on the application. In broader terms, hydro/solvo-thermal process can be defined as "any heterogeneous or homogeneous chemical reaction in the presence of a solvent (whether aqueous or nonaqueous) above room temperature and at pressures greater than 1 atm in a closed system". Under these conditions, the reactants which are otherwise difficult to dissolve go into solution. Therefore some workers define hydrothermal reactions as a special case of chemical transport reactions.[117] According to the reaction temperature, hydro/solvo-thermal syntheses can be classified as subcritical (100 °C – 240 °C) or supercritical (could reach 1000 °C and 0.3 GPa).[116]

In some cases, hydro/solvo thermal reactions offer an attractive alternative and mild synthetic method over solid-state reactions. Solid-state reactions depend on the diffusion of the raw materials at interfaces whereas for hydro/solvo-thermal the

reactant ions and/or molecules are in solution. The difference of reaction mechanism may lead to different products even if the same reactants are used.[116]

The main disadvantage of the hydro/solvo-thermal system is the “black-box” nature of the experiment, because one typically cannot observe directly the reaction processes.[117] However it is known that during the reaction, many of the fundamental physical properties of the solvent like viscosity, dielectric constant, density, etc., undergo considerable changes during the reaction at higher temperature and pressure. Due to the high solvation power, high compressibility and mass transport properties of these solvents, powders or single crystals are formed by chemical reaction. [116,117]

The solvent used under high temperature and pressure conditions can play an important role in the reaction. In hydrothermal, water can act as a solvent as well as one of the reactants. This potential double role is a key to change the chemical and physical properties of reactants and products, accelerate reactions and transfer pressure. In solvothermal synthesis, an organic solvent is used. This solvent is the medium of the reaction but also a way to dissolve or partially dissolve the reactants. This solubility property will affect the chemical reaction rate, the concentration and state of the reactants, and thus finally change the reaction process.[116]

The pressure and temperature conditions and the corrosion resistance needed for the experiments are the parameters that are considered for the selection of the autoclave. The most commonly used autoclaves in hydrothermal research are listed in Table 2.1.[117,118]

Table 2.1. Autoclaves. [117]

Type	Characteristic data
Pyrex tube 5 mm i.d. 2 mm wall thickness	6 bar at 250 °C
Quartz tube 5 mm i.d. 2 mm wall thickness	6 bar at 300 °C
Flat-plate seal, Morey type	400 bar at 400 °C
Welded Walker-Buchler closure 2600 bar at 350 °C	2kbar at 480 °C
Delta ring, unsupported area	2.3 kbar at 400 °C
Modified Bridgman, unsupported area	3.7 kbar at 500 °C
Full Bridgman, unsupported area	3.7 kbar at 750 °C
Cold-cone seal, Tuttle-Roy type (batch reactors)	5 kbar at 750 °C
Piston cylinder	40 kbar at 1000 °C
Belt apparatus	100 kbar at > 1500 °C
Opposed anvil	200 kbar at > 1500 °C
Opposed diamond anvil	Up to 500 kbar at > 2000 °C
Continuous flow reactor	2 kbar at 600 °C

In general, thick glass or quartz cylinder and high refractory alloys are usually used to build the autoclave. In order to prevent any corrosive attacks from reagents, inert linings, liners or cans are usually used. These are made from Teflon, Pyrex, quartz, graphite, Armco iron, titanium, silver, platinum, tantalum, copper, nickel, and gold. Detailed descriptions of various autoclaves are discussed in literature.[117]

Experiments within this thesis were performed using two types of autoclaves: (1) A Parr Instruments 5500 Series high pressure controlled atmosphere autoclave (Figure **2**.**4**). The maximum temperature is 350 °C and maximum pressure is 200 atm or 20.3 MPa for a volume of 300 mL with ability to initially control the type of atmosphere of

the autoclave. A sketch of the autoclave with internal setup for experiments is shown in Figure **2.5**.

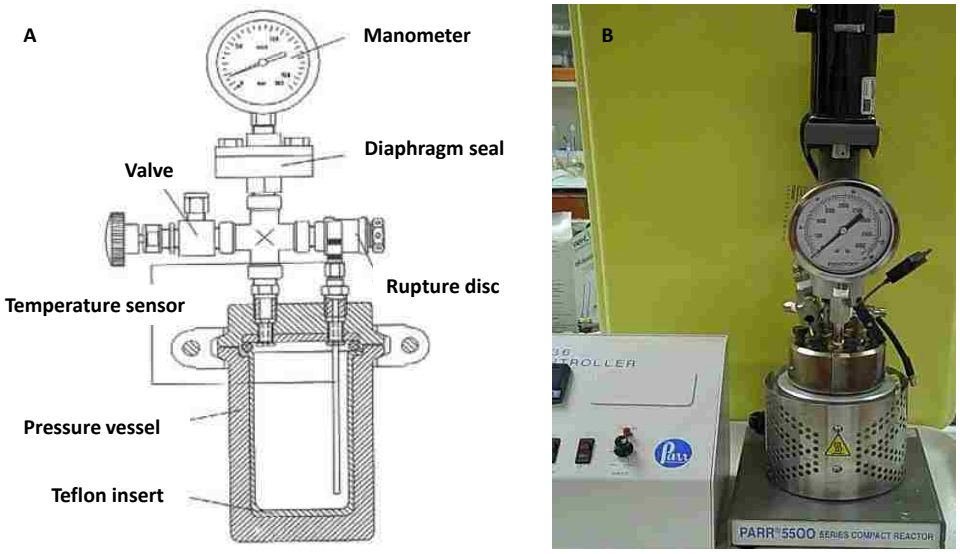

Figure 2.4. A: Schematic of commercially available autoclave parts [116]. B: Picture of the Parr instrument 5500 series compact reactor with temperature controller on the left.

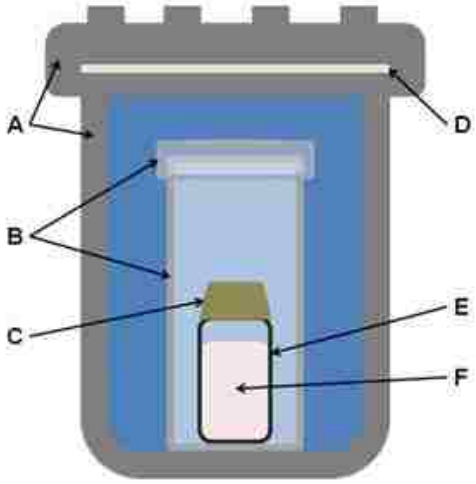

Figure 2.5. A sketch of the internal setup of the autoclave: A, Parr Instruments 5521 series 300mL high pressure autoclave. B, 100 mL fused quartz beaker with cover, C, 10 mL Teflon inverted cup used as a loose cover. D, replaceable Teflon gasket (one use only), E, 20 mL glass scintillation vial, F, solution containing reactants.

(2) A Parr instrument 4749 general purpose bomb autoclave (Figure **2**.**6**). Maximum temperature is around 250 °C and maximum pressure is 120 atm for a volume of 23 mL and an inert Teflon liner. One disadvantage is the atmosphere of the 4749 autoclave is not controlled unless steps are taken to produce a special atmosphere with large error in final pressure of the system. A sketch of the autoclave with internal setup for experiments is shown in Figure **2**.**6**.

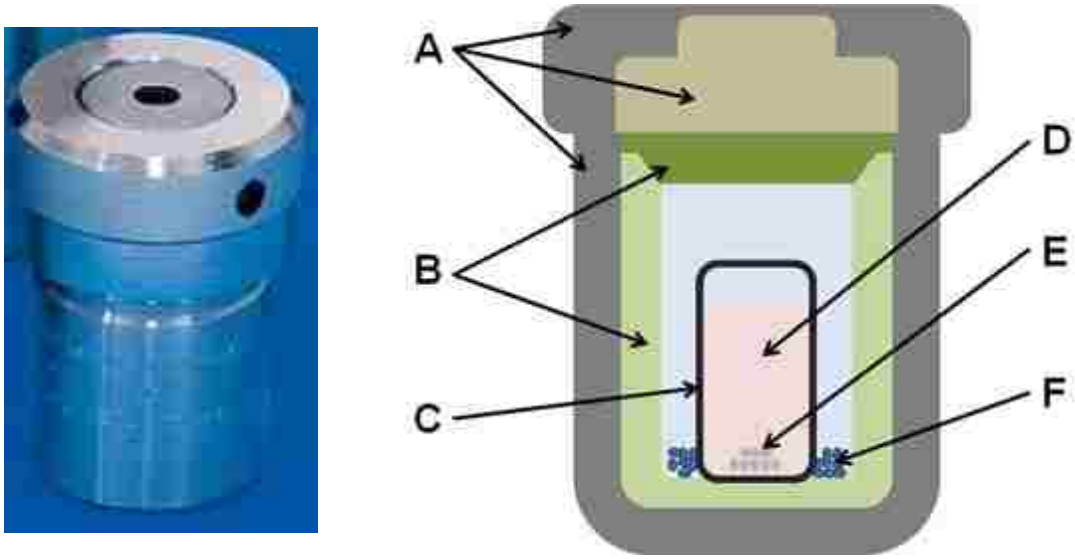

Figure 2.6. Parr Instrument 4749 autoclave. Left picture of the outside, right sketch of the internal setup: (A) stainless steel screw cap, body, pressure plates, and rupture discs, (B) 23 mL Teflon liner, (C) 9 mL glass vial (1.8 cm I.D. x 3.5 cm H), (D) liquid reagents, (E) $KTcO_4$, (F) $NaBH_4$ solid.

The biggest difference between the two autoclave systems, besides volume, is controlling of atmosphere. The Parr 5550 can be monitored during the experiment to verify the internal pressures at any given temperature (internal thermocouple). The 4749 is unable to record or display internal pressure and only an external thermocouple

provides temperature of the system. The two main reasons for using the 4749 autoclave are high throughput, i.e., between 4-6 autoclaves can be used simultaneously compared to only one run in the same time period using the Parr 5500. The second reason, which is most important, is corrosion of the stainless steel body and fittings on the Parr 5500 requires constant cleaning and replacement of parts. The Parr 4749 is a Teflon lined autoclave that can withstand halogenated solvents and mineral acids. Minimal maintenance is required for the 4749 autoclave, just a few inexpensive rupture discs and routine cleaning of the internal cell. Both autoclave systems were influential in the hydro/solvothermal synthesis of the technetium cluster compounds presented in chapters 3-5.

2.2 **Characterization techniques**

2.2.1 ***Single crystal X-ray Diffraction (SC-XRD)***

2.2.1.1 Principle

X-ray diffraction is used to determine crystal structure and atomic spacing. X-ray diffraction is based on constructive interference of monochromatic X-rays and a crystalline sample. [119]

In an X-ray tube, evacuated to low pressure, across the two end electrodes a high voltage is placed and electrons are accelerated and directed against a metal target and pass through a window usually made of beryllium (low atomic number for low absorption) (Figure **2**.**7**). This slows the electrons by multiple collisions producing a

continuum of radiation. [120,121] In most X-ray work, a monochromatic wavelength is needed so X-rays are filtered.

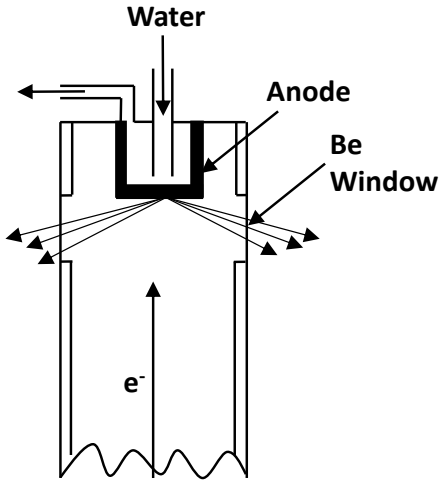

Figure 2.7. Scheme of X-ray tube.

During the experiment, when the X-rays interact with the sample some constructive interferences are produced when conditions satisfy the Bragg's Law showed in Equation 2.1:

$$n\lambda = 2d \sin\theta \qquad \text{Equation 2.1}$$

The Bragg's law shows that the lattice spacing in a crystalline sample is related to the wavelength of the emitted radiation at a specific diffraction angle.

Crystals are characterized by well-defined structures and symmetry of the unit cell forming smooth faces and specific angles between any pair of these faces. Table **2.2** describes the various crystal systems and the Bravais lattice associated.

Table 2.2. Crystal systems and Bravais lattices.

System	Axial lengths and angles	Bravais lattice	Lattice symbol
Cubic	Three equal axes at right angles $a = b = c$, $\alpha = \beta = \gamma = 90°$	Simple Body-centered Face-centered	P I F
Tetragonal	Three axes at right angles, two equal $a = b \neq c$, $\alpha = \beta = \gamma = 90°$	Simple Body-centered	P I
Orthorhombic	Three unequal axes at right angles $a \neq b \neq c$, $\alpha = \beta = \gamma = 90°$	Simple Body-centered Base-centered Face-centered	P I C F
Rhombohedral (or Trigonal)	Three equal axes, equally inclined $a = b = c$, $\alpha = \beta = \gamma \neq 90°$	Simple	R
Hexagonal	Two equal coplanar axes at 120°, third axis at right angles $a = b \neq c$, $\alpha = \beta = 90°$, $\gamma = 120°$	Simple	P
Monoclic	Three unequal axes, one pair not at right angles $a \neq b \neq c$, $\alpha = \gamma = 90° \neq \beta$	Simple Base-centered	P C
Triclinic	Three unequal axes, unequally inclined and none at right angles $a \neq b \neq c$, $\alpha \neq \beta \neq 90°$	Simple	P

Note: the symbol ≠ implies non-equality by reason of symmetry. Accidental equality may occur.

2.2.1.2 Procedure

For single crystal analysis, first a good crystal is selected, usually under an optical microscope, and then fixed with epoxy, glue, or Paratone to the tip of a thin glass fiber or a Kaptan cryoloop. The capillary is mounted on a goniometer to allow positioning and rotation in the instrument (Figure **2**.**8**). The crystal is normally cooled to 100 K by computer controlled Oxford nitrogen cryostream system, to minimize thermal motion and thus enhancing diffraction data resolution.

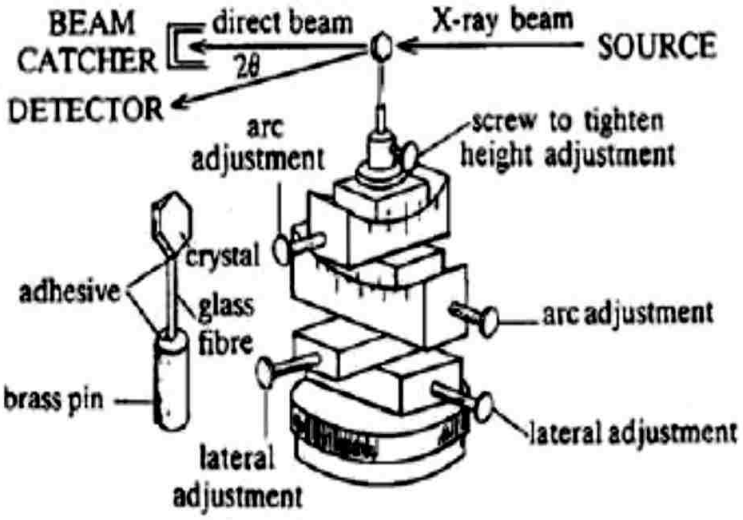

Figure 2.8. Scheme of goniometer and capillary for SC-XRD analysis. [122]

When the crystal is installed inside the instrument, various steps are necessary to prepare data collection since it is an automated procedure.

First the crystal needs to be centered, which means that the diffracted beam from crystal's reflections at its maximum intensity must pass into the center of the detector.

[122] Then a simple cell and matrix are chosen to assign integral indices to all reflections. When the original primitive cell is found, the Bravais lattice is established. Peak-top measurements or a rapid data collection within the chosen range should identify sufficiently intense reflections. Reflections should be chosen so that the precision of the matrix is as similar as possible in all directions.[122]

2.2.1.3 SC-XRD Instrument and Software

Single crystal X-ray diffraction data were collected on a Bruker Apex II CCD diffractometer using Mo-K_α radiation (λ = 0.71073 Å). The Apex II suite was used to perform data processing and an absorption correction performed with SADABS. Solution to the structure was performed by Direct Methods and refinement was carried out using SHELX[123] and OLEX2.[124]

If required anisotropic approximations of all atoms except hydrogen were refined against F^2, whereas the hydrogen atoms positions were determined geometrically and refined using the riding model. All crystal structure visualizations were prepared in Mercury 3.3 software.[125] or Diamond 3.2[126]

In certain cases, such as crystal structure elucidation for $K[Tc_8(\mu\text{-}I)_8I_4]I$, the resulting data showed the crystal was a non-merohedral twin and refinement against both crystal domains was attempted but produced a substantially higher R-value after which refinement against a single merged domain provided a reasonable R-value.

2.2.1.4 Solving Crystal Structures

After data collection, the data are combined computationally with complementary chemical information to produce an electron density map. The calculation of the electron density map from an X-ray diffraction pattern is obtained by a Fourier analysis. Then the atoms are fitted to this map. After refinement and model fitting a crystal structure can be obtained.[122,127]

Solving a crystal structure is often a result of successive approximations knowing that the repeating structure and the diffraction pattern are related to one another by Fourier summations. A structure is generally said to be solved when most of the atoms have been located in the unit cell. The choice of parameters and how they are fitted to the experimental data affects the result of the whole structure analysis. The structural refinement is evaluated from the agreement between the calculated and the measured structure factors. Having a fully refined structure with a set of coordinates and displacement parameters for each atom, it is possible to derive bond lengths, other non-bonded distances, bond angles, torsion angles and hydrogen bonds. The results can be presented as graphics of the final structure, lists of table and they can be archived as CIF Format. A summary of SC-XRD technique is presented in Figure **2.9**.

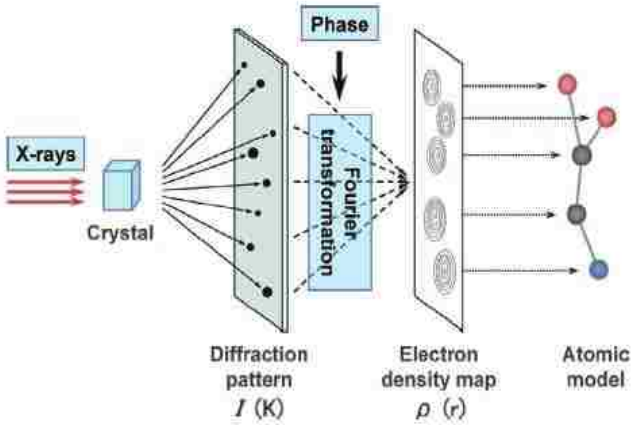

Figure 2.9. Summary of SC-XRD technique. [127]

2.2.1.5 CIF (Crystallographic Information File)

Informal meanings for CIF are used to describe the format, the data output by a control or refinement program, as well as the data file (comprising two or more data blocks) submitted as a manuscript for electronic publication.[122] It is a free-format ASCII archive file for the transmission of the crystallographic data. It is based around the Self-defining Text Archive and Retrieval (STAR) procedure. This final organized data set in unique to the diffracted crystal motif and the CIF file is transferrable to many different software programs and databases for analysis and viewing.

2.2.2 ***Other techniques***

2.2.2.1 Magnetic susceptibility

Magnetic susceptibility is the physical quantity describing material properties in the external magnetic field.[128] It is defined by the ratio between magnetization (M) of the materiel in the magnetic field and the field intensity (H) by the Equation 2.2:

$$M = \chi \cdot H \qquad \text{Equation 2.2}$$

where X is the magnetic moment of the molecule in the direction of the applied field and is unitless, M is measured in units of amperes per meter [$A.m^{-1}$] and H is measured in [$A.m^{-1}$] which is related to the magnetic induction B measured in tesla [T]. Applying a Boltzmann distribution with Avogadro's number, equation 1.2 is transformed into magnetic susceptibility which leads to Curies law's and calculating μ_{eff}, the effective bohr magneton value also referred to as effective magnetic moment.[129]

All materials can be classified by value of magnetic susceptibility into three groups: [130]

- Diamagnetic materials: $-1 < \chi < 0$. Materials create an induced magnetic field in the opposite direction of the externally applied magnetic field.
- Paramagnetic materials: $0 < \chi << 1$. Materials that are attracted by externally applied magnetic field and create an induced magnetic field in the same direction as the externally applied magnetic field.
- Ferromagnetic materials: $\chi >> 1$. Materials that can be magnetized by an external magnetic field and remain magnetized after the field is removed.

Various techniques can be used to determine the magnetic susceptibility of materials. Compounds $Tc_2(O_2CCH_3)_4(\mu\text{-}O_2CCH_3)$ and $Tc_2(O_2CCH_3)_4I$ were analyzed using a Quantum Design PPMS (Physical Property Measurement System) in a DC magnetometer mode at UNLV by Professor Andrew Cornelius and Daniel Antonio. During

measurements, the sample is placed inside a constant persistent field, H, at 0.1 T using the superconducting magnet and a moment, M, is created in the sample. It is then moved quickly through the detection coils and a signal is induced according to Faraday's law and the magnetic susceptibility is measured according to Equation 2.2.

Compound Tc_5I_{13} was analyzed using a Quantum Design MPMS5 SQUID (Magnetic Properties Measurement System – 5 Superconducting Quantum Interference Device) magnetometer, at Northwestern University by Dr. Christos D. Malliakas. A SQUID is an extremely sensitive magnetometer that can measure very small magnetic fields (as low as 5 x 10^{-18} T). Polycrystalline powdered Tc_5I_{13} was loaded in a gelatin capsule. Temperature-dependent data were collected under zero-field-cooled (ZFC) and field-cooled (FC) conditions between 2 and 300 K, with an applied field *H* = 500 Oe. The experimental data were fitted against the modified Curie-Weiss law (Equation 2.3)

$$[\chi = \chi_0 + C/(T-\theta)] \qquad \text{Equation 2.3}$$

where χ is the molar magnetic susceptibility, χ_0 is the temperature independent paramagnetic term, C is the Curie constant, and θ is the Curie temperature. Background (plastic straw and gelatin capsule) was subtracted from the susceptibility data and diamagnetic contribution of the elements was corrected using Pascal's constants.

2.2.2.2 UV-Visible spectroscopy

During ultraviolet-visible (UV-Vis) spectroscopy photons from the ultraviolet (UV), Visible and near infrared (NIR) regions are absorbed by the sample and electronic

transitions are observed.[131,132] Equation 2.4 gives the Beer-Lambert law [133] that can be used to determine quantitative concentrations of an absorbing species in solution [134]:

$$A = - \log_{10} (I / I_0) = \varepsilon \, . \, c \, . \, l \qquad \text{Equation 2.4}$$

where, at a given wavelength, A is the measured absorbance from the species in solution, I_0 is the intensity of the incident light, I is the transmitted intensity measured, l the path length through the sample, c the concentration of the absorbing species, and ε the molar absorptivity or extinction coefficient. The latter is a constant determined for each species at a particular wavelength.

This technique was used to determine speciation of the species present in solution.[131,132] The apparatus used was a Cary 6000i UV-Vis-NIR Spectrophotometer. Analyses were performed at room temperature between 190 and 800 nm. The spectra were baseline corrected using the same solvent as the sample analyzed.

2.2.2.3 Liquid Scintillation Counting

This technique was used to determine the concentration of technetium-99 in solution.[135] For the measurement, around 5 mg of compound was dissolved in 5 mL of concentrated ammonium hydroxide for multiple days and the solution was diluted to 1000 with DI H_2O. Samples for liquid scintillation counting (LSC) contained 10 mL of scintillation cocktail ULTIMA GOLD ABTM (Packard), 100 µL of diluted sample solution and 100 µL of DI H_2O to correspond to calibration curves. The measurements were performed on a Perkin Elmer liquid scintillation counter Tri-Carb 3100TR coupled with

QuantaSmart software. A calibration curve of $KTcO_4$ in water was used to determine the concentration of the solutions and thus the quantity of ^{99}Tc in the solid.

2.2.2.4 Iodide elemental analysis

US-EPA Method 345.1 was used to determine the amount of iodide (2-20 mg/L I^-). The desired compound is dissolved and prepared for titration. Bromine is used to convert iodide into iodate which is then titrated by sodium thiosulfate. A sample of the compound containing iodide is dissolved in 10 mL of ammonium hydroxide with two drop of 30% hydrogen peroxide. The dissolution time may take up to 24 hours to be complete depending of the compound. Using pH electrode, the solution is then adjusted to approximately 7 by dropwise addition of 3.6 M H_2SO_4. To prepare for titration several solutions are added to the dissolved compound: 15 mL of 2.0 M $NaC_2H_3O_2$, 5 mL of 3.5 M $HC_2H_3O_2$, 40 mL 7.8 mM Br_2 in (H_2O). The solution is mixed for 5 minutes and then 2 mL of 7.4 M $NaCHO_2$ is added and mixed into the solution for 2 minutes. Solution is titrated with 0.0375 M $Na_2S_2O_3$ sodium thiosulfate and few drops of indicator, 1% starch in water, until the light yellow solution becomes colorless.[136]

2.2.2.5 Infrared spectroscopy

IR spectroscopy is usually used to obtain information about the structure of a compound. Molecular structure of sample can be determined by analyzing in the IR spectrum the position, shape and intensity of the peaks.[132] This technique, performed on a Varian 3100 FTIR Excalibur Series equipped with a diamond attenuated total

reflection (ATR) apparatus, was principally used to detect the presence of carbonyl functional groups through characteristic C-O and C=O stretching modes. The samples were analyzed using attenuated total reflectance attachment.

This technique enables to analyze directly the powder onto the diamond ATR and thus no further sample preparation is needed.

2.2.2.6 Energy Dispersive X-ray spectroscopy

In order to determine the elemental composition of the sample, energy dispersive X-ray spectroscopy (EDS) can be used. This technique uses a focused beam of electrons to interact with the sample. At this point, core electrons in the sample are ejected, and during the filling of this hole with an outer shell electron, characteristic X-rays are emitted. The analysis of energies and intensities of these signature X-rays permits one to identify and quantify the elements present in the sample.[137,138] The EDS measurements were accomplished using two different instruments and techniques. The first method was through transmission electron microscopy (TECNAI-G2-F30 Super-twin) with a 300 keV field emission gun. The EDS spectrum was collected under STEM (scanning transmission electron microscopy) mode [139]. The technetium samples were prepared by the solution-drop method [140] on carbon film supported on a copper grid. The second method used was through Scanning Electron Microscopy (SEM JEOL JSM-5610). The technetium samples were spread onto carbon tape, coated with carbon and analyzed by EDS mapping.

2.2.2.7 X-ray Absorption Fine Structure spectroscopy

During X-ray Absorption Fine Structure (XAFS) spectroscopy experiments, incident X-ray photons from a source, such as a synchrotron, equal to the binding energy of the core-level electron of element probed are absorbed promoting electron out of the core creating a photo-electron in continuum space.[141,142] These photo-electrons act as very sensitive probes that see charge distribution and the arrangement of surrounding "neighboring" atoms. This occurs when an ejected photoelectron wave interacts with a backscattered wave from neighboring atom electrons causing an interference or modulated pattern on the central atom. The interferences happen on different scales within the absorption spectra leading to specific information about the central atom as well as its close neighbors. The X-ray absorption spectrum is divided into two regions, shown in Figure **2.10**: X-ray absorption near-edge spectroscopy (XANES) and extended X-ray absorption fine structure spectroscopy (EXAFS). The XANES section of the spectrum is sensitive to formal oxidation state and coordination chemistry of the absorbing atom. The XANES absorption is classified by all scattering pathways of the photo-electron wave, meaning multiple interactions with neighboring atoms. The EXAFS section allows for determination of distances, coordination number, and neighboring elements of the absorbing atom. Although multiple scattering can be considered for EXAFS, traditionally EXAFS is classified as a single scattering photo-electron with by a single neighboring atom, which allows for bond lengths between the central and neighboring atoms to be determined.[141,143]

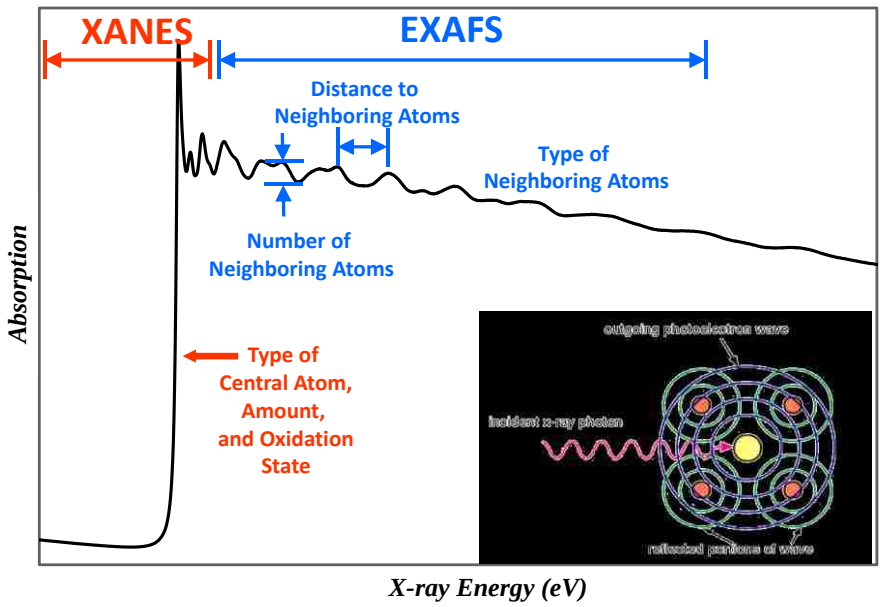

Figure 2.10 Principles of XAFS of X-ray absorption spectroscopy.

Measurements at the Tc K-edge were performed at the Advanced Photon Source (APS) at the BESSRC-CAT 12 BM station at Argonne National Laboratory. Solids were diluted by mass to about 1% technetium with boron nitride and placed in an aluminum sample holder of local design (Figure **2.11** A). The 100 µL solutions were injected in a special aluminum liquid sample holder (Figure **2.11** B).

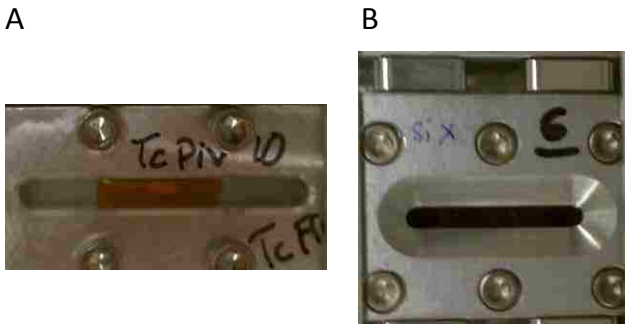

Figure 2.11. A: solid sample holder and B: liquid sample holder for XAFs experiment at APS.

During XAFS experiment, a double crystal of Si[111] was used as a monochromator and the spectra were recorded at the Tc K-edge (i.e., 21,044 eV). The energy was calibrated using a molybdenum foil (K-edge = 20,000 eV). The XAFS spectra were recorded in transmission mode and in fluorescence mode at room temperature using a 13 element germanium detector. To analyze the data, the raw data are background subtracted and normalized using ATHENA software [144]. Using known crystallographic structures input files were generated by Atoms [145] and the amplitude and phase shift function were calculated using FEFF 8.2 [146]. These theoretical data were then used for the fitting procedure comparing the theory with the experimental data through *k*-weight and Fourier transform into *R*-space using WINXAS [147].

Chapter 3: Molecular Metal-Metal Bonded Technetium Compounds

3.1 Introduction

In this chapter, reliable, high yield syntheses of $Tc_2(O_2CCH_3)_4Cl_2$ and $Tc_2(O_2CCH_3)_4Br_2$ are described as well as their characterization by single crystal x-ray diffraction. $Tc_2(O_2CCH_3)_4Cl_2$ was first reported in the Russian literature in 1980, followed by the synthesis of $Tc_2(O_2CCH_3)_4Br_2$ in 1992.[47,148] Subsequently, some sketchy details on the preparation of the chloride using hydrothermal techniques were provided in a 1981 Russian patent.[149] A handful of additional publications dealing with $Tc_2(O_2CCH_3)_4Cl_2$ and its bromide analog have appeared since the patent and alternative methods for its preparation have been described. Preetz and coworkers [150] modeled their synthesis of $Tc_2(O_2CCH_3)_4Cl_2$ after that used by Cotton, et al., to prepare $Re_2(O_2CCH_3)_4Cl_2$ (Equation 3.1).[151] This reaction provides $Tc_2(O_2CCH_3)_4Cl_2$ in about 40% yield, but requires the prior preparation of $[n\text{-}Bu_4N]_2[Tc_2Cl_8]$. Interestingly, the substitution reaction from $[n\text{-}Bu_4N]_2[Tc_2Br_8]$ with acetic acid and anhydride yields about 79%, $Tc_2(O_2CCH_3)_4Br_2$ this may be due to more labile bromine atom. [148,152]

$$[Re_2Cl_8]^{2-} \xrightarrow{\text{excess } CH_3COOH} Re_2(O_2CCH_3)_4Cl_2 + 4\ HCl + 2\ Cl^- \qquad \text{Equation 3.1}$$

The compound $[n\text{-}Bu_4N]_2[Tc_2Cl_8]$ is accessible in comparable yield (40-50%) from ammonium pertechnetate, but the synthesis involves 4 steps and takes a minimum of 2 days. Given the fact that both reactions are performed on a small scale, an overall yield

of $Tc_2(O_2CCH_3)_4Cl_2$ and $Tc_2(O_2CCH_3)_4Br_2$ on the order of 20% is far from satisfactory. Two other technetium(III) tetracarboxylate complexes are known, but both were isolated in low yield. The tetrapivalate, $Tc_2(O_2CCMe_3)_4Cl_2$, was prepared from the reaction of $(NH_4)_3Tc_2Cl_8$ with molten pivalic acid,[52] and $[Tc_2(O_2CCH_3)_4](TcO_4)_2$ was isolated from the aerial oxidation of solutions containing $[Tc_2(O_2CCH_3)_4Cl_2]^{1-}$.[153]

Until recently the single crystal structure of $Tc_2(O_2CCH_3)_4Cl_2$, and $Tc_2(O_2CCH_3)_4Br_2$, were unknown, and the complexes were characterized by EXAFS, IR and Raman spectroscopy.[48,148-150,152] Single crystal solid state elucidation is important for helping to understand the metal-metal bonded chemistry of technetium.

3.2 **Experimental**

3.2.1 ***Preparation of $Tc_2(O_2CCH_3)_4Cl_2$***

The synthesis of tetraacetatodichloroditechnetate(III), $Tc_2(O_2CCH_3)_4Cl_2$, was a local and improved (see below) modification of the procedure first reported by Rezvov, et al.[149] To a 20 mL glass scintillation vial was added $KTcO_4$ (55.0 mg, 0.27 mmol) and an 18 mL mixture of glacial acetic acid and concentrated hydrochloric acid (2:1 by volume). The vial was loosely capped with an inverted 10 mL Teflon cup and placed inside of a 100 mL fused quartz beaker with cover. This dual containment, depicted in Figure 2.6, allows for gases to permeate the reaction mixture and minimizes the spread of technetium to the autoclave. The apparatus is sealed in a 300 mL Parr Instruments 5521 series high pressure autoclave, Figure 2.5. The autoclave was purged two times with 5 atm of H_2, filled to a starting pressure of 35 atm H_2, and then heated to 210 °C at 5

°C/min. After 14 hours, the heater was switched off and the autoclave was allowed to cool slowly to room temperature. At that point, the autoclave was carefully depressurized and opened to reveal a deep red-orange mother-liquor covering a crop of dark red elongated hexagonal crystals, shown in Figure **3**.**1**. The air-stable product was rinsed with acetic acid, followed by isopropyl alcohol, and diethyl-ether, and allowed to dry in air. The reaction produced 48.1 mg (0.095 mmol) of $Tc_2(O_2CCH_3)_4Cl_2$ for a yield of 70%, a significant improvement over the 51% yield reported in the patent.[149] The compound is insoluble in common organic solvents (e.g., acetone, acetonitrile, tetrahydrofuran, and methylene chloride) and aqueous acids including hydrochloric, sulfuric, and acetic, but hydrolyze under alkaline conditions consistent with the observations of Zaitseva, et al.[47] An ATR-FTIR spectrum, Figure **3**.**2**, of $Tc_2(O_2CCH_3)_4Cl_2$ reveals COO stretches at 1441 cm^{-1} (vs) and 1375 *(*vs) cm^{-1}, characteristic of bridging acetate groups and similar in energy to the analogous vibrations in $Re_2(O_2CCH_3)_4Cl_2$, *viz.*, at 1456 and 1385 cm^{-1}, as reported by Taha and Wilkinson.[42]

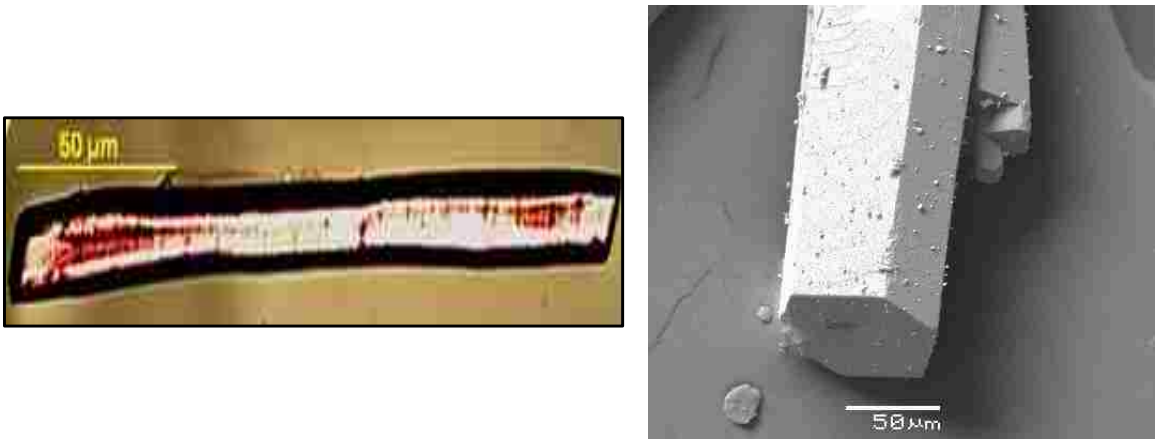

Figure 3.1. Leica optical microscope images of $Tc_2(O_2CCH_3)_4Cl_2$ on the right and SEM image magnification x350 in back scattering mode on the left.

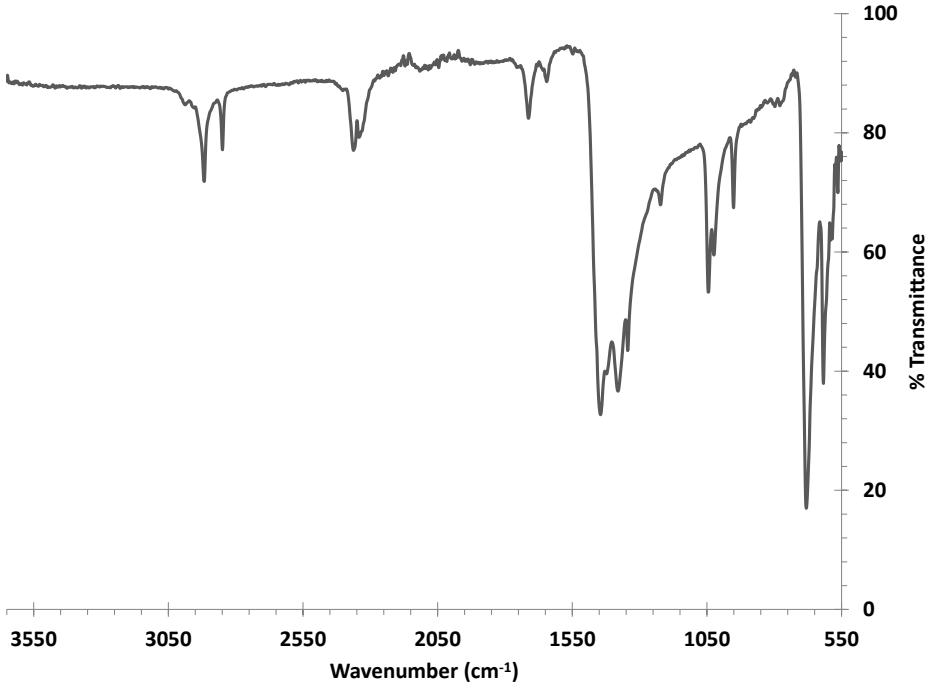

Figure 3.2. ATR-FTIR spectrum of $Tc_2(O_2CCH_3)_4Cl_2$.

3.2.2 ***Preparation of $Tc_2(O_2CCH_3)_4Br_2$***

The synthesis of tetraacetatodibromoditechnetate(III), $Tc_2(O_2CCH_3)_4Br_2$, was performed by a modification of the experimental setup described in Section 3.2.1. To the glass vial was added 52.0 mg (0.257 mmol) $KTcO_4$, and a starting solution with an altered composition of 18 mL of glacial acetic acid to hydrobromic acid (20:1 by volume) ratio. Larger amounts of HBr in acetic acid (2:1 or 5:1 by volume) lead to a final product of $K_2TcBr_{6(s)}$. By reducing the molar ratio of bromide ion in solution it is believed that $TcBr_6^{2-}$ ion was not completely formed in high enough concentration to precipitate out before reduction of Tc(+7) to low valent oxidation state, e.g., Tc(+3), Tc(+4). The thought process of systematically changing concentration of hydrobromic acid was derived from the work of Resvov, et al., in the synthesis of dichloro species.[149]

All other conditions were followed as described in Section 3.2.1. The reaction produced clusters of dark red-orange short hexagonal crystals shown in Figure **3.3**. In the final synthesis, 49.6 mg (0.084 mmol) of $Tc_2(O_2CCH_3)_4Br_2$ was isolated in a yield of 65%. The compound is insoluble in common organic solvents (e.g., acetone, acetonitrile, tetrahydrofuran, and methylene chloride) and aqueous acids including hydrochloric, sulfuric, and acetic, but hydrolyzes under alkaline conditions, identical to $Tc_2(O_2CCH_3)_4Cl_2$. An FTIR spectrum, Figure **3.4** , of $Tc_2(O_2CCH_3)_4Br_2$ reveals COO stretches at 1440 cm^{-1} (vs) and 1389 *(*vs) cm^{-1}, 1355 cm^{-1} characteristic of bridging acetate groups and similar in energy to the analogous vibrations in $Re_2(O_2CCH_3)_4Br_2$, *viz.*, at 1451 and 1382 cm^{-1}.[148]

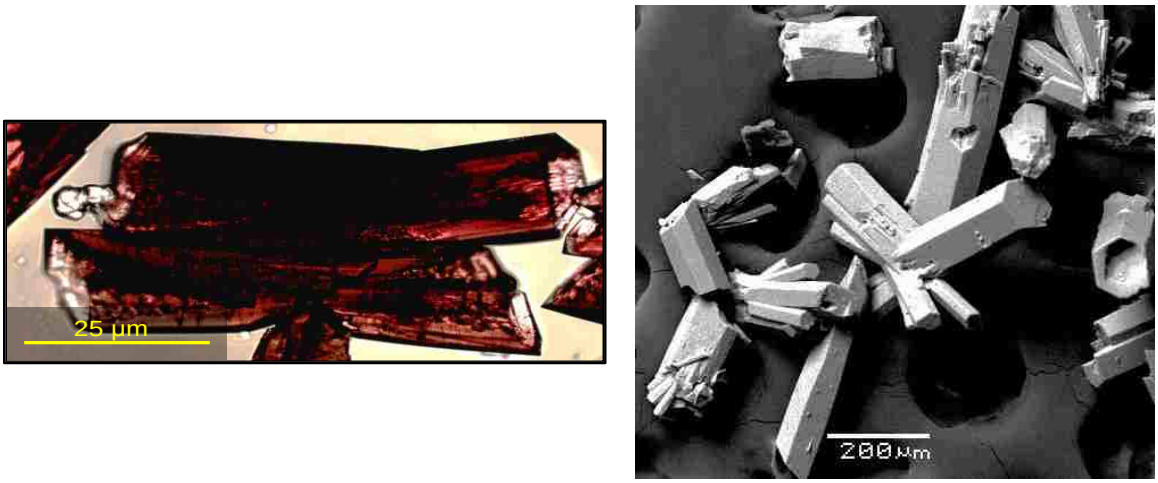

Figure 3.3. Leica optical microscope images of $Tc_2(O_2CCH_3)_4Br_2$ on the right and SEM image magnification x90 in back scattering mode on the left.

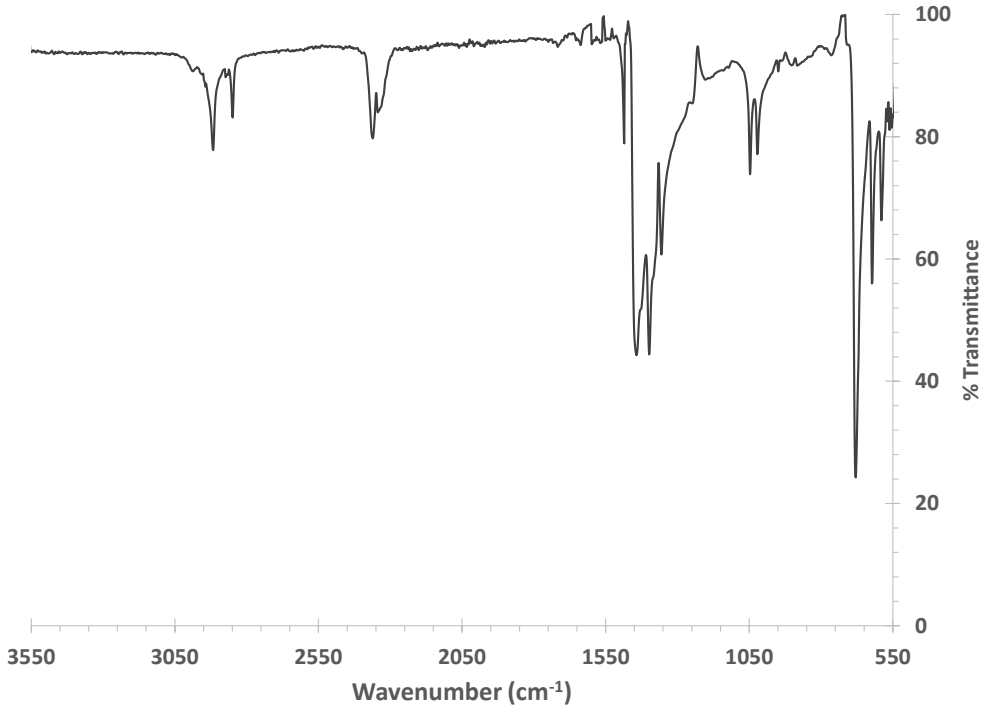

Figure 3.4. ATR-FTIR spectrum of $Tc_2(O_2CCH_3)_4Br_2$.

3.2.3 ***Preparation of $Tc_2(O_2CCH_3)_3Cl_2(H_2O)_2 \cdot H_2O$***

The synthesis of triacetatodiaquadichloroditechnetate(III) monohydrate, $Tc_2(O_2CCH_3)_3Cl_2(H_2O)_2 \cdot H_2O$, was performed by the experimental setup described above in Section 3.2.1 and is a byproduct of the reaction. At post procedure, the mother liquor presented no crystals of $Tc_2(O_2CCH_3)_4Cl_2$ and the solution was capped (exposed to normal atmosphere) and set aside for two days. After the two days, visual inspection of the vial revealed crystals growing on the glass shown in Figure **3**.**5**. Upon decanting of the mother liquor, dark red elongated hexagonal crystals of $Tc_2(O_2CCH_3)_4Cl_2$ and rectangular turquoise crystals of $Tc_2(O_2CCH_3)_3Cl_2(H_2O)_2 \cdot H_2O$ were isolated and are shown in Figure **3**.**6**. The single crystal structure data obtained by XRD encouraged dissolving the small amount of crystals into acetonitrile for the UV-vis absorption, shown in Figure **3**.**7**, indicating a broad band at 1000 nm. Liquid scintillation counting on the acetonitrile solution determine the amount of technetium in solution was 2.86 µM or 1.4 mg of $Tc_2(O_2CCH_3)_3Cl_2(H_2O)_2 \cdot H_2O$.

Figure 3.5. Mother liquor solution removed from original vial after two days, revealing crystals of $Tc_2(O_2CCH_3)_3Cl_2(H_2O)_2 \cdot H_2O$ seen on the bottom and sides of the empty vial. The clear liquid in the bottom of the vial on the right is paratone oil used to obtain single crystals for XRD.

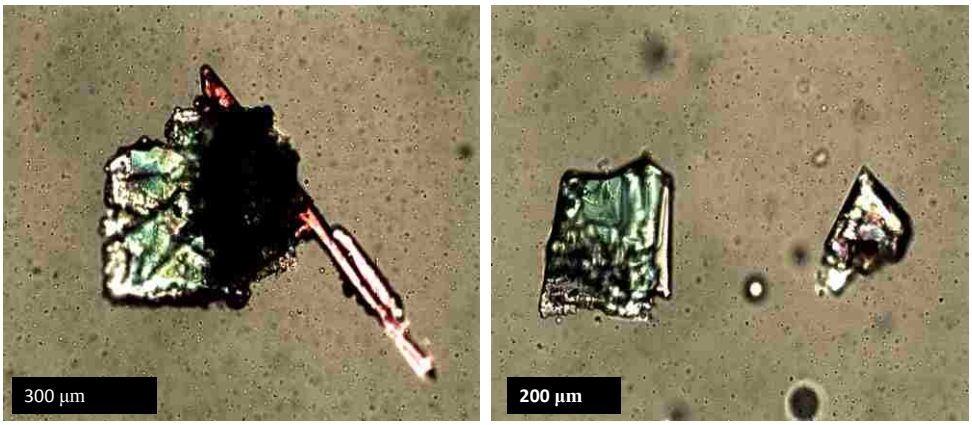

Figure 3.6. Leica optical microscope images of $Tc_2(O_2CCH_3)_3Cl_2(H_2O)_2{\cdot}H_2O$ (turquoise, rectangular)growing alongside $Tc_2(O_2CCH_3)_4Cl_2$ (red, elongated needle) on the right and $Tc_2(O_2CCH_3)_3Cl_2(H_2O)_2{\cdot}H_2O$ isolated on the left.

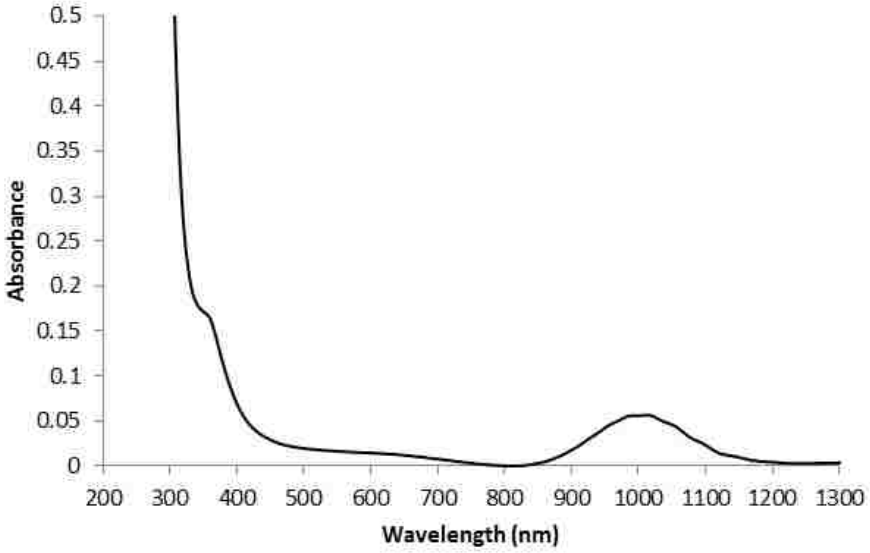

Figure 3.7. UV-Visible spectrum of $Tc_2(O_2CCH_3)_3Cl_2(H_2O)_2{\cdot}H_2O$ in acetonitrile.

3.2.4 ***Single Crystal X-ray Diffraction***

A long dark red hexagonal crystal of $Tc_2(O_2CCH_3)_4Cl_2$, Figure **3.1**, dark red-orange hexagonal cone cluster crystal of $Tc_2(O_2CCH_3)_4Br_2$, Figure **3.3**, and irregular rectangular

turquoise crustal of $Tc_2(O_2CCH_3)_3Cl_2(H_2O)_2 \cdot H_2O$, Figure **3.6** were mounted under Paratone on a Kaptan cryoloop for data collection. Single crystal X-ray diffraction data were collected on a Bruker Apex II CCD diffractometer using Mo-K_α radiation (λ = 0.71073 Å). The crystal was maintained at 100 K during data collection using an Oxford nitrogen cryostream system. The Apex II suite was used to perform data processing and an absorption correction performed with SADABS. Solution to the structure was performed by Direct Methods and refinement was carried out using SHELX-97.[123] Anisotropic approximations of all atoms except hydrogen were refined against F^2, whereas the hydrogen atoms positions were determined geometrically and refined using the riding model.

3.3 **Results and Discussion**

Interest in exploring hydrothermal methods was spurred by the need for a higher yield route to $Tc_2(O_2CCH_3)_4Cl_2$ (see Chapter 1). The Russian literature suggested that $Tc_2(O_2CCH_3)_4Cl_2$ was accessible from potassium pertechnetate, $KTcO_4$, in what could be described euphemistically as a "one-pot reaction." Treatment of a solution of $KTcO_4$ in a 20:1 mixture of acetic acid and concentrated aqueous hydrochloric acid with excess hydrogen for 14 hr at 210 °C provides $Tc_2(O_2CCH_3)_4Cl_2$ in 70% yield in the form of dark red crystals that can be recovered by filtration of the mother liquor (Equation 3.2). The details of how $Tc_2(O_2CCH_3)_4Cl_2$ is generated during the course of this procedure are not known, but it would appear from other papers in the technetium literature that reduction of the metal below the +4 oxidation state invariably leads to coupling of metal

centers and the formation of dinuclear or polynuclear clusters.[16] This process is likely encouraged by the presence of bridging acetate ligands. Once formed, $Tc_2(O_2CCH_3)_4Cl_2$ is insoluble in common organic solvents and the mother liquor from whence it was isolated.

$$2\ KTcO_4 + 4\ HCl + 4\ CH_3CO_2H + 4\ H_2 \rightarrow Tc_2(O_2CCH_3)_4Cl_2 + 2\ KCl + 8\ H_2O$$ Equation 3.2

The compound $Tc_2(O_2CCH_3)_4Cl_2$ crystallizes in the monoclinic space group $P2_1/n$ with a = 6.4258 (8) Å, b = 8.8474(11) Å, c = 12.5285(16) Å, and β = 90.778(2)°, broadly consistent with the isostructural Re analog.[154] Crystallographic data and refinement parameters are summarized in Table **3.1**, with full information and cif in Appendix B. The molecular structure of the $Tc_2(O_2CCH_3)_4Cl_2$ is shown in Figure **3.8** and Figure **3.9**. In Figure **3.8**, a normal view of the molecular structure shows the expected ditechnetium paddle wheel motif, capped with axial chlorines. Figure **3.9** shows a unit cell along the *a*- and *b*-axes. Selected bond lengths are summarized in Table **3.2** and Table **3.3**. The refined Tc-Tc quadruple bond length (2.1758(3) Å) is essentially identical to the published extended x-ray absorption fine structure (EXAFS) value (Tc-Tc = 2.18(2) Å),[152] and is slightly shorter than that estimated (2.19 Å) from an analysis of the Raman spectrum.[148] It is also marginally shorter than the Tc-Tc separation reported (2.192 (2) Å) for the related pivalate derivative.[52]

Table 3.1. Crystallographic data and refinement parameters for $Tc_2(O_2CCH_3)_4X_2$ [X = Cl, Br] and $Tc_2(O_2CCH_3)_3Cl_2(H_2O)_2 \cdot H_2O$, 1-3 respectively.

Crystallographic data	1	2	3
Empirical Formula	$C_8H_{12}Cl_2O_8Tc_2$	$C_8H_{12}Br_2O_8Tc_2$	$C_6H_{15}Cl_2O_9Tc_2$
Formula weight	504.90	593.80	499.90
Temperature (K)	100	100	100
Wavelength (Å)	0.71073	0.71073	0.71073
Crystal system	Monoclinic	Monoclinic	Monoclinic
Space group	$P2_1/n$	$P2_1/n$	$P2_1$
a (Å)	6.4258(8)	6.5299(7)	7.7102(7)
b (Å)	8.8474(11)	9.0483(9)	11.4786(11)
c (Å)	12.5285(16)	12.5915(13)	8.3468(8)
α (°)	90.00	90.00	90.00
β (°)	90.778(2)	90.718	94.8430(10)
γ (°)	90.00	90.00	90.00
V ($Å^3$)	712.20(15)	743.90	736.07(12)
Z	2	2	2
Density calculated (Mg m^{-3})	2.346	2.643	2.256
Absorption coefficient (mm^{-1})	2.346	7.259	2.273
F(000)	488	560	486
Range of 2θ (°)	2.82 – 30.51	2.77 – 30.51	2.45 – 31.50
Index ranges (*h, k, l*)	$-9 \le h \le 9$, $-12 \le k \le 12$, $-17 \le l \le 17$	$-9 \le h \le 9$, $-12 \le k \le 12$, $-17 \le l \le 17$	$-11 \le h \le 11$, $-16 \le k \le 16$, $-12 \le l \le 12$
Reflections collected	11170	11863	12743
Independent reflections	2169 [$R_{(int)}$ = 0.0277]	2265 [$R_{(int)}$ = 0.0280]	4868 [$R_{(int)}$ = 0.0203]
Complete to 2θ (%)	100.0	100.0	100.0
Refinement method	Full-matrix least-sq on F^2	Full-matrix least-sq on F^2	Full-matrix least-sq on F^2
Data/restraints/parameters	2169 / 0 / 93	2265 / 0 / 93	4868 / 4 / 194
Goodness-of-fit on F^2	1.076	1.046	1.027
Final R indices [$I > 2\sigma(I)$]	R1 = 0.0180, wR2 = 0.0467	R1 = 0.0184, wR2 = 0.0400	R1 = 0.0152, wR2 = 0.0363
R indices (all data)	R1 = 0.0204, wR2 = 0.0476	R1 = 0.0219, wR2 = 0.0409	R1 = 0.0157, wR2 = 0.0365

The paddlewheel unit is quite regular with the exception of the capping chlorides, which are bent roughly 8° from linear (Tc(1a)-Tc(1)-Cl(1) = 171.903(13)°). A smaller distortion (~3.5°) is observed in the corresponding dirhenium analog,[154] and no distortion is observed for the pivalate complex,[52] which crystallizes in a tetragonal space group. We suspect that crystal packing is responsible for these small distortions. The packing for $Tc_2(O_2CCH_3)_4Cl_2$ is illustrated in Figure **3.9**. The distorted Tc-Tc-Cl angle may impact Tc-Cl distance. We find the latter to be 2.5078(4) Å, or considerably longer than the estimates of 2.43(1) Å from EXAFS [152] and 2.41 Å from the Raman data [148]. In the EXAFS analysis, the number of Cl atoms attached to Tc was fixed at one, and the Tc-Cl distance and the Debye-Waller factor (DWF) for the Tc-Cl scattering were refined.[152] The DWF fit, i.e., 0.012 $Å^2$, is significantly higher than the ones reported in other Tc chloride complexes, which are typically on the order of 0.003 $Å^2$. The value of the residual (difference between the experimental spectra and the fit) is also high (17%) and suggests that the fit may not be optimal. Further analysis of the EXAFS spectra of $Tc_2(O_2CCH_3)_4Cl_2$ by fixing the DWF to those determined in reference samples such as $(n\text{-}Bu_4N)_2Tc_2Cl_8$ and refining the distance and the number of Cl atoms will be necessary to ascertain if the Tc-Cl distance found by EXAFS spectroscopy converges on the SC-XRD value. Table **3.2** summarizes important bond distances/angles determined by the various methods.

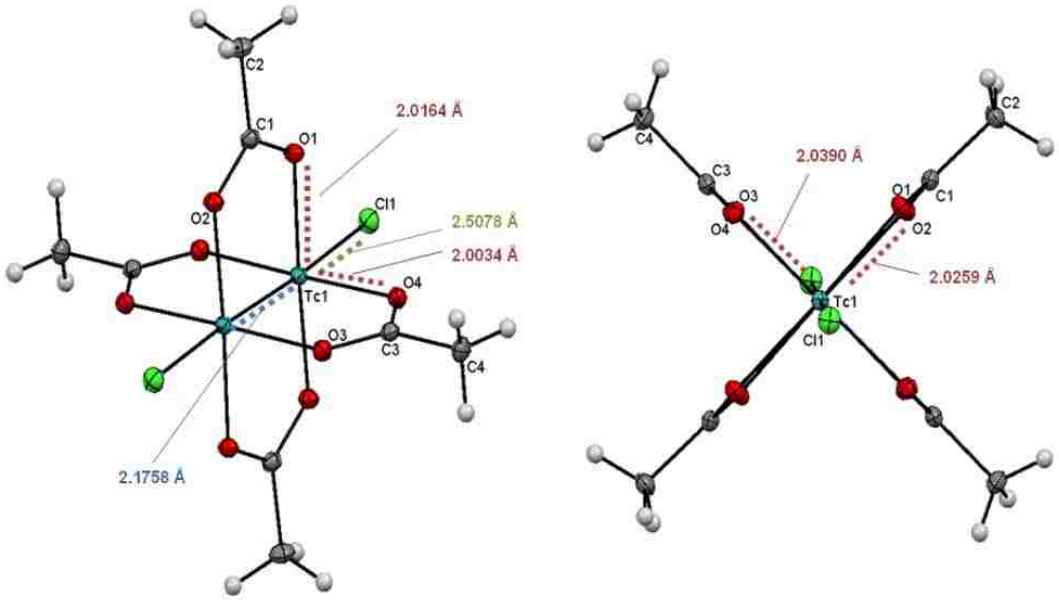

Figure 3.8. X-ray crystal structure of $Tc_2(O_2CCH_3)_4Cl_2$. The ORTEP representations display ellipsoids at the 50% probability level with key bond lengths shown.

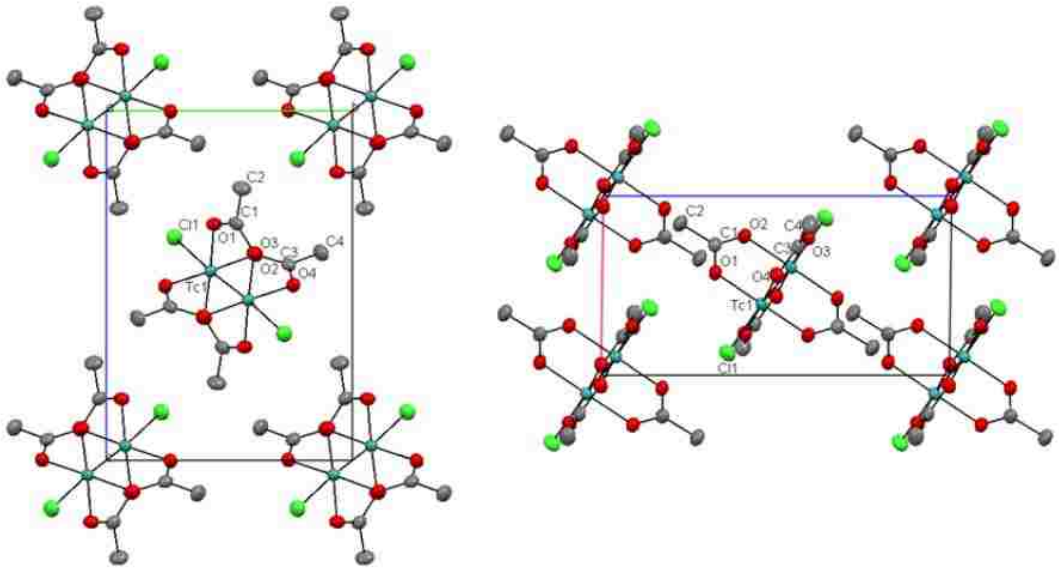

Figure 3.9. Unit cell views of $Tc_2(O_2CCH_3)_4Cl_2$ along the a-axis (left image) and b-axis (right image). Hydrogen atoms are omitted for clarity.

Table 3.2. Selected interatomic distances [Å] and angles [°] for $Tc_2(O_2CCH_3)_4X_2$ [X = Cl, Br], $Tc_2(O_2CC(CH_3)_3)_4Cl_2$, and $Re_2(O_2CCH_3)_4X_2$ [X = Cl, Br].

Compound [ref.]	*d* M-M	*d* M-X	*d* M-O (av.)	M-M-X	M-M-O (av.)
$Tc_2(O_2CCH_3)_4Cl_2$ [152]	2.18(1)	2.43(1)	2.03(1)	-	-
[148]	2.192	2.41	2.03	-	-
[this work,48]	2.1758(3)	2.5078(4)	2.0211(12)	171.903(13)	90.63(4)
$Tc_2(O_2CCH_3)_4Br_2$[152]	2.19(1)	2.63(1)	2.03(2)	-	-
[148]	2.192	2.600	2.032	-	-
[this work]	2.1764(3)	2.6554(3)	2.0223(12)	173.563(12)	90.82(4)
$Tc_2(O_2CC(CH_3)_3)_4Cl_2$ [52]	2.192(2)	2.408(4)	2.032(4)	180.00	90.67(11)
$Re_2(O_2CCH_3)_4Cl_2$ [154]	2.224(4)	2.5213(4)	2.0181(14)	176.519(5)	90.074(5)
$Re_2(O_2CCH_3)_4Br_2$ [148]	2.224	2.022	2.603	-	-

Table 3.3. Selected bond lengths and angles for $Tc_2(O_2CCH_3)_4Cl_2$.

Bond length [Å]			Bond Angle [°]
Tc(1)-O(1)	2.0164(12)	O(1)-Tc(1)-O(3)	89.59(5)
Tc(1)-O(2)	2.0259(12)	O(1)-Tc(1)-O(2a)	177.47(5)
Tc(1)-O(3)	2.0390(12)	O(1)-Tc(1)-O(4a)	89.63(5)
Tc(1)-O(4)	2.0034(12)	O(1)-Tc(1)-Tc(1a)	91.22(4)
Tc(1)-Tc(1a)	2.1758(3)	Tc(1a)-Tc(1)-Cl(1)	171.903(13)
Tc(1)-Cl(1)	2.5078(4)	O(1)-Tc(1)-Cl(1)	91.12(4)
O - C(avg.)	1.280(2)	C(3)-O(3)-Tc(1)	120.94(11)
C - C(avg.)	1.484(2)	O(2)-C(1)-C(2)	120.23(15)

Inevitably, interest quickly shifted to the synthesis of the bromo analogue. At first several experiments resulted in crystals of $K_2TcBr_{6(s)}$ and it was puzzling that a direct molar ratio of 2:1 acetic acid to hydrobromic acid did not afford $Tc_2(O_2CCH_3)_4Br_2$ as it did for the chloro species. A review of the original Russian patent on $Tc_2(O_2CCH_3)_4Cl_2$, revealed that changing the molar amount of chloride in the system influenced the synthesis and yield of the compound. Steps were then taken to systematically increase the molar ratio of acetic acid:HBr in the system to synthesize $Tc_2(O_2CCH_3)_4Br_2$. Only one ratio provided crystals of $Tc_2(O_2CCH_3)_4Br_2$ which is not to say that the compound did not exist in solution for other molar ratios. The compound could not be characterized by UV-

Vis spectroscopy because the mother-liquor solution saturated the detector and dilution revealed no further information.

The optimal condition for the preparation of $Tc_2(O_2CCH_3)_4Br_2$ involves the treatment of a solution of $KTcO_4$ with a 20:1 mixture of acetic acid and concentrated aqueous hydrobromic acid with excess hydrogen for 14 hr at 210 °C. This provides $Tc_2(O_2CCH_3)_4Br_2$ in 65% yield in the form of beautiful dark red-orange crystals that can be recovered by filtration of the mother liquor (Equation 3.3). As with $Tc_2(O_2CCH_3)_4Cl_2$ details of how $Tc_2(O_2CCH_3)_4Br_2$ is generated during the course of this procedure are not known or obvious.

$$2\ KTcO_4 + 4\ HBr + 4\ CH_3CO_2H + 4\ H_2 \rightarrow Tc_2(O_2CCH_3)_4Br_2 + 2\ KBr + 8\ H_2O$$ Equation 3.3

The complex $Tc_2(O_2CCH_3)_4Br_2$ crystallizes in the monoclinic space group $P2_1/n$ with a = 6.5299 (7) Å, b = 9.0483(9) Å, c = 12.5915(13) Å, and β = 90.718(2)°, a slight elongation of the unit cell along a- and b-axis and broadly consistent with the isostructural Re-Cl analog.[154] Crystallographic data and refinement parameters are summarized in Table **3.1**, with full information and cif in Appendix B. The molecular structure of the $Tc_2(O_2CCH_3)_4Br_2$ is shown in Figure **3.10** and Figure **3.11**. In Figure **3.10**, a normal view of the molecular structure shows the expected ditechnetium paddle wheel motif, capped with axial bromines. Figure **3.11** shows a unit cell along the a- and b-axes. Selected bond lengths are summarized in Table **3.2** and Table **3.4**. The refined Tc-Tc separation

(2.1764(3) Å)[48] is consistent with the presence of a quadruple bond. The Tc-Tc separation found by SC-XRD essentially identical to the published extended x-ray absorption fine structure (EXAFS) value (Tc-Tc = 2.19(2) Å),[152] and is slightly shorter than that estimated (2.192 Å) from Raman spectroscopy.[148] It is also marginally shorter than the Tc-Tc separation reported (2.192(2) Å) for the related pivalate derivative.[52] The Tc-Tc bond lengths of the chloro (2.1758(3) Å) and the bromo (2.1764(3) Å) are essentially identical and indicate that the nature of the coordinating halogen ligand has minor effect on the $[Tc_2(O_2CCH_3)_4]^{2+}$ unit.

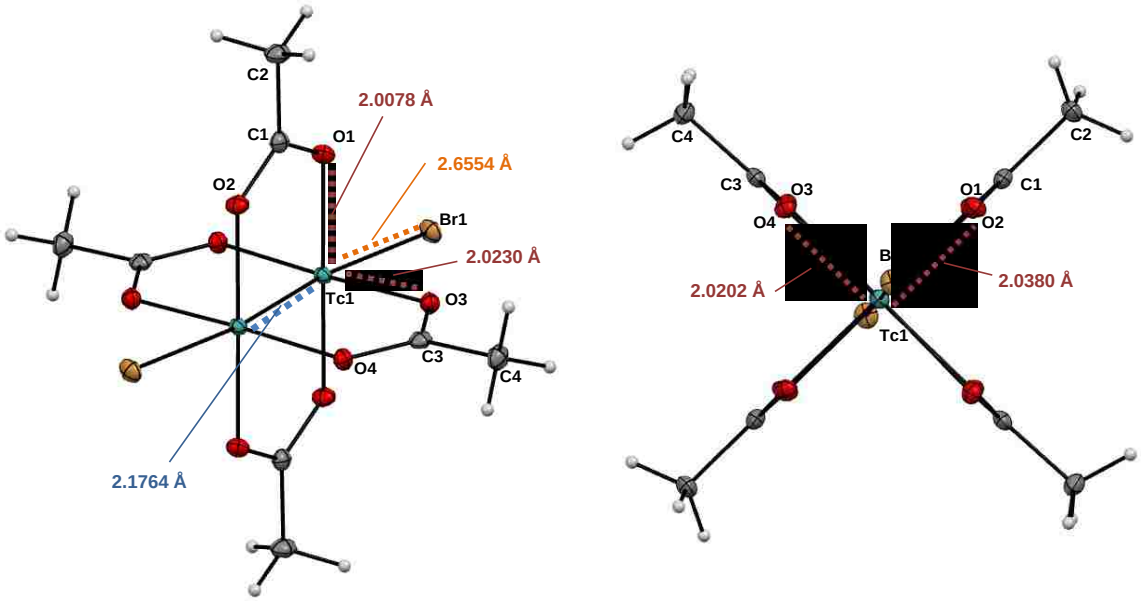

Figure 3.10. X-ray crystal structure of $Tc_2(O_2CCH_3)_4Br_2$. The ORTEP representations display ellipsoids at the 50% probability level with key bond lengths shown.

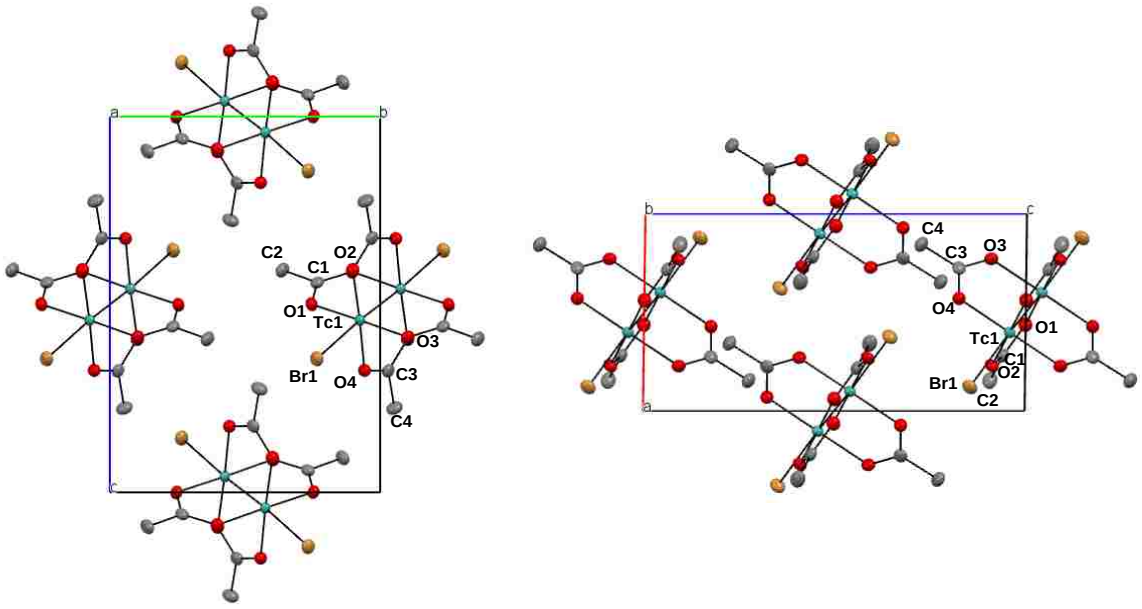

Figure 3.11 Unit cell views of $Tc_2(O_2CCH_3)_4Br_2$ along the a-axis (left image) and b-axis (right image). Hydrogen atoms are omitted for clarity.

Similar to $Tc_2(O_2CCH_3)_4Cl_2$, $Tc_2(O_2CCH_3)_4Br_2$ adopts a paddlewheel structure with capping bromides that are bent slightly (about 6.5°) from linear (Tc(1a)-Tc(1)-Br(1) = 173.563(12)°). The smaller angle of distortion of bromide from the Tc-Tc bond is due to more electron density present than in the chloride, ~8° from the 180°. It is suspected that crystal packing is responsible for these small distortions. The packing for $Tc_2(O_2CCH_3)_4Br_2$ is illustrated in Figure **3.11**, and identical to the packing of $Tc_2(O_2CCH_3)_4Cl_2$.

The distorted Tc-Tc-Br angle may impact Tc-Br distance as discussed with Tc-Cl above. The bond distance of Tc-Br was found to be 2.6554(3) Å, considerably longer than the estimates of 2.600 Å from the Raman data [148] but just a few hundreds of

angstrom larger from EXAFS, 2.63(1) Å.[152] Considering the rhenium bromo analogue, $Re_2(O_2CCH_3)_4Br_2$, the Re-Br bond distance (Raman spectroscopy) is reported to be 2.603 Å having significant error in M-Br, (M = Tc, Re) when compared to single crystal data. An increase in bond length of the M-Br is expected but is not observed, Tc-Br (2.6554(3) Å), and Re-Br (2.603 Å). Within the Cambridge Crystal Data Centre (CCDC) no single crystal structure for $Re_2(O_2CCH_3)_4Br_2$ has been reported to date. But an example of the dirhenium-dibromo paddlewheel has been reported; $Re_2(O_2CCMe_3)_4Br_2$, with a rhenium-bromide bond distance of 2.603(1) Å which identical to the Re-Br bond distance reported by Raman spectroscopy for tetraacetate compound; $Re_2(O_2CCH_3)_4Br_2$.[155]

Table 3.4. Selected bond lengths and angles for $Tc_2(O_2CCH_3)_4Br_2$.

Bond length [Å]			Bond Angle [°]
Tc(1)-O(1)	2.0078(14)	O(1)-Tc(1)-O(3)	88.41(6)
Tc(1)-O(2)	2.0380(14)	O(1)-Tc(1)-O(2a)	178.72(6)
Tc(1)-O(3)	2.0230(14)	O(1)-Tc(1)-O(4a)	89.64(6)
Tc(1)-O(4)	2.0202(14)	O(1)-Tc(1)-Tc(1a)	92.80(4)
Tc(1)-Tc(1a)	2.1764(3)	Tc(1a)-Tc(1)-Br(1)	173.563(12)
Tc(1)-Br(1)	2.6554(3)	O(1)-Tc(1)-Br(1)	93.41(4)
O - C(avg.)	1.280(2)	C(3)-O(3)-Tc(1)	119.943(13)
C - C(avg.)	1.483(3)	O(2)-C(1)-C(2)	119.96(18)

The discovery of $Tc_2(O_2CCH_3)_3Cl_2(H_2O)_2{\cdot}H_2O$ was by chance and never repeated due to unknown conditions that caused the compound to crystallize out of the mother liquor from the reaction of $KTcO_4$ with acetic acid and hydrochloric acid, Equation 3.2, with air oxidation for two days at room temperature. The complex $Tc_2(O_2CCH_3)_3Cl_2(H_2O)_2{\cdot}H_2O$ crystallizes in the monoclinic space group $P2_1$ with *a* = 7.7102(7) Å, *b* = 11.4786(11) Å, *c* = 8.3468(8) Å, and β = 94.8430(10)°, with a monohydrate which seems to have no bearing or influence on the molecular structure. Crystallographic data and refinement parameters are summarized in Table **3**.**1**, with full information and cif in Appendix B. The molecular structure of the $Tc_2(O_2CCH_3)_3Cl_2(H_2O)_2{\cdot}H_2O$, Figure **3**.**12** showing the triacetate paddlewheel with chlorides in the equatorial position and water ligands axial to the paddlewheel. Within the literature no known structures of molecular triacetate halide paddlewheels have been reported for rhenium tricarboxylates such as; $Re_2(O_2CH)_3Cl_3$ and $Re_2(O_2CCMe_3)_3Cl_3$ have been reported but are linear chains with linkage through a chloride atom, not molecular species.[156,157] It should be noted that one Ru_2^{+5} molecular triaceatate has been reported, $Ru_2(O_2CCH_3)_3$(dcnp), [dcnp = 1,8-napthyridine-2,7-dicarboxylate], prepared from $Ru_2(O_2CCH_3)_4Cl$ by substitution reaction with H_2dcnp in methanol at room temperature.[158] The compound $Tc_2(O_2CCH_3)_3Cl_2(H_2O)_2{\cdot}H_2O$ is the first solid molecular triacetate to be reported in literature, where the Tc-Tc bond distance is 2.1152(2) Å and is comparable to other paddlewheel Tc_2^{+5} bonds distance listed in Table **1**.**2** and Table **4**.**3**. Selected bond lengths and angles are summarized in Table **3**.**5**.

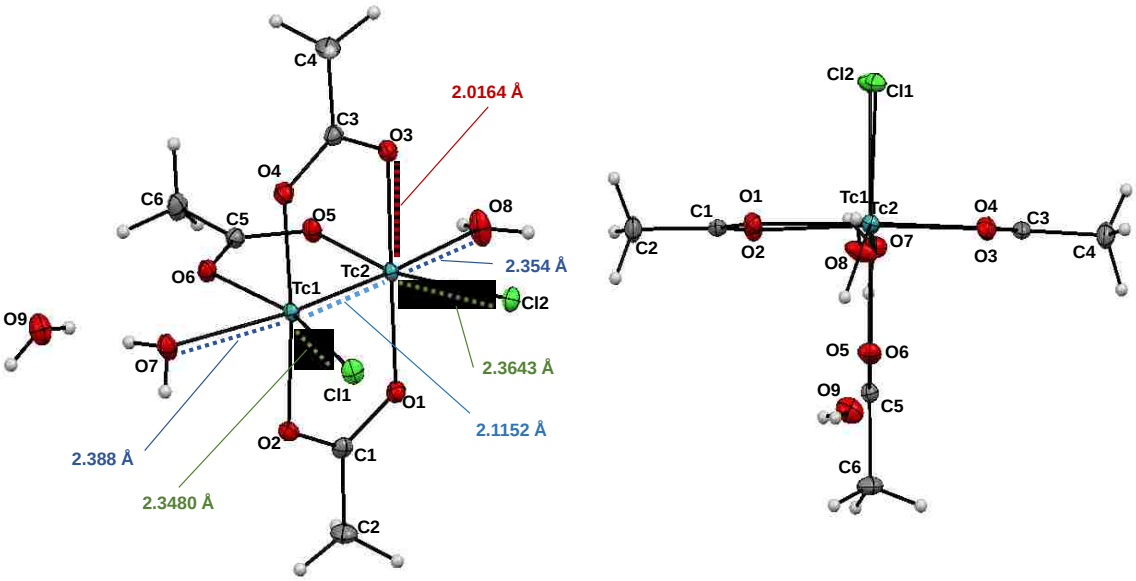

Figure 3.12. X-ray crystal structure of $Tc_2(O_2CCH_3)_3Cl_2(H_2O)_2{\cdot}H_2O$. The ORTEP representations display ellipsoids at the 50% probability level with key bond lengths shown.

The structure of $Tc_2(O_2CCH_3)_3Cl_2(H_2O)_2{\cdot}H_2O$, (Tc-Tc, 2.1152 Å, $\sigma^2\pi^4\delta^2\delta^{*1}$) is quite different than that of $Tc_2(O_2CCH_3)_4Cl_2$, (Tc-Tc, 2.1758 Å, $\sigma^2\pi^4\delta^2\delta^{*2}$) and $Tc_2(O_2CCH_3)_4Br_2$, (Tc-Tc, 2.1764 Å, $\sigma^2\pi^4\delta^2\delta^{*2}$) in that the halogen (chlorides) are not in line with the Tc-Tc bond of the molecule as seen in the $Tc_2(O_2CCH_3)_4X_2$. The bond lengths of the chloride in $Tc_2(O_2CCH_3)_3Cl_2(H_2O)_2{\cdot}H_2O$ are significantly shorter (Tc-Cl, 2.3643 Å and 2.3480 Å) than in $Tc_2(O_2CCH_3)_4Cl_2$ (Tc-Cl, 2.5078 Å). This can be attributed to the dz^2 orbital bonding in the $Tc_2(O_2CCH_3)_4Cl_2$ as well as the change in bond order. In Figure **3.12** the Tc-Tc-Cl bond angles should be 90°, but are not and chloride atoms are flexed out from each other (104.66° and 107.14°) causing the a noticeable change in angle of the Tc-Tc-OH_2 (172.31° and 167.30°) from the expected 180° as seen in the $Tc_2(O_2CCMe_3)_4Cl_2$. This is not a surprise considering both $Tc_2(O_2CCH_3)_4Cl_2$, and $Tc_2(O_2CCH_3)_4Br_2$ have non-linear Tc-Tc-X angles (171.903° and 173.563° respectively).

Table 3.5. Selected bond lengths and angles for $Tc_2(O_2CCH_3)_3Cl_2(H_2O)_2 \cdot H_2O$.

Bond length [Å]			Bond Angle [°]
Tc(1)-O(4)	2.0480(13)	O(4)-Tc(1)-O(6)	88.44(5)
Tc(1)-O(6)	2.0579(13)	O(2)-Tc(1)-O(4)	175.29(5)
Tc(2)-O(3)	2.0549(13)	O(3)-Tc(2)-O(5)	88.62(5)
Tc(2-O(5)	2.0683(13)	O(3)-Tc(2)-O(1)	176.41(7)
Tc(1)-Tc(2)	2.1152(2)	O(5)-Tc(2)-Cl(2)	161.79(4)
Tc(1)-Cl(1)	2.3480(5)	Tc(2)-Tc(1)-Cl(1)	104.661(14)
Tc(2)-Cl(2)	2.3643(5)	Tc(1)-Tc(2)-Cl(2)	107.142(13)
Tc(1)-O(7)	2.3884(15)	Tc(2)-Tc(1)-O(7)	172.31(4)
Tc(2)-O(8)	2.3543(14)	Tc(1)-Tc(2)-O(8)	167.30(4)
O - C(avg.)	1.276(3)	C(5)-O(5)-Tc(21)	118.87(12)
C - C(avg.)	1.490(3)	O(5)-C(5)-O(6)	120.82(17)

Why is the $Tc_2(O_2CCH_3)_3Cl_2(H_2O)_2 \cdot H_2O$ structure important? The argument can be made that the formation mechanism for $Tc_2(O_2CCH_3)_4Cl_2$ under the conditions described in Section 3.2.1 and Equation 3.2 may require the intermediate Tc_2^{+5} triacetate in order to oxidized to the Tc_2^{+6} tetraacetate structure in solution, shown in Figure **3.13**. Oxidation of the $Tc_2(O_2CCH_3)_3Cl_2(H_2O)_2$ in solution by addition of acetate anion to one of the Tc atoms in an SN_2 type mechanism levitating two water ligands while forcing the chlorides to axial position which would distribute the electron density throughout the

molecule more evenly forming $Tc_2(O_2CCH_3)_4Cl_2$. More investigation into the triacetate structure is needed but attempts to synthesize this compound again have failed.

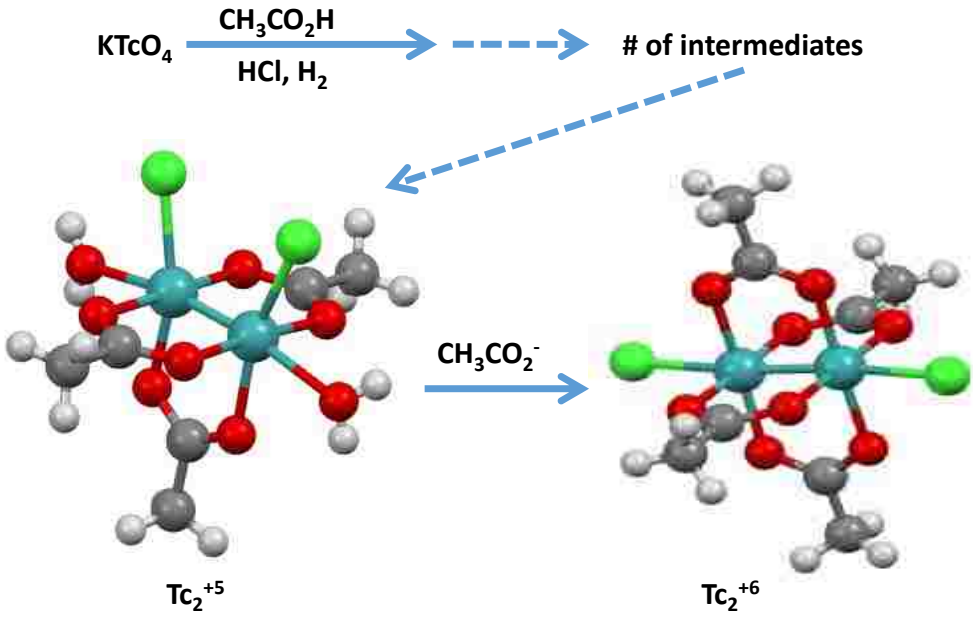

Figure 3.13. Proposed mechanism of the formation of $Tc_2(O_2CCH_3)_4Cl_2$ from addition of acetate anion to $Tc_2(O_2CCH_3)_3Cl_2(H_2O)_2$.Color of atoms: Tc in turquoise, C in dark gray, H in light gray, O in red, Cl in green.

3.4 Conclusion

A reliable, high-yield method for the synthesis of both $Tc_2(O_2CCH_3)_4Cl_2$ and $Tc_2(O_2CCH_3)_4Br_2$ has been developed based on a modification of an earlier report in the Russian patent literature. It is attractive because of its simplicity. $Tc_2(O_2CCH_3)_4Cl_2$ is an important starting material for a range of other molecular and solid-state compounds of technetium(III).[40] Now that a high yield route to $Tc_2(O_2CCH_3)_4Br_2$ exists, expansion of technetium (III) bromide compounds maybe more obtainable as well as technetium (III) chloride compounds. The x-ray structures of $Tc_2(O_2CCH_3)_4X_2$ (X = Cl, Br) are reported for

the first time and brings to 9 the total number of structurally characterized, quadruply bonded technetium(III) dimers, see Table 1.1.[16,36] By comparison, the number of structurally characterized rhenium(III) dimers with Re-Re quadruple bonds easily exceeds one hundred.[82]

The compound $Tc_2(O_2CCH_3)_3Cl_2(H_2O)_2 \cdot H_2O$ is the first ditechnetium triacetate dimer to be synthesis to-date. Investigations into the synthesis of the $Tc_2(O_2CCH_3)_3Cl_2(H_2O)_2 \cdot H_2O$, are needed as it could potentially be an intermediate molecule in the formation of $Tc_2(O_2CCH_3)_4Cl_2$. In-situ spectroscopy could enlighten the proposed mechanism. With that a deeper exploration into solubility of $Tc_2(O_2CCH_3)_4X_2$ (X = Cl, Br) is desperately needed, currently normal common organic solvents do not dissolve $Tc_2(O_2CCH_3)_4Cl_2$, ie., CH_2Cl_2, hexane, isopropyl alcohol. If a solvent were to dissolve $Tc_2(O_2CCH_3)_4Cl_2$ then expanding potential reaction routes to new compounds may be possible in turn increasing the knowledge of low-valent technetium chemistry. Currently gas flowing reactions or direct molten substitution are the only methods used to synthesis compounds from this otherwise potentially great starting material, $Tc_2(O_2CCH_3)_4X_2$ (X = Cl, Br).[16,36,40,82,152]

It should be noted that attempts to produce $Tc_2(O_2CCH_3)_4X_2$ (X = F, I) failed but lead to the discovery of new Tc-dimers and polynuclear structures presented in chapter 4, 5, and Appendix A. A good starting point for future reactions to synthesis $Tc_2(O_2CCH_3)_4F_2$, would be to start from TcF_6^{2-} anion under a lower pressure of hydrogen but retain the temperature at 200 °C. Although HCl and HBr were used in the synthesis of $Tc_2(O_2CCH_3)_4X_2$ (X = Cl, Br) the use of HF was not attempted due to concerns of HF

volatilization if the autoclaves were to rupture. If appropriate measures are taken then HF should be considered as a reactant and replaced for the HCl in Equation 3.2 to attempt the formation of $Tc_2(O_2CCH_3)_4F_2$. A suggestion for future synthesis route to $Tc_2(O_2CCH_3)_4I_2$ would be to start from TcI_6^{2-} anion in excess acetic acid under H_2 at 200 °C or addition of iodine in a sealed quartz tube with $Tc_2(O_2CCH_3)_4I$ (presented in chapter 4) under vacuum and argon conditions at various temperatures up to 350 °C (decomposition of starting materials ~380 °C).

Appendix A, contains three compounds that were synthesized in attempts to obtain $Tc_2(O_2CCH_3)_4X_2$ (X = Br, I) by the reaction of $KTcO_4$, potassium iodide or cesium iodide with a molar ratio of 1:4 technetium:iodide under same conditions sections 3.2.1, and 4.2.1. Synthesis resulted in low yield or mixture of solid crystals containing $Tc_2(O_2CCH_3)_4X$, $M[Tc_2(O_2CCH_3)_4X_2]$, M_2TcX_6, and MX, (where; M = K, Cs; and X =Br, I), similar to the description of the Russian reactions by Spitsyn, et. al., 1981 and Koz'min, et. al., 1982 to obtaining a mixture of $Tc_2(O_2CCH_3)_4Cl$, $K[Tc_2(O_2CCH_3)_4Cl_2]$, K_2TcCl_6, and KCl from the $K_3Tc_2Cl_8$ and acetic acid under hydrogen/argon atmospheres.[45,69,164] Single crystal structures of $K[Tc_2(O_2CCH_3)_4Br_2]$, $Cs[Tc_2(O_2CCH_3)_4Br_2]$, and $Cs[Tc_2(O_2CCH_3)_4I_2]$ were obtained and data tabulated in Appendix B, Section B10-12 respectively, but no further characterization was performed.

Chapter 4: Polymeric Carboxylate Chain Technetium Compounds

4.1 Introduction

Analysis of the literature indicates that ruthenium and technetium are capable of forming compounds having M_2^{5+} core structures that are linked by one atom or unit, e.g., $M_2(O_2CR)_4X$ (M = Tc, Ru; R = alkyl; X = bridging ligand).[16,104] These compounds are called extended metal atoms chains (EMAC).

For ruthenium, over 50 EMAC species containing the paddlewheel Ru_2^{5+} cores bridged by carboxylate ligands are known ($Ru_2(O_2CR)_4X$, R = alkyl; X = halide). The compound $Ru_2(O_2CPr^n)_4Cl$ was the first compound structurally characterized and is also one the most used starting compound for ruthenium metal-metal bonded compound synthesis.[104] The structural characterization of other $Ru_2(O_2CR)_4X$ showed that the polymeric chain could be linear or bent, and the chain structure seems to depend on the nature of the alkyl group.[159] Some Ru_2^{5+} tetracarboxylates exhibit non-polymeric structures in the solid state but they have the formula $Ru_2(O_2CR)_4XL$ (R = alkyl; X = halide; L = neutral donor ligand or solvent molecule). The type of axial ligand seems to play an important role to the formation of the compound and determine if it will adopt an extended or molecular structure. Unfortunately the mechanism and the factors determining the structure remain unclear.[104] Further investigation of the alkyl group in the bridging carboxylate was pursued showing the possible existence of both ionic and polymeric forms in the solid and liquid states.[160] In addition to carboxylate ligands, some chains exist with O,N- or N,N- bridging ligands for ruthenium and osmium.[104] In

order to modify magnetic or electronic properties, other ligands like OCN^- or $[Ag(OCN)_2]^-$ have been used as connectors, for example, $\{[Ru_2(O_2CCH_3)_4][Ag\text{-}(OCN)_2]\}_n$.[161]

For technetium, only EMAC containing metal-metal bonds are known within literature: Tc_2(2-hydroxypyridine)$_4Cl$, $Tc_2(O_2CCH_3)_4Cl$ and $Tc_2(O_2CCH_3)_4Br$ (see Table **1.2**).[16] These compounds consist of single chains with the halogen atom linking Tc metal-metal bonded units. For the ditechnetium tetraacetate compounds, the units are linked by chlorine and bromine. No iodine complex was reported. Some effort was focused on the synthesis of $Tc_2(O_2CCH_3)_4I$. It was discovered that $KTcO_4$ in acetic acid/MI media (M = Na, K, H), Tc:MI molar ratio 1:2, could be reduced in an autoclave to produce $Tc_2(O_2CCH_3)_4I$. The structure of the compound was solved by single-crystal X-ray diffraction and magnetic susceptibility measurements were performed. The structure of $Tc_2(O_2CCH_3)_4I$ consists of infinite chains of $Tc_2(O_2CCH_3)_4^+$ units linked by bridging iodides, an arrangement similar to the one found in $Tc_2(O_2CCH_3)_4X$ (X = Cl, Br), with a Tc_2^{5+} core unit and Tc-Tc bond of order 3.5.[162]

In exploring the synthetic routes to $Tc_2(O_2CCH_3)_4X_2$ (X = Cl, Br) as described in Chapter 3, fluoride was substituted for chloride as LiF, resulting in an unforeseen product, $Tc_2(O_2CCH_3)_4(\mu\text{-}O_2CCH_3)$ discussed below. Since it has been shown for ruthenium that the change of the alkyl group in the bridging unit could be of influence in the formation of a polymeric species, some more experiments were performed using various carboxylate ligands and different conditions. In this context, we found that $KTcO_4$ suspended in excess carboxylic acid [RCOOH] was reduced in an autoclave under a hydrogen atmosphere at 120 – 200 °C to produce $Tc_2(O_2CR)_4(\mu\text{-}O_2CR)$ where [R = $-CH_3$,

-CH_2CH_3, -C_6H_5, $C(CH_3)_3$]. These compounds possess carboxylate connector unit between the Tc_2^{5+} cores. Details of the synthesis and characterization are presented in this chapter.

The characterization of these compounds showed a special type of structural motif shared by technetium and ruthenium that is not seen with other group 7 elements. In fact, it is important to note that technetium under these conditions has a very different chemistry than rhenium and no polymeric chains are observed for rhenium.

4.2 **Experimental**

4.2.1 ***Preparation of $Tc_2(O_2CCH_3)_4I$***

Route a. A 4 dram borosilicate glass vial of original dimensions 2.1 x 7.0 cm, inner diameter 1.8 cm, was custom-cut to 3.5 cm in height. Potassium pertechnetate (104.4 mg, 0.517 mmol) and sodium iodide (151.2 mg, 1.01 mmol) were added to this vessel with a molar ratio of 1:2 technetium:iodide. The glass vial was placed in a 23 mL Teflon acid digestion autoclave (Parr Instruments) and 6.00 mL of glacial acetic acid was dispensed into the glass vial. To the Teflon autoclave, outside the glass vial, sodium borohydride (322 mg, 8.51 mmol) and 0.200 mL of deionized water was added. An illustration of the experimental autoclave setup is shown in Figure **2.6**. The system was sealed and placed in an oven at 210 °C for 3 days. Sodium borohydride reacts with water and acid to generate hydrogen gas *in situ*. Complete reaction would result in approximately 60-70 atm of H_2 pressure at 210 °C. After 3 days, the autoclave was allowed to cool to room temperature on an aluminum block, and then opened in a

sealed bag revealing well-formed, light brown crystals of $Tc_2(O_2CCH_3)_4I$. The mother liquor was removed by glass pipet, the product was washed with acetic acid (2 x 2 mL), isopropyl alcohol (2 x 2 mL), and diethyl ether (2 x 2 mL), then dried in open air. Yield: 120.1 mg (0.213 mmol, 82.8%). Anal. Calcd. for $C_8H_{12}O_8ITc_2$: Tc, 35.29; I, 22.62. Found: Tc, 35.08; I, 22.49. FT-IR (ATR, cm^{-1}): 2916s (ν_{as} CH_3), 2848s (ν_s CH_3), 1459s (ν_{as} COO), 1437s (ν_s COO), see Figure **4.1**. The compound decomposes at around 380 °C.

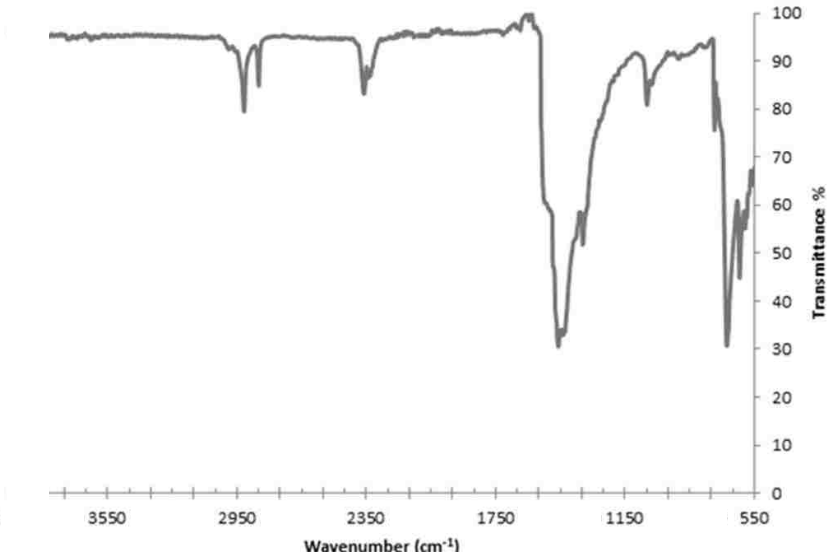

Figure 4.1. Infrared-spectrum of $Tc_2(O_2CCH_3)_4I$.

Route b. The reaction was performed using the same procedure as the one described in route a. Potassium pertechnetate (91.3 mg, 0.452 mmol) and potassium iodide (135.1 mg, 0.814 mmol) was added to the glass vial (Tc:KI molar ratio ~1:2). The glass vial was placed in a 23 mL Teflon acid digestion autoclave and 6.00 mL of glacial acetic acid was dispensed into the glass vial. To the Teflon autoclave, outside the glass

vial, sodium borohydride (321 mg, 8.49 mmol) and 0.200 mL of deionized water was added. The system was sealed and placed in an oven at 210 °C for 3 days. After 3 days, the autoclave was allowed to cool to room temperature on an aluminum block, and opened. The mother liquor was removed by glass pipet, the brown product ($Tc_2(O_2CCH_3)_4I$) was washed with acetic acid (2 x 2 mL), isopropyl alcohol (2 x 2 mL), and diethyl ether (2 x 2 mL), then dried in air. Yield: 104.1 mg (0.186 mmol, 82.1%).

Route c. The reaction was performed using the same experimental set-up as the one described in route a. Potassium pertechnetate (98.1 mg, 0.486 mmol) was added to the glass vial. The glass vial was placed in a 23 mL Teflon acid digestion autoclave and 6.00 mL of glacial acetic acid was dispensed into the glass vial followed by concentrated hydroiodic acid (120 µL, 0.908 mmol) for a molar ratio of 1:2 technetium:iodide. To the Teflon autoclave, outside the glass vial, sodium borohydride (324 mg, 8.56 mmol) and 0.200 mL of deionized water was added. The system was sealed and placed in an oven at 210 °C for 3 days. After 3 days, the autoclave was allowed to cool to room temperature on an aluminum block, and opened**.** The mother liquor was removed by glass pipet, the brown product ($Tc_2(O_2CCH_3)_4I$) was washed with acetic acid (2 x 2 mL), isopropyl alcohol (2 x 2 mL), and diethyl ether (2 x 2 mL), then dried in air. Yield: 125.2 mg (0.223 mmol, 92%).

4.2.2 ***Preparation of $Tc_2(O_2CCH_3)_4(\mu\text{-}O_2CCH_3)$***

Potassium pertechnetate (100.0 mg, 0.495 mmol) was added to a 3.5 cm in height custom-cut 4 dram borosilicate glass vial of original dimensions 2.1 x 7.0 cm, inner

diameter 1.8 cm. The glass vial was placed in a 23 mL Teflon acid digestion autoclave (Parr Instruments 4749) and 6.00 mL of glacial acetic acid was dispensed into the glass vial. To the Teflon autoclave, outside the glass vial, sodium borohydride (310 mg, 8.19 mmol) and 0.200 mL of deionized water was added. See chapter 2 for an illustration of the experimental setup in detail. The system was sealed and placed in an oven at 200 °C for 3 days. Sodium borohydride reacts with water and acid to produce hydrogen gas *in situ*. Complete reaction would result in approximately 60-70 atm of H_2 at 200 °C. After 3 days, the autoclave was allowed to cool to room temperature on an aluminum block, and then opened in a sealed bag revealing medium sized light purple crystals of $Tc_2(O_2CCH_3)_4(O_2CCH_3)$. The mother liquor was removed by glass pipet, the product was washed with acetic acid (2 x 2 mL), isopropyl alcohol (2 x 2 mL), and diethyl ether (2 x 2 mL), then dried in open air. Yield: 101.4 mg (0.206 mmol, 83.1%). Elemental Analysis, $C_{10}H_{15}O_{10}Tc_2$ (493.04): Calcd.: Tc, 40.16; Found: Tc, 39.82. FT-IR (ν(cm^{-1}) ATR-neat), 2916 (str CH_3-ν_{as}), 2850 (str CH_3-ν_s), 1543 (str, COO- ν_{as}), 1435 (str, COO-ν_s). Decomposition ~ 380 °C.

4.2.3 ***Preparation of $Tc_2(O_2CCH_2CH_3)_4(\mu\text{-}O_2CCH_2CH_3)$***

The procedure used for the preparation of $Tc_2(O_2CCH_2CH_3)_4(\mu\text{-}O_2CCH_2CH_3)$ is identical to the one presented above (4.2.2) except using propionic acid (ethanecarboxylic acid) in place of glacial acetic acid. After cleaning of the crystals, medium-sized, elongated light purple to reddish-pink crystals of tetrapropionatoditechnetium (II,III) propionate, $Tc_2(O_2CCH_2CH_3)_4(\mu\text{-}O_2CCH_2CH_3)$, were

isolated. Yield: 80.7 mg (0.144 mmol, 58.1%). Elemental Analysis, $C_{15}H_{25}O_{10}Tc_2$ (561.35): Calcd.: Tc, 35.27; Found: Tc, 36.01. FT-IR (ν(cm^{-1}) ATR-neat), 2916 (str CH_3-ν_{as}), 2850 (str CH_3-ν_s), 1465 (str, COO- ν_{as}), 1431 (str, COO- ν_s). Decomposition ~ 380 °C.

4.2.4 ***Preparation of $Tc_2(O_2CC_6H_5)_4(\mu\text{-}O_2CC_6H_5)$***

The procedure used for the preparation of $Tc_2(O_2CC_6H_5)_4(\mu\text{-}O_2CC_6H_5)$ is identical to the one presented above (4.2.2) except using benzoic acid in place of glacial acetic acid. After cleaning of the crystals, medium-sized reddish-purple crystals of tetrabenzoatoditechnetium (II,III) benzoate, $Tc_2(O_2CC_6H_5)_4(\mu\text{-}O_2CC_6H_5)$, were isolated. Yield: 80.7 mg (0.144 mmol, 51.3%). Elemental Analysis, $C_{15}H_{25}O_{10}Tc_2$ (561.35): Calcd.: Tc, 35.27; Found Tc, 36.01. FT-IR was not acquired. Decomposition ~ 380 °C.

4.2.5 ***Preparation of $Tc_2[O_2CC(CH_3)_3]_4[\mu\text{-}O_2CC(CH_3)_3]$***

The procedure used for the preparation of $Tc_2[O_2CC(CH_3)_3]_4[\mu\text{-}O_2CC(CH_3)_3]$ is identical to the one presented above (4.2.2) except using pivalic acid in place of glacial acetic acid. Product was soluble in excess pivalic acid and no solid product was obtained. LSC of Tc-99 provided 0.446 mmol technetium in liquid product but does not confirm that all technetium is a pivalate dimer. Analysis of product by XAFS shows evidence of a tetrapivalatoditechnetium (II,III) pivalate; $Tc_2[O_2CC(CH_3)_3]_4[\mu\text{-}O_2CC(CH_3)_3]$ structure.

4.2.6 ***Analysis***

4.2.6.1 Single Crystal X-ray Diffraction

Crystals synthesized in section 4.2.1 through 4.2.4 were obtained directly from the washed precipitate and mounted under Paratone on a Kaptan cryoloop for data collection. Single crystal X-ray diffraction data were collected on a Bruker Apex II CCD diffractometer using Mo-K_α radiation (λ = 0.71073 Å). The crystals were maintained at 100 K during data collection using an Oxford nitrogen cryostream system. The Apex II suite was used to perform data processing and an absorption correction performed with SADABS. Solution to the structure was performed by Direct Methods and refinement was carried out using SHELX [123] and OLEX2.[124]

For $Tc_2(O_2CCH_3)_4I$, anisotropic approximations of all atoms except hydrogen were refined against F^2, whereas the hydrogen atoms positions were determined geometrically and refined using the riding model. All crystal structure visualizations were prepared in Mercury 3.3 software.[125] Crystallographic data and refinement parameters for $Tc_2(O_2CCH_3)_4(\mu\text{-}O_2CCH_3)$, $Tc_2(O_2CCH_2CH_3)_4(\mu\text{-}O_2CCH_2CH_3)$, are shown in Table **4.1**, $Tc_2(O_2CC_6H_5)_4(\mu\text{-}O_2CC_6H_5)$ and $Tc_2(O_2CCH_3)_4I$, are shown in Table **4.2** and accounting for hydrogens the final R-factor = 0.0167. Full details on crystallographic data for the structures are shown in Appendix B.

Table 4.1. Crystallographic data and refinement parameters for $Tc_2(O_2CCH_3)_4(\mu\text{-}O_2CCH_3)$ and $Tc_2(O_2CCH_2CH_3)_4(\mu\text{-}O_2CCH_2CH_3)$.

Crystallographic data		
Empirical Formula	$C_{10}H_{15}O_{10}Tc_2$	$C_{15}H_{25}O_{10}Tc_2$
Formula weight	493.04	561.35
Temperature (K)	100	100
Wavelength (Å)	0.71073	0.71073
Crystal system	Monoclinic	Orthorhombic
Space group	C2/c	$P2_12_12_1$
a (Å)	13.0754(5)	8.7086(4)
b (Å)	8.3466(3)	13.8192(6)
c (Å)	15.0242(5)	16.8542(7)
α (°)	90.00	90.00
β (°)	106.1770(10)	90.00
γ (°)	90.00	90.00
V ($Å^3$)	1574.75(10)	2028.33(15)
Z	4	4
Density calc. (Mg m^{-3})	2.072	1.838
Absorption coef. (mm^{-1})	1.801	1.411
F(000)	964	1124
Range of 2θ (°)	2.83 – 30.51	1.91 – 30.51
Index ranges (*h, k, l*)	-18 ≤ *h* ≤ 18, -11 ≤ *k* ≤ 11, -21 ≤ *l* ≤ 21	-12 ≤ *h* ≤ 13, -19 ≤ *k* ≤ 19, -24 ≤ *l* ≤ 24
Reflections collected	11879	33356
Independent reflections	2400 [R(int) = 0.0155]	6201 [R(int) = 0.0239]
Complete to 2θ (%)	100.0	100.0
Refinement method	Full-matrix least-sq. on F^2	Full-matrix least-sq. on F^2
Data / restraints / parameters	2400 / 6 / 112	6201 / 0 / 279
Goodness-of-fit on F^2	1.129	1.050
Final R indices [$I > 2\sigma(I)$]	R1 = 0.0175, wR2 = 0.0495	R1 = 0.0208, wR2 = 0.0481
R indices (all data)	R1 = 0.0188, wR2 = 0.0467	R1 = 0.0222, wR2 = 0.0488

Table 4.2. Crystallographic data and refinement parameters for $Tc_2(O_2CC_6H_5)_4(\mu\text{-}O_2CC_6H_5)$ and $Tc_2(O_2CCH_3)_4I$.

Crystallographic data		
Empirical Formula	$C_{35}H_{25}O_{10}Tc_2$	$C_8H_{12}IO_8Tc_2$
Formula weight	803.55	560.90
Temperature (K)	100	100
Wavelength (Å)	0.71073	0.71073
Crystal system	Triclinic	Monoclinic
Space group	P-1	C 2/m
a (Å)	10.9468(3)	7.1994(6)
b (Å)	11.7511(3)	14.5851(13)
c (Å)	14.3525(4)	7.1586(6)
α (°)	67.5170(10)	90.00
β (°)	71.2040(10)	110.954(10)
γ (°)	78.4840(10)	90.00
V ($Å^3$)	1608.78(10)	701.97(10)
Z	2	2
Density calc. (Mg m^{-3})	1.655	2.645
Absorption coef. (mm^{-1})	0.918	4.197
F(000)	802	526
Range of 2θ (°)	1.88 – 30.51	2.793 – 29.564
Index ranges (*h, k, l*)	-15 ≤ *h* ≤ 15, -16 ≤ *k* ≤ 16, -20 ≤ *l* ≤ 20	-9 ≤ *h* ≤ 9, -19 ≤ *k* ≤ 19, -9 ≤ *l* ≤ 9
Reflections collected	26379	4112
Independent reflections	9772 [R(int) = 0.0174]	1021 [R(int) = 0.0170]
Complete to 2θ (%)	100.0	100.0
Refinement method	Full-matrix least-sq. on F^2	Full-matrix least-sq. on F^2
Data / restraints / parameters	9772 / 0 / 424	1021 / 0 / 48
Goodness-of-fit on F^2	1.029	1.125
Final R indices [$I > 2\sigma(I)$]	R1 = 0.0217, wR2 = 0.0558	R1 = 0.0167, wR2 = 0.0419
R indices (all data)	R1 = 0.0243, wR2 = 0.0572	R1 = 0.0178, wR2 = 0.0425

4.2.6.2 Elemental analyses

For ^{99}Tc elemental analyses using liquid scintillation counting, weighed amounts of the compounds (*ca.* 5 mg) were suspended in 5 mL of ammonium hydroxide for several days. After complete dissolution, the solutions were diluted to 10 mL with DI H_2O. Samples for LSC were prepared by mixing 100 µL of sample solution containing ^{99}Tc and

100 µL of DI H_2O, to correspond to calibration curves, with 10 mL of scintillation cocktail. ^{99}Tc concentrations were determined by liquid scintillation counting using a Perkin Elmer liquid scintillation counter Tri-Carb 3100TR. The scintillation cocktail was ULTIMA GOLD ABTM (Packard). US-EPA Method 345.1 was used to determine the amount of iodide in $Tc_2(O_2CCH_3)_4I$, See chapter 2.[163]

4.2.6.3 Magnetic measurements

Magnetic susceptibility measurements were performed on samples in a 0.1 T applied magnetic field from 10 to 300 K using a Quantum Design PPMS. The sample (83.3 mg, 0.146 mmol) was placed in a medical gel-capsule and packed with cotton. The capsule was wrapped, sealed with Parafilm and inserted securely into the bottom of a plastic straw fitted onto the PPMS sample holder.

4.2.6.4 Infrared spectroscopy

Infrared spectra were measured in an attenuated total reflectance (ATR) module with germanium objective using a Varian 3100 FT-IR Excalibur spectrometer.

4.2.6.5 XAFS spectroscopy

XAFS measurements were done at the Advanced Photon Source (APS) at the BESSRC-CAT 12 BM station at Argonne National Laboratory. The dry powder containing the Tc-pivalate complex was placed in an aluminium sample holder equipped with kapton windows. XAFS spectra were recorded at the Tc-K edge (21,044 eV) in

fluorescence mode at room temperature using a 13 element germanium detector. A double crystal of Si [1 1 1] was used as a monochromator. The energy was calibrated using a molybdenum foil (Mo-K edge = 20,000 eV).

4.3 **Results and discussion**

Historically, $Tc_2(O_2CCH_3)_4Cl_2$ was the first dinuclear technetium complex coordinated to acetate ligands to be reported.[47,162] This compound was synthesized by treating potassium pertechnetate ($KTcO_4$) in an acetic acid/HCl mixture at 210 °C in large stainless steel autoclaves that were pressurized to 30 atm with hydrogen gas (see chapter 3). In these earlier preparations, the autoclaves corroded rapidly upon exposure to the hot concentrated mineral acid. In our syntheses, Teflon-coated vessels were used and hydrogen was generated *in-situ* from the reaction of solid sodium borohydride with H_2O/HX vapors (Figure **2**.**6**) during the course of the reaction. The reaction of $KTcO_4$, with iodide salts and/or hydroiodic acid in glacial acetic acid with a Tc:MI molar ratio of 1:2 (M = K, Na, H) at 210 °C under 60-70 atm hydrogen afforded $Tc_2(O_2CCH_3)_4I$ in approximately 80-90% yield. Under these experimental conditions, the paddlewheel technetium(III, III) dimer, $Tc_2(O_2CCH_3)_4I_2$, was not observed. The halogen analogues of $Tc_2(O_2CCH_3)_4I$, i.e., $Tc_2(O_2CCH_3)_4Cl$[164] and $Tc_2(O_2CCH_3)_4Br$,[165] were respectively synthesized in autoclaves after treatment of $K_3Tc_2Cl_8{\cdot}2H_2O$ in glacial acetic acid at 120 °C under 30 atm of argon or hydrogen, and after treatment of $K_2Tc_2Br_6{\cdot}2H_2O$ in acetic acid at 230 °C under argon.

The compound $Tc_2(O_2CCH_3)_4I$ crystallizes in the monoclinic space group C2/m with *a* = 7.1194(6) Å, *b* = 14.5851(13) Å, *c* = 7.1586(6) Å, and β = 110.9540(10)° (Table **4.2**). The structure of $Tc_2(O_2CCH_3)_4I$ consists of infinite chains of $[Tc_2(O_2CCH_3)_4]^+$ units linked by bridging iodide ligand (Figure 4.2). The structure of $Tc_2(O_2CCH_3)_4I$ is similar to that of $Tc_2(O_2CCH_3)_4Br$, but differs slightly from that of $Tc_2(O_2CCH_3)_4Cl$. In $Tc_2(O_2CCH_3)_4Cl$, the Tc-Tc-X angle is 120°, resulting in a zig-zag chain, while a value of 180° is observed in $Tc_2(O_2CCH_3)_4X$ (X = Br, I) (Table 4.3). The compound $Tc_2(O_2CCH_3)_4I$ packs as parallel chains along the *a*-axis with the *b*- and *c*-axes exhibiting staggered parallel chains within the unit cell, a similar arrangement is observed in $Tc_2(O_2CCH_3)_4Br$ (Figure 4.3). Extended metal atom chains containing carboxylate bridged metal dimers are also known for ruthenium and rhenium. For ruthenium, more than 20 compounds containing the Ru_2^{5+} core have been reported;[104] these include $Ru_2(O_2CCH_3)_4Cl$ [103] and $Ru_2(O_2CH)_4Br$.[166] Surprisingly, EMAC compounds that contain the Re_2^{5+} core coordinated to carboxylate ligands have been not reported. This is an example of where technetium chemistry follows ruthenium rather than rhenium. We note that several EMACs with Re_2^{6+} tricarboxylate cores bridged by chloride ligands have been reported, [82] including $Re_2(O_2CCMe_3)_3Cl_3$. In the latter compound, the Re-Re separation is 2.229(3) Å and the Re-Cl-Re angle is 134°.[157]

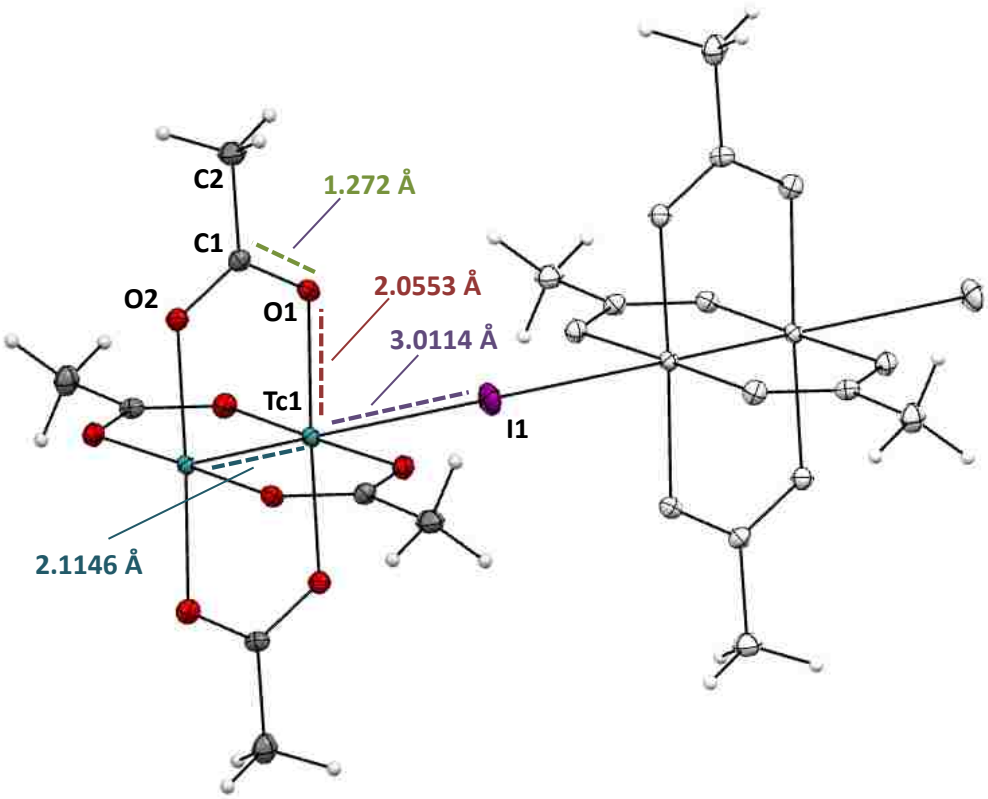

Figure 4.2. Ball and stick representation of $Tc_2(O_2CCH_3)_4I$. Ellipsoids are shown at the 50% probability level with selected bond lengths in Å. Color of atoms: Tc in turquoise, I in purple, C in gray, O in red and H in white.

In $Tc_2(O_2CCH_3)_4I$, the Tc-Tc separation of 2.1146(4) Å is slightly longer than the one found in $Tc_2(O_2CCH_3)_4Br$ (2.112(1) Å) and slightly shorter than the one in $Tc_2(O_2CCH_3)_4Cl$ (2.117(1) Å) (Table **4.3**). The Tc-Tc separations in $Tc_2(O_2CCH_3)_4X$ (X = Cl, Br, I) are consistent with the presence of the Tc_2^{5+} core (electronic configuration $\sigma^2\pi^4\delta^2\delta^{*1}$).[16] The Tc-Tc separations in $Tc_2(O_2CCH_3)_4X$ (X = Cl, Br, I) are shorter than those in $Tc_2(O_2CCH_3)_4Cl_2$ (2.1785(3) Å)[48] and $Tc_2(O_2CCMe_3)_4Cl_2$ (2.192(2) Å).[52] This phenomenon is likely due to stronger metal-metal π bonding in the Tc_2^{5+} core than in the Tc_2^{6+} core as was previously discussed for the $Tc_2X_8^{n-}$ (n = 2, 3; X = Cl, Br) systems.[36] It should be

noted that the same trend is observed in rhenium metal-metal bonding for $[Re_2Cl_4(PMe_2Ph)_4]PF_6$, Re_2^{5+} core (electronic configuration $\sigma^2\pi^2\delta^2\delta^{*1}$) and $Re_2Cl_6(PEt_3)_2$, Re^{6+} core (electronic configuration $\sigma^2\pi^4\delta^2$) compounds described by Cotton et al., concluding an increase in Re-Re bond length based on increase from 3.5 to 4 in bond order.[167]

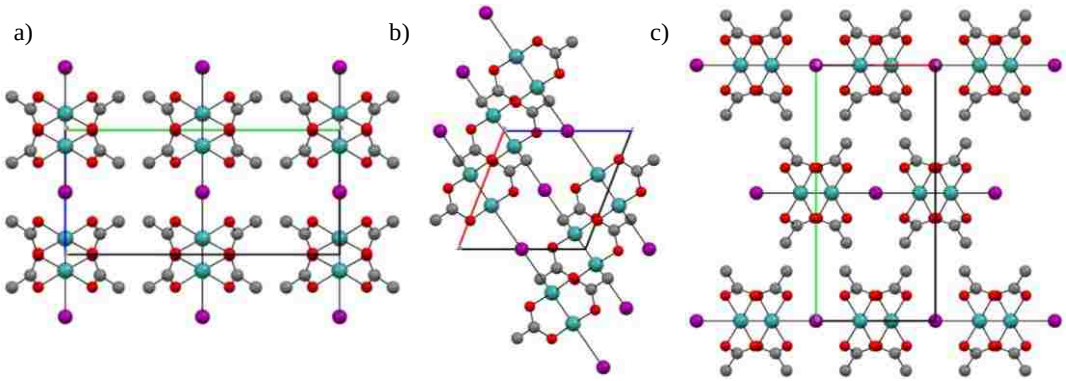

Figure 4.3. Unit cell packing for $Tc_2(O_2CCH_3)_4I$ along the a) a-axis, b) b-axis and c) c-axis. Color of atoms: Tc in turquoise, I in purple, C in gray, O in red and H omitted for clarity.

*Table 4.3. Selected interatomic distances (Å) and angles (°) for compounds with M_2^{5+} and M_2^{6+} cores coordinated to carboxylate and halogen ligands.*EXAFS, all other SC-XRD. †This Work. Uncertainties of the values given are shown in Appendix B and the given references.*

Compound [ref.]	dM-M	$M\text{-}O_{eq(avg)}$	$M\text{-}X_{ax}$ $M\text{-}O_{ax}$	$M\text{-}M\text{-}X_{ax}$ $M\text{-}M\text{-}O_{ax}$	M-X-M M-O-C
$Tc_2(O_2CCH_3)_4Cl$ [40]	2.117	2.065	2.656	176.07	119.32
$Tc_2(O_2CCH_3)_4Br$ [42]	2.112	2.060	2.843	179.63	180
$Tc_2(O_2CCH_3)_4I$ [†,162]	2.1146	2.0553	3.0114	179.534	180
$Tc_2(ONCC_5H_4)_4Cl$ [73]	2.095	2.087	2.679	93.07	180
$Ru_2(O_2CCH_3)_4Cl$ [103]	2.281	2.03	2.571	177.0	180
$Ru_2(O_2CH)_4Br$ [166]	2.2897	2.026	2.7170	176.43	109.99
	2.2901	2.026	2.7313	177.07	-
$Ru_2(O_2CCH_2CH_2CH_3)_4Cl$ [101]	2.281	2.00	2.587	175.1	-
$Tc_2(O_2CCH_3)_4(\mu\text{-}O_2CCH_3)$ [†]	2.1124	2.0660	2.2125	176.65	145
$Tc_2(O_2CCH_2H_3)_4(\mu\text{-}O_2CCH_2CH_3)$[†]	2.1139	2.0630	2.2249	176.40	147
$Tc_2(O_2CC_6H_5)_4(\mu\text{-}O_2CC_6H_5)$ [†]	2.1233	2.0603	2.2067	168.00	128
$Tc_2[O_2CC(CH_3)_3]_4[\mu\text{-}O_2CC(CH_3)_3]$[†]*	2.13	2.08	-	-	-
$Ru_2(O_2CCF_3)_4(\mu\text{-}O_2CCF_3)$[168]	2.278	2.022	2.157	178.9	148
$Ru_2(O_2CCH_2H_3)_4(\mu\text{-}O_2CCH_2CH_3)$[168]	2.273	2.025	2.165	174.6	148
$Ru_2(O_2CC_6H_5)_5\cdot C_6H_5CO_2H$ [169]	2.277	2.016	2.244	175.57	-
$Tc_2(O_2CCH_3)_4Cl_2$ [48]	2.1758	2.0211	2.5078	171.903	-
$Tc_2(O_2CCMe_3)_4Cl_2$ [52]	2.192	2.032	2.408	180	-

In the current literature, there are no reports of $Tc_2(O_2CR)_4(\mu\text{-}O_2CR)$ compounds, where [R = alkyl] despite the fact that over 50 are known for ruthenium. The first technetium pentacarboxylate to be synthesized was the acetate, $Tc_2(O_2CCH_3)_4(\mu$-

O_2CCH_3), purple in color, forming in no visual particular shape. An optical image of the pentaacetate technetium dimer is shown in Figure **4**.**4** together with an SEM-image. The compound $Tc_2(O_2CCH_3)_4(\mu\text{-}O_2CCH_3)$ crystallizes in the monoclinic space group C2/c with *a* = 13.0754(5) Å, *b* = 8.3466(3) Å, *c* = 15.0242(5) Å, and β = 106.1770(10)°. (Table 4.1). The structure of $Tc_2(O_2CCH_3)_4(\mu\text{-}O_2CCH_3)$ consists of infinite chains of $[Tc_2(O_2CCH_3)_4]^+$ units linked by bridging acetate ligands (Figure 4.5). No comparable ruthenium pentaacetate is known but the trifluoroacetate analog is, $Ru_2(O_2CCF_3)_4(\mu\text{-}O_2CCF_3)$.[168] The structure of $Tc_2(O_2CCH_3)_4(\mu\text{-}O_2CCH_3)$ is completely analogous to that of $Ru_2(O_2CCF_3)_4(\mu\text{-}O_2CCF_3)$, with spiraling disordered positions of the carboxylate linkers, in an up-down configuration. In $Ru_2(O_2CCF_3)_4(\mu\text{-}O_2CCF_3)$, the Ru-Ru-O angle is 178.9°, resulting in a slight zig-zag chain, while a value of 176.65° is observed in $Tc_2(O_2CCH_3)_4(\mu\text{-}O_2CCH_3)$ (Table 4.3), the latter may be due to the electron withdrawing $-CF_3$ groups as well as the small increase in the ionic radius of ruthenium causing a more linear bond angle.

The M-M bond lengths in $M_2(O_2CR)_4(\mu\text{-}O_2CR)$ [M = Tc, Ru; R = alkyl] are larger for M= Ru than the one for M = Tc This effect is due to the two extra electrons within the Ru-Ru bonding orbitals [3 unpaired electrons, $\sigma^2\pi^4\delta^2(\pi^*\delta^*)^3$]. The $Tc_2(O_2CCH_3)_4(\mu\text{-}O_2CCH_3)$ bond lengths can be compared with those listed in Table 4. In $Tc_2(O_2CCH_3)_4(\mu\text{-}O_2CCH_3)$, the Tc-Tc separation of 2.1124(2) Å is comparable to those Tc_2^{+5} bond lengths found in $Tc_2(O_2CCH_3)_4X$, (Cl, Br, and I), i.e., 2.117(1) Å, 2.112(1) Å, and 2.1146(4) Å respectively (Table **4**.**3**). The Tc-Tc separations in $Tc_2(O_2CCH_3)_4X$ (X = Cl, Br, I, and O_2CCH_3) are all consistent with the presence of the Tc_2^{5+} core (electronic configuration $\sigma^2\pi^4\delta^2\delta^{*1}$).[16]

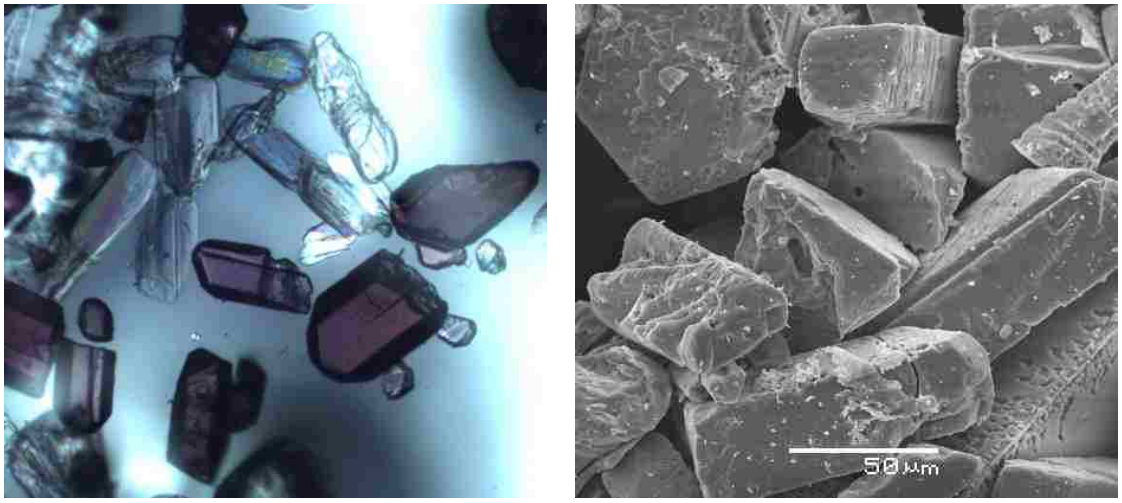

Figure 4.4. Optical microscope view (right) of single crystals $Tc_2(O_2CCH_3)_4(\mu\text{-}O_2CCH_3)$, and SEM-image magnification x500 in scanning electron mode(left).

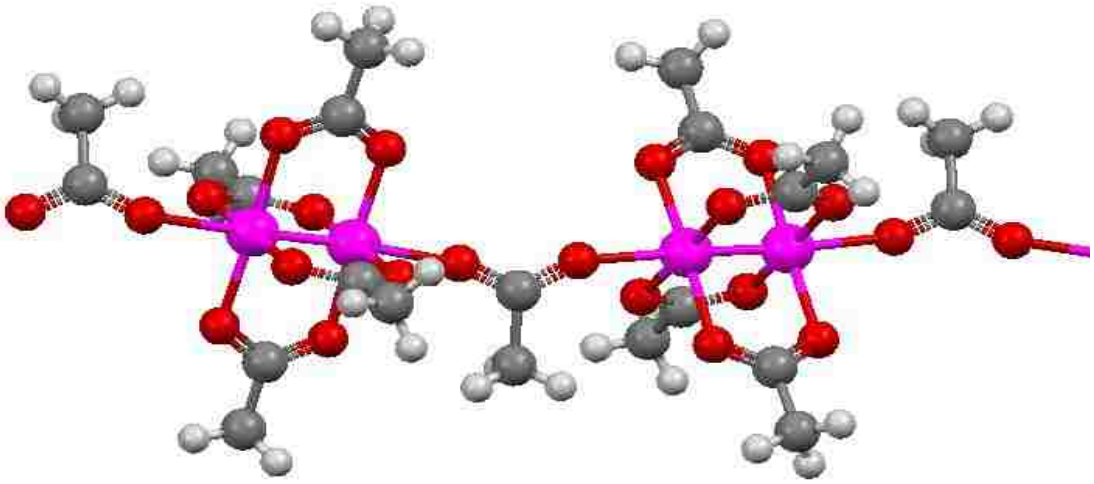

Figure 4.5. Ball and stick representation of $Tc_2(O_2CCH_3)_4(\mu\text{-}O_2CCH_3)$. Color of atoms: Tc in pink, C in gray, O in red and H in white.

The second carboxylate technetium dimer to be prepared was $Tc_2(O_2CCH_2H_3)_4(\mu\text{-}O_2CCH_2CH_3)$. It forms having elongated reddish-pink-purple crystals shown in Figure **4.6**

including an SEM-image. The compound $Tc_2(O_2CCH_2CH_3)_4(\mu\text{-}O_2CCH_2CH_3)$ crystallizes in the orthorhombic space group $P2_12_12_1$ with a = 8.7086(4) Å, b = 13.8192(6) Å, c = 16.8542(7) Å, and $\alpha = \beta = \gamma = 90°$(Table **4.1**). The structure of $Tc_2(O_2CCH_2CH_3)_4(\mu\text{-}O_2CCH_2CH_3)$ consists of infinite chains of $[Tc_2(O_2CCH_2CH_3)_4]^+$ units linked by bridging propionate ligand (Figure **4.7**).

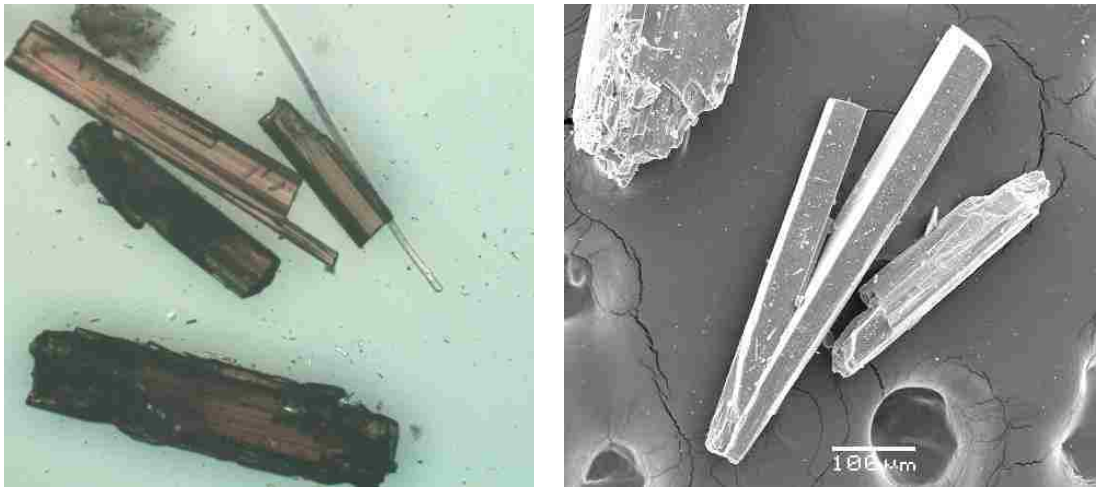

Figure 4.6. Optical microscope view (right) of single crystals $Tc_2(O_2CCH_2CH_3)_4(\mu\text{-}O_2CCH_2CH_3)$, and SEM-image magnification x150 in scanning electron mode (left).

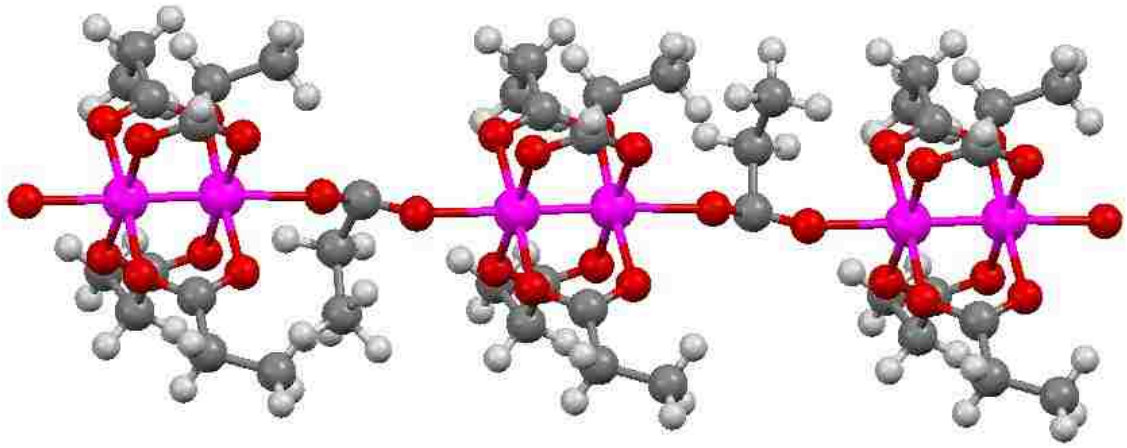

Figure 4.7. Ball and stick representation of $Tc_2(O_2CCH_2CH_3)_4(\mu\text{-}O_2CCH_2CH_3)$. Color of atoms: Tc in pink, C in gray, O in red and H in white.

The structure of $Tc_2(O_2CCH_2CH_3)_4(\mu\text{-}O_2CCH_2CH_3)$ is similar to that of $Ru_2(O_2CCH_2CH_3)_4(\mu\text{-}O_2CCH_2CH_3)$, but from $Tc_2(O_2CCH_3)_4(\mu\text{-}O_2CCH_3)$ where the acetate linkage is in alternating positions of up-down-up-down, etc., with a spiraling chain, whereas $Ru_2(O_2CCH_3)_4(\mu\text{-}O_2CCH_3)$ has the linker consistently on the same side of the polymeric chain and metal-metal bond. The compounds $Tc_2(O_2CCH_2CH_3)_4(\mu\text{-}O_2CCH_2CH_3)$ and $Ru_2(O_2CCH_2CH_3)_4(\mu\text{-}O_2CCH_2CH_3)$[168] are isostructural but bond the lengths cannot be directly compared as explained above due to change in the number of antibonding electrons in the metal-metal bond. One interesting comparison is the ruthenium pentapropionate and technetium pentapropionate have similar M-M-O_{ax} bond angles at 174.6° and 176.40° respectively, even though the $Tc_2(O_2CCH_2CH_3)_4(\mu\text{-}O_2CCH_2CH_3)$ has a spiraling chain and disordered within its crystal packing. The metal-metal bond of $Tc_2(O_2CCH_2CH_3)_4(\mu\text{-}O_2CCH_2CH_3)$ is also closely comparable to the other known Tc_2^{+5} carboxylate linkage chains listed in Table 4.3 with all having a metal-metal separation of

2.11XX Å. It should be noted that a slight increase in bond length that occurs between the $Tc_2(O_2CCH_3)_4(\mu\text{-}O_2CCH_3)$, $Tc_2(O_2CCH_2CH_3)_4(\mu\text{-}O_2CCH_2CH_3)$, and $Tc_2(O_2CC_6H_5)_4(\mu\text{-}O_2CC_6H_5)$ from 2.1124(2) Å, 2.1139(2) Å to 2.1233(2) Å, is mostly likely related to the increasing size of the alkyl group.

As mentioned, the larger steric effect seen in the increase of bond length brings up the third technetium pentacarboxylate, $Tc_2(O_2CC_6H_5)_4(\mu\text{-}O_2CC_6H_5)$ forming regular reddish purple crystals that are shown in Figure **4.8** together with an SEM-image. The compound $Tc_2(O_2CC_6H_5)_4(\mu\text{-}O_2CC_6H_5)$ crystallizes in the triclinic space group P-1 with *a* = 10.9468(3) Å, *b* = 11.7511(3) Å, *c* = 14.3525(4) Å, and α = 67.5170(10)°, β = 71.2040(10)°, γ = 78.4840(10)° (Table **4.2**). The structure of $Tc_2(O_2CC_6H_5)_4(\mu\text{-}O_2CC_6H_5)$, consists of infinite chains of $[Tc_2(O_2CC_6H_5)_4]^+$ units linked by bridging benzoate ligands (Figure **4.9**). The compound $Tc_2(O_2CC_6H_5)_4(\mu\text{-}O_2CC_6H_5)$ is isostructural to its ruthenium neighbor (Table **4.3** $Ru_2(O_2CC_6H_5)_4(\mu\text{-}O_2CC_6H_5)\cdot C_6H_5CO_2H$) that also crystallizes in the triclinic space group P-1. Other than structure, not much is comparable between the Ru and Tc complexes. $Tc_2(O_2CC_6H_5)_4(\mu\text{-}O_2CC_6H_5)$ has a type of compacted packing where the linking benzoate is turned almost 90 degrees facing the Tc-Tc paddlewheel. The benzoic acid in $Ru_2(O_2CC_6H_5)_4(\mu\text{-}O_2CC_6H_5)\cdot C_6H_5CO_2H$ takes on a similar roll allowing a straighter linkage in the chain, compared to the forced zig-zag in $Tc_2(O_2CC_6H_5)_4(\mu\text{-}O_2CC_6H_5)$.

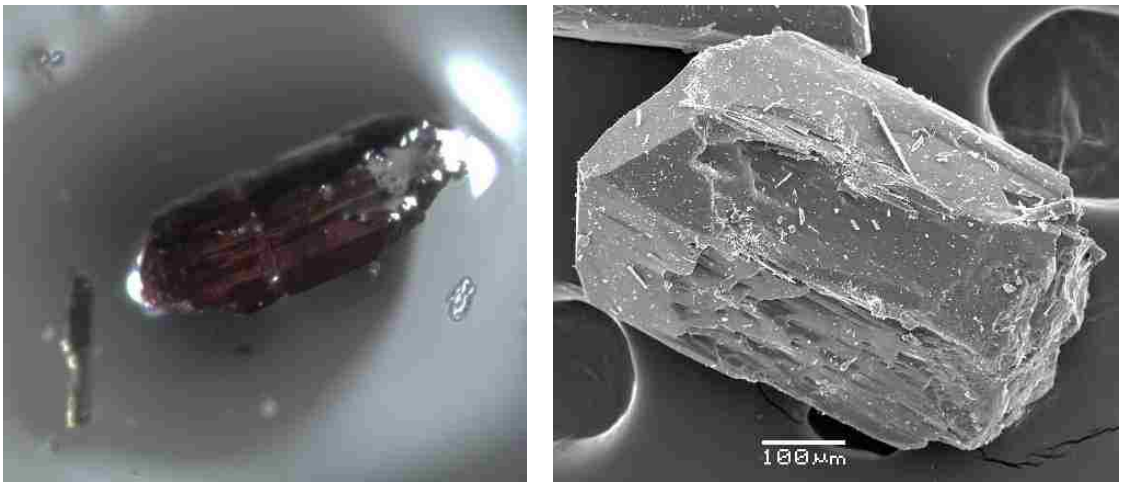

Figure 4.8. Optical microscope view (right) of single crystals $Tc_2(O_2CC_6H_5)_4(\mu\text{-}O_2CC_6H_5)$, and SEM-image magnification x150 in scanning electron mode (left).

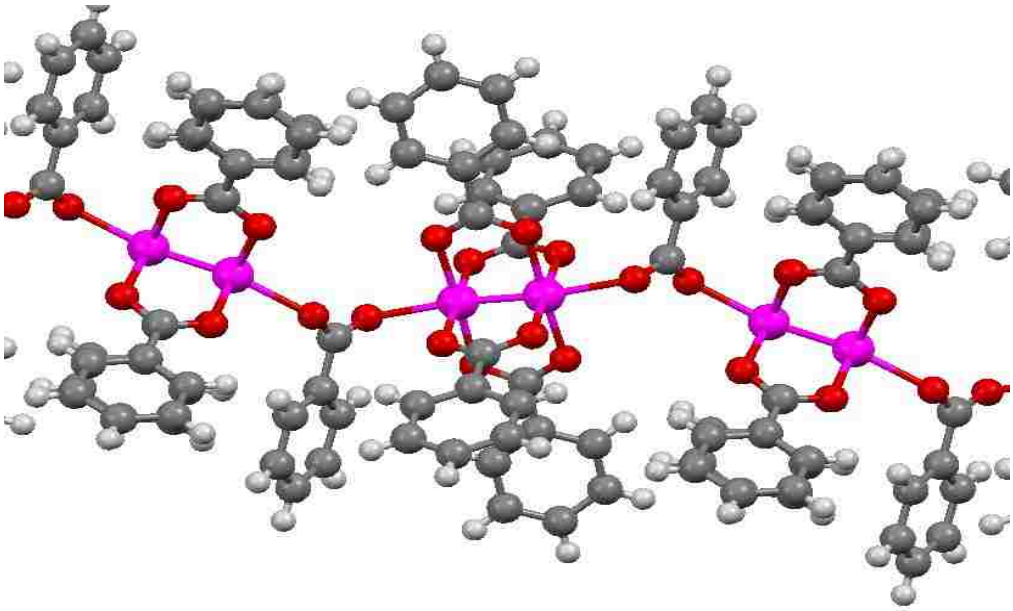

Figure 4.9. Ball and stick representation of $Tc_2(O_2CC_6H_5)_4(\mu\text{-}O_2CC_6H_5)$. Color of atoms: Tc in pink, C in gray, O in red and H in white.

The last technetium pentacarboxylate to be synthesized was $Tc_2[O_2CC(CH_3)_3]_4[\mu\text{-}O_2CC(CH_3)_3]$. The compound was soluble in pivalic acid and even after multiple purification processes no single crystals were obtained. Thus, the structure was studied

by EXAFS spectroscopy. Twenty spectra were recorded in the *k* range [0 - 15] $Å^{-1}$ and averaged. EXAFS spectra were extracted using Athena [170] software and data analysis was performed using Winxas.[147] For the fitting procedure, amplitude and phase shift function were calculated by FEFF 8.2.[146] Input files were generated by Atoms [145] using crystallographic structures of $Tc_2(O_2CCH_3)_4Cl_2$.[48] The EXAFS spectra was fitted using the Tc-O, Tc-Tc and Tc-C scattering calculated in $Tc_2(O_2CCH_3)_4Cl_2$. For the adjustment, the Debye-Waller factors for the Tc-O, Tc-Tc and Tc-C scatterings were fixed to the one previously determined in $Tc_2(O_2CCH_3)_4Cl_2$.[152] Adjustments of the k^3 -weighted EXAFS spectra were performed under the constraints $S_0^2 = 0.9$. A single value of energy shift (ΔE_0) was used for all scattering,

The fitted k^3-EXAFS spectra and the Fourier transform are presented in Figure **4.10**. The results Table **4.4** of the adjustment indicates that the fist coordination sphere around the Tc atom is constituted by 4.3(9) O atoms at 2.08(2) Å and 0.8(2) Tc atoms at 2.13(2) Å. The second coordination shell is constituted by 5(1) C atom at 2.90(3) Å. The results are in agreement with the present of a technetium pivalate compound with multiple Tc-Tc bonds. The Tc-Tc distance (i.e., 2.13(2) Å) is in agreement with the ones found for similar compounds with the Tc_2^{5+} core. Considering the XAFS measurement is not completed at 100 K like the data obtained from SC-XRD, the Tc-Tc bond distance of $Tc_2[O_2CC(CH_3)_3]_4[\mu\text{-}O_2CC(CH_3)_3]$ structure is slightly larger than that of the other $Tc_2(O_2CR)_4(\mu\text{-}O_2CR)$ where [R = $-CH_3$, $-CH_2CH_3$, $-C_6H_5$] due to thermal noise in the XAFS measurement. Nonetheless, the Tc-Tc bond distance follows the trend of an increase in length based on the size of the alkyl ligand.

Table 4.4. Structural parameters obtained by adjustment of the k^3- EXAFS spectra of $Tc_2[O_2CC(CH_3)_3]_4[\mu\text{-}O_2CC(CH_3)_3]$. Adjustment between k= [3.5 - 12.5] $Å^{-1}$. ΔE_0 (eV) = 7.96.

Scattering	Structural parameter		
	C. N.	R(Å)	$\sigma^2(Å^2)$
Tc0-O	4.3(9)	2.08(2)	0.0049
Tc0-Tc	0.8(2)	2.13(2)	0.0025
Tc0-C	5(1)	2.90(3)	0.0044

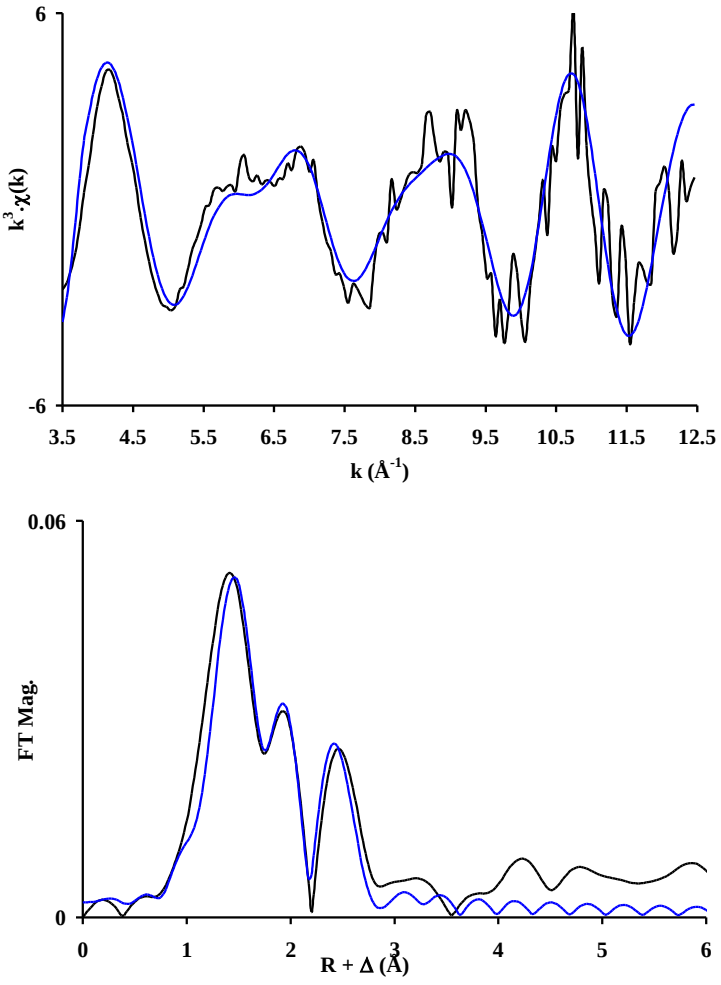

Figure 4.10. Fitted experimental k^3-EXAFS spectra (top) and Fourier transform of k^3 – EXAFS spectra (bottom) of the $Tc_2[O_2CC(CH_3)_3]_4[\mu\text{-}O_2CC(CH_3)_3]$ complex. Adjustment between k = [3.5 - 12.5] $Å^{-1}$. Experimental data are in black and the fits are in blue.

Magnetic susceptibility measurements were performed in the temperature range from 10-300 K. The data (Figure **4.11**) indicates the compound to be paramagnetic, which is consistent with the presence of a single unpaired electron in the Tc_2^{5+} core (i.e., $\sigma^2\pi^4\delta^2\delta^{*1}$). The magnetic moment in Bohr magnetons, μ_{eff}, was determined at 300 K using Equation 4.1:

$$\mu_{eff} = \sqrt{\frac{3 \cdot k \cdot X_m \cdot T}{N \cdot \beta^2}} = \sqrt{7.9971 \cdot X_m \cdot T} \qquad \text{Equation 4.1}$$

where *k* is the Boltzmann constant (1.38 x 10^{-16} erg.deg^{-1}.mol^{-1}), *N* is Avogadro's number (6.022 x 10^{23} atom.mol^{-1}), β is the Bohr magneton (9.2731 x 10^{-21} erg.gauss^{-1}), X_m is the magnetic susceptibility and T is the temperature in Kelvin. The equation is simplified by $3k/N\beta^2$ = 7.9971 mol.gauss^2.erg^{-1}.deg^{-1}. Therefore for a X_m = 0.00141 mol^{-1} at 300 K, the μ_{eff} for $Tc_2(O_2CCH_3)_4I$ is calculated to be 1.84 B.M. or close to what one would expect for a single unpaired electron.

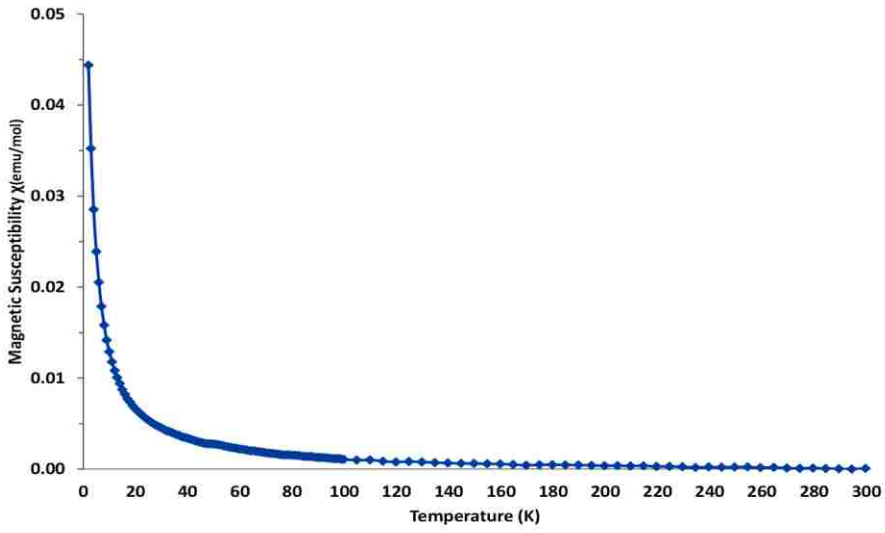

Figure 4.11. Magnetic susceptibility as a function of the temperature for $Tc_2(O_2CCH_3)_4I$

The magnetic moment for $Tc_2(O_2CCH_3)_4I$ (μ_{eff} = 1.84 B.M.) is comparable to the ones reported previously for $Tc_2(O_2CCH_3)_4Cl$ and $Tc_2(O_2CCH_3)_4Br$, i.e., 1.73 and ~2.0 B.M, respectively.[171] The μ_{eff} for $Tc_2(O_2CCH_3)_4I(\mu\text{-}O_2CCH_3)$ was determined to be 1.40 B.M. based on a x_m = 0.00141 mol^{-1} at 300 K, as shown in Figure **4.12**. Unfortunately, there is no data to compare this magnetic information within the technetium literature. The isostructural ruthenium complexes, listed in table 4.3, have magnetic susceptibilities much larger than $Tc_2(O_2CCH_3)_4X$, (X = Cl, Br, I, O_2CCH_3), i.e., $Ru_2(O_2CCH_3)_4Cl$ (μ_{eff} = 2.79 B.M.) is due to the fact that the Ru_5^{+2} $[\sigma^2\pi^4\delta^2(\pi^*\delta^*)^3]$ core has three unpaired electrons where as Tc_2^{+5} $[\sigma^2\pi^4\delta^2\delta^{*1}]$ core has one unpaired electron.[172]

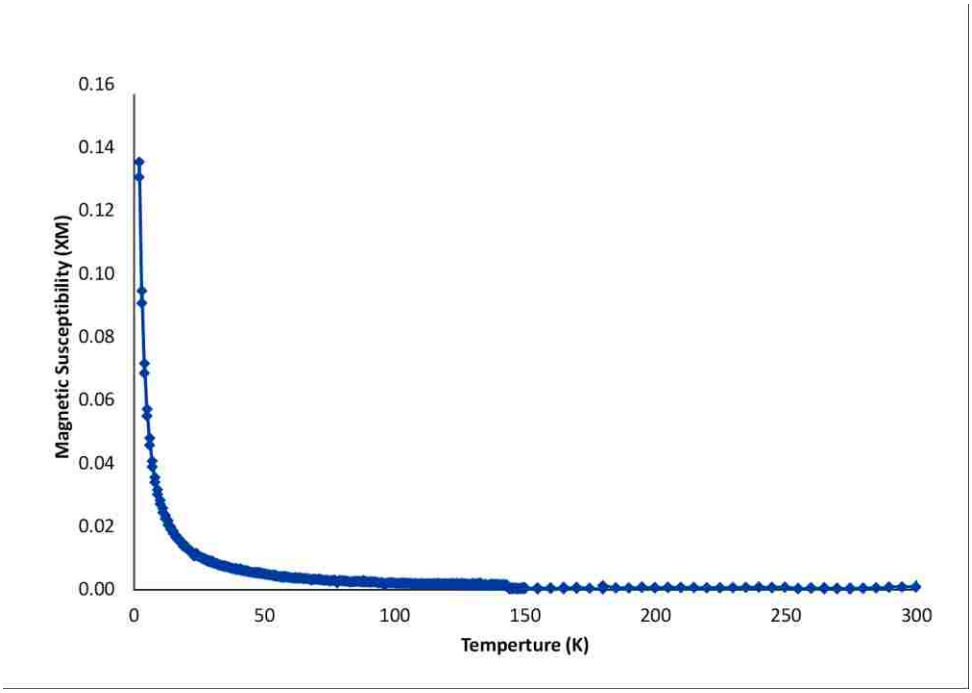

Figure 4.12. Magnetic susceptibility as a function of temperature for $Tc_2(O_2CCH_3)_4(\mu\text{-}O_2CCH_3)$.

4.4 **Conclusion**

A new technetium metal-metal bonded iodide compound, $Tc_2(O_2CCH_3)_4I$ was synthesized via the hydrothermal reduction of $KTcO_4$ in acetic acid/MI (M = Na, K, H) media and its X-ray crystal structure elucidated. The discovery of $Tc_2(O_2CCH_3)_4I$ brings to four the number of structurally characterized complexes with the Tc_2^{5+} unit coordinated to acetate ligands. The Tc-Tc separation in $Tc_2(O_2CCH_3)_4I$ is consistent with the presence of the Tc_2^{5+} core with the electronic configuration $\sigma^2\pi^4\delta^2\delta^{*1}$. Magnetic measurements were performed on $Tc_2(O_2CCH_3)_4I$. The results show the compound to be paramagnetic, consistent with the electronic configuration $\sigma^2\pi^4\delta^2\delta^{*1}$. It is expected that $Tc_2(O_2CCH_3)_4I$ will serve as a precursor for the synthesis of other multiply metal-metal bonded complexes, e.g., $Tc_2I_8^{2-}$ or $Tc_2(O_2CCH_3)_4I_2$. Proposed future reaction as indicated in conclusion of chapter 3, would be to oxidize the $Tc_2(O_2CCH_3)_4I$ in a sealed quartz tube with iodine at various temperatures in vacuum or argon atmosphere to form $Tc_2(O_2CCH_3)_4I_2$.

Several new EMAC with the stoichiometry $Tc_2(O_2CR)_4(\mu\text{-}O_2CR)$ where [R = $-CH_3$, $-CH_2CH_3$, $-C_6H_5$, $C(CH_3)_3$] were prepared and characterized by SC-XRD or EXAFS. These new structures have expanded the number of known polymeric Tc_2^{+5} compounds from 3 to 8. In the future it is believed that $Tc_2(O_2CCH_3)_4(\mu\text{-}O_2CCH_3)$ compound could become a new starting material for Tc-Tc metal-metal bond chemistry as well as a useful precursor to Tc-halides. The compound has already been shown to be a starting material for synthesis of pure technetium disulfide. The reaction of $Tc_2(O_2CCH_3)_4(\mu\text{-}O_2CCH_3)$ with flowing hydrogen sulfide gas at 450 °C for 1 hour provides 99.8% conversion to TcS_2, as

potential waste form.[173] The reactions presented demonstrate that the chemistry of technetium and especially that of metal-metal bonded systems merits further exploration.

Chapter 5: Technetium Cluster Chemistry

5.1 Introduction

As of 1993, only 9 technetium polynuclear cluster halide compounds were known. At UNLV the technetium group within the radiochemistry program has synthesized 3 more clusters in the last 2 years, two of which are discussed in this chapter. The first of the original 9 cluster compounds discovered in 1982 was $[H(H_2O)_2]\{[Tc_8((\mu\text{-}Br)_8Br_4]Br\}$, (shown in Figure **5.1** as the cation). Research in this area expanded over the next few years to include a few additional octa-nuclear and hexa-nuclear structures of chloride, bromide and iodide compounds listed in Table 1.2. The cluster compounds were obtained using various starting materials such as $MTcO_4$ and M_nTcX_6 ($M = H^+, NH_4^+, NR_4^+$; n = 1, 2; X = Cl, Br, I) under a reducing hydrogen atmosphere as described in Chapter 1 from concentrated HBr and HI solutions. The clusters $[Tc_8(\mu\text{-}Br)_8Br_4]Br\cdot 2H_2O$,[76,78] $(H_5O_2)[Tc_8(\mu\text{-}Br)_8Br_4]Br$,[77,78] and $(H_5O_2)_2[Tc_8(\mu\text{-}Br)_8Br_4]Br_2$[78] have properties consistent with the presence of one unpaired electron.[174] The $[Tc_8(\mu\text{-}Br)_8Br_4]^+$ cluster exhibits four very different types of Tc–Tc bonds; Tc(1)-Tc(2) distance of 2.145(2) Å , Tc(1)–Tc(4), 2.689(2) Å , Tc(3)–Tc(4), 2.521(2) Å, and Tc(3)–Tc(4A), 2.147(2) Å. The clusters clearly possess four Tc–Tc bonds of high multiplicity concluded to be “electron-rich triple bonds”, similar to those in the hexanuclear-Tc-chloro cluster $(Me_4N)_3\{[Tc_6(\mu\text{-}Cl)_6Cl_6]Cl_2$, shown in Figure **5.1**.[175]

In the effort to synthesize $Tc_2(O_2CCH_3)_4I$ (Chapter 4), $KTcO_4$ was reduced in an autoclave in a mixture of acetic acid and alkali metal iodide salts. Using the mixture

Tc:MI (M = K, Na, H) at a molar ratio 1:2 $Tc_2(O_2CCH_3)_4I$ was synthesized. With the combination Tc:KI:HI in a molar ratio 1:1:3 a mixture of $K[Tc_8(\mu\text{-}I)_8I_4]I$ and $Tc_2(O_2CCH_3)_4I$ was produced. The compound $K[Tc_8(\mu\text{-}I)_8I_4]I$, is the first octanuclear technetium iodide cluster to be reported.

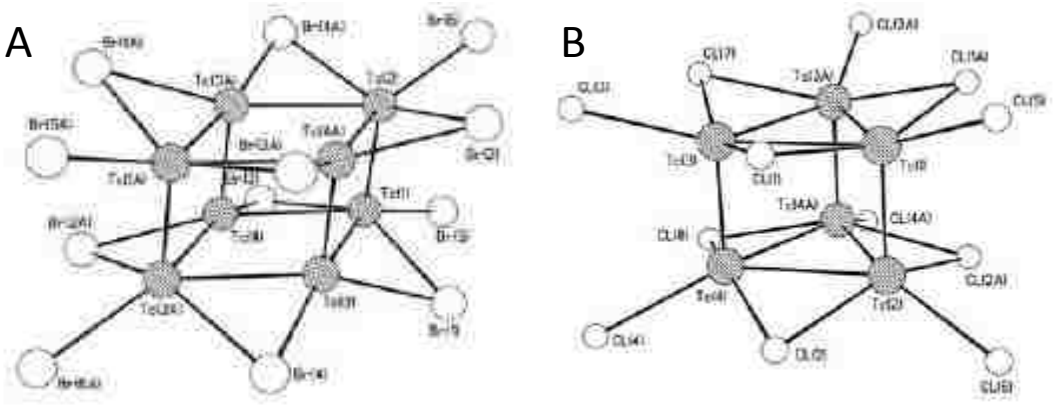

Figure 5.1. A: Structure of $[Tc_8(\mu\text{-}Br)_8Br_4]^+$ cation in $[Tc_8(\mu\text{-}Br)_8Br_4]Br{\cdot}2H_2O$.[176] B: Structure of the trigonal prismatic cluster anion, $[Tc_6Cl_6(\mu\text{-}Cl)_6]^-$ in $(Me_4N)_3\{[Tc_6(\mu\text{-}Cl)_6Cl_6]Cl_2$. Capping chloride ions have been omitted. The structure of $[Tc_6Cl_6(\mu\text{-}Cl)_6]^{2-}$ is similar.[177]

Prior to 2014, pentanuclear technetium clusters were unknown. Pentanuclear clusters of the neighboring elements molybdenum and tungsten are reported, i.e., $[(Mo_5Cl_8)Cl_5]^{2-}$ and $[(W_5I_8)I_5]^{n-}$ (n = 1, 2) (Figure **5.2**), and $W_{15}I_{47}$, which contains 3 core units of $[W_5I_8]I_x$ (x = 1, 2) linked by $(I_3)_y$ units (y = 1, 3/2, 2) between clusters. [114,178,179] In the conclusion section of the $W_{15}I_{47}$ paper, the authors suggested that from the Extended-Hückel molecular orbital (EHMO) calculations on $[(W_5I_8)I_5]^{1-}$ with comparison to EHMO calculation on $[(Mo_5Cl_8)Cl_5]^{2-}$ that these clusters have 18 electrons per cluster in HOMOs and that the LUMO that is an essentially nonbonding level. This means higher occupation numbers up to 22 electrons are possible and most likely stable. The

importance of a 22 electron core cluster is that stability of a technetium pentanuclear cluster structurally similar to $[(Mo_5Cl_8)Cl_5]^{2-}$, and $[(W_5I_8)I_5]^{1-}$ may be possible. Assuming Tc as a pentanuclear core with 13 halogen atoms either terminal and/or bridging like that of $[(W_5I_8)I_5]^{1-}$ but as a molecular species, the magic number of 22 electron core is achieved and Tc_5X_{13} (X= halogen or equivalent ligand) should exist. In fact, a Tc_5I_{13} cluster has been synthesized and will be discussed later in this chapter. It should also be noted that there is no evidence within the literature of pentanuclear rhenium halide structures.

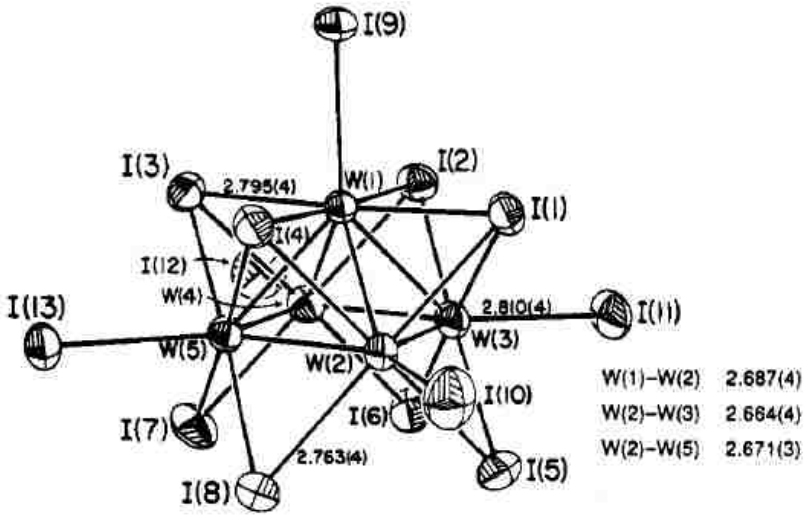

Figure 5.2. Structure of $(Pr_4N)[W_5I_5(\mu\text{-}I)_4(\eta\text{-}I)_4]\cdot THF$ or written as $(Pr_4N)[W_5I_{13}]\cdot THF$. Both the $(PrN)^+$ and THF have been omitted.[179]

5.2 **Experimental**

5.2.1 ***Preparation of $K[Tc_8(\mu\text{-}I)_8I_4]$***

The reaction was performed using the same experimental set-up as the one described for $Tc_2(O_2CCH_3)_4I$ (Chapter 4) and Figure **2.6**. Potassium pertechnetate (101.3

mg, 0.501 mmol) and potassium iodide (84.3 mg, 0.508 mmol) were added to the glass vial. The glass vial was placed in a 23 mL Teflon acid digestion autoclave and glacial acetic acid (6 mL) was added into the glass vial followed by concentrated hydroiodic acid (198 μL, 1.50 mmol). The Tc:KI:HI molar ratio is ~1:1:3. To the Teflon autoclave, outside the glass vial, sodium borohydride (319 mg, 8.43 mmol) and 0.200 mL of deionized water were added. The system was sealed and placed in an oven at 210 °C for 3 days. After 3 days, the autoclave was allowed to cool to room temperature on an aluminum block and opened. The mother liquor was removed by glass pipet, the product was washed with acetic acid (2 x 2 mL), isopropyl alcohol (2 x 2 mL), and diethyl ether (2 x 2 mL), then dried in air, revealing two crystalline solids: tan $Tc_2(O_2CCH_3)_4I$ and purple $K[Tc_8(\mu\text{-}I)_8I_4]I$ (144.1 mg total mass). An approximate 2:1 mixture of $Tc_2(O_2CCH_3)_4I$ and $K[Tc_8(\mu\text{-}I)_8I_4]I$ was estimated visually. The dark purple-black, elongated rectangular $K[Tc_8(\mu\text{-}I)_8I_4]I$ crystals are readily distinguishable to the naked eye from the light brown $Tc_2(O_2CCH_3)_4I$ crystals and were mechanically separated under a microscope.

5.2.2 ***Preparation of Tc_5I_{13}, or $Tc_5I_5(\mu\text{-}I)_4(\eta\text{-}I)_4$***

A weighed quantity of potassium pertechnetate (100 mg, 0.495 mmol) was placed in a glass vial and addition of 7.0 mL of hydroiodic acid then placed in a Parr Instruments 4749 autoclave. To the outside of the vial but inside the autoclave were added (250 mg, 6.61 mmol) of sodium borohydride and 200 μL of water. The autoclave was heated at 200 ºC for 72 hours removed and allowed to cool to room temperature, providing deep dark purple-black crystalline rectangular needles of Tc_5I_{13}, 70% yield. The composition of

Tc_5I_{13} was determined by technetium elemental analysis LSC and iodide titration (Anal. Calcd. for Tc_5I_{13}: Tc, 23.1; I, 76.9. Found: Tc, 22.9; I, 77.0). FT-IR (KBr) spectrum showed the absence of stretching modes from 4000 to 500 cm^{-1} confirming a no hydronium ion or hydrated species. Decomposition of the product in a sealed evacuated capillary tube occurs at temperatures above 290 °C to a grey metallic powder and headspace filled with purple iodine gas.

5.2.3 ***Analysis***

5.2.3.1 Single Crystal X-ray Diffraction

Dark purple rectangular crystals of $K[Tc_8(\mu\text{-}I)_8I_4]I$, and dark "black" purple needle-like crystals of Tc_5I_{13}, were obtained directly from the washed precipitate and mounted under Paratone on a Kaptan cryoloop for data collection. See Chapter 2 for instrumentation and analysis parameters for SC-XRD. Solution to the structure was performed by Direct Methods and refinement was carried out using SHELX [123] and OLEX2.[124] For $K[Tc_8(\mu\text{-}I)_8I_4]I$, the resulting data showed the crystal was a non-merohedral twin and refinement against both crystal domains was attempted but produced a substantially higher R-values after which refinement against a single merged domain provided an R-value of 0.0277. Crystallographic data and refinement parameters for each compound, $K[Tc_8(\mu\text{-}I)_8I_4]I$ and $Tc_5I_5(\mu\text{-}I)_4(\eta\text{-}I)_4$ are shown in Table **5.1**. Full details on crystallographic data for the structure of $K[Tc_8(\mu\text{-}I)_8I_4]I$ and $Tc_5I_5(\mu\text{-}I)_4(\eta\text{-}I)_4$ are tabled in Appendix B.

Table 5.1. Crystallographic data and refinement parameters for $K[Tc_8(\mu\text{-}I)_8I_4]I$ and $Tc_5I_5(\mu\text{-}I)_4(\eta\text{-}I)_4$.

Crystallographic data		
Empirical Formula	$I_{13}KTc_8$	$I_{13}Tc_5$
Formula weight	2480.08	2144.25
Temperature (K)	100	100
Wavelength (Å)	0.71073	0.71073
Crystal system	Monoclinic	Monoclinic
Space group	$P2_1/n$	$P2_1/n$
a (Å)	8.00180(5)	9.7648(9)
b (Å)	14.5125(10)	15.5838(15)
c (Å)	13.1948(9)	15.7621(13)
α (°)	90.00	90.00
β (°)	102.3090(10)	91.7520
γ (°)	90.00	90.00
V ($Å^3$)	1497.04(17)	2397.4(4)
Z	2	4
Density calc. ($Mg\ m^{-3}$)	5.486	5.928
Absorption coef. (mm^{-1})	17.114	19.536
F(000)	2104	3616
Range of 2θ (°)	2.113 – 28.281	1.838 – 28.282
Index ranges (*h, k, l*)	$-10 \le h \le 10$, $-19 \le k \le 19$, $-17 \le l \le 17$	$-13 \le h \le 13$, $-20 \le k \le 20$, $-21 \le l \le 21$
Reflections collected	5888	33760
Independent reflections	3710 [R(int) = 0.0277]	5940 [R(int) = 0.0473]
Complete to 2θ (%)	99.7	100.0
Refinement method	Full-matrix least-squares on F^2	Full-matrix least-squares on F^2
Data / restraints / parameters	3710 / 37 / 106	5940 / 0 / 163
Goodness-of-fit on F^2	1.092	1.086
Final R indices [$I > 2\sigma(I)$]	R1 = 0.0277, wR2 = 0.0564	R1 = 0.0269, wR2 = 0.0470
R indices (all data)	R1 = 0.0353, wR2 = 0.0588	R1 = 0.0361, wR2 = 0.0495

5.2.3.2 Elemental analyses

For ^{99}Tc elemental analyses using liquid scintillation counting, weighed amounts of the compounds (*ca.* 5 mg) were suspended in 5 mL of ammonium hydroxide for several days. After complete dissolution, the solutions were diluted to 10 mL with DI H_2O. Samples for LSC were prepared by mixing 100 µL of sample solution containing ^{99}Tc and 100 µL of DI H_2O, to correspond to calibration curves, with 10 mL of scintillation cocktail. ^{99}Tc concentrations were determined by LSC using a Perkin Elmer liquid scintillation counter Tri-Carb 3100TR. The scintillation cocktail was ULTIMA GOLD ABTM (Packard). US-EPA Method 345.1, explained in Chapter 2, was used to determine the amount of iodide.

5.3 **Results and discussion**

5.3.1 ***$K[Tc_8(\mu\text{-}I)_8I_4]I$***

The reaction of $KTcO_4$, with iodide salts and/or hydroiodic acid in glacial acetic acid at 210 °C under 60-70 atm hydrogen afforded $Tc_2(O_2CCH_3)_4I$ and $K[Tc_8(\mu\text{-}I)_8I_4]I$. Experiments performed in acetic acid with a Tc:MI molar ratio of 1:2 (M = K, Na, H) provided exclusively $Tc_2(O_2CCH_3)_4I$ in a ca. ~80-90% yield. Experiments performed with a Tc:MI:HI molar ratio of 1:1:3 provided a mixture of $K[Tc_8(\mu\text{-}I)_8I_4]I$ and $Tc_2(O_2CCH_3)_4I$. An approximate ratio of $Tc_2(O_2CCH_3)_4I$:$K[Tc_8(\mu\text{-}I)_8I_4]I$ of ~2:1 was visually estimated. Crystals of the individual compounds were hand separated under a microscope; $Tc_2(O_2CCH_3)_4I$ is light brown and $K[Tc_8(\mu\text{-}I)_8I_4]I$ is purple. See chapter 4 for other synthesis and characterization data on $Tc_2(O_2CCH_3)_4I$. The solid state structure of $K[Tc_8(\mu\text{-}I)_8I_4]I$ was

solved by single-crystal X-ray diffraction and crystallizes in the monoclinic space group $P2_1/n$ with a = 8.0018(5) Å, b = 14.5125(10) Å, c = 13.1948(9) Å, and β = 102.3090(10)°. The Tc-Tc separations in the $[Tc_8(\mu\text{-}I)_8I_4]$ cluster (i.e., 2.164(3) Å, 2.5308(8) Å and 2.72(3) Å) suggest the presence of Tc≡Tc triple bonds, Tc=Tc double bonds and Tc-Tc single bonds, shown in Figure **5.3**.

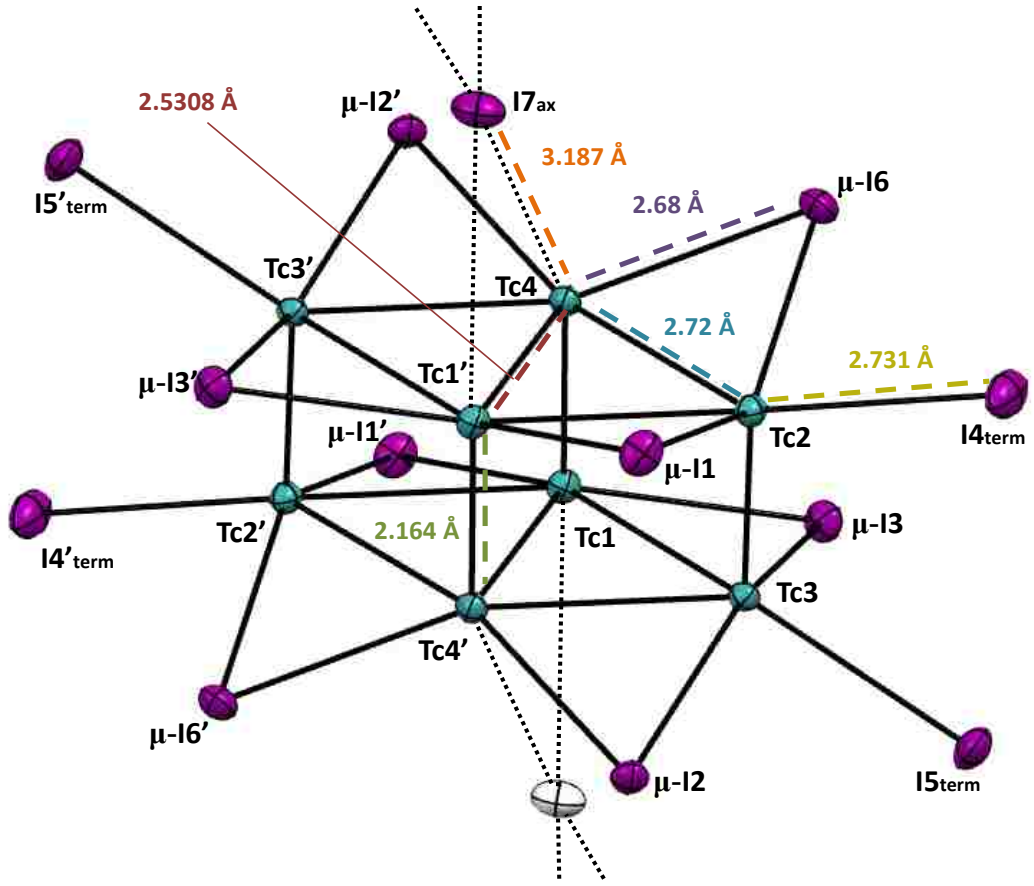

Figure 5.3. Ball and stick representation of $K[Tc_8(\mu\text{-}I)_8I_4]I$. Ellipsoids are shown at the 70% probability level with selected bond lengths (Å). Color of atoms: Tc in turquoise, K in white and I in purple.

The octanuclear technetium bromide clusters ($[H(H_2O)_2]_2\{[Tc_8((\mu\text{-}Br)_8Br_4]Br_2\}$, $[H(H_2O)_2]\{[Tc_8((\mu\text{-}Br)_8Br_4]Br\}$, and $\{[Tc_8(\mu\text{-}Br)_8Br_4]Br\}\cdot 2H_2O$) were synthesized from the reaction of $HTcO_4$ or H_2TcBr_6 with hydrobromic acid in autoclaves (30-50 atm hydrogen) in the temperature range 130-200 °C.[18] Previous attempts to synthesize iodide clusters from the hydrothermal reaction of $HTcO_4$ in HI at 140-220 °C under hydrogen were unsuccessful. Those reactions produced a small amount of black powder that was only characterized through elemental analysis as $TcI_2\cdot 0.5H_2O$.[180] In our reaction, the preferential formation of $K[Tc_8(\mu\text{-}I)_8I_4]I$ over a divalent iodide hydrate might be due to the presence of glacial acetic acid as a solvent which minimizes hydrolysis of the reaction products. The formation mechanism(s) of polynuclear technetium halide clusters under hydrothermal conditions are not well understood. It was previously postulated that the hexa- and octanuclear bromide and chloride clusters were formed from the cycloaddition of $Tc_2X_8^{n-}$ (n = 4, 5; X = Cl, Br) anions, but no experimental evidence has been provided.

The compound contains the tetragonal-prismatic $[Tc_8(\mu\text{-}I)_8I_4]$ cluster (Figure 5.3) and is the first octanuclear technetium cluster coordinated solely to iodide ligands to be reported. In the $[Tc_8(\mu\text{-}I)_8I_4]$ cluster, there are nominally four Tc(+2) atoms and four Tc(+1) atoms (44 cluster electrons). Three distinct metal-metal separations are observed: four short Tc-Tc bonds (2.164(3) Å) along the edges of the tetragonal pyramid, two Tc-Tc bonds forming the short diagonals of the prism faces (2.5308(8) Å), and eight longer Tc-Tc longer bonds (2.72(3) Å) forming the bases of the prism. The shortest metal-metal separation (2.164(3) Å) is characteristic of electron-rich Tc≡Tc

triple bonds, while the longest (2.72(3) Å) is characteristic of Tc-Tc single bonds. The Tc-Tc separations of 2.5308(8) Å suggest the presence of Tc=Tc double bonds (or at least Tc-Tc bonds with some degree of multiple bond character).[181] The overall geometry of the $[Tc_8(\mu\text{-}I)_8I_4]$ cluster is similar to the ones found in the $[Tc_8(\mu\text{-}Br)_8Br_4]^n$ (n = 0, 1) clusters. Within literature only one paper probing the metal-metal bonding in an octanuclear technetium cluster of the type described here.[175] Unfortunately, few details were provided. It would seem that $[Tc_8(\mu\text{-}X)_8X_4]$ clusters (X = Br, I) are prime targets for additional theoretical investigations. Selected interatomic bond distances for hexa-and octanuclear technetium bromide and iodide clusters are shown in Table 5.2. The shortest Tc-Tc separations in the isoelectronic $[Tc_8(\mu\text{-}Br)_8Br_4]$ cluster (i.e., 2.155(3) Å and 2.152(9) Å) are slightly shorter than the ones found in $[Tc_8(\mu\text{-}I)_8I_4]$. In the trigonal-prismatic $[Tc_6(\mu\text{-}I)_6I_6]^{1-}$ cluster,[54] the shortest Tc-Tc separation (2.18(1) Å) is slightly longer than the one in $[Tc_8(\mu\text{-}I)_8I_4]$. The $[Tc_8(\mu\text{-}I)_8I_4]$ cluster contains eight bridging ($Tc\text{-}I_{bri}$ = 2.68[3] Å) and four terminal ($Tc\text{-}I_{term}$ = 2.731[12] Å) iodide ligands. The $[Tc_8(\mu\text{-}I)_8I_4]$ cluster is also capped by one iodine atom, with the shortest $Tc\text{-}I_{cap}$ distance being 3.187(53) Å. The packing of the $[Tc_8(\mu\text{-}I)_8I_4]$ cluster within the unit cell (Figure **5.4**) along the *a*-axis and *b*-axis shows the rhombohedral face of the top half of the cluster. The shortest I···I separation between clusters is 3.7455(2) Å through terminal-equatorial iodide contacts, or somewhat less than the sum of the Van der Waals radii (~ 4.2 Å).[182]

Table 5.2. Selected Interatomic bond distances (Å) in hexa- and octanuclear technetium clusters

Compound [ref.]	Tc-Tc	Tc-Xterm	Tc-XBri	Tc-Xcap
$K[Tc_8(\mu\text{-}I)_8I_4]I$ [this work,162]	2.164/3/, 2.5308(8), 2.72/3/	2.731/12/	2.68/3/	3.187/53/
$[FeCp_2]_3\{Tc_6(\mu\text{-}I)_6I_6]I_2\}$[55]	2.18(1), 2.67(1)	2.71(1)	2.61/2/	3.26(2)
$[H(H_2O)_2]\{[Tc_8(\mu\text{-}Br)_8Br_4]Br\}$ [78,183]	2.155/3/, 2.531/2/ 2.70/2/	2.53/2/	2.51/2/	2.99/7/
$[H(H_2O)_2]_2\{[Tc_8(\mu\text{-}Br)_8Br_4]Br_2\}$ [78,183]	2.152/9/, 2.520/9/ 2.69(1)	2.52/1/	2.52/1/	2.90/2/
$[Tc_8(\mu\text{-}Br)_8Br_4]Br\cdot 2H_2O$ [76]	2.146(2), 2.521(2) 2.69/2/	2.509/8/	2.50/2/	3.00/7/

Standard errors are given in rounded brackets and deviations from mean values—/x/.

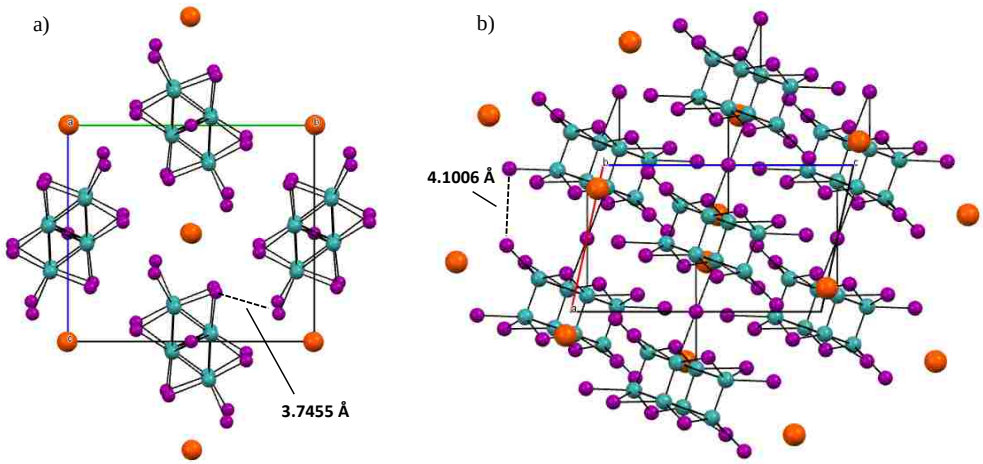

Figure 5.4. Unit cell packing along the (a) a-axis and (b) b-axis. Color of atoms: Tc in turquoise, I in purple and K in orange. The iodine-iodine Van der Waals distances for terminal-equatorial (a) and terminal-terminal (b) are shown.

5.3.2 ***Tc_5I_{13} compound: $(Tc_5(\mu\text{-}I)_4(\mu_3\text{-}I)_4I_5)$***

The compound Tc_5I_{13} is the first example of a pentanuclear binary halide within the group 7 elements. Rhenium has exhibited the pentanuclear Re_5 metal cluster in $Re_5(CO)_{14}(\mu_4\text{-}PMe)(\mu\text{-}PMe_2)(\mu_3\text{-}P[Re(CO)_5])$ but there are no known Re_5X_{13} (X = Cl, Br, I) clusters.[184]

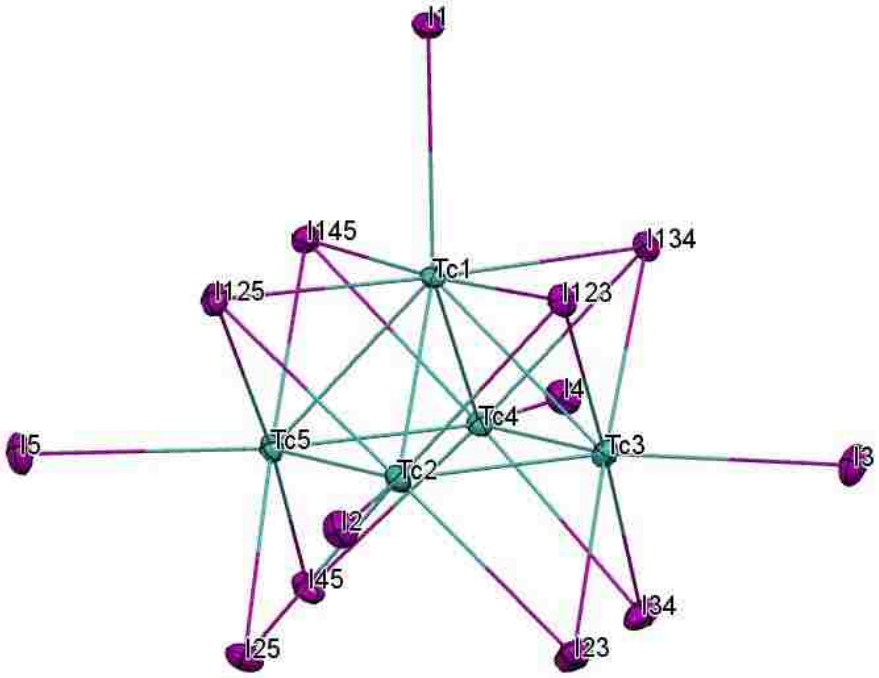

Figure 5.5. Ball and stick representation of $Tc_5(\mu\text{-}I)_4(\mu_3\text{-}I)_4I_5$ "Tc_5I_{13}". Ellipsoids are shown at the 70% probability level. Color of atoms: Tc in turquoise and I in purple.

The structure of the compound was investigated by SCXRD. An SEM image of the type of crystals picked for SC-XRD analysis shown in Figure 5.6, on the order of 100 µm in length. The compound contains a square-pyramidal technetium pentanuclear cluster with five terminal, four edge bridging, and four triangular face capping iodides as shown in Figure 5.5. Crystal data for Tc_5I_{13}: $P2_1/n$ [a = 9.7648(9) Å, b = 15.5838(15) Å, and c =

15.7621(15) Å; α = γ = 90°, β = 91.7520(14)°], R1 2.69%. The Tc-Tc bond distances of the square base (Tc_{2-5}) in the pyramid, Figure 5.5, have a large range of 2.6040 – 2.6557 Å suggesting that the bonds are sharing electrons evenly throughout the base of the pyramid. Whereas, Tc_1-Tc_x (x is Tc 2-5 of the square base) bonds from top of the pyramid to the square base (Tc_{2-5}) of the pyramid are a tighter range of 2.6470 – 2.6662 Å suggesting less electron sharing between Tc1 and the other Tc atoms in the pyramid

Table **5.3**. The Tc-Tc distances are more consistent with Tc-Tc rather than Tc=Tc bonding based on previous theoretical studies, it was shown the that Tc-Tc = 2.56 Å, Tc=Tc = 2.4 Å and Tc≡Tc = 2.20 Å.[181]

The Tc_5I_{13} cluster is isostructural with $[Mo_5Cl_{13}]^{2-}$ and $[W_5I_{13}]^{-1}$ anions and exhibits the same range of M—M bond lengths. [77,179] The only other known Tc-I polynuclear clusters are $\{[Tc_6I_6(\mu\text{-}I)_6]I_2\}^{3-}$ and $\{[Tc_8I_4(\mu\text{-}I)_8]I\}^{-}$ anions both containing triply bonded Tc atoms 2.18 Å and 2.164 Å respectively, connecting the a two triangular Tc_3 faces for a Tc_6 core and two Tc_4 rhomboidal units for Tc_8 core.[78,162] Tc_5I_{13} does not have such electron rich metal-metal bonds within the structure. The Tc-I bonding in Tc_5I_{13} has similar trends to the Mo-Cl and W-I bonding where the terminal metal-iodide bonds are longer then the bridging iodides. The trend is also seen in $\{[Tc_6I_6(\mu\text{-}I)_6]I_2\}^{3-}$ and $\{[Tc_8I_4(\mu\text{-}I)_8]I\}^{-}$ anions with terminal iodides as well.

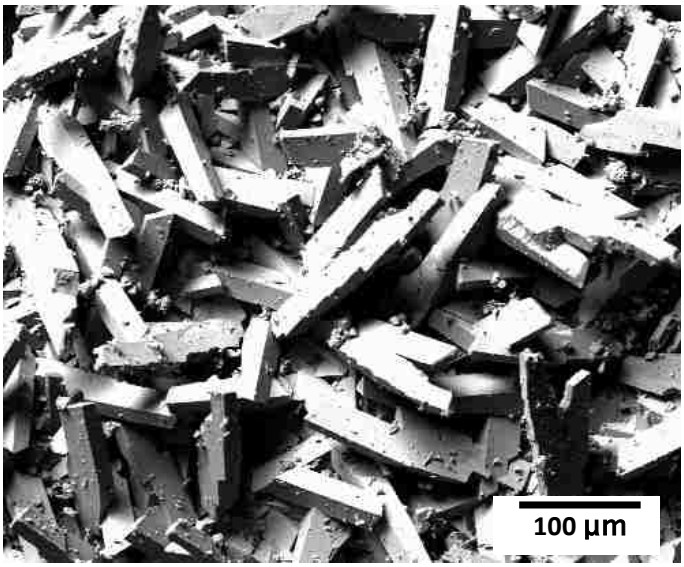

Figure 5.6. Tc_5I_{13} SEM image magnification x200 in backscattering mode.

Table 5.3. Selected Interatomic bond distances (Å) in penta-, hexa- and octanuclear molybdenum, tungsten, and technetium clusters.

Compound [ref.]	M-M (Å)	M-X terminal (Å)	Tc-X Bridged (Å)
$(Tc_5I_8)I_5$ [this work]	2.6470 – 2.6662(8)	2.7268 – 2.7670(8)	2.6851 – 2.7571(8)
$[Mo_5Cl_8)Cl_5]^{2-}$ [178]	2.602 – 2.563(3)	2.418 – 2.440	2.434 – 2.473
$[(W_5I_8)I_5]^-$ [179]	2.673 – 2.692 (1)	2.763 – 2.843 (2)	2.741 – 2.788(2)
$\{[Tc_6I_6(\mu\text{-}I)_6]I_2\}^{3-}$ [54]	2.18 – 2.67(1)	2.71(1)	2.61(2)
$\{[Tc_8I_4(\mu\text{-}I)_8]I\}^-$ [162]	2.164(3), 2.531(8), 2.72(3)	2.731(2)	2.68(3)

Multiple batches of Tc_5I_{13} were synthesized. On several occasions micro-crystalline powder was made and SEM images of those powders are shown in Figure **5**.**7**. Images A and C of Figure **5**.**7** are of powder like globes and to the naked eye looks as if the solid is black and metallic. At first glance it was thought to be Tc-metal powder but when high

magnification the material, seen in images B and D (under 20 um in length) proved to be Tc_5I_{13} in element ratio of 1:2.6, Tc:I; 23.1 wt.% technetium to 76.9 wt.% iodine determined by SEM-EDS. The SEM-EDS measurements indicate that there was no contribution from Tc-metal in the sample prepared for magnetic susceptibility measurements. The temperature dependence of the magnetic susceptibility of Tc_5I_{13} showed a paramagnetic behavior and data can be fitted with a modified Curie law, Figure **5.8** An effective magnetic moment of 0.43(2) μ_B was extracted from the fit. The relatively small value of the magnetic moment suggests a small fraction of unpaired electrons. A broad weak feature of unknown origin centered around 100 K was also observed.

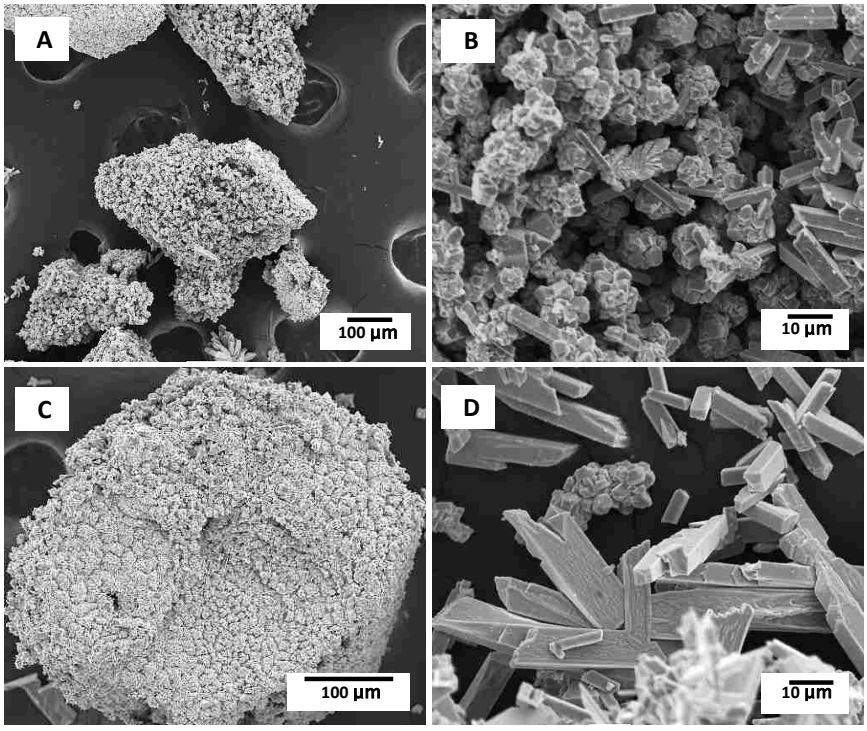

Figure 5.7. Tc_5I_{13} SEM images in secondary electron mode. A: magnification x100, B: magnification x1000, C: magnification x200, D: magnification x1000.

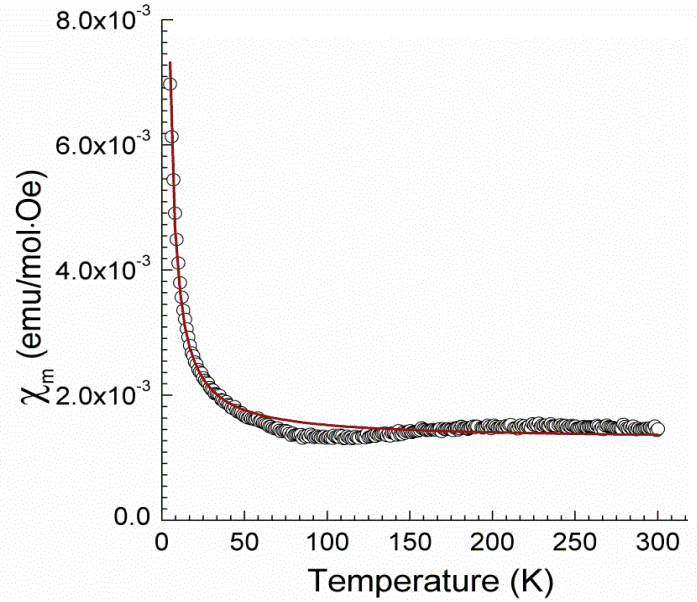

Figure 5.8. Magnetic susceptibility data of Tc_5I_{13} showing paramagnetic behavior.

5.4 **Conclusion**

In summary, two new technetium metal-metal bonded iodide cluster compounds (1) $K[Tc_8(\mu\text{-}I)_8I_4]I$, and (2) $Tc_5(\mu\text{-}I)_4(\mu_3\text{-}I)_4I_5$ "Tc_5I_{13}" were synthesized via the hydrothermal reduction of (1) $KTcO_4$ in acetic acid/MI (M = K, H) and (2) $KTcO_4$ in hydroiodic acid media, respectively and their X-ray crystal structures elucidated.

The compound $K[Tc_8(\mu\text{-}I)_8I_4]I$ is the first technetium iodide octanuclear cluster to be reported. The Tc-Tc separations in $K[Tc_8(\mu\text{-}I)_8I_4]I$ are consistent with the presence of Tc-Tc single bonds, Tc=Tc double bonds and Tc≡Tc triple bonds. Other routes to $M[Tc_8(\mu\text{-}I)_8I_4]I$ are being explored for weighable quantities and free of other solid products.

The compound $Tc_5(\mu\text{-}I)_4(\mu_3\text{-}I)_4I_5$ is the first pentanuclear technetium iodide cluster to be reported within the group 7 elements. The synthesis route to Tc_5I_{13} produces high yields of material which will allow for further experimental work on the compound.

Chapter 6: Conclusions and Future work

The goal of the work presented in this thesis was to revisit some Russian routes from the 1980's for synthesis of technetium metal-metal bonded compounds using hydrothermal technique. The synthesis and characterization of new technetium species helped to provide details and insight into fundamental technetium metal-metal bonded chemistry and potential applications. The M_2^{+n} carboxylate core "paddlewheel" and M_nX multi-cluster core chemistry for technetium was and still is poorly studied compared to that of its neighbors (Mo, Ru, Re and W). This work resulted in the synthesis and characterization of 7 new species; $Tc_2(O_2CCH_3)_4I$, $Tc_2(O_2CR)_4(\mu\text{-}O_2CR)$ where [R = $-CH_3$, $-CH_2CH_3$, $-C_6H_5$, $C(CH_3)_3$], $K[Tc_8(\mu\text{-}I)_8I_4]I$, and $Tc_5(\mu\text{-}I)_4(\mu_3\text{-}I)_4I_5$. In addition, the solid structures of $Tc_2(O_2CCH_3)_4Cl_2$ and $Tc_2(O_2CCH_3)_4Br_2$ were obtained, which were unknown. These 7 compounds were characterized by single crystal X-ray diffraction as well as various spectroscopic and physical techniques. This work described different synthesis routes to produce technetium metal-metal bond compounds from pertechnetate using hydrothermal techniques in a new and novel one-step method. A summary of the reactions pursued is shown in Figure **6.1**. The number of known technetium metal-metal bonded compounds forming polymeric chains has increased and lead to the characterization of 5 new compounds. This new chemistry indicated that a special type of structural motif is shared with ruthenium while it is not seen in other group 7 elements.

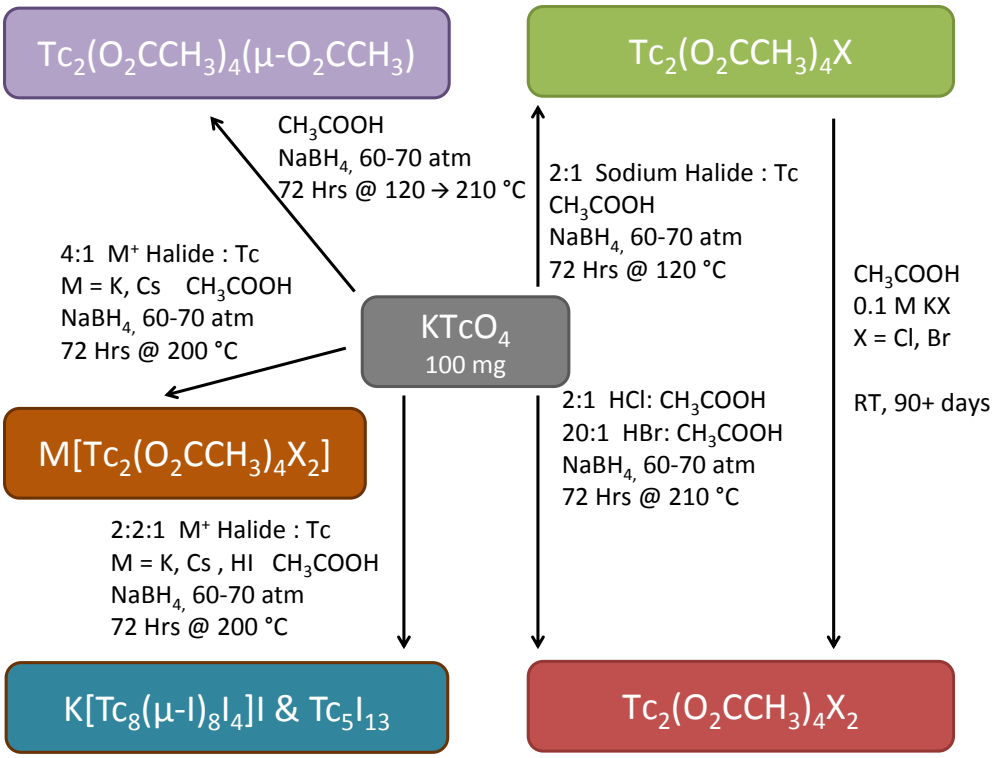

Figure 6.1. Summary of synthesis routes from pertechnetate explored using hydrothermal techniques to prepare technetium metal-metal bond compounds.

First, reactions involving the reduction of pertechnetate in carboxylic acid, under a 60-70 atmosphere of H_2 (obtained from the decomposition of $NaBH_4$) at moderate temperature (120 °C to 210 °C) for 72 hours lead to the formation of $Tc_2(O_2CR)_4(\mu\text{-}O_2CR)$ [R = $-CH_3$, $-CH_2CH_3$, $-C_6H_5$, $C(CH_3)_3$]. These compounds consists of infinite chains of $Tc_2(O_2CR)_4^+$ units linked by bridging carboxylic acid units.

When this reaction is performed in acetic acid, with a molar ratio of 2:1 for sodium halide:technetium under 60-70 atmosphere of H_2 at 120 °C the connector unit between the Tc_2^{5+} cores is a halide atom. For the first time, the structure of $Tc_2(O_2CCH_3)_4I$ has been determined and has an arrangement similar to the one found in the known $Tc_2(O_2CCH_3)_4X$ (X = Cl, Br), with a Tc_2^{5+} core unit and Tc-Tc bond of order 3.5. When

these compounds, $Tc_2(O_2CCH_3)_4X$ (X = Cl, Br), are left in vials at room temperature for over 3 months in a mixture of acetic acid and 0.1 M KCl or KBr the molecular dimeric crystals $Tc_2(O_2CCH_3)_4X_2$ (X = Cl, Br) are observed on the side wall of the vial. Unfortunately this reaction was not observed for the iodide species.

Molecular technetium metal-metal bond species have also been prepared for the first time with a reliable, high yield, simple method based on a modification of an earlier report in the Russian patent literature. The reaction involved the reduction of pertechnetate in acetic acid and HCl or HBr, under a 60-70 atmosphere of H_2 (obtained from $NaBH_4$) at 210 °C for 72 hours. The X-ray structures of $Tc_2(O_2CCH_3)_4X_2$ (X = Cl, Br) are reported for the first time and brings to 9 the total number of structurally characterized, quadruply bonded technetium(III) dimers. It is well known that $Tc_2(O_2CCH_3)_4Cl_2$ is used as a starting compound for various Tc(III) chloride compounds. With the easily preparation of $Tc_2(O_2CCH_3)_4Br_2$, expansion of Tc(III) bromide compounds is expected and currently being explored. Further investigation into synthesis of $Tc_2(O_2CCH_3)_4X_2$ (X = F, I) should be explored from TcX_6^{-2} anion and for the difluoride, a reaction with HF in acetic acid under the same conditions described in Section 3.2.1.

Molecular technetium metal-metal bonded salts have also been synthesized from the reduction of pertechnetate in acetic acid in presence of excess potassium or cesium halide under a 60-70 atmosphere of H_2 obtained from $NaBH_4$ at 200 °C for 72 hours, see Appendix A for more information. These reactions have not been fully characterized and thus were not presented in this work. As a result, the repeatability and the full characterization of these compounds should be performed in the near future.

Finally new polynuclear technetium iodides have been prepared and characterized. Reactions of pertechnetate under hydrothermal conditions provided the formation of two new technetium iodide clusters; $K[Tc_8(\mu\text{-}I)_8I_4]I$ and $Tc_5(\mu\text{-}I)_4(\mu_3\text{-}I)_4I_5$.

The compound $K[Tc_8(\mu\text{-}I)_8I_4]I$, is the first technetium iodide octanuclear cluster to be reported, and was synthesized via the hydrothermal reduction of $KTcO_4$ in acetic acid and MI (M = K, H) under a 60-70 atmosphere of H_2 at 210 °C for 72 hours. The Tc-Tc separations in $K[Tc_8(\mu\text{-}I)_8I_4]I$ are consistent with the presence of Tc-Tc single bonds, Tc=Tc double bonds and Tc≡Tc triple bonds similar to those of the known bromide compound, i.e., $(H_5O_2)[Tc_8(\mu\text{-}Br)_8Br_4]Br$.

The compound $Tc_5(\mu\text{-}I)_4(\mu_3\text{-}I)_4I_5$, the first pentanuclear technetium iodide cluster to be reported within the group 7 elements, was synthesized via the hydrothermal reduction of $KTcO_4$ in hydroiodic acid media 60-70 atmosphere of H_2 obtained from $NaBH_4$ at 210 °C for 72 hours. The metal-metal separation in Tc_5I_{13} is primarily consistent with the presence of Tc-Tc single bonds. Nevertheless, theoretical calculation needs to be performed in order to determine the Tc-Tc bond order within the Tc_5^{13+} core. Due to its yield formation, the compound can be used as a precursor in inorganic chemistry. One of the challenges will be to derive Tc_5I_{13} in order to obtain soluble salts containing the Tc_5I_{13} unit. One reaction that was pressured to solubilize Tc_5I_{13} was to react with $NOPF_6$ in dichloromethane but no suitable product was obtained but the reaction was conducted in open air, so future studies should investigate argon atmosphere reaction.

Future challenges include the synthesis and characterization of $Tc_2(O_2CCH_3)_4I_2$. Most of the chemistry accomplished in chapters 3-5, was in some way directly related to completing this challenge. It is our view that there is more technetium cluster chemistry to be discovered.

APPENDIX A **: Tc-Tc Dimer Salts**

A.1 ***Background***

First reported acetate paddlewheel dimer salt of technetium was potassium tetraacetatedichloroditechnetium(III, II); $K[Tc_2(O_2CCH_3)_4Cl_2]$ by Spitsyn 1981 in a mixture of other compounds such as, $Tc_2(O_2CCH_3)_4Cl$, K_2TcCl_6, and KCl. The compound was synthesis by two different routes starting from $K_3[Tc_2Cl_8]\cdot 2H_2O$; (1) under 30 atmosphere argon at 110 °C in acetic acid for 2 hours, and (2) under 30 atmosphere molecular hydrogen at 120 °C in acetic acid for 20 hours and in both instances the crystals were separated by microscope.[164] Single crystal data obtained by Koz'min 1981 for the $Tc_2(O_2CCH_3)_4Cl$, and 1982 for the $K[Tc_2(O_2CCH_3)_4Cl_2]$.[45,69] The compound $K[Tc_2(O_2CCH_3)_4Cl_2]$ crystallizes in the tetragonal space group $P4_2/n$; a = b = 11.9885(3) Å, c = 11.2243(2) Å. The reported Tc-Tc bond distance for $K[Tc_2(O_2CCH_3)_4Cl_2]$ is 2.1260(5) Å, and Tc-Tc-Cl bond angle of 175.90(5)° similar to other Tc_2^{+5} core compounds, $[Tc_2(O_2CCH_3)_4X_2]^-$, X = Br, discussed below in Section A.2 and A.3.

A.2 ***Experimental***

The compounds: $K[Tc_2(O_2CCH_3)_4Br_2]$, $Cs[Tc_2(O_2CCH_3)_4Br_2]$, and $Cs[Tc_2(O_2CCH_3)_4I_2]$ were synthesized by the reaction of $KTcO_4$, potassium iodide or cesium iodide with a molar ratio of 1:4 technetium:iodide under same conditions sections 3.2.1, and 4.2.1. Single crystal XRD data was obtained and tabulated in Appendix B, Sections B10-12. No

further characterization was performed. The basic structure of the $M[Tc_2(O_2CCH_3)_4X_2]$, (where M = K, Cs; and X = Br, I) is shown in Figure A.**1**.

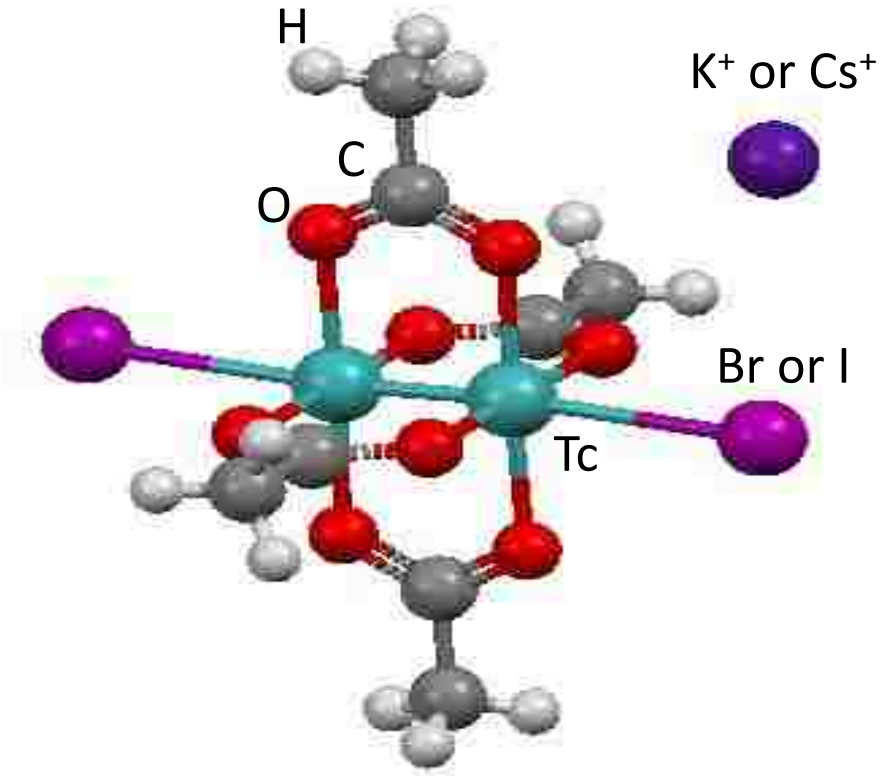

Figure A.1. Ball and stick model $M[Tc_2(O_2CCH_3)_4X_2]$, where M = K, Cs; and X = Br, I. Color of atoms: Tc in turquoise, C in dark gray, H in light gray, O in red, Br/I in light purple, and K/Cs in dark purple.

A.3 ***Discussion/Conclusion***

The compounds synthesized; $K[Tc_2(O_2CCH_3)_4Br_2]$, $Cs[Tc_2(O_2CCH_3)_4Br_2]$, and $Cs[Tc_2(O_2CCH_3)_4I_2]$ crystallize in the tetragonal space group $P4_2/n$, same as in $K[Tc_2(O_2CCH_3)_4Cl_2]$. The Tc-Tc bond distances and selected bond angles have been tabulated in Table A.**1**. The Tc-Tc bonds are consitant throughout the structures with

very little deviation average about 2.127 Å for the Tc_2^{+5} core with electronic configuration of $\sigma^2\pi^4\delta^2\delta^{*2}\pi^{*1}$. The Tc-Tc-X bond angle seems to broadened with the increase in ionic size for cation (K^+ to Cs^+) by ~ 2°, from 175 to 173°, again a non-linear Tc-Tc-X bond angle as seen through the Tc_2^{+n}, (n= 5, 6) tetraacetate paddlewheels.

Table A.1. Selected bond distances (Å) and bond angles (°) for $M[Tc_2(O_2CCH_3)_4X_2]$, (where M = K, Cs; and X = Cl, Br, I). corresponds to the work presented in this appendix.*

Compound [ref.]	*d* M-M	*d* M-X	*d* M-O (av.)	M-M-X
$K[Tc_2(O_2CCH_3)_4Cl_2]$[164]	2.1260(5)	2.589(1)	2.07	175.90(5)
$K[Tc_2(O_2CCH_3)_4Br_2]$[*]	2.1274(3)	2.7467(3)	2.060(13)	175.608(12)
$Cs[Tc_2(O_2CCH_3)_4Br_2]$[*]	2.1298(3)	2.7453(3)	2.068(16)	173.744(14)
$Cs[Tc_2(O_2CCH_3)_4I_2]$[*]	2.1275(4)	2.9813(3)	2.067(16)	173.735(13)

APPENDIX B **: Crystal structures**

B.1 ***$Tc_2(O_2CCH_3)_4Cl_2$***

Single crystal X-ray diffraction data for the structural analysis has been deposited with the Cambridge Crystallographic Data Centre, CCDC No. 890709. Copies of this information may be obtained free of charge from the Director, CCDC, 12 Union Road, Cambridge, CB2 1EZ, UK (fax: +44 1223 336033; email: deposit@ccdc.cam.ac.uk or www.ccdc.cam.ac.uk). Crystallographic data are given in Table B.**1** and Table B.**4**.

Table B.1. Crystal data and structure refinement for $Tc_2(O_2CCH_3)_4Cl_2$.

Empirical formula	C8H12Cl2O8Tc2	
Formula weight	504.90	
Temperature	100 K	
Wavelength	0.71073 Å	
Crystal system	Monoclinic	
Space group	P 21/n	
Unit cell dimensions	a = 6.4258(8) Å	α = 90°.
	b = 8.8474(11) Å	β = 90.778(2)°.
	c = 12.5285(16) Å	γ = 90°.
Volume	712.20(15) $Å^3$	
Z	2	
Density (calculated)	2.346 Mg/m^3	
Absorption coefficient	2.346 mm^{-1}	
F(000)	488	
Crystal size	0.05 x 0.05 x 0.05 mm^3	
Theta range for data collection	2.82 to 30.51°.	
Index ranges	-9<=h<=9, -12<=k<=12, -17<=l<=17	
Reflections collected	11170	
Independent reflections	2169 [R(int) = 0.0277]	
Completeness to theta = 25.242°	100.0%	
Absorption correction	Semi-empirical from equivalents	

Max. and min. transmission	0.9703 and 0.8457
Refinement method	Full-matrix least-squares on F^2
Data / restraints / parameters	2169 / 0 / 93
Goodness-of-fit on F^2	1.076
Final R indices [I>2sigma(I)]	R1 = 0.0180, wR2 = 0.0467
R indices (all data)	R1 = 0.0204, wR2 = 0.0476
Largest diff. Peak and hole	1.119 and -0.657 $e.A^{-3}$

Table B.2. Atomic coordinates (x 10^4) and equivalent isotropic displacement parameters ($Å^2$ x 10^3) for $Tc_2(O_2CCH_3)_4Cl_2$. U(eq) is defined as one third of the trace of the orthogonalized U^{ij} tensor.

	x	y	z	U(eq)
Tc(1)	1033(1)	768(1)	9584(1)	9(1)
Cl(1)	3770(1)	2232(1)	8620(1)	14(1)
O(3)	2687(2)	-1075(1)	9109(1)	12(1)
O(1)	-722(2)	620(1)	8241(1)	12(1)
O(2)	-2766(2)	-1015(1)	9064(1)	12(1)
C(3)	2168(3)	-2401(2)	9398(1)	11(1)
O(4)	567(2)	-2608(1)	9986(1)	12(1)
C(2)	-3471(3)	-512(2)	7216(1)	15(1)
C(1)	-2284(2)	-279(2)	8226(1)	11(1)
C(4)	3415(3)	-3724(2)	9059(1)	15(1)

Table B.3. Bond lengths (Å) and angles (°) for $Tc_2(O_2CCH_3)_4Cl_2$.

Tc(1)-O(4)#1	2.0034(12)
Tc(1)-O(1)	2.0164(12)
Tc(1)-O(2)#1	2.0259(12)
Tc(1)-O(3)	2.0390(12)
Tc(1)-Tc(1)#1	2.1758(3)
Tc(1)-Cl(1)	2.5078(4)
O(3)-C(3)	1.274(2)
O(1)-C(1)	1.281(2)
O(2)-C(1)	1.277(2)
O(2)-Tc(1)#1	2.0259(12)

C(3)-O(4)	1.287(2)
C(3)-C(4)	1.484(2)
O(4)-Tc(1)#1	2.0034(12)
C(2)-C(1)	1.483(2)
O(4)#1-Tc(1)-O(1)	89.63(5)
O(4)#1-Tc(1)-O(2)#1	88.05(5)
O(1)-Tc(1)-O(2)#1	177.47(5)
O(4)#1-Tc(1)-O(3)	178.42(5)
O(1)-Tc(1)-O(3)	89.59(5)
O(2)#1-Tc(1)-O(3)	92.71(5)
O(4)#1-Tc(1)-Tc(1)#1	93.44(4)
O(1)-Tc(1)-Tc(1)#1	91.22(4)
O(2)#1-Tc(1)-Tc(1)#1	89.92(4)
O(3)-Tc(1)-Tc(1)#1	87.95(4)
O(4)#1-Tc(1)-Cl(1)	94.33(4)
O(1)-Tc(1)-Cl(1)	91.12(4)
O(2)#1-Tc(1)-Cl(1)	88.05(4)
O(3)-Tc(1)-Cl(1)	84.31(4)
Tc(1)#1-Tc(1)-Cl(1)	171.903(13)
C(3)-O(3)-Tc(1)	120.94(11)
C(1)-O(1)-Tc(1)	118.83(11)
C(1)-O(2)-Tc(1)#1	119.75(10)
O(3)-C(3)-O(4)	120.57(15)
O(3)-C(3)-C(4)	120.03(15)
O(4)-C(3)-C(4)	119.39(15)
C(3)-O(4)-Tc(1)#1	117.09(10)
O(2)-C(1)-O(1)	120.15(15)
O(2)-C(1)-C(2)	120.23(15)
O(1)-C(1)-C(2)	119.56(15)

Symmetry transformations used to generate equivalent atoms:
#1 -x+1,-y,-z+2

Table B.4. Anisotropic displacement parameters ($Å^2 x\ 10^3$) for $Tc_2(O_2CCH_3)_4Cl_2$. The anisotropic displacement factor exponent takes the form: $-2p^2[h^2\ a^{*2}U^{11} + ... + 2\ h\ k\ a^*\ b^*\ U^{12}]$.

	U^{11}	U^{22}	U^{33}	U^{23}	U^{13}	U^{12}
Tc(1)	9(1)	9(1)	8(1)	0(1)	1(1)	-1(1)
Cl(1)	15(1)	14(1)	15(1)	0(1)	3(1)	-3(1)
O(3)	12(1)	12(1)	12(1)	0(1)	1(1)	1(1)
O(1)	13(1)	14(1)	9(1)	0(1)	-1(1)	-1(1)
O(2)	12(1)	13(1)	10(1)	0(1)	-1(1)	-1(1)
C(3)	13(1)	12(1)	9(1)	-2(1)	-2(1)	0(1)
O(4)	14(1)	10(1)	11(1)	1(1)	2(1)	1(1)
C(2)	15(1)	19(1)	11(1)	-2(1)	-3(1)	0(1)
C(1)	12(1)	12(1)	10(1)	-2(1)	0(1)	2(1)
C(4)	18(1)	13(1)	15(1)	-2(1)	0(1)	4(1)

B.2 ***$Tc_2(O_2CCH_3)_4Br_2$***

Single crystal X-ray diffraction data for $Tc_2(O_2CCH_3)_4Br_2$ has been deposited with the Cambridge Crystallographic Data Centre, CCDC No. 897437. Copies of this information may be obtained free of charge from the Director, CCDC, 12 Union Road, Cambridge, CB2 1EZ, UK (fax: +44 1223 336033; email: deposit@ccdc.cam.ac.uk or www.ccdc.cam.ac.uk). Crystallographic data are given in Table B.**5** and Table B.**9**.

Table B.5. Crystal data and structure refinement for $Tc_2(O_2CCH_3)_4Br_2$.

Identification code	bk_tc2oac4br2_0m_a	
Empirical formula	C8 H12 Br2 O8 Tc2	
Formula weight	593.8	
Temperature	100(2) K	
Wavelength	0.71073 Å	
Crystal system	Monoclinic	
Space group	P2(1)/n	
Unit cell dimensions	a = 6.5299(7) Å	α= 90°.
	b = 9.0483(9) Å	β= 90.718(2)°.

	c = 12.5915(13) Å γ = 90°.
Volume	743.90(13) $Å^3$
Z	2
Density (calculated)	2.643 Mg/m^3
Absorption coefficient	7.259 mm^{-1}
F(000)	560
Crystal size	0.08 x 0.03 x 0.03 mm^3
Theta range for data collection	2.77 to 30.51°.
Index ranges	-9<=h<=9,-12<=k<=12,-17<=l<=17
Reflections collected	11863
Independent reflections	2265 [R(int) = 0.0280]
Completeness to theta = 30.51°	100.0%
Absorption correction	Semi-empirical from equivalents
Max. and min. transmission	0.7462 and 0.5214
Refinement method	Full-matrix least-squares on F^2
Data / restraints / parameters	2265 / 0 / 93
Goodness-of-fit on F^2	1.046
Final R indices [I>2sigma(I)]	R1 = 0.0184, wR2 = 0.0400
R indices (all data)	R1 = 0.0219, wR2 = 0.0409
Largest diff. peak and hole	0.567 and -0.528 $e.Å^{-3}$

Table B.6. Atomic coordinates (x 10^4) and equivalent isotropic displacement parameters ($Å^2$ x 10^3) for $Tc_2(O_2CCH_3)_4Br_2$. U(eq) is defined as one third of the trace of the orthogonalized U^{ij} tensor.

	x	y	z	U(eq)
Tc(1)	6010(1)	4247(1)	9583(1)	7(1)
Br(1)	8774(1)	2658(1)	8556(1)	12(1)
O(4)	5711(2)	5578(2)	11756(1)	10(1)
O(3)	7715(2)	3986(2)	10922(1)	11(1)
O(2)	2308(2)	3970(2)	10873(1)	11(1)
O(1)	4383(2)	2464(2)	10006(1)	11(1)
C(1)	2809(3)	2671(2)	10586(2)	10(1)
C(3)	7252(3)	4698(2)	11764(2)	10(1)
C(2)	1561(3)	1386(2)	10917(2)	14(1)
C(4)	8448(3)	4468(2)	12758(2)	14(1)

Table B.7. Bond lengths (Å) and angles (°) for $Tc_2(O_2CCH_3)_4Br_2$.

Tc(1)-O(1)	2.0078(14)
Tc(1)-O(4)#1	2.0202(14)
Tc(1)-O(3)	2.0230(14)
Tc(1)-O(2)#1	2.0380(14)
Tc(1)-Tc(1)#1	2.1764(3)
Tc(1)-Br(1)	2.6554(3)
O(4)-C(3)	1.283(2)
O(4)-Tc(1)#1	2.0202(14)
O(3)-C(3)	1.280(2)
O(2)-C(1)	1.274(2)
O(2)-Tc(1)#1	2.0380(14)
O(1)-C(1)	1.282(2)
C(1)-C(2)	1.483(3)
C(3)-C(4)	1.482(3)
O(1)-Tc(1)-O(4)#1	89.64(6)
O(1)-Tc(1)-O(3)	88.41(6)
O(4)#1-Tc(1)-O(3)	177.77(6)
O(1)-Tc(1)-O(2)#1	178.72(6)
O(4)#1-Tc(1)-O(2)#1	89.96(6)
O(3)-Tc(1)-O(2)#1	91.96(6)
O(1)-Tc(1)-Tc(1)#1	92.80(4)
O(4)#1-Tc(1)-Tc(1)#1	91.12(4)
O(3)-Tc(1)-Tc(1)#1	90.05(4)
O(2)#1-Tc(1)-Tc(1)#1	88.42(4)
O(1)-Tc(1)-Br(1)	93.41(4)
O(4)#1-Tc(1)-Br(1)	90.61(4)
O(3)-Tc(1)-Br(1)	88.43(4)
O(2)#1-Tc(1)-Br(1)	85.39(4)
Tc(1)#1-Tc(1)-Br(1)	173.563(12)
C(3)-O(4)-Tc(1)#1	118.91(13)
C(3)-O(3)-Tc(1)	119.93(13)
C(1)-O(2)-Tc(1)#1	120.62(13)
C(1)-O(1)-Tc(1)	117.68(12)
O(2)-C(1)-O(1)	120.48(17)
O(2)-C(1)-C(2)	119.96(18)

O(1)-C(1)-C(2)	119.57(18)
O(3)-C(3)-O(4)	119.92(18)
O(3)-C(3)-C(4)	120.13(18)
O(4)-C(3)-C(4)	119.92(18)

Symmetry transformations used to generate equivalent atoms:
#1 -x+1,-y+1,-z+2

Table B.8. Anisotropic displacement parameters ($Å^2$x 10^3) for $Tc_2(O_2CCH_3)_4Br_2$. The anisotropic displacement factor exponent takes the form: $-2p^2[h^2 a^{*2}U^{11} + ... + 2 h k a^* b^* U^{12}]$.

	U^{11}	U^{22}	U^{33}	U^{23}	U^{13}	U^{12}
Tc(1)	7(1)	7(1)	8(1)	0(1)	1(1)	1(1)
Br(1)	12(1)	11(1)	14(1)	-1(1)	3(1)	3(1)
O(4)	10(1)	10(1)	10(1)	0(1)	0(1)	1(1)
O(3)	10(1)	11(1)	12(1)	0(1)	0(1)	1(1)
O(2)	10(1)	10(1)	12(1)	0(1)	2(1)	-2(1)
O(1)	12(1)	9(1)	11(1)	-1(1)	0(1)	-1(1)
C(1)	11(1)	11(1)	9(1)	2(1)	-2(1)	0(1)
C(3)	10(1)	10(1)	11(1)	2(1)	1(1)	-4(1)
C(2)	17(1)	11(1)	14(1)	3(1)	-1(1)	-5(1)
C(4)	13(1)	17(1)	11(1)	3(1)	-3(1)	0(1)

Table B.9. Hydrogen coordinates (x 10^4) and isotropic displacement parameters ($Å^2$ x 10^3) for $Tc_2(O_2CCH_3)_4Br_2$.

	x	y	z	U(eq)
H(2A)	1697	1250	11687	21
H(2B)	2039	496	10554	21
H(2C)	120	1564	10730	21
H(4A)	8452	5382	13176	20
H(4B)	9859	4199	12585	20
H(4C)	7825	3672	13172	20

B.3 ***$Tc_2(O_2CCH_3)_3Cl_2(H_2O)_2 \cdot H_2O$***

Single crystal X-ray diffraction data for $Tc_2(O_2CCH_3)_3Cl_2(H_2O)_2 \cdot H_2O$ has not been deposited with the Cambridge Crystallographic Data Centre. Crystallographic data are given in Table B.**10** and Table B.**14**.

Table B.10. Crystal data and structure refinement for $Tc_2(O_2CCH_3)_3Cl_2(H_2O)_2 \cdot H_2O$.

Identification code	bk_tc2_ac_4_cl2_k_0m
Empirical formula	C6 H15 Cl2 O9 Tc2
Formula weight	499.90
Temperature	100(2) K
Wavelength	0.71073 Å
Crystal system	Monoclinic
Space group	P 21
Unit cell dimensions	a = 7.7102(7) α= 90°.
	b = 11.4786(11) Å β= 94.8430(10)°.
	c = 8.3468(8) Å γ = 90°.
Volume	736.07(12) $Å^3$
Z	2
Density (calculated)	2.256 Mg/m^3
Absorption coefficient	2.273 mm^{-1}
F(000)	486
Crystal size	0.06 x 0.04 x 0.04 mm^3
Theta range for data collection	2.45 to 31.50°.
Index ranges	-11<=h<=11, -16<=k<=16, -12<=l<=12
Reflections collected	12743
Independent reflections	4868 [R(int) = 0.0203]
Completeness to theta = 31.50°	100.0%
Refinement method	Full-matrix least-squares on F^2
Data / restraints / parameters	4868 / 4 / 194
Goodness-of-fit on F^2	1.027
Final R indices [I>2sigma(I)]	R1 = 0.0152, wR2 = 0.0363
R indices (all data)	R1 = 0.0157, wR2 = 0.0365

Absolute structure parameter	0.00(14)
Largest diff. peak and hole	0.723 and -0.364 e.Å^{-3}

Table B.11. Atomic coordinates (x 10^4) and equivalent isotropic displacement parameters (Å^2 x 10^3) for $Tc_2(O_2CCH_3)_3Cl_2(H_2O)_2 \cdot H_2O$. U(eq) is defined as one third of the trace of the orthogonalized U^{ij} tensor.

	x	y	z	U(eq)
Tc(1)	1060(1)	7544(1)	7039(1)	8(1)
Tc(2)	2387(1)	9037(1)	6299(1)	8(1)
Cl(1)	2845(1)	5961(1)	6413(1)	13(1)
Cl(2)	5008(1)	8394(1)	5356(1)	12(1)
O(1)	1088(2)	8939(1)	4004(1)	11(1)
O(4)	2280(2)	7661(2)	9319(2)	12(1)
O(3)	3651(2)	9244(1)	8539(2)	12(1)
O(2)	-362(2)	7412(1)	4826(1)	11(1)
O(5)	440(2)	10104(1)	6993(2)	12(1)
O(7)	-681(2)	6035(1)	8052(2)	14(1)
O(6)	-943(2)	8544(1)	7805(2)	12(1)
C(5)	-850(2)	9646(2)	7618(2)	11(1)
O(9)	-3774(2)	6938(1)	8699(2)	19(1)
C(1)	-57(2)	8143(2)	3733(2)	11(1)
C(2)	-1017(3)	8068(2)	2108(2)	16(1)
C(3)	3329(2)	8509(2)	9617(2)	11(1)
C(4)	4190(3)	8632(2)	11276(2)	17(1)
O(8)	3257(2)	10895(1)	5481(2)	19(1)
C(6)	-2251(2)	10409(2)	8152(3)	16(1)

Table B.12. Bond lengths (Å) and angles (°) for $Tc_2(O_2CCH_3)_3Cl_2(H_2O)_2 \cdot H_2O$.

Tc(1)-O(4)	2.0549(12)
Tc(1)-O(6)	2.0683(13)
Tc(1)-O(2)	2.0719(12)
Tc(1)-Tc(2)	2.1152(2)
Tc(1)-Cl(1)	2.3643(5)
Tc(1)-O(7)	2.3884(15)
Tc(2)-O(3)	2.0480(13)

Tc(2)-O(5)	2.0579(13)
Tc(2)-O(1)	2.0887(12)
Tc(2)-Cl(2)	2.3481(5)
Tc(2)-O(8)	2.3543(14)
O(1)-C(1)	1.277(2)
O(4)-C(3)	1.277(2)
O(3)-C(3)	1.273(2)
O(2)-C(1)	1.276(2)
O(5)-C(5)	1.275(2)
O(6)-C(5)	1.277(2)
C(5)-C(6)	1.489(2)
C(1)-C(2)	1.491(2)
C(3)-C(4)	1.491(3)
O(4)-Tc(1)-O(6)	88.44(5)
O(4)-Tc(1)-O(2)	175.29(5)
O(6)-Tc(1)-O(2)	87.91(5)
O(4)-Tc(1)-Tc(2)	91.27(4)
O(6)-Tc(1)-Tc(2)	91.88(4)
O(2)-Tc(1)-Tc(2)	91.81(4)
O(4)-Tc(1)-Cl(1)	91.45(4)
O(6)-Tc(1)-Cl(1)	163.45(4)
O(2)-Tc(1)-Cl(1)	91.21(4)
Tc(2)-Tc(1)-Cl(1)	104.661(14)
O(4)-Tc(1)-O(7)	86.94(5)
O(6)-Tc(1)-O(7)	80.59(6)
O(2)-Tc(1)-O(7)	89.54(5)
Tc(2)-Tc(1)-O(7)	172.31(4)
Cl(1)-Tc(1)-O(7)	82.88(4)
O(3)-Tc(2)-O(5)	88.62(5)
O(3)-Tc(2)-O(1)	176.41(7)
O(5)-Tc(2)-O(1)	89.16(5)
O(3)-Tc(2)-Tc(1)	91.85(4)
O(5)-Tc(2)-Tc(1)	91.00(4)
O(1)-Tc(2)-Tc(1)	91.00(4)
O(3)-Tc(2)-Cl(2)	89.20(4)
O(5)-Tc(2)-Cl(2)	161.79(4)
O(1)-Tc(2)-Cl(2)	92.03(4)

Tc(1)-Tc(2)-Cl(2)	107.142(13)
O(3)-Tc(2)-O(8)	91.97(5)
O(5)-Tc(2)-O(8)	77.00(5)
O(1)-Tc(2)-O(8)	84.79(6)
Tc(1)-Tc(2)-O(8)	167.30(4)
Cl(2)-Tc(2)-O(8)	85.02(4)
C(1)-O(1)-Tc(2)	118.16(12)
C(3)-O(4)-Tc(1)	117.62(12)
C(3)-O(3)-Tc(2)	117.51(12)
C(1)-O(2)-Tc(1)	118.28(12)
C(5)-O(5)-Tc(2)	118.87(12)
C(5)-O(6)-Tc(1)	117.43(12)
O(5)-C(5)-O(6)	120.82(17)
O(5)-C(5)-C(6)	119.40(17)
O(6)-C(5)-C(6)	119.78(16)
O(2)-C(1)-O(1)	120.66(16)
O(2)-C(1)-C(2)	120.32(16)
O(1)-C(1)-C(2)	119.01(16)
O(3)-C(3)-O(4)	121.72(16)
O(3)-C(3)-C(4)	119.71(16)
O(4)-C(3)-C(4)	118.57(16)

Symmetry transformations used to generate equivalent atoms:

Table B.13. Anisotropic displacement parameters ($Å^2$x 10^3) for $Tc_2(O_2CCH_3)_3Cl_2(H_2O)_2 \cdot H_2O$. The anisotropic displacement factor exponent takes the form: $-2p^2[h^2 a^{*2}U^{11} + ... + 2 h k a^* b^* U^{12}]$.

	U^{11}	U^{22}	U^{33}	U^{23}	U^{13}	U^{12}
Tc(1)	8(1)	7(1)	9(1)	0(1)	1(1)	0(1)
Tc(2)	8(1)	7(1)	9(1)	1(1)	1(1)	0(1)
Cl(1)	13(1)	9(1)	19(1)	0(1)	3(1)	2(1)
Cl(2)	10(1)	13(1)	13(1)	1(1)	3(1)	2(1)
O(1)	12(1)	11(1)	11(1)	1(1)	1(1)	0(1)
O(4)	12(1)	13(1)	12(1)	2(1)	1(1)	-1(1)
O(3)	10(1)	14(1)	13(1)	0(1)	1(1)	-2(1)
O(2)	11(1)	10(1)	12(1)	0(1)	0(1)	-1(1)
O(5)	12(1)	8(1)	16(1)	0(1)	3(1)	0(1)
O(7)	13(1)	11(1)	20(1)	-1(1)	4(1)	-1(1)

O(6)	10(1)	10(1)	14(1)	-1(1)	3(1)	0(1)
C(5)	10(1)	12(1)	10(1)	-1(1)	0(1)	0(1)
O(9)	16(1)	17(1)	24(1)	3(1)	4(1)	-2(1)
C(1)	10(1)	10(1)	12(1)	-2(1)	1(1)	3(1)
C(2)	17(1)	19(1)	11(1)	-1(1)	-3(1)	0(1)
C(3)	9(1)	14(1)	10(1)	-1(1)	1(1)	1(1)
C(4)	16(1)	24(1)	12(1)	-2(1)	-2(1)	-2(1)
O(8)	14(1)	11(1)	33(1)	7(1)	7(1)	2(1)
C(6)	12(1)	14(1)	22(1)	-3(1)	6(1)	2(1)

Table B.14. Hydrogen coordinates (x 10^4) and isotropic displacement parameters ($Å^2$ x 10^3) for $Tc_2(O_2CCH_3)_3Cl_2(H_2O)_2 \cdot H_2O$.

	x	y	z	U(eq)
H(1O7)	-820(30)	5460(17)	7540(30)	17
H(2O7)	-1570(30)	6250(20)	8270(30)	17
H(1O9)	-4510(30)	6570(20)	8420(30)	23
H(2O9)	-3610(30)	7490(30)	8220(30)	23
H(2A)	-1831	7411	2081	24
H(2B)	-186	7951	1297	24
H(2C)	-1664	8792	1880	24
H(4A)	5056	9257	11294	26
H(4B)	4766	7898	11602	26
H(4C)	3314	8820	12021	26
H(1O8)	2530(30)	11414(19)	5350(30)	23
H(2O8)	4060(30)	11040(30)	5000(30)	23
H(6A)	-1848	10783	9172	24
H(6B)	-3287	9940	8300	24
H(6C)	-2540	11008	7337	24

B.4 ***$Tc_2(O_2CCH_3)_4(\mu\text{-}O_2CCH_3)$***

Single crystal X-ray diffraction data for $Tc_2(O_2CCH_3)_4(\mu\text{-}O_2CCH_3)$ has not been deposited with the Cambridge Crystallographic Data Centre. Crystallographic data are given in Table B.**15** and Table B.**19**.

Table B.15. Crystal data and structure refinement for $Tc_2(O_2CCH_3)_4(\mu\text{-}O_2CCH_3)$.

Identification code	bk_tcoac5_100k_0m_a
Empirical formula	C10 H15 O10 Tc2
Formula weight	493.04
Temperature	100(2) K
Wavelength	0.71073 Å
Crystal system	Monoclinic
Space group	C2/c
Unit cell dimensions	a = 13.0754(5) Å α= 90°
	b = 8.3466(3) Å β= 106.1770(10)°
Volume	1574.75(10) $Å^3$
Z	4
Density (calculated)	2.072 Mg/m^3
Absorption coefficient	1.801 mm^{-1}
F(000)	964
Crystal size	0.25 x 0.2 x 0.2 mm^3
Theta range for data collection	2.82 to 30.51°.
Index ranges	-18<=h<=18, -11<=k<=11, -21<=l<=21
Reflections collected	11879
Independent reflections	2400 [R(int) = 0.0155]
Completeness to theta = 30.51−	100.0%
Absorption correction	Semi-empirical from equivalents
Max. and min. transmission	0.7465 and 0.6819
Refinement method	Full-matrix least-squares on F^2
Data / restraints / parameters	2400 / 6 / 112
Goodness-of-fit on F^2	1.129

Final R indices [I>2sigma(I)]	R1 = 0.0175, wR2 = 0.0459
R indices (all data)	R1 = 0.0188, wR2 = 0.0467
Largest diff. peak and hole	1.145 and -0.549 e.Å^{-3}

Table B.16. Atomic coordinates (x 10^4) and equivalent isotropic displacement parameters (Å^2 x 10^3) for $Tc_2(O_2CCH_3)_4(\mu\text{-}O_2CCH_3)$. U(eq) is defined as one third of the trace of the orthogonalized U^{ij} tensor.

	x	y	z	U(eq)
Tc(1)	1804(1)	2595(1)	9440(1)	14(1)
O(3)	867(1)	1653(1)	10204(1)	18(1)
O(2)	2969(1)	4648(1)	11052(1)	19(1)
O(1)	1504(1)	4864(1)	9872(1)	19(1)
O(4)	2325(1)	1442(1)	11389(1)	18(1)
C(1)	2141(1)	5416(2)	10606(1)	19(1)
C(3)	1324(1)	1282(2)	11045(1)	17(1)
C(4)	671(1)	645(2)	11633(1)	22(1)
C(2)	1922(1)	7014(2)	10966(1)	27(1)
O(5)	378(1)	2932(2)	8250(1)	25(1)
C(5)	96(9)	3636(3)	7449(9)	15(1)
C(6)	325(4)	5385(4)	7368(3)	48(1)

Table B.17. Bond lengths (Å) and angles (°) for $Tc_2(O_2CCH_3)_4(\mu\text{-}O_2CCH_3)$.

Tc(1)-O(3)	2.0540(10)
Tc(1)-O(2)#1	2.0646(10)
Tc(1)-O(4)#1	2.0709(10)
Tc(1)-O(1)	2.0743(10)
Tc(1)-Tc(1)#1	2.1124(2)
Tc(1)-O(5)	2.2125(11)
O(3)-C(3)	1.2757(16)
O(2)-C(1)	1.2758(17)
O(2)-Tc(1)#1	2.0646(10)
O(1)-C(1)	1.2684(17)
O(4)-C(3)	1.2737(17)

O(4)-Tc(1)#1	2.0709(10)
C(1)-C(2)	1.497(2)
C(3)-C(4)	1.4872(19)
O(5)-C(5)#2	1.212(13)
O(5)-C(5)	1.297(12)
C(5)-O(5)#2	1.212(13)
C(5)-C(6)	1.502(4)
O(3)-Tc(1)-O(2)#1	91.19(4)
O(3)-Tc(1)-O(4)#1	176.91(4)
O(2)#1-Tc(1)-O(4)#1	88.75(4)
O(3)-Tc(1)-O(1)	88.89(4)
O(2)#1-Tc(1)-O(1)	176.88(4)
O(4)#1-Tc(1)-O(1)	91.00(4)
O(3)-Tc(1)-Tc(1)#1	92.43(3)
O(2)#1-Tc(1)-Tc(1)#1	92.23(3)
O(4)#1-Tc(1)-Tc(1)#1	90.66(3)
O(1)-Tc(1)-Tc(1)#1	90.89(3)
O(3)-Tc(1)-O(5)	90.09(4)
O(2)#1-Tc(1)-O(5)	89.93(4)
O(4)#1-Tc(1)-O(5)	86.82(4)
O(1)-Tc(1)-O(5)	86.94(4)
Tc(1)#1-Tc(1)-O(5)	176.65(3)
C(3)-O(3)-Tc(1)	117.30(9)
C(1)-O(2)-Tc(1)#1	116.95(9)
C(1)-O(1)-Tc(1)	117.90(9)
C(3)-O(4)-Tc(1)#1	118.16(9)
O(1)-C(1)-O(2)	121.97(13)
O(1)-C(1)-C(2)	119.53(13)
O(2)-C(1)-C(2)	118.50(13)
O(4)-C(3)-O(3)	121.42(12)
O(4)-C(3)-C(4)	119.46(12)
O(3)-C(3)-C(4)	119.13(12)
C(5)#2-O(5)-C(5)	14.6(7)
C(5)#2-O(5)-Tc(1)	151.0(4)

C(5)-O(5)-Tc(1)	140.0(4)
O(5)#2-C(5)-O(5)	121.9(3)
O(5)#2-C(5)-C(6)	117.8(9)
O(5)-C(5)-C(6)	120.3(9)

Symmetry transformations used to generate equivalent atoms:
#1 -x+1/2,-y+1/2,-z+2 #2 -x,y,-z+3/2

Table B.18. Anisotropic displacement parameters ($Å^2 x\ 10^3$) for $Tc_2(O_2CCH_3)_4(\mu\text{-}O_2CCH_3)$. The anisotropic displacement factor exponent takes the form: $-2p^2[h^2\ a^{*2}U^{11} + ... + 2\ h\ k\ a^*\ b^*\ U^{12}]$.

	U^{11}	U^{22}	U^{33}	U^{23}	U^{13}	U^{12}
Tc(1)	14(1)	15(1)	14(1)	0(1)	4(1)	-2(1)
O(3)	17(1)	20(1)	18(1)	0(1)	6(1)	-3(1)
O(2)	20(1)	18(1)	19(1)	-4(1)	6(1)	-2(1)
O(1)	20(1)	17(1)	22(1)	0(1)	6(1)	1(1)
O(4)	20(1)	20(1)	17(1)	1(1)	6(1)	-2(1)
C(1)	21(1)	16(1)	22(1)	-1(1)	11(1)	-2(1)
C(3)	20(1)	14(1)	18(1)	-2(1)	8(1)	-2(1)
C(4)	25(1)	23(1)	22(1)	-2(1)	13(1)	-5(1)
C(2)	33(1)	19(1)	31(1)	-6(1)	14(1)	1(1)
O(5)	23(1)	27(1)	20(1)	4(1)	0(1)	-2(1)
C(5)	13(3)	15(1)	19(3)	0(1)	8(2)	1(1)
C(6)	64(3)	15(1)	51(3)	6(2)	-6(2)	-4(1)

Table B.19. Hydrogen coordinates ($x\ 10^4$) and isotropic displacement parameters ($Å^2\ x\ 10^3$) for $Tc_2(O_2CCH_3)_4(\mu\text{-}O_2CCH_3)$.

	x	y	z	U(eq)
H(4A)	-7	1178	11477	33
H(4B)	1033	831	12274	33
H(4C)	565	-485	11527	33
H(2A)	1895	6903	11595	40
H(2B)	1252	7415	10592	40
H(2C)	2479	7749	10944	40

H(6A)	1078	5539	7481	72
H(6B)	80	5980	7816	72
H(6C)	-37	5754	6756	72

B.5 ***$Tc_2(O_2CCH_2CH_3)_4(\mu\text{-}O_2CCH_2CH_3)$***

Single crystal X-ray diffraction data for $Tc_2(O_2CCH_2CH_3)_4(\mu\text{-}O_2CCH_2CH_3)$ has not been deposited with the Cambridge Crystallographic Data Centre. Crystallographic data are given in Table B.**20** and Table B.**24**.

Table B.20. Crystal data and structure refinement for $Tc_2(O_2CCH_2CH_3)_4(\mu\text{-}O_2CCH_2CH_3)$.

Identification code	bk_tcprop5_0m	
Empirical formula	C15 H25 O10 Tc2	
Formula weight	561.35	
Temperature	100(2) K	
Wavelength	0.71073 Å	
Crystal system	Orthorhombic	
Space group	P2(1)2(1)2(1)	
Unit cell dimensions	a = 8.7086(4) Å	α = 90°.
	b = 13.8192(6) Å	β = 90°.
	c = 16.8542(7) Å	γ = 90°.
Volume	2028.33(15) $Å^3$	
Z	4	
Density (calculated)	1.838 Mg/m^3	
Absorption coefficient	1.411 mm^{-1}	
F(000)	1124	
Crystal size	? x ? x ? mm^3	
Theta range for data collection	1.91 to 30.51°.	
Index ranges	-12<=h<=12, -19<=k<=19, -24<=l<=24	
Reflections collected	33356	
Independent reflections	6201 [R(int) = 0.0239]	
Completeness to theta = 30.51°	100.0%	

Absorption correction	None
Refinement method	Full-matrix least-squares on F^2
Data / restraints / parameters	6201 / 0 / 279
Goodness-of-fit on F^2	1.050
Final R indices [I>2sigma(I)]	R1 = 0.0208, wR2 = 0.0481
R indices (all data)	R1 = 0.0222, wR2 = 0.0488
Absolute structure parameter	0.00
Largest diff. peak and hole	1.181 and -0.504 e.Å^{-3}

Table B.21. Atomic coordinates (x 10^4) and equivalent isotropic displacement parameters (Å^2 x 10^3) for $Tc_2(O_2CCH_2CH_3)_4(\mu\text{-}O_2CCH_2CH_3)$. U(eq) is defined as one third of the trace of the orthogonalized U^{ij} tensor.

	x	y	z	U(eq)
Tc(1)	3496(1)	2921(1)	1854(1)	16(1)
Tc(2)	1077(1)	3031(1)	1901(1)	18(1)
O(8)	1071(2)	2753(1)	3103(1)	28(1)
O(9)	6051(2)	2892(1)	1844(1)	23(1)
O(10)	8521(2)	3058(1)	1978(1)	29(1)
O(1)	3706(2)	4385(1)	2073(1)	20(1)
O(7)	3621(2)	2628(1)	3053(1)	24(1)
O(4)	961(2)	3348(1)	707(1)	24(1)
O(3)	3498(2)	3218(1)	657(1)	22(1)
O(5)	3399(2)	1455(1)	1640(1)	22(1)
O(2)	1159(2)	4491(1)	2131(1)	22(1)
O(6)	855(2)	1567(1)	1682(1)	26(1)
C(4)	2221(3)	3411(2)	328(1)	23(1)
C(2)	2603(3)	5952(2)	2271(1)	27(1)
C(1)	2491(2)	4881(2)	2160(1)	20(1)
C(5)	2219(3)	3775(2)	-511(1)	31(1)
C(10)	2360(3)	2600(2)	3434(1)	29(1)
C(8)	1938(3)	-10(2)	1509(2)	36(1)
C(7)	2075(2)	1066(2)	1611(1)	24(1)
C(11)	2362(3)	2378(3)	4306(2)	45(1)
C(6)	2542(4)	4857(2)	-517(2)	40(1)
C(9)	3446(3)	-532(2)	1380(2)	38(1)
C(3)	2239(4)	6472(2)	1508(2)	42(1)

C(12)	3929(4)	2151(3)	4645(2)	65(1)
C(13A)	7279(10)	3382(6)	1788(4)	17(1)
C(14A)	7297(5)	4338(3)	1350(3)	29(1)
C(15A)	7207(6)	4176(4)	457(3)	40(1)
C(13B)	7279(14)	3225(8)	1572(5)	13(1)
C(14B)	7230(6)	3832(4)	828(4)	26(1)
C(15B)	7511(10)	4895(5)	1025(4)	44(2)

Table B.22. Bond lengths (Å) and angles (°) for $Tc_2(O_2CCH_2CH_3)_4(\mu\text{-}O_2CCH_2CH_3)$.

Tc(1)-O(3)	2.0584(15)
Tc(1)-O(5)	2.0588(14)
Tc(1)-O(7)	2.0636(15)
Tc(1)-O(1)	2.0651(14)
Tc(1)-Tc(2)	2.1139(2)
Tc(1)-O(9)	2.2250(13)
Tc(2)-O(2)	2.0550(15)
Tc(2)-O(8)	2.0617(17)
Tc(2)-O(4)	2.0622(16)
Tc(2)-O(6)	2.0661(15)
Tc(2)-O(10)#1	2.2301(14)
O(8)-C(10)	1.272(3)
O(9)-C(13B)	1.251(12)
O(9)-C(13A)	1.269(9)
O(10)-C(13A)	1.213(9)
O(10)-C(13B)	1.301(12)
O(10)-Tc(2)#2	2.2301(14)
O(1)-C(1)	1.270(2)
O(7)-C(10)	1.273(3)
O(4)-C(4)	1.273(3)
O(3)-C(4)	1.271(3)
O(5)-C(7)	1.273(2)
O(2)-C(1)	1.280(2)
O(6)-C(7)	1.274(3)
C(4)-C(5)	1.500(3)
C(2)-C(1)	1.495(3)
C(2)-C(3)	1.506(4)
C(5)-C(6)	1.522(4)

C(10)-C(11)	1.501(3)
C(8)-C(7)	1.501(3)
C(8)-C(9)	1.514(3)
C(11)-C(12)	1.512(4)
C(13A)-C(14A)	1.514(10)
C(14A)-C(15A)	1.523(7)
C(13B)-C(14B)	1.509(13)
C(14B)-C(15B)	1.526(9)
O(3)-Tc(1)-O(5)	91.44(6)
O(3)-Tc(1)-O(7)	176.94(6)
O(5)-Tc(1)-O(7)	88.91(6)
O(3)-Tc(1)-O(1)	88.81(6)
O(5)-Tc(1)-O(1)	177.27(6)
O(7)-Tc(1)-O(1)	90.70(6)
O(3)-Tc(1)-Tc(2)	91.33(4)
O(5)-Tc(1)-Tc(2)	92.10(4)
O(7)-Tc(1)-Tc(2)	91.70(4)
O(1)-Tc(1)-Tc(2)	90.61(4)
O(3)-Tc(1)-O(9)	89.77(6)
O(5)-Tc(1)-O(9)	91.31(6)
O(7)-Tc(1)-O(9)	87.19(6)
O(1)-Tc(1)-O(9)	85.98(5)
Tc(2)-Tc(1)-O(9)	176.40(4)
O(2)-Tc(2)-O(8)	89.89(6)
O(2)-Tc(2)-O(4)	88.71(6)
O(8)-Tc(2)-O(4)	176.69(6)
O(2)-Tc(2)-O(6)	176.59(6)
O(8)-Tc(2)-O(6)	89.58(7)
O(4)-Tc(2)-O(6)	91.65(7)
O(2)-Tc(2)-Tc(1)	92.48(4)
O(8)-Tc(2)-Tc(1)	91.49(4)
O(4)-Tc(2)-Tc(1)	91.57(4)
O(6)-Tc(2)-Tc(1)	90.90(4)
O(2)-Tc(2)-O(10)#1	90.42(6)
O(8)-Tc(2)-O(10)#1	86.76(6)
O(4)-Tc(2)-O(10)#1	90.25(6)
O(6)-Tc(2)-O(10)#1	86.19(6)

Tc(1)-Tc(2)-O(10)#1	176.61(4)
C(10)-O(8)-Tc(2)	117.44(14)
C(13B)-O(9)-C(13A)	19.3(3)
C(13B)-O(9)-Tc(1)	148.3(5)
C(13A)-O(9)-Tc(1)	146.5(4)
C(13A)-O(10)-C(13B)	19.0(4)
C(13A)-O(10)-Tc(2)#2	151.7(4)
C(13B)-O(10)-Tc(2)#2	143.4(5)
C(1)-O(1)-Tc(1)	118.44(13)
C(10)-O(7)-Tc(1)	117.11(14)
C(4)-O(4)-Tc(2)	117.54(14)
C(4)-O(3)-Tc(1)	117.99(14)
C(7)-O(5)-Tc(1)	117.39(14)
C(1)-O(2)-Tc(2)	116.94(13)
C(7)-O(6)-Tc(2)	118.11(14)
O(3)-C(4)-O(4)	121.4(2)
O(3)-C(4)-C(5)	118.9(2)
O(4)-C(4)-C(5)	119.7(2)
C(1)-C(2)-C(3)	110.6(2)
O(1)-C(1)-O(2)	121.51(19)
O(1)-C(1)-C(2)	119.63(19)
O(2)-C(1)-C(2)	118.82(19)
C(4)-C(5)-C(6)	109.5(2)
O(8)-C(10)-O(7)	122.3(2)
O(8)-C(10)-C(11)	117.8(2)
O(7)-C(10)-C(11)	120.0(2)
C(7)-C(8)-C(9)	114.8(2)
O(5)-C(7)-O(6)	121.4(2)
O(5)-C(7)-C(8)	119.70(19)
O(6)-C(7)-C(8)	118.84(19)
C(10)-C(11)-C(12)	114.4(2)
O(10)-C(13A)-O(9)	122.4(7)
O(10)-C(13A)-C(14A)	116.2(7)
O(9)-C(13A)-C(14A)	120.7(7)
C(13A)-C(14A)-C(15A)	110.6(4)
O(9)-C(13B)-O(10)	116.9(8)
O(9)-C(13B)-C(14B)	119.0(9)
O(10)-C(13B)-C(14B)	124.0(9)

C(13B)-C(14B)-C(15B)	110.5(6)

Symmetry transformations used to generate equivalent atoms:
#1 x-1,y, z #2 x+1,y, z,

Table B.23. Anisotropic displacement parameters ($Å^2 x\ 10^3$) for $Tc_2(O_2CCH_2CH_3)_4(\mu\text{-}O_2CCH_2CH_3)$. The anisotropic displacement factor exponent takes the form: $-2p^2[h^2\ a^{*2}U^{11} + ... + 2\ h\ k\ a^*\ b^*\ U^{12}]$.

	U^{11}	U^{22}	U^{33}	U^{23}	U^{13}	U^{12}
Tc(1)	7(1)	17(1)	23(1)	0(1)	-1(1)	-1(1)
Tc(2)	7(1)	20(1)	29(1)	-1(1)	0(1)	0(1)
O(8)	16(1)	38(1)	30(1)	2(1)	6(1)	0(1)
O(9)	10(1)	26(1)	33(1)	5(1)	1(1)	0(1)
O(10)	11(1)	31(1)	44(1)	1(1)	0(1)	-1(1)
O(1)	12(1)	20(1)	29(1)	-3(1)	-2(1)	-2(1)
O(7)	17(1)	32(1)	24(1)	4(1)	-1(1)	0(1)
O(4)	16(1)	27(1)	29(1)	-3(1)	-6(1)	2(1)
O(3)	15(1)	28(1)	24(1)	-1(1)	-1(1)	0(1)
O(5)	13(1)	17(1)	35(1)	-1(1)	-1(1)	-1(1)
O(2)	12(1)	22(1)	33(1)	-5(1)	1(1)	2(1)
O(6)	12(1)	20(1)	46(1)	-2(1)	-1(1)	-1(1)
C(4)	19(1)	24(1)	26(1)	-6(1)	-5(1)	-1(1)
C(2)	27(1)	20(1)	35(1)	-9(1)	-2(1)	2(1)
C(1)	16(1)	20(1)	24(1)	-5(1)	-2(1)	0(1)
C(5)	31(1)	40(1)	22(1)	-5(1)	-6(1)	3(1)
C(10)	26(1)	34(1)	28(1)	4(1)	3(1)	-1(1)
C(8)	20(1)	18(1)	69(2)	-3(1)	0(1)	-3(1)
C(7)	14(1)	21(1)	38(1)	-2(1)	-3(1)	-2(1)
C(11)	31(1)	74(2)	30(1)	12(1)	4(1)	-1(1)
C(6)	52(2)	42(2)	27(1)	7(1)	-4(1)	-2(1)
C(9)	28(1)	19(1)	67(2)	-4(1)	-8(1)	4(1)
C(3)	64(2)	24(1)	38(1)	-1(1)	12(1)	-5(1)
C(12)	41(2)	118(3)	35(1)	26(2)	-7(1)	-9(2)
C(13A)	13(2)	23(3)	16(3)	-4(2)	4(3)	2(2)
C(14A)	20(2)	27(2)	41(2)	11(2)	5(2)	1(2)
C(15A)	25(2)	57(3)	38(3)	21(2)	-2(2)	-1(2)
C(13B)	13(2)	14(3)	13(4)	-6(3)	2(3)	5(2)
C(14B)	14(2)	33(3)	30(3)	17(3)	-6(2)	-7(2)

C(15B)	55(5)	31(4)	45(4)	16(3)	0(3)	6(3)

Table B.24. Hydrogen coordinates (x 10^4) and isotropic displacement parameters ($Å^2$ x 10^3) for $Tc_2(O_2CCH_2CH_3)_4(\mu\text{-}O_2CCH_2CH_3)$.

	x	y	z	U(eq)
H(2A)	3655	6123	2445	33
H(2B)	1877	6160	2689	33
H(5A)	1208	3646	-759	37
H(5B)	3014	3431	-822	37
H(8A)	1259	-142	1051	43
H(8B)	1436	-282	1987	43
H(11A)	1678	1819	4403	54
H(11B)	1930	2939	4595	54
H(6A)	1732	5196	-224	61
H(6B)	2566	5090	-1066	61
H(6C)	3537	4981	-264	61
H(9A)	3932	-292	894	57
H(9B)	3255	-1228	1330	57
H(9C)	4126	-414	1833	57
H(3A)	3005	6303	1106	63
H(3B)	2257	7172	1600	63
H(3C)	1217	6279	1323	63
H(12A)	4404	1629	4338	97
H(12B)	3821	1948	5199	97
H(12C)	4577	2730	4618	97
H(14A)	8252	4693	1479	35
H(14B)	6415	4738	1523	35
H(15A)	7165	4803	185	60
H(15B)	6281	3803	331	60
H(15C)	8116	3818	280	60
H(14C)	6215	3760	570	31
H(14D)	8025	3603	452	31
H(15D)	7430	5283	540	66
H(15E)	8540	4970	1252	66
H(15F)	6743	5115	1410	66

B.6 ***$Tc_2(O_2CC_6H_5)_4(\mu\text{-}O_2CC_6H_5)$***

Single crystal X-ray diffraction data for $Tc_2(O_2CC_6H_5)_4(\mu\text{-}O_2CC_6H_5)$ has not been deposited with the Cambridge Crystallographic Data Centre. Crystallographic data are given in Table B.**25** and Table B.**29**.

Table B.25. Crystal data and structure refinement for $Tc_2(O_2CC_6H_5)_4(\mu\text{-}O_2CC_6H_5)$.

Identification code	bk_tc2_o2cph_5_0m
Empirical formula	C35 H25 O10 Tc2
Formula weight	803.55
Temperature	100(2) K
Wavelength	0.71073 Å
Crystal system	Triclinic
Space group	P-1
Unit cell dimensions	a = 10.9468(3) Å α = 67.5170(10)°.
	b = 9.0483(9) Å β = 71.2040(10)°.
	c = 12.5915(13) Å γ = 78.4840(10)°.
Volume	1608.78(8) $Å^3$
Z	2
Density (calculated)	1.655 Mg/m^3
Absorption coefficient	0.918 mm^{-1}
F(000)	802
Crystal size	0.2 x 0.2 x 0.02 mm^3
Theta range for data collection	1.88 to 30.51°.
Index ranges	-15<=h<=15,-16<=k<=16,-20<=l<=20
Reflections collected	26379
Independent reflections	9772 [R(int) = 0.0174]
Completeness to theta = 30.51°	99.5%
Absorption correction	Semi-empirical from equivalents
Max. and min. transmission	0.7466 and 0.6484
Refinement method	Full-matrix least-squares on F^2
Data / restraints / parameters	9772 / 0 / 424
Goodness-of-fit on F^2	1.029
Final R indices [I>2sigma(I)]	R1 = 0.0217, wR2 = 0.0558
R indices (all data)	R1 = 0.0243, wR2 = 0.0572
Largest diff. peak and hole	0.894 and -0.474 $e.Å^{-3}$

Table B.26. Atomic coordinates (x 10^4) and equivalent isotropic displacement parameters ($Å^2$ x 10^3) for $Tc_2(O_2CC_6H_5)_4(\mu\text{-}O_2CC_6H_5)$. U(eq) is defined as one third of the trace of the orthogonalized U^{ij} tensor.

	x	y	z	U(eq)
Tc(1)	335(1)	5380(1)	4172(1)	11(1)
Tc(2)	4508(1)	5115(1)	732(1)	11(1)
O(10)	2016(1)	5750(1)	4335(1)	15(1)
O(3)	6119(1)	5754(1)	750(1)	14(1)
O(1)	5073(1)	3363(1)	1600(1)	14(1)
O(5)	1315(1)	6275(1)	2498(1)	16(1)
O(8)	1123(1)	3673(1)	4075(1)	16(1)
O(6)	3441(1)	5765(1)	2051(1)	16(1)
C(16)	2708(1)	7873(1)	1846(1)	17(1)
C(2)	6355(1)	1458(1)	1630(1)	15(1)
C(15)	2478(1)	6548(1)	2149(1)	14(1)
C(10)	8334(1)	6462(1)	866(1)	20(1)
C(23)	1391(1)	1490(1)	4881(1)	19(1)
C(7)	7172(1)	745(1)	1051(1)	19(1)
C(9)	8296(1)	6273(1)	-30(1)	16(1)
C(1)	5821(1)	2702(1)	1074(1)	13(1)
C(31)	4238(1)	6436(1)	4461(1)	19(1)
C(8)	7122(1)	5840(1)	-33(1)	14(1)
C(3)	6089(1)	1018(1)	2721(1)	20(1)
C(11)	9468(2)	6771(1)	909(1)	25(1)
C(29)	2135(1)	5501(1)	5245(1)	14(1)
C(6)	7739(2)	-396(1)	1561(1)	25(1)
C(30)	3259(1)	5903(1)	5352(1)	16(1)
C(22)	956(1)	2750(1)	4923(1)	15(1)
C(21)	1670(2)	8782(1)	1816(1)	25(1)
C(14)	9382(1)	6441(1)	-895(1)	21(1)
C(32)	5283(2)	6830(2)	4564(2)	28(1)
C(17)	3965(2)	8206(2)	1571(1)	24(1)
C(35)	3334(2)	5771(1)	6341(1)	23(1)
C(12)	10550(2)	6932(2)	51(2)	28(1)
C(28)	2278(2)	1332(2)	3983(1)	27(1)
C(24)	890(2)	476(1)	5736(1)	25(1)
C(4)	6653(2)	-128(2)	3224(1)	26(1)

C(13)	10502(1)	6785(2)	-856(1)	27(1)
C(34)	4390(2)	6154(2)	6438(2)	31(1)
C(5)	7490(2)	-826(1)	2646(1)	27(1)
C(18)	4169(2)	9442(2)	1279(2)	36(1)
C(33)	5363(2)	6684(2)	5550(2)	33(1)
C(20)	1893(2)	10015(2)	1499(1)	36(1)
C(25)	1279(2)	-709(2)	5694(2)	35(1)
C(27)	2677(2)	140(2)	3958(2)	38(1)
C(19)	3140(2)	10340(2)	1231(2)	41(1)
C(26)	2172(2)	-868(2)	4810(2)	41(1)
O(9)	1292(1)	4928(1)	6072(1)	15(1)
O(4)	7135(1)	5538(1)	-800(1)	15(1)
O(2)	6143(1)	3100(1)	81(1)	14(1)
O(7)	425(1)	2874(1)	5816(1)	16(1)

Table B.27. Bond lengths (Å) and angles (°) for $Tc_2(O_2CC_6H_5)_4(\mu\text{-}O_2CC_6H_5)$.

Tc(1)-O(9)#1	2.0447(9)
Tc(1)-O(8)	2.0578(9)
Tc(1)-O(7)#1	2.0585(9)
Tc(1)-O(10)	2.0746(9)
Tc(1)-Tc(1)#1	2.1218(2)
Tc(1)-O(5)	2.2100(9)
Tc(2)-O(1)	2.0496(9)
Tc(2)-O(4)#2	2.0535(9)
Tc(2)-O(3)	2.0613(9)
Tc(2)-O(2)#2	2.0824(9)
Tc(2)-Tc(2)#2	2.1247(2)
Tc(2)-O(6)	2.2034(9)
O(10)-C(29)	1.2692(16)
O(3)-C(8)	1.2812(16)
O(1)-C(1)	1.2802(15)
O(5)-C(15)	1.2657(15)
O(8)-C(22)	1.2720(16)
O(6)-C(15)	1.2623(16)
C(16)-C(21)	1.395(2)
C(16)-C(17)	1.397(2)
C(16)-C(15)	1.4986(18)

C(2)-C(3)	1.3958(19)
C(2)-C(7)	1.3961(19)
C(2)-C(1)	1.4777(18)
C(10)-C(11)	1.387(2)
C(10)-C(9)	1.400(2)
C(23)-C(24)	1.391(2)
C(23)-C(28)	1.394(2)
C(23)-C(22)	1.4804(18)
C(7)-C(6)	1.389(2)
C(9)-C(14)	1.3961(19)
C(9)-C(8)	1.4752(18)
C(1)-O(2)	1.2673(16)
C(31)-C(32)	1.385(2)
C(31)-C(30)	1.3959(19)
C(8)-O(4)	1.2746(16)
C(3)-C(4)	1.388(2)
C(11)-C(12)	1.388(2)
C(29)-O(9)	1.2820(16)
C(29)-C(30)	1.4734(18)
C(6)-C(5)	1.390(2)
C(30)-C(35)	1.3952(19)
C(22)-O(7)	1.2772(16)
C(21)-C(20)	1.390(2)
C(14)-C(13)	1.388(2)
C(32)-C(33)	1.388(3)
C(17)-C(18)	1.392(2)
C(35)-C(34)	1.385(2)
C(12)-C(13)	1.395(3)
C(28)-C(27)	1.391(2)
C(24)-C(25)	1.391(2)
C(4)-C(5)	1.390(2)
C(34)-C(33)	1.389(3)
C(18)-C(19)	1.381(3)
C(20)-C(19)	1.384(3)
C(25)-C(26)	1.383(3)
C(27)-C(26)	1.386(3)
O(9)-Tc(1)#1	2.0447(9)
O(4)-Tc(2)#2	2.0535(9)

O(2)-Tc(2)#2	2.0824(9)
O(7)-Tc(1)#1	2.0585(9)
O(9)#1-Tc(1)-O(8)	87.80(4)
O(9)#1-Tc(1)-O(7)#1	91.77(4)
O(8)-Tc(1)-O(7)#1	176.98(4)
O(9)#1-Tc(1)-O(10)	176.95(4)
O(8)-Tc(1)-O(10)	92.71(4)
O(7)#1-Tc(1)-O(10)	87.55(4)
O(9)#1-Tc(1)-Tc(1)#1	94.26(3)
O(8)-Tc(1)-Tc(1)#1	91.51(3)
O(7)#1-Tc(1)-Tc(1)#1	91.51(3)
O(10)-Tc(1)-Tc(1)#1	88.73(3)
O(9)#1-Tc(1)-O(5)	95.78(4)
O(8)-Tc(1)-O(5)	90.35(4)
O(7)#1-Tc(1)-O(5)	86.71(4)
O(10)-Tc(1)-O(5)	81.22(4)
Tc(1)#1-Tc(1)-O(5)	169.86(3)
O(1)-Tc(2)-O(4)#2	88.79(4)
O(1)-Tc(2)-O(3)	90.06(4)
O(4)#2-Tc(2)-O(3)	176.91(4)
O(1)-Tc(2)-O(2)#2	177.06(4)
O(4)#2-Tc(2)-O(2)#2	90.16(4)
O(3)-Tc(2)-O(2)#2	90.85(4)
O(1)-Tc(2)-Tc(2)#2	94.36(3)
O(4)#2-Tc(2)-Tc(2)#2	91.88(3)
O(3)-Tc(2)-Tc(2)#2	91.07(3)
O(2)#2-Tc(2)-Tc(2)#2	88.42(3)
O(1)-Tc(2)-O(6)	97.40(4)
O(4)#2-Tc(2)-O(6)	90.75(4)
O(3)-Tc(2)-O(6)	86.55(4)
O(2)#2-Tc(2)-O(6)	79.86(4)
Tc(2)#2-Tc(2)-O(6)	168.00(3)
C(29)-O(10)-Tc(1)	119.54(8)
C(8)-O(3)-Tc(2)	117.83(8)
C(1)-O(1)-Tc(2)	115.61(8)
C(15)-O(5)-Tc(1)	124.59(8)
C(22)-O(8)-Tc(1)	117.41(8)

C(15)-O(6)-Tc(2)	131.31(8)
C(21)-C(16)-C(17)	119.74(14)
C(21)-C(16)-C(15)	120.12(13)
C(17)-C(16)-C(15)	120.13(13)
C(3)-C(2)-C(7)	120.21(13)
C(3)-C(2)-C(1)	120.51(12)
C(7)-C(2)-C(1)	119.23(12)
O(6)-C(15)-O(5)	123.53(12)
O(6)-C(15)-C(16)	118.87(12)
O(5)-C(15)-C(16)	117.60(12)
C(11)-C(10)-C(9)	119.90(14)
C(24)-C(23)-C(28)	120.80(14)
C(24)-C(23)-C(22)	119.30(13)
C(28)-C(23)-C(22)	119.89(14)
C(6)-C(7)-C(2)	119.73(14)
C(14)-C(9)-C(10)	120.11(13)
C(14)-C(9)-C(8)	120.38(13)
C(10)-C(9)-C(8)	119.44(12)
O(2)-C(1)-O(1)	121.61(12)
O(2)-C(1)-C(2)	118.77(11)
O(1)-C(1)-C(2)	119.60(11)
C(32)-C(31)-C(30)	119.68(15)
O(4)-C(8)-O(3)	121.59(12)
O(4)-C(8)-C(9)	119.52(12)
O(3)-C(8)-C(9)	118.88(12)
C(4)-C(3)-C(2)	119.56(14)
C(10)-C(11)-C(12)	119.94(15)
O(10)-C(29)-O(9)	121.70(12)
O(10)-C(29)-C(30)	119.01(12)
O(9)-C(29)-C(30)	119.28(12)
C(7)-C(6)-C(5)	120.06(14)
C(35)-C(30)-C(31)	120.08(13)
C(35)-C(30)-C(29)	120.05(13)
C(31)-C(30)-C(29)	119.86(12)
O(8)-C(22)-O(7)	122.05(12)
O(8)-C(22)-C(23)	119.30(12)
O(7)-C(22)-C(23)	118.66(12)
C(20)-C(21)-C(16)	119.94(16)

C(13)-C(14)-C(9)	119.54(15)
C(31)-C(32)-C(33)	120.12(16)
C(18)-C(17)-C(16)	119.64(16)
C(34)-C(35)-C(30)	119.84(15)
C(11)-C(12)-C(13)	120.25(14)
C(27)-C(28)-C(23)	119.07(17)
C(23)-C(24)-C(25)	119.55(16)
C(3)-C(4)-C(5)	120.29(15)
C(14)-C(13)-C(12)	120.19(15)
C(35)-C(34)-C(33)	119.95(16)
C(4)-C(5)-C(6)	120.12(14)
C(19)-C(18)-C(17)	120.29(17)
C(32)-C(33)-C(34)	120.31(15)
C(19)-C(20)-C(21)	120.09(17)
C(26)-C(25)-C(24)	119.71(17)
C(26)-C(27)-C(28)	120.06(17)
C(18)-C(19)-C(20)	120.29(16)
C(25)-C(26)-C(27)	120.79(16)
C(29)-O(9)-Tc(1)#1	115.47(8)
C(8)-O(4)-Tc(2)#2	117.62(8)
C(1)-O(2)-Tc(2)#2	119.95(8)
C(22)-O(7)-Tc(1)#1	117.24(8)

Symmetry transformations used to generate equivalent atoms:
#1 -x,-y+1,-z+1 #2 -x+1,-y+1,-z

Table B.28. Anisotropic displacement parameters ($Å^2 x\ 10^3$) for $Tc_2(O_2CC_6H_5)_4(\mu\text{-}O_2CC_6H_5)$. The anisotropic displacement factor exponent takes the form: $-2p^2[h^2\ a^{*2}U^{11} + ... + 2\ h\ k\ a^*\ b^*\ U^{12}]$.

	U^{11}	U^{22}	U^{33}	U^{23}	U^{13}	U^{12}
Tc(1)	12(1)	12(1)	10(1)	-4(1)	-2(1)	0(1)
Tc(2)	10(1)	11(1)	11(1)	-4(1)	-3(1)	0(1)
O(10)	14(1)	18(1)	13(1)	-5(1)	-4(1)	-2(1)
O(3)	13(1)	16(1)	16(1)	-7(1)	-4(1)	-2(1)
O(1)	16(1)	13(1)	13(1)	-5(1)	-4(1)	0(1)
O(5)	14(1)	21(1)	13(1)	-5(1)	-2(1)	-3(1)
O(8)	17(1)	15(1)	15(1)	-6(1)	-2(1)	1(1)

O(6)	17(1)	17(1)	13(1)	-6(1)	-3(1)	1(1)
C(16)	21(1)	17(1)	13(1)	-7(1)	-1(1)	-3(1)
C(2)	15(1)	12(1)	18(1)	-3(1)	-6(1)	-1(1)
C(15)	14(1)	17(1)	9(1)	-5(1)	-1(1)	-1(1)
C(10)	18(1)	18(1)	27(1)	-10(1)	-9(1)	-1(1)
C(23)	18(1)	15(1)	26(1)	-10(1)	-8(1)	4(1)
C(7)	22(1)	14(1)	21(1)	-6(1)	-6(1)	1(1)
C(9)	13(1)	13(1)	23(1)	-6(1)	-7(1)	-1(1)
C(1)	14(1)	12(1)	15(1)	-5(1)	-5(1)	-1(1)
C(31)	16(1)	15(1)	25(1)	-6(1)	-6(1)	-1(1)
C(8)	13(1)	12(1)	17(1)	-4(1)	-6(1)	0(1)
C(3)	21(1)	19(1)	18(1)	-3(1)	-5(1)	0(1)
C(11)	23(1)	20(1)	39(1)	-13(1)	-17(1)	1(1)
C(29)	14(1)	12(1)	16(1)	-5(1)	-5(1)	1(1)
C(6)	25(1)	15(1)	32(1)	-7(1)	-8(1)	4(1)
C(30)	16(1)	12(1)	21(1)	-7(1)	-8(1)	2(1)
C(22)	14(1)	14(1)	18(1)	-7(1)	-4(1)	1(1)
C(21)	28(1)	19(1)	22(1)	-7(1)	-2(1)	2(1)
C(14)	15(1)	19(1)	27(1)	-8(1)	-5(1)	-2(1)
C(32)	17(1)	21(1)	47(1)	-13(1)	-7(1)	-3(1)
C(17)	26(1)	25(1)	21(1)	-8(1)	-3(1)	-8(1)
C(35)	26(1)	23(1)	24(1)	-10(1)	-12(1)	-1(1)
C(12)	17(1)	21(1)	51(1)	-13(1)	-15(1)	-1(1)
C(28)	24(1)	25(1)	33(1)	-17(1)	-4(1)	4(1)
C(24)	29(1)	16(1)	30(1)	-7(1)	-10(1)	1(1)
C(4)	28(1)	23(1)	21(1)	1(1)	-8(1)	1(1)
C(13)	15(1)	23(1)	40(1)	-9(1)	-4(1)	-4(1)
C(34)	36(1)	33(1)	40(1)	-21(1)	-23(1)	2(1)
C(5)	26(1)	15(1)	32(1)	1(1)	-11(1)	1(1)
C(18)	43(1)	32(1)	33(1)	-11(1)	-2(1)	-20(1)
C(33)	24(1)	31(1)	59(1)	-25(1)	-20(1)	0(1)
C(20)	52(1)	18(1)	31(1)	-9(1)	-4(1)	5(1)
C(25)	42(1)	16(1)	49(1)	-10(1)	-18(1)	2(1)
C(27)	35(1)	33(1)	53(1)	-31(1)	-6(1)	9(1)
C(19)	65(1)	21(1)	35(1)	-9(1)	-3(1)	-14(1)
C(26)	45(1)	21(1)	64(1)	-24(1)	-20(1)	11(1)
O(9)	15(1)	18(1)	12(1)	-4(1)	-4(1)	-2(1)
O(4)	12(1)	18(1)	16(1)	-7(1)	-3(1)	-2(1)

O(2)	16(1)	13(1)	13(1)	-5(1)	-4(1)	1(1)
O(7)	18(1)	13(1)	15(1)	-5(1)	-5(1)	1(1)

Table B.29. Hydrogen coordinates (x 10^4) and isotropic displacement parameters ($Å^2$ x 10^3) for $Tc_2(O_2CC_6H_5)_4(\mu\text{-}O_2CC_6H_5)$.

	x	y	z	U(eq)
H(10)	7584	6378	1444	24
H(7)	7340	1040	309	23
H(31)	4187	6529	3787	23
H(3)	5525	1499	3116	24
H(11)	9504	6873	1525	29
H(6)	8297	-883	1169	30
H(21)	812	8558	2011	30
H(14)	9356	6321	-1506	25
H(32)	5946	7201	3958	33
H(17)	4677	7593	1584	28
H(35)	2661	5420	6947	27
H(12)	11327	7142	82	33
H(28)	2607	2027	3397	32
H(24)	286	593	6345	30
H(4)	6466	-436	3966	32
H(13)	11236	6921	-1448	32
H(34)	4450	6054	7111	38
H(5)	7892	-1599	2993	32
H(18)	5020	9669	1113	43
H(33)	6086	6948	5617	40
H(20)	1187	10636	1466	44
H(25)	933	-1406	6271	42
H(27)	3295	18	3357	46
H(19)	3288	11184	1013	50
H(26)	2444	-1679	4785	49

B.7 ***$Tc_2(O_2CCH_3)_4I$***

Single crystal X-ray diffraction data for $Tc_2(O_2CCH_3)_4I$ has been deposited with the Cambridge Crystallographic Data Centre, CCDC No. 995651. Copies of this information may be obtained free of charge from the Director, CCDC, 12 Union Road, Cambridge, CB2 1EZ, UK (fax: +44 1223 336033; email: deposit@ccdc.cam.ac.uk or www.ccdc.cam.ac.uk). Crystallographic data are given in Table B.**30** and Table B.**34**.

Table B.30. Crystal data and structure refinement for $Tc_2(O_2CCH_3)_4I$.

Identification code	BK_0611B_3_0m_a
Empirical formula	C8 H12 I O8 Tc2
Formula weight	560.90
Temperature	100(2) K
Wavelength	0.71073 Å
Crystal system	Monoclinic
Space group	C 2/m
Unit cell dimensions	a = 7.1994(6) Å α = 90°. b = 14.5851(13) Å β = 110.9540(10)°. c = 7.1586(6) Å γ = 90°.
Volume	701.97(10) $Å^3$
Z	2
Density (calculated)	2.645 Mg/m^3
Absorption coefficient	4.197 mm^{-1}
F(000)	526
Crystal size	0.2 x 0.2 x 0.06 mm^3
Theta range for data collection	2.793 to 29.567°.
Index ranges	-9<=h<=9, -19<=k<=19, -9<=l<=9
Reflections collected	4112
Independent reflections	1021 [R(int) = 0.0170]
Completeness to theta = 25.242°	100.0%
Absorption correction	Semi-empirical from equivalents
Max. and min. transmission	0.7466 and 0.6136
Refinement method	Full-matrix least-squares on F^2

Data / restraints / parameters	1021 / 0 / 48
Goodness-of-fit on F^2	1.125
Final R indices [I>2sigma(I)]	R1 = 0.0167, wR2 = 0.0419
R indices (all data)	R1 = 0.0178, wR2 = 0.0425
Extinction coefficient	n/a
Largest diff. peak and hole	1.027 and -0.618 e.Å^{-3}

Table B.31. Atomic coordinates (x 10^4) and equivalent isotropic displacement parameters (Å^2 x 10^3) for $Tc_2(O_2CCH_3)_4I$. U(eq) is defined as one third of the trace of the orthogonalized U^{ij} tensor.

	x	y	z	U(eq)
I(1)	0	0	5000	16(1)
Tc(1)	3695(1)	0	8706(1)	7(1)
O(1)	2411(2)	-986(1)	9904(2)	10(1)
O(2)	5147(2)	-985(1)	12621(2)	10(1)
C(1)	3392(3)	-1266(1)	11669(3)	10(1)
C(2)	2465(3)	-1944(1)	12638(3)	14(1)

Table B.32. Bond lengths (Å) and angles (°) for $Tc_2(O_2CCH_3)_4I$.

I(1)-Tc(1)#1	3.0114(3)
I(1)-Tc(1)	3.0114(3)
Tc(1)-O(1)	2.0559(13)
Tc(1)-O(1)#2	2.0559(13)
Tc(1)-O(2)#3	2.0566(13)
Tc(1)-O(2)#4	2.0566(13)
Tc(1)-Tc(1)#4	2.1146(4)
O(1)-C(1)	1.274(2)
O(2)-C(1)	1.270(2)
O(2)-Tc(1)#4	2.0565(13)
C(1)-C(2)	1.495(3)
Tc(1)#1-I(1)-Tc(1)	180.0
O(1)-Tc(1)-O(1)#2	88.82(7)
O(1)-Tc(1)-O(2)#3	91.20(5)
O(1)#2-Tc(1)-O(2)#3	177.10(6)

O(1)-Tc(1)-O(2)#4	177.10(6)
O(1)#2-Tc(1)-O(2)#4	91.20(5)
O(2)#3-Tc(1)-O(2)#4	88.64(7)
O(1)-Tc(1)-Tc(1)#4	91.47(4)
O(1)#2-Tc(1)-Tc(1)#4	91.47(4)
O(2)#3-Tc(1)-Tc(1)#4	91.42(4)
O(2)#4-Tc(1)-Tc(1)#4	91.42(4)
O(1)-Tc(1)-I(1)	88.86(4)
O(1)#2-Tc(1)-I(1)	88.86(4)
O(2)#3-Tc(1)-I(1)	88.24(4)
O(2)#4-Tc(1)-I(1)	88.24(4)
Tc(1)#4-Tc(1)-I(1)	179.534(14)
C(1)-O(1)-Tc(1)	117.73(12)
C(1)-O(2)-Tc(1)#4	117.86(12)
O(2)-C(1)-O(1)	121.41(17)
O(2)-C(1)-C(2)	119.22(17)
O(1)-C(1)-C(2)	119.38(17)

Symmetry transformations used to generate equivalent atoms:

#1 -x,-y,-z+1 #2 x,-y,z #3 -x+1,y,-z+2 #4 -x+1,-y,-z+2

Table B.33. Anisotropic displacement parameters ($Å^2 x\ 10^3$) for $Tc_2(O_2CCH_3)_4I$. The anisotropic displacement factor exponent takes the form: $-2p^2[h^2\ a^{*2}U^{11} + ... + 2\ h\ k\ a^*\ b^*\ U^{12}]$.

	U^{11}	U^{22}	U^{33}	U^{23}	U^{13}	U^{12}
I(1)	10(1)	20(1)	11(1)	0	-3(1)	0
Tc(1)	6(1)	8(1)	6(1)	0	1(1)	0
O(1)	9(1)	11(1)	10(1)	0(1)	3(1)	-2(1)
O(2)	9(1)	11(1)	10(1)	1(1)	3(1)	0(1)
C(1)	9(1)	10(1)	11(1)	-1(1)	5(1)	0(1)
C(2)	14(1)	15(1)	14(1)	3(1)	6(1)	-2(1)

Table B.34. Hydrogen coordinates (x 10^4) and isotropic displacement parameters ($Å^2$ x 10^3) for $Tc_2(O_2CCH_3)_4I$.

	x	y	z	U(eq)
H(1)	1018	-1940	11949	21
H(2)	2786	-1778	14045	21
H(3)	2981	-2558	12553	21

B.8 ***K[$Tc_8(\mu\text{-}I)_8I_4$]***

Single crystal X-ray diffraction data for $K[Tc_8(\mu\text{-}I)_8I_4]I$ has been deposited in Fachinformationszentrum Karlsruhe (FIZ) 76344 Eggenstein-Leopoldshafen, Germany (e-mail: crysdata@fiz-karlsruhe.de/request_for_deposited_data.html, fax: (+49) 7247-808-666) for deposition number CSD-427573. Crystallographic data are given in Table B.**35** and Table B.**38**.

Table B.35. Crystal data and structure refinement for $K[Tc_8(\mu\text{-}I)_8I_4]I$.

Identification code	twin4_a	
Empirical formula	I13 K Tc8	
Formula weight	2480.08	
Temperature	100(2) K	
Wavelength	0.71073 Å	
Crystal system	Monoclinic	
Space group	P 21/n	
Unit cell dimensions	a = 8.0018(5) Å	α = 90°.
	b = 14.5125(10) Å	β = 102.3090(10)°.
	c = 13.1948(9) Å	γ = 90°.
Volume	1497.04(17) $Å^3$	
Z	2	
Density (calculated)	5.486 Mg/m^3	
Absorption coefficient	17.114 mm^{-1}	
F(000)	2104	
Crystal size	0.2 x 0.2 x 0.05 mm^3	

Theta range for data collection	2.113 to 28.281°.
Index ranges	-10<=h<=10, -19<=k<=19, -17<=l<=17
Reflections collected	5888
Independent reflections	3710
Completeness to theta = 25.242°	99.7%
Absorption correction	Semi-empirical from equivalents
Max. and min. transmission	0.746634 and 0.387931
Refinement method	Full-matrix least-squares on F^2
Data / restraints / parameters	3710 / 37 / 106
Goodness-of-fit on F^2	1.092
Final R indices [I>2sigma(I)]	R1 = 0.0277, wR2 = 0.0564
R indices (all data)	R1 = 0.0353, wR2 = 0.0588
Extinction coefficient	n/a
Largest diff. peak and hole	2.499 and -1.261 e.Å^{-3}

Table B.36. Atomic coordinates (x 10^4) and equivalent isotropic displacement parameters (Å^2 x 10^3) for $K[Tc_8(\mu\text{-}I)_8I_4]I$. U(eq) is defined as one third of the trace of the orthogonalized U^{ij} tensor.

	x	y	z	U(eq)
I(2)	7402(1)	2763(1)	9485(1)	9(1)
I(6)	8834(1)	4090(1)	12511(1)	11(1)
I(1)	11885(1)	2765(1)	9110(1)	11(1)
I(3)	13375(1)	3994(1)	12270(1)	10(1)
I(7)	15000	5000	10000	14(1)
I(5)	5481(1)	3513(1)	6847(1)	13(1)
I(4)	10240(1)	3560(1)	6279(1)	15(1)
Tc(4)	8891(1)	4230(1)	10504(1)	7(1)
Tc(2)	10358(1)	4283(1)	8214(1)	7(1)
Tc(3)	7755(1)	4313(1)	8428(1)	6(1)
Tc(1)	11523(1)	4192(1)	10329(1)	7(1)
K(1)	3391(4)	5030(2)	5015(3)	17(1)

Table B.37. Bond lengths (Å) and angles (°) for $K[Tc_8(\mu\text{-}I)_8I_4]I$.

I(2)-Tc(4)	2.6602(7)
I(2)-Tc(3)	2.6933(7)
I(6)-Tc(4)	2.6660(7)
I(6)-Tc(2)#1	2.6790(7)
I(1)-Tc(2)	2.6693(7)
I(1)-Tc(1)	2.6754(7)
I(3)-Tc(1)	2.6872(7)
I(3)-Tc(3)#1	2.7104(7)
I(3)-K(1)#2	3.918(4)
I(7)-Tc(1)#3	3.1341(6)
I(7)-Tc(1)	3.1341(6)
I(5)-Tc(3)	2.7191(7)
I(5)-K(1)	3.430(3)
I(5)-K(1)#4	3.502(3)
I(4)-Tc(2)	2.7434(8)
I(4)-K(1)#4	3.665(3)
I(4)-K(1)#5	3.936(3)
Tc(4)-Tc(1)	2.1674(8)
Tc(4)-Tc(1)#1	2.5308(8)
Tc(4)-Tc(3)	2.6983(8)
Tc(4)-Tc(2)#1	2.7291(8)
Tc(2)-Tc(3)	2.1611(8)
Tc(2)-I(6)#1	2.6790(7)
Tc(2)-Tc(4)#1	2.7292(8)
Tc(2)-Tc(1)	2.7508(8)
Tc(3)-Tc(1)#1	2.7065(8)
Tc(3)-I(3)#1	2.7104(7)
Tc(1)-Tc(4)#1	2.5309(8)
Tc(1)-Tc(3)#1	2.7064(8)
K(1)-K(1)#4	2.585(7)
K(1)-I(5)#4	3.502(3)
K(1)-I(4)#4	3.665(3)
K(1)-I(3)#6	3.918(4)
K(1)-I(4)#7	3.936(3)
Tc(4)-I(2)-Tc(3)	60.53(2)

Tc(4)-I(6)-Tc(2)#1	61.41(2)
Tc(2)-I(1)-Tc(1)	61.95(2)
Tc(1)-I(3)-Tc(3)#1	60.18(2)
Tc(1)-I(3)-K(1)#2	137.08(5)
Tc(3)#1-I(3)-K(1)#2	84.35(5)
Tc(1)#3-I(7)-Tc(1)	180.0
Tc(3)-I(5)-K(1)	114.37(7)
Tc(3)-I(5)-K(1)#4	92.86(6)
K(1)-I(5)-K(1)#4	43.77(10)
Tc(2)-I(4)-K(1)#4	94.96(6)
Tc(2)-I(4)-K(1)#5	106.81(6)
K(1)#4-I(4)-K(1)#5	90.90(7)
Tc(1)-Tc(4)-Tc(1)#1	90.99(3)
Tc(1)-Tc(4)-I(2)	105.45(3)
Tc(1)#1-Tc(4)-I(2)	120.11(3)
Tc(1)-Tc(4)-I(6)	109.03(3)
Tc(1)#1-Tc(4)-I(6)	118.19(3)
I(2)-Tc(4)-I(6)	109.87(2)
Tc(1)-Tc(4)-Tc(3)	91.04(3)
Tc(1)#1-Tc(4)-Tc(3)	62.24(2)
I(2)-Tc(4)-Tc(3)	60.34(2)
I(6)-Tc(4)-Tc(3)	159.77(3)
Tc(1)-Tc(4)-Tc(2)#1	89.74(3)
Tc(1)#1-Tc(4)-Tc(2)#1	62.93(2)
I(2)-Tc(4)-Tc(2)#1	164.15(3)
I(6)-Tc(4)-Tc(2)#1	59.53(2)
Tc(3)-Tc(4)-Tc(2)#1	125.17(3)
Tc(3)-Tc(2)-I(1)	108.80(3)
Tc(3)-Tc(2)-I(6)#1	109.94(3)
I(1)-Tc(2)-I(6)#1	139.74(3)
Tc(3)-Tc(2)-Tc(4)#1	89.65(3)
I(1)-Tc(2)-Tc(4)#1	110.99(3)
I(6)#1-Tc(2)-Tc(4)#1	59.06(2)
Tc(3)-Tc(2)-I(4)	106.65(3)
I(1)-Tc(2)-I(4)	91.06(2)
I(6)#1-Tc(2)-I(4)	88.17(2)
Tc(4)#1-Tc(2)-I(4)	147.01(3)
Tc(3)-Tc(2)-Tc(1)	89.78(3)

I(1)-Tc(2)-Tc(1)	59.133(19)
I(6)#1-Tc(2)-Tc(1)	110.42(2)
Tc(4)#1-Tc(2)-Tc(1)	55.01(2)
I(4)-Tc(2)-Tc(1)	149.66(3)
Tc(2)-Tc(3)-I(2)	105.11(3)
Tc(2)-Tc(3)-Tc(4)	90.35(3)
I(2)-Tc(3)-Tc(4)	59.128(19)
Tc(2)-Tc(3)-Tc(1)#1	90.47(3)
I(2)-Tc(3)-Tc(1)#1	112.84(3)
Tc(4)-Tc(3)-Tc(1)#1	55.84(2)
Tc(2)-Tc(3)-I(3)#1	103.60(3)
I(2)-Tc(3)-I(3)#1	150.34(3)
Tc(4)-Tc(3)-I(3)#1	113.66(3)
Tc(1)#1-Tc(3)-I(3)#1	59.48(2)
Tc(2)-Tc(3)-I(5)	113.38(3)
I(2)-Tc(3)-I(5)	85.05(2)
Tc(4)-Tc(3)-I(5)	141.75(3)
Tc(1)#1-Tc(3)-I(5)	145.98(3)
I(3)#1-Tc(3)-I(5)	90.35(2)
Tc(4)-Tc(1)-Tc(4)#1	89.01(3)
Tc(4)-Tc(1)-I(1)	108.42(3)
Tc(4)#1-Tc(1)-I(1)	117.39(3)
Tc(4)-Tc(1)-I(3)	104.63(3)
Tc(4)#1-Tc(1)-I(3)	120.34(3)
I(1)-Tc(1)-I(3)	112.45(2)
Tc(4)-Tc(1)-Tc(3)#1	90.11(3)
Tc(4)#1-Tc(1)-Tc(3)#1	61.92(2)
I(1)-Tc(1)-Tc(3)#1	161.46(3)
I(3)-Tc(1)-Tc(3)#1	60.33(2)
Tc(4)-Tc(1)-Tc(2)	88.84(3)
Tc(4)#1-Tc(1)-Tc(2)	62.06(2)
I(1)-Tc(1)-Tc(2)	58.91(2)
I(3)-Tc(1)-Tc(2)	166.15(3)
Tc(3)#1-Tc(1)-Tc(2)	123.98(3)
Tc(4)-Tc(1)-I(7)	156.43(3)
Tc(4)#1-Tc(1)-I(7)	68.833(19)
I(1)-Tc(1)-I(7)	89.599(19)
I(3)-Tc(1)-I(7)	81.175(18)

Tc(3)#1-Tc(1)-I(7)	72.709(18)
Tc(2)-Tc(1)-I(7)	87.72(2)
K(1)#4-K(1)-I(5)	69.60(12)
K(1)#4-K(1)-I(5)#4	66.63(12)
I(5)-K(1)-I(5)#4	136.23(10)
K(1)#4-K(1)-I(4)#4	134.84(17)
I(5)-K(1)-I(4)#4	154.94(10)
I(5)#4-K(1)-I(4)#4	68.49(5)
K(1)#4-K(1)-I(3)#6	77.31(16)
I(5)-K(1)-I(3)#6	108.07(9)
I(5)#4-K(1)-I(3)#6	62.24(5)
I(4)#4-K(1)-I(3)#6	86.43(7)
K(1)#4-K(1)-I(4)#7	135.93(17)
I(5)-K(1)-I(4)#7	67.26(5)
I(5)#4-K(1)-I(4)#7	155.36(10)
I(4)#4-K(1)-I(4)#7	89.10(7)
I(3)#6-K(1)-I(4)#7	107.91(9)

Symmetry transformations used to generate equivalent atoms:

#1 -x+2,-y+1,-z+2 #2 x+1, y, z+1 #3 -x+3, -y+1, -z+2

#4 -x+1,-y+1,-z+1 #5 x+1, y, z #6 x-1, y, z-1 #7 x-1, y, z

Table B.38. Anisotropic displacement parameters ($Å^2 x\ 10^3$) for $K[Tc_8(\mu\text{-}I)_8I_4]I$. The anisotropic displacement factor exponent takes the form: $-2p^2[h^2\ a^{*2}U^{11} + ... + 2\ h\ k\ a^*\ b^*\ U^{12}]$.

	U^{11}	U^{22}	U^{33}	U^{23}	U^{13}	U^{12}
I(2)	11(1)	6(1)	9(1)	1(1)	2(1)	-2(1)
I(6)	12(1)	12(1)	9(1)	1(1)	4(1)	-2(1)
I(1)	11(1)	8(1)	13(1)	-2(1)	2(1)	2(1)
I(3)	10(1)	8(1)	10(1)	2(1)	0(1)	1(1)
I(7)	11(1)	13(1)	18(1)	2(1)	6(1)	-1(1)
I(5)	13(1)	12(1)	11(1)	0(1)	-3(1)	-3(1)
I(4)	13(1)	21(1)	13(1)	-8(1)	4(1)	-1(1)
Tc(4)	7(1)	6(1)	7(1)	1(1)	1(1)	0(1)
Tc(2)	7(1)	7(1)	7(1)	-1(1)	2(1)	0(1)
Tc(3)	6(1)	6(1)	6(1)	0(1)	1(1)	0(1)
Tc(1)	7(1)	5(1)	7(1)	0(1)	1(1)	1(1)
K(1)	14(2)	20(2)	17(2)	17(1)	4(1)	7(1)

B.9 ***$Tc_5(\mu\text{-}I)_4(\mu_3\text{-}I)_4I_5$***

Single crystal X-ray diffraction data for $Tc_5(\mu\text{-}I)_4(\mu_3\text{-}I)_4I_5$ has not been deposited in Fachinformationszentrum Karlsruhe (FIZ) 76344 Eggenstein-Leopoldshafen, Germany. Crystallographic data are given in Table B.**39** and Table B.**42**.

Table B.39. Crystal data and structure refinement for $Tc_5(\mu\text{-}I)_4(\mu_3\text{-}I)_4I_5$.

Identification code	BK_0703B_0m_a
Empirical formula	I13 Tc5
Formula weight	2144.25
Temperature	100(2) K
Wavelength	0.71073 Å
Crystal system	Monoclinic
Space group	P 21/n
Unit cell dimensions	a = 9.7648(9) Å α= 90°.
	b = 15.5838(15) Å β= 91.7520(14)°.
	c = 15.7621(15) Å γ = 90°.
Volume	2397.4(4) $Å^3$
Z	4
Density (calculated)	5.928 Mg/m^3
Absorption coefficient	19.536 mm^{-1}
F(000)	3616
Crystal size	0.3 x 0.02 x 0.02 mm^3
Theta range for data collection	1.838 to 28.282°.
Index ranges	-13<=h<=13, -20<=k<=20, -21<=l<=21
Reflections collected	33760
Independent reflections	5940 [R(int) = 0.0473]
Completeness to theta = 25.242°	100.0%
Refinement method	Full-matrix least-squares on F^2
Data / restraints / parameters	5940 / 0 / 163
Goodness-of-fit on F^2	1.086
Final R indices [I>2sigma(I)]	R1 = 0.0269, wR2 = 0.0470
R indices (all data)	R1 = 0.0361, wR2 = 0.0495
Largest diff. peak and hole	1.400 and -1.365 e.$Å^{-3}$

Table B.40. Atomic coordinates (x 10^4) and equivalent isotropic displacement parameters ($Å^2$ x 10^3) for $Tc_5(\mu\text{-}I)_4(\mu_3\text{-}I)_4I_5$. U(eq) is defined as one third of the trace of the orthogonalized U^{ij} tensor.

	x	y	z	U(eq)
I(34)	3390(1)	1997(1)	3122(1)	11(1)
I(25)	858(1)	4501(1)	1930(1)	11(1)
I(45)	178(1)	3103(1)	3808(1)	10(1)
I(23)	3825(1)	3265(1)	1203(1)	12(1)
I(123)	1455(1)	1763(1)	-127(1)	8(1)
I(145)	-2059(1)	1605(1)	2450(1)	8(1)
I(134)	1038(1)	335(1)	1825(1)	8(1)
I(125)	-1666(1)	3088(1)	531(1)	9(1)
Tc(1)	-268(1)	1723(1)	1181(1)	6(1)
Tc(5)	-622(1)	3082(1)	2158(1)	6(1)
Tc(4)	693(1)	1760(1)	2782(1)	6(1)
Tc(2)	1111(1)	3157(1)	894(1)	7(1)
Tc(3)	2406(1)	1831(1)	1526(1)	7(1)
I(4)	686(1)	706(1)	4171(1)	10(1)
I(5)	-2819(1)	4097(1)	2590(1)	13(1)
I(3)	4692(1)	922(1)	1127(1)	12(1)
I(2)	1505(1)	4216(1)	-454(1)	11(1)
I(1)	-1908(1)	657(1)	199(1)	10(1)

Table B.41. Bond lengths (Å) and angles (°) for $Tc_5(\mu\text{-}I)_4(\mu_3\text{-}I)_4I_5$.

I(34)-Tc(3)	2.6776(8)
I(34)-Tc(4)	2.6970(8)
I(25)-Tc(5)	2.6716(8)
I(25)-Tc(2)	2.6722(8)
I(45)-Tc(5)	2.6928(8)
I(45)-Tc(4)	2.7013(8)
I(23)-Tc(2)	2.6851(8)
I(23)-Tc(3)	2.6866(8)
I(123)-Tc(1)	2.7014(8)
I(123)-Tc(2)	2.7300(8)
I(123)-Tc(3)	2.7419(8)

I(145)-Tc(1)	2.7030(8)
I(145)-Tc(4)	2.7332(8)
I(145)-Tc(5)	2.7420(8)
I(134)-Tc(1)	2.6943(7)
I(134)-Tc(4)	2.7131(7)
I(134)-Tc(3)	2.7357(8)
I(125)-Tc(1)	2.7113(7)
I(125)-Tc(5)	2.7315(8)
I(125)-Tc(2)	2.7571(8)
Tc(1)-Tc(5)	2.6470(8)
Tc(1)-Tc(2)	2.6543(8)
Tc(1)-Tc(3)	2.6554(8)
Tc(1)-Tc(4)	2.6662(8)
Tc(1)-I(1)	2.7524(7)
Tc(5)-Tc(4)	2.6041(8)
Tc(5)-Tc(2)	2.6557(9)
Tc(5)-I(5)	2.7670(8)
Tc(4)-Tc(3)	2.6327(9)
Tc(4)-I(4)	2.7370(7)
Tc(2)-Tc(3)	2.6040(8)
Tc(2)-I(2)	2.7268(8)
Tc(3)-I(3)	2.7336(8)
Tc(3)-I(34)-Tc(4)	58.66(2)
Tc(5)-I(25)-Tc(2)	59.60(2)
Tc(5)-I(45)-Tc(4)	57.73(2)
Tc(2)-I(23)-Tc(3)	57.99(2)
Tc(1)-I(123)-Tc(2)	58.51(2)
Tc(1)-I(123)-Tc(3)	58.39(2)
Tc(2)-I(123)-Tc(3)	56.83(2)
Tc(1)-I(145)-Tc(4)	58.74(2)
Tc(1)-I(145)-Tc(5)	58.168(19)
Tc(4)-I(145)-Tc(5)	56.798(19)
Tc(1)-I(134)-Tc(4)	59.08(2)
Tc(1)-I(134)-Tc(3)	58.55(2)
Tc(4)-I(134)-Tc(3)	57.78(2)
Tc(1)-I(125)-Tc(5)	58.198(19)
Tc(1)-I(125)-Tc(2)	58.068(19)

Tc(5)-I(125)-Tc(2)	57.87(2)
Tc(5)-Tc(1)-Tc(2)	60.13(2)
Tc(5)-Tc(1)-Tc(3)	88.58(2)
Tc(2)-Tc(1)-Tc(3)	58.74(2)
Tc(5)-Tc(1)-Tc(4)	58.69(2)
Tc(2)-Tc(1)-Tc(4)	88.71(2)
Tc(3)-Tc(1)-Tc(4)	59.30(2)
Tc(5)-Tc(1)-I(134)	119.49(3)
Tc(2)-Tc(1)-I(134)	120.24(3)
Tc(3)-Tc(1)-I(134)	61.51(2)
Tc(4)-Tc(1)-I(134)	60.81(2)
Tc(5)-Tc(1)-I(123)	121.41(3)
Tc(2)-Tc(1)-I(123)	61.29(2)
Tc(3)-Tc(1)-I(123)	61.57(2)
Tc(4)-Tc(1)-I(123)	120.86(3)
I(134)-Tc(1)-I(123)	90.43(2)
Tc(5)-Tc(1)-I(145)	61.65(2)
Tc(2)-Tc(1)-I(145)	121.78(3)
Tc(3)-Tc(1)-I(145)	120.48(3)
Tc(4)-Tc(1)-I(145)	61.20(2)
I(134)-Tc(1)-I(145)	88.63(2)
I(123)-Tc(1)-I(145)	176.77(3)
Tc(5)-Tc(1)-I(125)	61.28(2)
Tc(2)-Tc(1)-I(125)	61.83(2)
Tc(3)-Tc(1)-I(125)	120.57(3)
Tc(4)-Tc(1)-I(125)	119.97(3)
I(134)-Tc(1)-I(125)	177.93(3)
I(123)-Tc(1)-I(125)	90.65(2)
I(145)-Tc(1)-I(125)	90.19(2)
Tc(5)-Tc(1)-I(1)	136.56(3)
Tc(2)-Tc(1)-I(1)	134.59(3)
Tc(3)-Tc(1)-I(1)	134.85(3)
Tc(4)-Tc(1)-I(1)	136.68(3)
I(134)-Tc(1)-I(1)	89.27(2)
I(123)-Tc(1)-I(1)	87.13(2)
I(145)-Tc(1)-I(1)	89.77(2)
I(125)-Tc(1)-I(1)	89.02(2)
Tc(4)-Tc(5)-Tc(1)	61.02(2)

Tc(4)-Tc(5)-Tc(2)	90.00(3)
Tc(1)-Tc(5)-Tc(2)	60.07(2)
Tc(4)-Tc(5)-I(25)	116.30(3)
Tc(1)-Tc(5)-I(25)	120.20(3)
Tc(2)-Tc(5)-I(25)	60.21(2)
Tc(4)-Tc(5)-I(45)	61.30(2)
Tc(1)-Tc(5)-I(45)	122.18(3)
Tc(2)-Tc(5)-I(45)	123.47(3)
I(25)-Tc(5)-I(45)	88.72(2)
Tc(4)-Tc(5)-I(125)	121.54(3)
Tc(1)-Tc(5)-I(125)	60.52(2)
Tc(2)-Tc(5)-I(125)	61.55(2)
I(25)-Tc(5)-I(125)	93.39(2)
I(45)-Tc(5)-I(125)	174.85(3)
Tc(4)-Tc(5)-I(145)	61.43(2)
Tc(1)-Tc(5)-I(145)	60.18(2)
Tc(2)-Tc(5)-I(145)	120.25(3)
I(25)-Tc(5)-I(145)	177.43(3)
I(45)-Tc(5)-I(145)	89.04(2)
I(125)-Tc(5)-I(145)	88.95(2)
Tc(4)-Tc(5)-I(5)	137.40(3)
Tc(1)-Tc(5)-I(5)	135.75(3)
Tc(2)-Tc(5)-I(5)	132.54(3)
I(25)-Tc(5)-I(5)	89.24(2)
I(45)-Tc(5)-I(5)	87.68(2)
I(125)-Tc(5)-I(5)	87.65(2)
I(145)-Tc(5)-I(5)	91.93(2)
Tc(5)-Tc(4)-Tc(3)	89.99(3)
Tc(5)-Tc(4)-Tc(1)	60.28(2)
Tc(3)-Tc(4)-Tc(1)	60.15(2)
Tc(5)-Tc(4)-I(34)	115.74(3)
Tc(3)-Tc(4)-I(34)	60.30(2)
Tc(1)-Tc(4)-I(34)	120.27(3)
Tc(5)-Tc(4)-I(45)	60.97(2)
Tc(3)-Tc(4)-I(45)	123.50(3)
Tc(1)-Tc(4)-I(45)	121.12(3)
I(34)-Tc(4)-I(45)	88.52(2)
Tc(5)-Tc(4)-I(134)	120.38(3)

Tc(3)-Tc(4)-I(134)	61.54(2)
Tc(1)-Tc(4)-I(134)	60.11(2)
I(34)-Tc(4)-I(134)	94.89(2)
I(45)-Tc(4)-I(134)	174.94(3)
Tc(5)-Tc(4)-I(145)	61.77(2)
Tc(3)-Tc(4)-I(145)	120.19(3)
Tc(1)-Tc(4)-I(145)	60.07(2)
I(34)-Tc(4)-I(145)	177.20(3)
I(45)-Tc(4)-I(145)	89.05(2)
I(134)-Tc(4)-I(145)	87.63(2)
Tc(5)-Tc(4)-I(4)	139.81(3)
Tc(3)-Tc(4)-I(4)	130.05(3)
Tc(1)-Tc(4)-I(4)	137.26(3)
I(34)-Tc(4)-I(4)	87.10(2)
I(45)-Tc(4)-I(4)	88.95(2)
I(134)-Tc(4)-I(4)	87.49(2)
I(145)-Tc(4)-I(4)	94.24(2)
Tc(3)-Tc(2)-Tc(1)	60.65(2)
Tc(3)-Tc(2)-Tc(5)	89.49(3)
Tc(1)-Tc(2)-Tc(5)	59.80(2)
Tc(3)-Tc(2)-I(25)	116.17(3)
Tc(1)-Tc(2)-I(25)	119.91(3)
Tc(5)-Tc(2)-I(25)	60.19(2)
Tc(3)-Tc(2)-I(23)	61.03(2)
Tc(1)-Tc(2)-I(23)	121.67(3)
Tc(5)-Tc(2)-I(23)	120.99(3)
I(25)-Tc(2)-I(23)	87.10(2)
Tc(3)-Tc(2)-I(2)	134.42(3)
Tc(1)-Tc(2)-I(2)	136.59(3)
Tc(5)-Tc(2)-I(2)	136.00(3)
I(25)-Tc(2)-I(2)	91.13(2)
I(23)-Tc(2)-I(2)	86.63(2)
Tc(3)-Tc(2)-I(123)	61.81(2)
Tc(1)-Tc(2)-I(123)	60.21(2)
Tc(5)-Tc(2)-I(123)	120.01(3)
I(25)-Tc(2)-I(123)	177.81(3)
I(23)-Tc(2)-I(123)	91.05(2)
I(2)-Tc(2)-I(123)	89.95(2)

Tc(3)-Tc(2)-I(125)	120.76(3)
Tc(1)-Tc(2)-I(125)	60.10(2)
Tc(5)-Tc(2)-I(125)	60.58(2)
I(25)-Tc(2)-I(125)	92.79(2)
I(23)-Tc(2)-I(125)	177.95(3)
I(2)-Tc(2)-I(125)	91.32(2)
I(123)-Tc(2)-I(125)	89.09(2)
Tc(2)-Tc(3)-Tc(4)	90.51(3)
Tc(2)-Tc(3)-Tc(1)	60.61(2)
Tc(4)-Tc(3)-Tc(1)	60.55(2)
Tc(2)-Tc(3)-I(34)	116.05(3)
Tc(4)-Tc(3)-I(34)	61.04(2)
Tc(1)-Tc(3)-I(34)	121.41(3)
Tc(2)-Tc(3)-I(23)	60.98(2)
Tc(4)-Tc(3)-I(23)	121.39(3)
Tc(1)-Tc(3)-I(23)	121.57(3)
I(34)-Tc(3)-I(23)	85.73(2)
Tc(2)-Tc(3)-I(3)	135.50(3)
Tc(4)-Tc(3)-I(3)	133.90(3)
Tc(1)-Tc(3)-I(3)	136.44(3)
I(34)-Tc(3)-I(3)	89.64(2)
I(23)-Tc(3)-I(3)	87.56(2)
Tc(2)-Tc(3)-I(134)	120.56(3)
Tc(4)-Tc(3)-I(134)	60.68(2)
Tc(1)-Tc(3)-I(134)	59.95(2)
I(34)-Tc(3)-I(134)	94.81(2)
I(23)-Tc(3)-I(134)	177.74(3)
I(3)-Tc(3)-I(134)	90.24(2)
Tc(2)-Tc(3)-I(123)	61.35(2)
Tc(4)-Tc(3)-I(123)	120.59(3)
Tc(1)-Tc(3)-I(123)	60.04(2)
I(34)-Tc(3)-I(123)	176.42(3)
I(23)-Tc(3)-I(123)	90.77(2)
I(3)-Tc(3)-I(123)	90.94(2)
I(134)-Tc(3)-I(123)	88.72(2)

Table B.42. Anisotropic displacement parameters ($Å^2 x\ 10^3$) for $Tc_5(\mu\text{-}I)_4(\mu_3\text{-}I)_4I_5$. The anisotropic displacement factor exponent takes the form: $-2p^2[h^2\ a^{*2}U^{11} + ... + 2\ h\ k\ a^*\ b^*\ U^{12}]$.

	U^{11}	U^{22}	U^{33}	U^{23}	U^{13}	U^{12}
I(34)	8(1)	16(1)	8(1)	0(1)	-1(1)	-1(1)
I(25)	14(1)	7(1)	10(1)	-1(1)	0(1)	-2(1)
I(45)	14(1)	9(1)	7(1)	-2(1)	-2(1)	2(1)
I(23)	9(1)	11(1)	16(1)	5(1)	-1(1)	-3(1)
I(123)	10(1)	9(1)	6(1)	-1(1)	2(1)	1(1)
I(145)	7(1)	9(1)	8(1)	-1(1)	2(1)	-1(1)
I(134)	9(1)	6(1)	8(1)	-1(1)	1(1)	1(1)
I(125)	9(1)	10(1)	7(1)	0(1)	-1(1)	2(1)
Tc(1)	6(1)	6(1)	5(1)	-1(1)	0(1)	0(1)
Tc(5)	7(1)	6(1)	5(1)	0(1)	0(1)	1(1)
Tc(4)	7(1)	6(1)	5(1)	0(1)	0(1)	1(1)
Tc(2)	8(1)	6(1)	7(1)	1(1)	0(1)	0(1)
Tc(3)	6(1)	8(1)	7(1)	1(1)	1(1)	0(1)
I(4)	13(1)	9(1)	7(1)	2(1)	1(1)	0(1)
I(5)	13(1)	12(1)	13(1)	-2(1)	2(1)	6(1)
I(3)	9(1)	16(1)	13(1)	0(1)	2(1)	4(1)
I(2)	13(1)	10(1)	9(1)	3(1)	1(1)	0(1)
I(1)	9(1)	11(1)	9(1)	-4(1)	-1(1)	-1(1)

B.10 ***K[$Tc_2(O_2CCH_3)_4Br_2$]***

Single crystal X-ray diffraction data for $K[Tc_2(O_2CCH_3)_4Br_2]$ has been deposited with the Cambridge Crystallographic Data Centre, CCDC No. 940547. Copies of this information may be obtained free of charge from the Director, CCDC, 12 Union Road, Cambridge, CB2 1EZ, UK (fax: +44 1223 336033; email: deposit@ccdc.cam.ac.uk or www.ccdc.cam.ac.uk). Crystallographic data are given in Table B.**43** and Table B.**47**.

Table B.43. Crystal data and structure refinement for $K[Tc_2(O_2CCH_3)_4Br_2]$.

Identification code	bk_tc2oac4br_120_0m
Empirical formula	C8 H12 Br2 K O8 Tc2
Formula weight	632.90
Temperature	100(2) K
Wavelength	0.71073 Å
Crystal system	Tetragonal
Space group	P42/n
Unit cell dimensions	a = 12.0675(3) Å α = 90°. b = 12.0675(3) Å β = 90°. c = 11.1236(5) Å γ = 90°.
Volume	1619.87(9) $Å^3$
Z	4
Density (calculated)	2.588 Mg/m^3
Absorption coefficient	6.926 mm^{-1}
F(000)	1196
Crystal size	0.07 x 0.02 x 0.02 mm^3
Theta range for data collection	2.39 to 30.51°.
Index ranges	-17<=h<=17, -17<=k<=17, -15<=l<=15
Reflections collected	25988
Independent reflections	2475 [R(int) = 0.0296]
Completeness to theta = 30.51°	100.0%
Absorption correction	Semi-empirical from equivalents
Max. and min. transmission	0.7466 and 0.5692
Refinement method	Full-matrix least-squares on F^2
Data / restraints / parameters	2475 / 0 / 98
Goodness-of-fit on F^2	1.125
Final R indices [I>2sigma(I)]	R1 = 0.0171, wR2 = 0.0392
R indices (all data)	R1 = 0.0206, wR2 = 0.0400
Largest diff. peak and hole	0.565 and -0.367 $e.Å^{-3}$

Table B.44. Atomic coordinates (x 10^4) and equivalent isotropic displacement parameters ($Å^2$ x 10^3) for $K[Tc_2(O_2CCH_3)_4Br_2]$. U(eq) is defined as one third of the trace of the orthogonalized U^{ij} tensor.

	x	y	z	U(eq)
Tc(1)	5289(1)	4190(1)	9790(1)	8(1)
Br(1)	5912(1)	2091(1)	9115(1)	12(1)
K(1)	7500	2500	6674(1)	23(1)
O(1)	6845(1)	4516(1)	10461(1)	11(1)
O(3)	4860(1)	3590(1)	11456(1)	12(1)
C(1)	7023(2)	5499(2)	10852(2)	10(1)
C(3)	4398(2)	4262(2)	12184(2)	10(1)
C(2)	8134(2)	5790(2)	11346(2)	14(1)
C(4)	4068(2)	3848(2)	13395(2)	15(1)
O(4)	4216(1)	5270(1)	11898(1)	11(1)
O(2)	6267(1)	6232(1)	10834(1)	11(1)

Table B.45. Bond lengths (Å) and angles (°) for $K[Tc_2(O_2CCH_3)_4Br_2]$.

Tc(1)-O(3)	2.0566(13)
Tc(1)-O(1)	2.0582(13)
Tc(1)-O(2)#1	2.0660(13)
Tc(1)-O(4)#1	2.0752(14)
Tc(1)-Tc(1)#1	2.1274(3)
Tc(1)-Br(1)	2.7467(2)
Tc(1)-K(1)#2	3.9583(4)
Br(1)-K(1)	3.3599(6)
Br(1)-K(1)#2	3.4668(6)
K(1)-O(1)#3	2.8925(14)
K(1)-O(1)#4	2.8925(14)
K(1)-Br(1)#5	3.3600(6)
K(1)-Br(1)#3	3.4668(6)
K(1)-Br(1)#4	3.4668(6)
K(1)-Tc(1)#3	3.9583(4)
K(1)-Tc(1)#4	3.9583(4)
O(1)-C(1)	1.281(2)
O(1)-K(1)#2	2.8924(14)
O(3)-C(3)	1.274(2)

C(1)-O(2)	1.271(2)
C(1)-C(2)	1.491(3)
C(3)-O(4)	1.276(2)
C(3)-C(4)	1.491(3)
O(4)-Tc(1)#1	2.0752(13)
O(2)-Tc(1)#1	2.0660(13)
O(3)-Tc(1)-O(1)	88.28(5)
O(3)-Tc(1)-O(2)#1	89.25(5)
O(1)-Tc(1)-O(2)#1	176.47(5)
O(3)-Tc(1)-O(4)#1	176.99(5)
O(1)-Tc(1)-O(4)#1	90.32(5)
O(2)#1-Tc(1)-O(4)#1	92.02(5)
O(3)-Tc(1)-Tc(1)#1	92.45(4)
O(1)-Tc(1)-Tc(1)#1	92.51(4)
O(2)#1-Tc(1)-Tc(1)#1	90.12(4)
O(4)#1-Tc(1)-Tc(1)#1	90.27(4)
O(3)-Tc(1)-Br(1)	89.46(4)
O(1)-Tc(1)-Br(1)	91.50(4)
O(2)#1-Tc(1)-Br(1)	85.95(4)
O(4)#1-Tc(1)-Br(1)	87.92(4)
Tc(1)#1-Tc(1)-Br(1)	175.608(12)
O(3)-Tc(1)-K(1)#2	60.72(4)
O(1)-Tc(1)-K(1)#2	44.92(4)
O(2)#1-Tc(1)-K(1)#2	131.56(4)
O(4)#1-Tc(1)-K(1)#2	116.55(4)
Tc(1)#1-Tc(1)-K(1)#2	125.323(11)
Br(1)-Tc(1)-K(1)#2	59.018(8)
Tc(1)-Br(1)-K(1)	103.982(6)
Tc(1)-Br(1)-K(1)#2	78.198(6)
K(1)-Br(1)-K(1)#2	109.107(6)
O(1)#3-K(1)-O(1)#4	124.40(6)
O(1)#3-K(1)-Br(1)	81.77(3)
O(1)#4-K(1)-Br(1)	153.75(3)
O(1)#3-K(1)-Br(1)#5	153.75(3)
O(1)#4-K(1)-Br(1)#5	81.77(3)
Br(1)-K(1)-Br(1)#5	72.170(15)
O(1)#3-K(1)-Br(1)#3	65.52(3)

O(1)#4-K(1)-Br(1)#3	69.42(3)
Br(1)-K(1)-Br(1)#3	131.571(4)
Br(1)#5-K(1)-Br(1)#3	131.571(4)
O(1)#3-K(1)-Br(1)#4	69.42(3)
O(1)#4-K(1)-Br(1)#4	65.52(3)
Br(1)-K(1)-Br(1)#4	131.570(4)
Br(1)#5-K(1)-Br(1)#4	131.571(4)
Br(1)#3-K(1)-Br(1)#4	69.616(14)
O(1)#3-K(1)-Tc(1)#3	30.16(3)
O(1)#4-K(1)-Tc(1)#3	111.77(3)
Br(1)-K(1)-Tc(1)#3	92.003(5)
Br(1)#5-K(1)-Tc(1)#3	145.153(10)
Br(1)#3-K(1)-Tc(1)#3	42.785(6)
Br(1)#4-K(1)-Tc(1)#3	82.219(12)
O(1)#3-K(1)-Tc(1)#4	111.77(3)
O(1)#4-K(1)-Tc(1)#4	30.16(3)
Br(1)-K(1)-Tc(1)#4	145.152(10)
Br(1)#5-K(1)-Tc(1)#4	92.003(5)
Br(1)#3-K(1)-Tc(1)#4	82.219(12)
Br(1)#4-K(1)-Tc(1)#4	42.785(6)
Tc(1)#3-K(1)-Tc(1)#4	116.074(17)
C(1)-O(1)-Tc(1)	116.94(12)
C(1)-O(1)-K(1)#2	125.06(11)
Tc(1)-O(1)-K(1)#2	104.92(5)
C(3)-O(3)-Tc(1)	117.29(12)
O(2)-C(1)-O(1)	121.23(17)
O(2)-C(1)-C(2)	119.19(17)
O(1)-C(1)-C(2)	119.58(17)
O(3)-C(3)-O(4)	121.58(17)
O(3)-C(3)-C(4)	118.52(17)
O(4)-C(3)-C(4)	119.90(17)
C(3)-O(4)-Tc(1)#1	118.38(12)
C(1)-O(2)-Tc(1)#1	119.09(12)

Symmetry transformations used to generate equivalent atoms:
#1 -x+1,-y+1,-z+2 #2 -y+1,x-1/2,z+1/2 #3 -y+1,x-1/2,z-1/2
#4 y+1/2,-x+1,z-1/2 #5 -x+3/2,-y+1/2,z

Table B.46. Anisotropic displacement parameters ($Å^2 x\ 10^3$) for $K[Tc_2(O_2CCH_3)_4Br_2]$. The anisotropic displacement factor exponent takes the form: $-2p^2[h^2\ a^{*2}U^{11} + ... + 2\ h\ k\ a^*\ b^*\ U^{12}]$.

	U^{11}	U^{22}	U^{33}	U^{23}	U^{13}	U^{12}
Tc(1)	8(1)	7(1)	8(1)	0(1)	0(1)	0(1)
Br(1)	12(1)	9(1)	14(1)	-1(1)	1(1)	1(1)
K(1)	17(1)	39(1)	14(1)	0	0	-11(1)
O(1)	10(1)	12(1)	12(1)	-1(1)	-1(1)	0(1)
O(3)	15(1)	11(1)	10(1)	1(1)	1(1)	0(1)
C(1)	10(1)	13(1)	7(1)	1(1)	0(1)	-1(1)
C(3)	9(1)	12(1)	10(1)	1(1)	-1(1)	-1(1)
C(2)	10(1)	19(1)	13(1)	-1(1)	-2(1)	-2(1)
C(4)	17(1)	18(1)	11(1)	3(1)	3(1)	1(1)
O(4)	13(1)	11(1)	10(1)	0(1)	1(1)	0(1)
O(2)	10(1)	11(1)	12(1)	-2(1)	-1(1)	-1(1)

Table B.47. Hydrogen coordinates ($x\ 10^4$) and isotropic displacement parameters ($Å^2 x\ 10^3$) for $K[Tc_2(O_2CCH_3)_4Br_2]$.

	x	y	z	U(eq)
H(2A)	8354	6523	11053	21
H(2B)	8679	5238	11084	21
H(2C)	8100	5799	12226	21
H(4A)	3757	4460	13867	23
H(4B)	4719	3548	13809	23
H(4C)	3510	3264	13306	23

B.11 ***Cs[Tc$_2$(O$_2$CCH$_3$)$_4$Br$_2$]***

Single crystal X-ray diffraction data for $Cs[Tc_2(O_2CCH_3)_4Br_2]$ has been deposited with the Cambridge Crystallographic Data Centre, CCDC No. 940548. Copies of this information may be obtained free of charge from the Director, CCDC, 12 Union Road,

Cambridge, CB2 1EZ, UK (fax: +44 1223 336033; email: deposit@ccdc.cam.ac.uk or www.ccdc.cam.ac.uk). Crystallographic data are given in Table B.**48** and Table B.**52**.

Table B.48. Crystal data and structure refinement for $Cs[Tc_2(O_2CCH_3)_4Br_2]$.

Identification code	bk_cstc2oac4br2_0m	
Empirical formula	C8 H12 Br2 Cs O8 Tc2	
Formula weight	726.71	
Temperature	100(2) K	
Wavelength	0.71073 Å	
Crystal system	Tetragonal	
Space group	P42/n	
Unit cell dimensions	a = 12.2300(3) Å	α = 90°.
	b = 12.2300(3) Å	β = 90°.
	c = 11.4330(5) Å	γ = 90°.
Volume	1710.07(10) $Å^3$	
Z	4	
Density (calculated)	2.816 Mg/m^3	
Absorption coefficient	8.416 mm^{-1}	
F(000)	1340	
Crystal size	0.08 x 0.02 x 0.02 mm^3	
Theta range for data collection	2.36 to 30.51°.	
Index ranges	-17<=h<=17, -17<=k<=17, -16<=l<=16	
Reflections collected	27324	
Independent reflections	2605 [R(int) = 0.0317]	
Completeness to theta = 30.51°	100.0%	
Absorption correction	Semi-empirical from equivalents	
Max. and min. transmission	0.7466 and 0.5187	
Refinement method	Full-matrix least-squares on F^2	
Data / restraints / parameters	2605 / 0 / 98	
Goodness-of-fit on F^2	1.032	
Final R indices [I>2sigma(I)]	R1 = 0.0186, wR2 = 0.0430	
R indices (all data)	R1 = 0.0219, wR2 = 0.0439	
Largest diff. peak and hole	0.606 and -0.999 $e.Å^{-3}$	

Table B.49. Atomic coordinates (x 10^4) and equivalent isotropic displacement parameters ($Å^2$ x 10^3) for $Cs[Tc_2(O_2CCH_3)_4Br_2]$. U(eq) is defined as one third of the trace of the orthogonalized U^{ij} tensor.

	x	y	z	U(eq)
Cs(1)	2500	7500	1848(1)	19(1)
Tc(1)	4203(1)	5291(1)	4790(1)	8(1)
Br(1)	2073(1)	5808(1)	4274(1)	12(1)
O(1)	3775(1)	3757(1)	4175(1)	11(1)
O(4)	5301(1)	4235(1)	6863(1)	11(1)
O(2)	5453(1)	3171(1)	4592(2)	12(1)
O(3)	3642(1)	4872(1)	6438(1)	12(1)
C(1)	4493(2)	3002(2)	4180(2)	10(1)
C(2)	4214(2)	1911(2)	3681(2)	15(1)
C(3)	4311(2)	4416(2)	7145(2)	11(1)
C(4)	3908(2)	4100(2)	8333(2)	16(1)

Table B.50. Bond lengths (Å) and angles (°) for $Cs[Tc_2(O_2CCH_3)_4Br_2]$.

Cs(1)-O(2)#1	3.1070(16)
Cs(1)-O(2)#2	3.1070(17)
Cs(1)-Br(1)#3	3.4999(3)
Cs(1)-Br(1)	3.5000(3)
Cs(1)-O(3)#4	3.5352(16)
Cs(1)-O(3)#5	3.5352(16)
Cs(1)-Br(1)#4	3.6357(3)
Cs(1)-Br(1)#5	3.6357(3)
Cs(1)-O(4)#6	3.7292(16)
Cs(1)-O(4)#7	3.7292(16)
Tc(1)-O(2)#6	2.0527(16)
Tc(1)-O(4)#6	2.0679(16)
Tc(1)-O(3)	2.0690(16)
Tc(1)-O(1)	2.0701(16)
Tc(1)-Tc(1)#6	2.1298(3)
Tc(1)-Br(1)	2.7453(3)
Tc(1)-Cs(1)#8	4.1441(2)
Br(1)-Cs(1)#8	3.6357(3)
O(1)-C(1)	1.274(3)

O(4)-C(3)	1.273(3)
O(4)-Tc(1)#6	2.0678(16)
O(4)-Cs(1)#6	3.7292(16)
O(2)-C(1)	1.282(3)
O(2)-Tc(1)#6	2.0528(16)
O(2)-Cs(1)#9	3.1070(16)
O(3)-C(3)	1.277(3)
O(3)-Cs(1)#8	3.5352(16)
C(1)-C(2)	1.491(3)
C(3)-C(4)	1.496(3)
O(2)#1-Cs(1)-O(2)#2	115.99(6)
O(2)#1-Cs(1)-Br(1)#3	159.39(3)
O(2)#2-Cs(1)-Br(1)#3	84.49(3)
O(2)#1-Cs(1)-Br(1)	84.49(3)
O(2)#2-Cs(1)-Br(1)	159.39(3)
Br(1)#3-Cs(1)-Br(1)	75.170(9)
O(2)#1-Cs(1)-O(3)#4	51.03(4)
O(2)#2-Cs(1)-O(3)#4	119.24(4)
Br(1)#3-Cs(1)-O(3)#4	118.33(3)
Br(1)-Cs(1)-O(3)#4	74.66(3)
O(2)#1-Cs(1)-O(3)#5	119.24(4)
O(2)#2-Cs(1)-O(3)#5	51.03(4)
Br(1)#3-Cs(1)-O(3)#5	74.66(3)
Br(1)-Cs(1)-O(3)#5	118.33(3)
O(3)#4-Cs(1)-O(3)#5	164.77(5)
O(2)#1-Cs(1)-Br(1)#4	62.38(3)
O(2)#2-Cs(1)-Br(1)#4	66.77(3)
Br(1)#3-Cs(1)-Br(1)#4	129.901(4)
Br(1)-Cs(1)-Br(1)#4	129.901(4)
O(3)#4-Cs(1)-Br(1)#4	55.40(3)
O(3)#5-Cs(1)-Br(1)#4	110.69(3)
O(2)#1-Cs(1)-Br(1)#5	66.77(3)
O(2)#2-Cs(1)-Br(1)#5	62.38(3)
Br(1)#3-Cs(1)-Br(1)#5	129.901(4)
Br(1)-Cs(1)-Br(1)#5	129.901(4)
O(3)#4-Cs(1)-Br(1)#5	110.69(3)
O(3)#5-Cs(1)-Br(1)#5	55.40(3)

Br(1)#4-Cs(1)-Br(1)#5	71.912(8)
O(2)#1-Cs(1)-O(4)#6	86.65(4)
O(2)#2-Cs(1)-O(4)#6	118.51(4)
Br(1)#3-Cs(1)-O(4)#6	85.15(3)
Br(1)-Cs(1)-O(4)#6	57.18(3)
O(3)#4-Cs(1)-O(4)#6	118.88(4)
O(3)#5-Cs(1)-O(4)#6	67.78(4)
Br(1)#4-Cs(1)-O(4)#6	144.32(3)
Br(1)#5-Cs(1)-O(4)#6	80.08(3)
O(2)#1-Cs(1)-O(4)#7	118.51(4)
O(2)#2-Cs(1)-O(4)#7	86.65(4)
Br(1)#3-Cs(1)-O(4)#7	57.18(3)
Br(1)-Cs(1)-O(4)#7	85.15(3)
O(3)#4-Cs(1)-O(4)#7	67.78(4)
O(3)#5-Cs(1)-O(4)#7	118.88(4)
Br(1)#4-Cs(1)-O(4)#7	80.08(3)
Br(1)#5-Cs(1)-O(4)#7	144.32(3)
O(4)#6-Cs(1)-O(4)#7	133.43(5)
O(2)#1-Cs(1)-C(1)#1	16.49(4)
O(2)#2-Cs(1)-C(1)#1	129.80(4)
Br(1)#3-Cs(1)-C(1)#1	144.89(3)
Br(1)-Cs(1)-C(1)#1	70.03(3)
O(3)#4-Cs(1)-C(1)#1	56.33(4)
O(3)#5-Cs(1)-C(1)#1	118.34(4)
Br(1)#4-Cs(1)-C(1)#1	78.61(3)
Br(1)#5-Cs(1)-C(1)#1	73.19(3)
O(4)#6-Cs(1)-C(1)#1	72.35(4)
O(4)#7-Cs(1)-C(1)#1	122.74(4)
O(2)#1-Cs(1)-C(1)#2	129.80(4)
O(2)#2-Cs(1)-C(1)#2	16.49(4)
Br(1)#3-Cs(1)-C(1)#2	70.03(3)
Br(1)-Cs(1)-C(1)#2	144.89(3)
O(3)#4-Cs(1)-C(1)#2	118.34(4)
O(3)#5-Cs(1)-C(1)#2	56.33(4)
Br(1)#4-Cs(1)-C(1)#2	73.19(3)
Br(1)#5-Cs(1)-C(1)#2	78.61(3)
O(4)#6-Cs(1)-C(1)#2	122.74(4)
O(4)#7-Cs(1)-C(1)#2	72.35(4)

C(1)#1-Cs(1)-C(1)#2	145.00(6)
O(2)#6-Tc(1)-O(4)#6	89.82(7)
O(2)#6-Tc(1)-O(3)	88.92(7)
O(4)#6-Tc(1)-O(3)	177.09(6)
O(2)#6-Tc(1)-O(1)	177.20(6)
O(4)#6-Tc(1)-O(1)	91.02(6)
O(3)-Tc(1)-O(1)	90.11(7)
O(2)#6-Tc(1)-Tc(1)#6	92.33(5)
O(4)#6-Tc(1)-Tc(1)#6	91.78(5)
O(3)-Tc(1)-Tc(1)#6	90.90(5)
O(1)-Tc(1)-Tc(1)#6	90.32(5)
O(2)#6-Tc(1)-Br(1)	93.29(5)
O(4)#6-Tc(1)-Br(1)	90.98(5)
O(3)-Tc(1)-Br(1)	86.46(5)
O(1)-Tc(1)-Br(1)	84.02(5)
Tc(1)#6-Tc(1)-Br(1)	173.744(14)
O(2)#6-Tc(1)-Cs(1)#8	46.39(5)
O(4)#6-Tc(1)-Cs(1)#8	118.89(5)
O(3)-Tc(1)-Cs(1)#8	58.51(5)
O(1)-Tc(1)-Cs(1)#8	131.04(5)
Tc(1)#6-Tc(1)-Cs(1)#8	123.348(12)
Br(1)-Tc(1)-Cs(1)#8	59.663(6)
Tc(1)-Br(1)-Cs(1)	99.492(7)
Tc(1)-Br(1)-Cs(1)#8	79.666(7)
Cs(1)-Br(1)-Cs(1)#8	106.458(6)
C(1)-O(1)-Tc(1)	118.74(14)
C(3)-O(4)-Tc(1)#6	117.48(15)
C(3)-O(4)-Cs(1)#6	133.26(14)
Tc(1)#6-O(4)-Cs(1)#6	108.03(6)
C(1)-O(2)-Tc(1)#6	117.54(14)
C(1)-O(2)-Cs(1)#9	120.03(14)
Tc(1)#6-O(2)-Cs(1)#9	105.02(6)
C(3)-O(3)-Tc(1)	118.14(15)
C(3)-O(3)-Cs(1)#8	124.47(14)
Tc(1)-O(3)-Cs(1)#8	91.55(5)
O(1)-C(1)-O(2)	121.0(2)
O(1)-C(1)-C(2)	119.3(2)
O(2)-C(1)-C(2)	119.7(2)

O(1)-C(1)-Cs(1)#9	139.50(15)
O(2)-C(1)-Cs(1)#9	43.48(11)
C(2)-C(1)-Cs(1)#9	87.67(13)
O(4)-C(3)-O(3)	121.7(2)
O(4)-C(3)-C(4)	119.9(2)
O(3)-C(3)-C(4)	118.5(2)

Symmetry transformations used to generate equivalent atoms:
#1 -y+1/2,x,-z+1/2 #2 y,-x+3/2,-z+1/2 #3 -x+1/2,-y+3/2,z
#4 y-1/2,-x+1,z-1/2 #5 -y+1,x+1/2,z-1/2 #6 -x+1,-y+1,-z+1
#7 x-1/2,y+1/2,-z+1 #8 -y+1,x+1/2,z+1/2 #9 y,-x+1/2,-z+1/2

Table B.51. Anisotropic displacement parameters ($Å^2 x\ 10^3$) for $Cs[Tc_2(O_2CCH_3)_4Br_2]$. The anisotropic displacement factor exponent takes the form: $-2p^2[h^2\ a^{*2}U^{11} + ... + 2\ h\ k\ a^*\ b^*\ U^{12}]$.

	U^{11}	U^{22}	U^{33}	U^{23}	U^{13}	U^{12}
Cs(1)	29(1)	15(1)	11(1)	0	0	-9(1)
Tc(1)	8(1)	8(1)	8(1)	0(1)	-1(1)	1(1)
Br(1)	9(1)	13(1)	15(1)	2(1)	-2(1)	1(1)
O(1)	12(1)	10(1)	12(1)	-1(1)	-2(1)	-1(1)
O(4)	12(1)	13(1)	10(1)	1(1)	0(1)	0(1)
O(2)	12(1)	10(1)	14(1)	-1(1)	-1(1)	1(1)
O(3)	11(1)	15(1)	10(1)	2(1)	0(1)	0(1)
C(1)	13(1)	10(1)	8(1)	2(1)	0(1)	-1(1)
C(2)	20(1)	10(1)	16(1)	-3(1)	0(1)	-2(1)
C(3)	14(1)	9(1)	10(1)	-1(1)	0(1)	-1(1)
C(4)	17(1)	18(1)	12(1)	4(1)	1(1)	2(1)

Table B.52. Hydrogen coordinates ($x\ 10^4$) and isotropic displacement parameters ($Å^2 x\ 10^3$) for $Cs[Tc_2(O_2CCH_3)_4Br_2]$.

	x	y	z	U(eq)
H(2A)	4215	1954	2825	23
H(2B)	3488	1689	3954	23
H(2C)	4757	1372	3937	23
H(4A)	4441	3613	8705	24
H(4B)	3205	3721	8260	24
H(4C)	3815	4758	8812	24

B.12 ***Cs[$Tc_2(O_2CCH_3)_4I_2$]***

Single crystal X-ray diffraction data for $Cs[Tc_2(O_2CCH_3)_4I_2]$ has not been deposited with the Cambridge Crystallographic Data Centre. Crystallographic data are given in Table B.**53** and Table B.**57**.

Table B.53. Crystal data and structure refinement for $Cs[Tc_2(O_2CCH_3)_4I_2]$.

Identification code	bk_cstc2oac4i2_0m_a	
Empirical formula	C8 H12 Cs I2 O8 Tc2	
Formula weight	820.71	
Temperature	100(2) K	
Wavelength	0.71073 Å	
Crystal system	Tetragonal	
Space group	P42/n	
Unit cell dimensions	a = 12.6139(7) Å	α = 90°.
	b = 12.6139(7) Å	β = 90°.
	c = 11.6608(6) Å	γ = 90°.
Volume	1855.36(17) $Å^3$	
Z	4	
Density (calculated)	2.932 Mg/m^3	
Absorption coefficient	6.778 mm^{-1}	
F(000)	1484	
Crystal size	0.07 x 0.07 x 0.03 mm^3	
Theta range for data collection	2.38 to 30.51°.	
Index ranges	-18<=h<=18, -17<=k<=18, -16<=l<=16	
Reflections collected	29756	
Independent reflections	2829 [R(int) = 0.0231]	
Completeness to theta = 30.51°	99.8%	
Absorption correction	Semi-empirical from equivalents	
Max. and min. transmission	0.7466 and 0.5958	
Refinement method	Full-matrix least-squares on F^2	
Data / restraints / parameters	2829 / 0 / 102	
Goodness-of-fit on F^2	1.210	
Final R indices [I>2sigma(I)]	R1 = 0.0181, wR2 = 0.0399	
R indices (all data)	R1 = 0.0188, wR2 = 0.0402	

Largest diff. peak and hole	0.830 and -0.986 e.Å^{-3}

Table B.54. Atomic coordinates (x 10^4) and equivalent isotropic displacement parameters (Å^2 x 10^3) for $Cs[Tc_2(O_2CCH_3)_4I_2]$. U(eq) is defined as one third of the trace of the orthogonalized U^{ij} tensor.

	x	y	z	U(eq)
Cs(1)	7465(9)	2580(7)	3241(1)	25(1)
I(1)	8027(1)	755(1)	5786(1)	15(1)
Tc(1)	5777(1)	264(1)	5212(1)	10(1)
O(2)	3853(1)	1218(1)	4147(1)	14(1)
O(4)	4712(1)	-762(1)	3182(1)	14(1)
O(1)	5485(1)	1756(1)	4575(1)	14(1)
O(3)	6329(1)	-185(1)	3615(1)	14(1)
C(1)	4561(2)	1936(2)	4166(2)	14(1)
C(3)	5682(2)	-619(2)	2923(2)	14(1)
C(2)	4304(2)	3008(2)	3703(2)	19(1)
C(4)	6075(2)	-979(2)	1776(2)	18(1)

Table B.55. Bond lengths (Å) and angles (°) for $Cs[Tc_2(O_2CCH_3)_4I_2]$.

Cs(1)-O(1)	3.121(11)
Cs(1)-O(1)#1	3.132(11)
Cs(1)-O(3)#1	3.648(11)
Cs(1)-I(1)#2	3.665(8)
Cs(1)-I(1)#3	3.682(8)
Cs(1)-I(1)#1	3.688(5)
Cs(1)-O(3)	3.797(11)
Cs(1)-I(1)	3.823(5)
Cs(1)-C(1)	3.904(12)
I(1)-Tc(1)	2.9813(3)
I(1)-Cs(1)#4	3.665(8)
I(1)-Cs(1)#5	3.682(8)
I(1)-Cs(1)#1	3.688(5)
Tc(1)-O(1)	2.0562(16)
Tc(1)-O(3)	2.0664(16)

Tc(1)-O(2)#6	2.0670(16)
Tc(1)-O(4)#6	2.0697(16)
Tc(1)-Tc(1)#6	2.1275(4)
O(2)-C(1)	1.271(3)
O(2)-Tc(1)#6	2.0669(16)
O(4)-C(3)	1.273(3)
O(4)-Tc(1)#6	2.0696(16)
O(1)-C(1)	1.280(3)
O(1)-Cs(1)#1	3.132(11)
O(3)-C(3)	1.272(3)
O(3)-Cs(1)#1	3.647(11)
C(1)-C(2)	1.492(3)
C(3)-C(4)	1.498(3)
Cs(1)#1-Cs(1)-O(1)	91(6)
Cs(1)#1-Cs(1)-O(1)#1	85(6)
O(1)-Cs(1)-O(1)#1	120.16(6)
Cs(1)#1-Cs(1)-O(3)#1	131(7)
O(1)-Cs(1)-O(3)#1	125.08(19)
O(1)#1-Cs(1)-O(3)#1	49.85(17)
Cs(1)#1-Cs(1)-I(1)#2	93(4)
O(1)-Cs(1)-I(1)#2	81.3(3)
O(1)#1-Cs(1)-I(1)#2	158.4(3)
O(3)#1-Cs(1)-I(1)#2	121.82(17)
Cs(1)#1-Cs(1)-I(1)#3	84(4)
O(1)-Cs(1)-I(1)#3	157.9(3)
O(1)#1-Cs(1)-I(1)#3	80.9(3)
O(3)#1-Cs(1)-I(1)#3	72.6(2)
I(1)#2-Cs(1)-I(1)#3	77.507(10)
Cs(1)#1-Cs(1)-I(1)#1	126.1(6)
O(1)-Cs(1)-I(1)#1	69.77(12)
O(1)#1-Cs(1)-I(1)#1	65.60(12)
O(3)#1-Cs(1)-I(1)#1	57.39(12)
I(1)#2-Cs(1)-I(1)#1	130.4(3)
I(1)#3-Cs(1)-I(1)#1	129.9(3)
Cs(1)#1-Cs(1)-O(3)	46(6)
O(1)-Cs(1)-O(3)	48.26(16)
O(1)#1-Cs(1)-O(3)	120.02(19)

O(3)#1-Cs(1)-O(3)	166.30(8)
I(1)#2-Cs(1)-O(3)	71.07(19)
I(1)#3-Cs(1)-O(3)	117.39(17)
I(1)#1-Cs(1)-O(3)	111.55(18)
Cs(1)#1-Cs(1)-I(1)	51.2(6)
O(1)-Cs(1)-I(1)	63.93(12)
O(1)#1-Cs(1)-I(1)	67.81(12)
O(3)#1-Cs(1)-I(1)	111.87(19)
I(1)#2-Cs(1)-I(1)	126.1(3)
I(1)#3-Cs(1)-I(1)	125.6(3)
I(1)#1-Cs(1)-I(1)	75.487(10)
O(3)-Cs(1)-I(1)	55.06(12)
Cs(1)#1-Cs(1)-C(1)	101(6)
O(1)-Cs(1)-C(1)	16.67(8)
O(1)#1-Cs(1)-C(1)	133.89(8)
O(3)#1-Cs(1)-C(1)	123.1(2)
I(1)#2-Cs(1)-C(1)	67.7(2)
I(1)#3-Cs(1)-C(1)	145.0(2)
I(1)#1-Cs(1)-C(1)	74.85(15)
O(3)-Cs(1)-C(1)	54.74(17)
I(1)-Cs(1)-C(1)	80.45(17)
Cs(1)#1-Cs(1)-Tc(1)#1	113(5)
O(1)-Cs(1)-Tc(1)#1	111.49(9)
O(1)#1-Cs(1)-Tc(1)#1	28.11(8)
O(3)#1-Cs(1)-Tc(1)#1	29.51(8)
I(1)#2-Cs(1)-Tc(1)#1	151.0(2)
I(1)#3-Cs(1)-Tc(1)#1	90.2(3)
I(1)#1-Cs(1)-Tc(1)#1	43.86(9)
O(3)-Cs(1)-Tc(1)#1	137.09(9)
I(1)-Cs(1)-Tc(1)#1	82.37(11)
C(1)-Cs(1)-Tc(1)#1	118.68(13)
Cs(1)#1-Cs(1)-Tc(1)	65(5)
O(1)-Cs(1)-Tc(1)	26.81(8)
O(1)#1-Cs(1)-Tc(1)	109.06(10)
O(3)#1-Cs(1)-Tc(1)	139.27(8)
I(1)#2-Cs(1)-Tc(1)	89.1(2)
I(1)#3-Cs(1)-Tc(1)	145.5(2)
I(1)#1-Cs(1)-Tc(1)	82.72(12)

O(3)-Cs(1)-Tc(1)	28.83(8)
I(1)-Cs(1)-Tc(1)	42.68(8)
C(1)-Cs(1)-Tc(1)	40.84(11)
Tc(1)#1-Cs(1)-Tc(1)	114.291(12)
Tc(1)-I(1)-Cs(1)#4	95.68(13)
Tc(1)-I(1)-Cs(1)#5	98.98(13)
Cs(1)#4-I(1)-Cs(1)#5	3.4(3)
Tc(1)-I(1)-Cs(1)#1	77.13(19)
Cs(1)#4-I(1)-Cs(1)#1	104.97(18)
Cs(1)#5-I(1)-Cs(1)#1	104.64(19)
Tc(1)-I(1)-Cs(1)	76.95(19)
Cs(1)#4-I(1)-Cs(1)	102.30(18)
Cs(1)#5-I(1)-Cs(1)	102.00(17)
Cs(1)#1-I(1)-Cs(1)	2.7(2)
O(1)-Tc(1)-O(3)	89.21(7)
O(1)-Tc(1)-O(2)#6	177.26(6)
O(3)-Tc(1)-O(2)#6	90.11(6)
O(1)-Tc(1)-O(4)#6	89.74(6)
O(3)-Tc(1)-O(4)#6	177.19(6)
O(2)#6-Tc(1)-O(4)#6	90.81(6)
O(1)-Tc(1)-Tc(1)#6	92.14(5)
O(3)-Tc(1)-Tc(1)#6	90.90(4)
O(2)#6-Tc(1)-Tc(1)#6	90.53(5)
O(4)#6-Tc(1)-Tc(1)#6	91.75(5)
O(1)-Tc(1)-I(1)	93.52(5)
O(3)-Tc(1)-I(1)	86.50(4)
O(2)#6-Tc(1)-I(1)	83.79(4)
O(4)#6-Tc(1)-I(1)	90.96(4)
Tc(1)#6-Tc(1)-I(1)	173.735(13)
O(1)-Tc(1)-Cs(1)#1	45.86(13)
O(3)-Tc(1)-Cs(1)#1	60.41(9)
O(2)#6-Tc(1)-Cs(1)#1	131.70(13)
O(4)#6-Tc(1)-Cs(1)#1	117.16(9)
Tc(1)#6-Tc(1)-Cs(1)#1	124.24(12)
I(1)-Tc(1)-Cs(1)#1	59.00(13)
O(1)-Tc(1)-Cs(1)	43.21(13)
O(3)-Tc(1)-Cs(1)	62.39(9)
O(2)#6-Tc(1)-Cs(1)	134.34(13)

O(4)#6-Tc(1)-Cs(1)	115.23(9)
Tc(1)#6-Tc(1)-Cs(1)	123.13(12)
I(1)-Tc(1)-Cs(1)	60.37(13)
Cs(1)#1-Tc(1)-Cs(1)	2.7(2)
C(1)-O(2)-Tc(1)#6	118.60(14)
C(3)-O(4)-Tc(1)#6	117.25(14)
C(1)-O(1)-Tc(1)	117.40(14)
C(1)-O(1)-Cs(1)	118.93(19)
Tc(1)-O(1)-Cs(1)	109.98(16)
C(1)-O(1)-Cs(1)#1	121.29(18)
Tc(1)-O(1)-Cs(1)#1	106.03(16)
Cs(1)-O(1)-Cs(1)#1	4.1(3)
C(3)-O(3)-Tc(1)	118.26(14)
C(3)-O(3)-Cs(1)#1	125.40(16)
Tc(1)-O(3)-Cs(1)#1	90.07(8)
C(3)-O(3)-Cs(1)	124.37(16)
Tc(1)-O(3)-Cs(1)	88.78(8)
Cs(1)#1-O(3)-Cs(1)	2.5(3)
O(2)-C(1)-O(1)	121.3(2)
O(2)-C(1)-C(2)	119.1(2)
O(1)-C(1)-C(2)	119.6(2)
O(2)-C(1)-Cs(1)	143.36(19)
O(1)-C(1)-Cs(1)	44.40(13)
C(2)-C(1)-Cs(1)	85.14(17)
O(3)-C(3)-O(4)	121.8(2)
O(3)-C(3)-C(4)	119.0(2)
O(4)-C(3)-C(4)	119.2(2)

Symmetry transformations used to generate equivalent atoms:
#1 -x+3/2,-y+1/2,z #2 y+1/2,-x+1,z-1/2 #3 -y+1,x-1/2,z-1/2
#4 -y+1,x-1/2,z+1/2 #5 y+1/2,-x+1,z+1/2 #6 -x+1,-y,-z+1

Table B.56. Anisotropic displacement parameters ($Å^2 x\ 10^3$) for $Cs[Tc_2(O_2CCH_3)_4I_2]$. The anisotropic displacement factor exponent takes the form: $-2p^2[h^2\ a^{*2}U^{11} + ... + 2\ h\ k\ a^*\ b^*\ U^{12}]$.

	U^{11}	U^{22}	U^{33}	U^{23}	U^{13}	U^{12}
Cs(1)	20(1)	42(2)	12(1)	-2(1)	0(1)	-14(1)
I(1)	11(1)	16(1)	18(1)	-4(1)	-1(1)	-1(1)

Tc(1)	10(1)	10(1)	10(1)	0(1)	-1(1)	-1(1)
O(2)	14(1)	13(1)	14(1)	1(1)	-3(1)	1(1)
O(4)	15(1)	16(1)	11(1)	-2(1)	0(1)	0(1)
O(1)	14(1)	11(1)	16(1)	2(1)	-1(1)	-2(1)
O(3)	13(1)	17(1)	12(1)	-2(1)	1(1)	-1(1)
C(1)	17(1)	13(1)	11(1)	0(1)	1(1)	1(1)
C(3)	17(1)	13(1)	12(1)	0(1)	0(1)	1(1)
C(2)	25(1)	12(1)	19(1)	3(1)	-1(1)	2(1)
C(4)	21(1)	22(1)	12(1)	-4(1)	3(1)	-1(1)

Table B.57. Hydrogen coordinates (x 10^4) and isotropic displacement parameters ($Å^2$ x 10^3) for $Cs[Tc_2(O_2CCH_3)_4I_2]$.

	x	y	z	U(eq)
H(2A)	4340	2992	2864	28
H(2B)	4815	3525	3998	28
H(2C)	3587	3210	3943	28
H(4A)	5955	-1742	1694	28
H(4B)	6836	-830	1716	28
H(4C)	5694	-599	1170	28

REFERENCES

[1] C. Perrier and E. Segré, *J. Chem. Phys.* **1937**, *5*, 712.

[2] C. Perrier and E. Segré, *J. Chem. Phys*. **1939**, *7*, 155.

[3] K. Schowchau, Technetium: Chemistry and Radiopharmaceutical Applications; Wiley-VCH: Weinheim, Germany, **2000.**

[4] J.A. Rard, M.H. Rand, G. Anderegg and H. Wanner, *Chemical Thermodynamics of Technetium*, M.C.A. Sandino and E. Östhols (ed) Chemical Thermodynamics 3, Elsevier, **1999.**

[5] J.P. Icenhower, N.P. Qafoku, W.J. Martin and J.M. Zachara, *Pacific Northwest National Laboratory report: The Geochemistry of Technetium: A Summary of the Behavior of an Artificial Element in the Natural Environment*, PNNL-18139, **2008**, 1.

[6] H. Kleykamp, *J. Nuc. Mater.* **1985**, *131*, 221.

[7] S. Utsunomiya and R.C. Ewing, *Radiochim. Acta* **2006**, *94*(9-11), 749.

[8] C. Soderquist and B. Hanson, *J. Nucl. Mater.* **2010**, *396*, 159.

[9] Y. Liu, J. Terry and S. Jurisson, *Radiochim. Acta* **2007**, *95*, 717.

[10] U. Abram and R. Alberto, *J. Braz. Chem. Soc.* **2006**, *17*(8), 1486-1500.

[11] C.J. Jones and J. Thomback, *Medicinal Applications of Coordination Chemistry*, Royal Society of Chemistry, Cambridge **2007.**

[12] J.A. McCleverty and T.J. Meyer, *Comprehensive Coordination Chemistry II*. E.C. Constable Volume 5 *Transition Metal Groups 7 and 8*. R. Alberto *Chapter 5.2 Technetium*. Elsevier Ltd, **2003**.

[13]http://nucleus.iaea.org/HHW/Radiopharmacy/VirRad/Eluting_the_Generator/Generator_Module/99Mo_-_99mTc_radionuclide_principles/index.html

[14] S. Banerjee, M.R.A. Pillai and N. Ramamoorthy, *Nuclear Medicine* **2001**, *XXXI* (4), 260-277.

[15] H.T. Chifotides, K.R. DunBar, *Acc. Chem. Res.* **2005**, *38*, 146.

[16] F.A. Cotton, *Multiple Bonds between Metal Atoms*, 3rd Ed., F.A. Cotton, C.A. Murillo, R.A. Walton (Eds), Springer, New York **2005,** chap. 7.

[17] See, for example: Parr Instrument Company, www.parrinst.com.

[18] S.V. Kryuchkov, Top. Curr. Chem. **1996**, *176*, 189.

[19] F.A. Cotton, *Multiple Bonds between Metal Atoms*, 3rd ed., F.A. Cotton, C.A. Murillo, R.A. Walton (eds.), Springer, NY, **2005**, chap. 1.

[20] J.H. Canterford and R.Colton, *Halides of the Second and Third Row Transition Metals,* John Wiley and Sons, NY, **1968**.

[21] F.A. Cotton, G. Wilkinson, C.A. Murillo and M. Bochmann, *Advanced Inorganic Chemistry*, 6th ed., John Wiley and Sons, NY, **1999**.

[22] N. Shtemenko, P. Collery and A. Shtemenko, *Anticancer Res.* **2007**, *27*, 2487.

[23] G. Hogarth, *Organomet. Chem.* **1995**, *24*, 184.

[24] F.A. Cotton, *Multiple Bonds between Metal Atoms*, 3rd ed., F.A. Cotton, C.A. Murillo, R.A. Walton, R. A. (eds.), Springer, NY, **2005**, chap. 13.

[25] E.L. Muetterties and M.J. Krause, *Angew. Chem. Int. Ed*. **1983**, *22*, 135.

[26] F.A. Cotton, *Multiple Bonds between Metal Atoms*, 3rd ed., F.A. Cotton, C.A. Murillo, R.A. Walton (eds.), Springer, NY, **2005**, chap. 15.

[27] M.H. Chisholm and A.M. Macintosh, *Chem. Rev.* **2005**, *105*, 2949.

[28] J. Lin and G.J. Miller, *Inorg. Chem*. **1993**, *32*, 1476–1487.

[29] B.H.S. Thimmappa, *Coord. Chem. Rev.* **1995**, *143*, 1-34.

[30] F.A. Cotton, *Inorg. Chem.* **1998**, *37*, 5710-5720.

[31] J. Lewis, *Pure and Applied Chemistry* **1965**, *10*(1), 11-36.

[32] J. Serre, *International Journal of Quantum Chemistry* **1981**, *19*, 1171-1183.

[33] F.A. Cotton, *Multiple Bonds between Metal Atoms*, 3rd ed., F.A. Cotton, C.A. Murillo, R.A. Walton (eds.), Springer, NY, **2005,** xxi-xxx.

[34] F.A. Cotton, *Multiple Bonds between Metal Atoms*, 3rd Ed., F.A. Cotton, C.A. Murillo, R.A. Walton (Eds), Springer, New York **2005,** chap. 16.

[35] D.L. Kepert and K. Vrieze, *Compounds of the Transition Elements Involving Metal-Metal Bonds: Pergamon Texts in Inorganic Chemistry*, Volume 27, Elsevier, Pergamon Press Inc, New York **2013**.

[36] F. Poineau, P.M. Forster, T.K. Todorova, L. Gagliardi, A.P. Sattelberger and K.R. Czerwinski, *Dalton Trans.* **2012**, *41*, 2869.

[37] P.F. Weck, E. Kim, F. Poineau, E. Rodriguez, A.P. Sattelberger and K.R. Czerwinski, *Inorg. Chem.* **2009**, *48*, 6555.

[38] F. Poineau, E.E. Rodriguez, P.M. Forster, A.P. Sattelberger, A.K. Cheetham and K.R. Czerwinski, *J. Am. Chem. Soc.* **2009**, *131*, 910.

[39] F. Poineau, C.D. Malliakas, P.F. Weck, B.L. Scott, E.V. Johnstone, P.M. Forster, E. Kim, M.G. Kanatzidis and K.R. Czerwinski, A. P. Sattelberger, *J. Am. Chem. Soc*. **2011**, *133*, 8814.

[40] F. Poineau, E.V. Johnstone, P. F. Weck, E. Kim, P.M. Forster, B.L. Scott, A.P. Sattelberger and K.R. Czerwinski, *J. Am. Chem. Soc.* **2010**, *132*, 15864.

[41] E.V. Johnstone, F. Poineau, J. Starkey, T. Hartmann, P.M. Forster, L. Ma, J. Hilger, E.E. Rodriguez, K.R. Czerwinski and A.P. Sattelberger, *Inorg. Chem.* **2013**, *52*, 14309.

[42] F. Taha and G. Wilkinson, J. Chem. Soc. **1963**, 5406.

[43] F. Poineau, E.V. Johnstone, K.R. Czerwinski and A.P. Sattelberger, *Acc. Chem. Res.* **2014**, *47*, 624.

[44] T.K. Todorova, F. Poineau, P.M. Forster, L. Gagliardi, K.R. Czerwinski and A.P. Sattelberger, *Polyhedron* **2014**, *70*, 144.

[45] P.A. Koz'min, T.B. Larina and M.D. Surazhskaya, *Koord. Khim*. **1981**, *7*, 1719.

[46] P.A. Koz'min, T.B. Larina and M.D. Surazhskaya, *Koord. Khim*. **1983**, *9*, 1114.

[47] L. Zaitseva, A. Kotel'nikova and A. Reszvov, *Russ. J. Inorg. Chem.* **1980**, *25*, 1449.

[48] W.M. Kerlin, F. Poineau, K.R. Czerwinski, P.M. Forster and A.P. Sattelberger, *Polyhedron* **2013**, *58*, 155.

[49] V.I. Spitsyn, A.F. Kuzina, A.A. Oblova and S.V. Kryuchkov, *Russ. Chem. Rev.* **1985**, *54*, 373.

[50] K.E. German, S.V. Kryuchkov, A.F. Kuzina and V.I. Spitsyn, *Dokl. Chem.* **1986**, *288*, 139.

[51] S.V. Kryuchkov, M.S. Grigoriev, A.I. Yanovskii, Y.T. Struchkov and V.I. Spitsyn, *Dokl. Chem.* **1988**, *297*, 520.

[52] F.A. Cotton and L.D. Gage, *Nouv. J. Chim.* **1977**, *1*, 441.

[53] N.A. Baturin, K.E. German, M.S. Grigoriev and S.V. Kryuchkov, *Sov. J. Coord. Chem.* **1991**, *17*, 732.

[54] M.S. Grigoriev and S.V. Kryutchkov*, Radiochim. Acta* **1993**, *63*, 187.

[55] J. Skowronek, W. Preetz and S.M. Jessen, *Z. Naturforsch*. **1991**, *46B*, 1305.

[56] F.A. Cotton, S.C. Haefner and A.P. Sattelberger, *Inorg. Chem*. **1996**, *35*, 1831.

[57] F.A. Cotton, S.C. Haefner and A.P. Sattelberger, *Inorg. Chem.* **1996**, *35*, 7350.

[58] C.J. Burns, A.K. Burrell, F.A. Cotton, S.C. Haefner and A.P. Sattelberger, *Inorg. Chem.* **1994**, *33*, 2257.

[59] F.A. Cotton, L.M. Daniels, S.C. Haefner and A.P. Sattelberger, *Inorg. Chim. Acta* **1999**, *288*, 69.

[60] E. Freiberg, A. Davison, A.G. Jones and W.M. Davis*, Inorg. Chem. Commun.* **1999,** *2*, 516.

[61] F.A. Cotton, L. Daniels, A. Davison and C. Orvig, *Inorg. Chem.* **1981**, *20*, 3051.

[62] S.V. Kryutchkov, *Topics in Current Chemistry* **1996**, *176*, 189.

[63] P.A. Koz'min and G.N. Novitskaya, *Russ. J. Inorg. Chem.* **1972**, *17*, 1652.

[64] F.A. Cotton and L.W. Shive, *Inorg. Chem.* **1975**, *14*, 2032.

[65] F.A. Cotton and W.K. Bratton, *J. Am. Chem. Soc.* **1965**, *87*, 921.

[66] W.K. Bratton and F.A. Cotton, *Inorg. Chem.* **1970**, *9*, 789.

[67] F.A. Cotton, A. Davison, V.W. Day, M.F. Fredrich, C. Orvig and R. Swanson, *Inorg. Chem.* **1982**, *21*, 1211.

[68] V.I. Spitsyn, A.F. Kuzina, A.A. Oblova and L.I. Belyaeva, *Dokl. Akad. Nauk. SSSR* **1977**, *237*, 1126.

[69] P.A. Koz'min, T.B. Larina and M.D. Surazhskaya, *Sov. J. Coord. Chem.* **1982**, *8*, 451.

[70] S.V. Kryuchkov, M.S. Grigorev, A.F. Kuzina, B.F. Gulev and V.I. Spitsyn, *Dokl. Chem.* **1986**, *288*, 147.

[71] F.A. Cotton, L.M. Daniels, L.R. Falvello, M.S. Grigoriev and S.V. Kryuchkov, *Inorg. Chim. Acta.* **1991**, *189*, 53.

[72] J.C. Bryan, F.A. Cotton, L.M. Daniels, S.C. Haefner and A.P. Sattelberger, *Inorg. Chem.* **1995**, *34*, 1875.

[73] F.A. Cotton, P.F. Fanwick and L.D. Gage, *J. Am. Chem. Soc.* **1980**, *102*, 1570.

[74] P.A. Koz'min, T.B. Larina and M.D. Surazhskaya, *Dokl. Phys. Chem.* **1983**, *271*, 577.

[75] P.A. Koz'min, M.D. Surazhskaya and T.B. Larina, *Sov. J. Coord. Chem.* **1985**, *11*, 888.

[76] S.V. Kryuchkov, M.S. Grigoriev, A.F. Kuzina, B.F. Gulev and V.I. Spitsyn, *Dokl. Chem.* **1986**, *288*, 172.

[77] P.A. Koz'min, M.D. Surazhskaya and T.B. Larina, *Dokl. Phys. Chem.* **1982**, *265*, 656.

[78] V.I. Spitzin, S.V. Kryuchkov, M.S. Grigoriev and A.F. Kuzina, *Z. anorg. allg. Chem*. **1988**, *563*, 136.

[79] J.D. Eakins, D.G. Humphreys and C.E. Mellish, *J. Chem. Soc.* **1963**, 6012.

[80] (a) A.S. Kotel'nikova and V.G. Tronev, *Russ. J. Inorg. Chem.* **1958**, *3*, 268. (b) F.A. Cotton, N.F. Curtis, B.F.G. Johnson and W.R. Robinson, *Inorg. Chem.* **1965**, *4*, 326. (c) A.S. Kotel'nikova, M.I. Glinkina, T.V. Misailova and V.G. Lebedev, *Russ. J. Inorg. Chem.* **1976**, *21*, 547. (d) A.S. Kotel'nikova, T.V. Misailova, I.Z. Babievskaya and V.G. Lebedov, *Russ. J. Inorg. Chem.* **1978**, *23*, 1326. (e) I.F. Golovaneva, T.V. Misailova, A.S. Kotel'nikova and A.V. Shtemenko, *Russ. J. Inorg. Chem.* **1986**, *31*, 517.

[81] (a) T.J. Barder and R. A. Walton, *Inorg. Chem.* **1982**, *21*, 2510. (b) T.J. Barder and R.A. Walton, *Inorg. Synth.* **1985**, *23*, 116.

[82] F.A. Cotton, *Multiple Bonds between Metal Atoms*, 3rd ed., F.A. Cotton, C.A. Murillo, R.A. Walton (eds.), Springer, NY, **2005**, chap. 8.

[83] (a) F.A. Cotton, N.F. Curtis, B.F.G. Johnson and W. R. Robinson, *Inorg. Chem.* **1965**, *4*, 326. (b) A.B. Brignole and F.A. Cotton, *Inorg. Synth.* **1972**, *13*, 81. (c) F.A. Cotton, C. Oldham and W.R. Robinson, *Inorg. Chem.* **1966**, *5*, 1798.

[84] A.V. Shtemenko, A.A. Golichenko and K.V. Domasevitch, *Z. Naturforsch.* **2001**, *56b*, 381.

[85] F.A. Cotton, *Multiple Bonds between Metal Atoms*, 3rd ed., F.A. Cotton, C.A. Murillo, R.A. Walton (eds.), Springer, NY, **2005**, chap. 3.

[86] (a) E.W. Abel, A. Singh and G. Wilkinson, *J. Chem. Soc.* **1959**, 3097. (b) E. Bannister and G. Wilkinson, *Chem. Ind.* (London) **1960**, 319. (c) G. Holste and H. Schafer, *Z. anorg. allg. Chem.* **1972**, *391*, 263.

[87] (a) E. Hochberg, P. Walks and E.H. Abbott, *Inorg. Chem.* **1974**, *13*, 1824. (b) A.B. Brignole and F.A. Cotton, *Inorg. Synth.* **1972**, *13*, 81. (c) R.E. McCarley, J.L. Templeton, T.J. Colburn, V. Katovic and R.J. Hoxmeier, *Adv. Chem. Ser.* **1976**, No. *150*, 318.

[88] F.A. Cotton, *Multiple Bonds between Metal Atoms*, 3rd Ed., F.A. Cotton, C.A. Murillo, R.A. Walton (Eds), Springer, New York **2005,** chap. 4.

[89] F.A. Cotton, *Multiple Bonds between Metal Atoms*, 3rd Ed., F.A. Cotton, C.A. Murillo, R.A. Walton (Eds), Springer, New York **2005,** chap. 5.

[90] T.A. Stephenson and D. Whittaker, *Inorg. Nucl. Chem. Lett.* **1969**, *5*, 569.

[91] F.A. Cotton and M. Jeremic, *Synth. Inorg. Metal-Org. Chem.* **1971**, *1*, 265.

[92] G. Holste, *Z. anorg. allg. Chem.* **1973**, *398*, 249.

[93] A.P. Sattelberger, K.W. McLaughlin and J. C. Huffman, *J. Am. Chem. Soc.* **1981**, *103*, 2880.

[94] D.J. Santure and A.P. Sattelberger, *Inorg. Synth.* **1989**, *26*, 219.

[95] D.J. Santure, J.C. Huffman and A.P. Sattelberger, *Inorg. Chem.* **1985**, *24*, 371.

[96] D.J. Santure, J.C. Huffman and A.P. Sattelberger, *Inorg. Chem.* **1984,** *23*, 938.

[97] F.A. Cotton, L.R. Falvello and W. Wang, *Inorg. Chim. Acta.* **1997**, *261*, 77.

[98] D.J. Santure, K.W. McLaughlin, J.C. Huffman and A.P. Sattelberger, *Inorg. Chem.* **1983**, *22*, 1877.

[99] T.A. Stephenson and G. Wilkinson, *J. Inorg. Nucl. Chem.* **1966**, *28*, 2285.

[100] M. Mukaida, T. Nomura and T. Ishimori, *Bull. Chem. Soc. Jpn.* **1967**, *40*, 2462.

[101] M.J. Bennet, K.G. Caulton and F.A. Cotton, *Inorg. Chem.* **1969**, *8*, 1.

[102] A. Bino, F.A. Cotton and T.R. Felthouse, *Inorg. Chem.* **1979**, *18*, 2599.

[103] T. Togano, M. Mukaida and T. Nomura, *Bull. Chem. Soc. Jpn.* **1980**, *53*, 2085.

[104] F.A. Cotton, *Multiple Bonds between Metal Atoms*, 3rd Ed., F.A. Cotton, C.A. Murillo, R.A. Walton (Eds), Springer, New York **2005,** chap. 9.

[105] F.A. Cotton and J. L. Thompson, *J. Am. Chem. Soc.* **1980**, *102*, 6437.

[106] F.A. Cotton, *Multiple Bonds between Metal Atoms*, 3rd Ed., F.A. Cotton, C.A. Murillo, R.A. Walton (Eds), Springer, New York **2005,** chap. 10.

[107] D.S. Moore, A.S. Alves and G. Wilkinson, *J. Chem. Soc., Chem. Comm.* **1981**, 1164.

[108] T. Behling, G. Wilkinson, T.A. Stephenson, D.A. Tocher and M.D. Walkinshaw, *J. Chem. Soc., Dalton Trans.* **1983**, 2109.

[109] (a) T.A. Stephenson, D.A. Tocher and M.D. Walkinshaw, *J. Organomet. Chem.* **1982**, *232*, c51. (b) F.A. Cotton, T. Ren and M.J. Wagner, *Inorg. Chem.* **1993**, *32*, 965. (c) F.A. Cotton, A.R. Chakravarty, D.A. Tocher and T.A. Stephenson*, Inorg. Chim. Acta* **1984**, *87*, 115.

[110] F.A. Cotton, *Multiple Bonds between Metal Atoms*, 3rd Ed., F.A. Cotton, C.A. Murillo, R.A. Walton (Eds), Springer, New York **2005,** chap. 4, 5, 7-10.

[111] F.A. Cotton, P. Haung, C. A. Murillo, D.J. Timmons, *Inorg Chem.Commun*. **2002**, 5, 501.

[112] F.A. Cotton, N.F. Curtis, C.B. Harris, B.F.G Johnson, S.J. Lippard, J.T. Mague, W.R. Robinson, J.S. Wood, *Science*, **1964**, *145*(3638), 1305.

[113] K. Jödden, H.G. von Schnering and H. Schäfer*, Angew. Chem.* **1975**, *87*, 594.

[114] M. Ströbele and H. Jürgen Meyer, *Z. Anorg. Allg. Chem.* **2010**, *636*, 62-66.

[115] R. Busey, R. Bevan and R. Gilbert, *J. Chem. Thermodynamics* **1972**, *4*(1), 77.

[116] S. Feng and G. Li, *Modern Inorganic Synthetic Chemistry*, R. Xu, W. Pang, Q. Huo (Eds), Elsevier B. V., **2011**, chap. 4.

[117] K. Byrappa and M. Yoshimura, *Handbook of Hydrothermal Technology*, 2nd Ed., William Andrew (Eds), Elsevier, **2013**.

[118] A. Rabenau, *The role of hydrothermal synthesis in preparative chemistry*, *Angew. Che. English Ed.* **1985**, *24*, 1026-1040.

[119] http://serc.carleton.edu/research_education/geochemsheets/techniques/SXD.html

[120] G.H. Stout and L.H. Jensen, *X-ray Structure Determination*, John Wiley & Sons Inc., 2nd Ed., **1989**.

[121] M. Laing, *An Introduction to the Scope, Potential and Applications of X-ray Analysis*, University College Cardiff Press for the International Union of Crystallography, **1981**.

[122] W. Clegg, A.J. Blake, R.O. Gould and P. Main*, Crystal Structure Analysis Principles and Practice*, Oxford science publications for International Union of Crystallography, **2001**.

[123] G.M. Sheldrick, *Acta. Cryst. A*. **2008,** *64*, 112.

[124] O.V. Dolomanov, L.J. Bourhis, R.J. Gildea, J.A.K. Howard and H. Puschmann, *OLEX2: A Complete Structure Solution, Refinement and Analysis Program*. *J. Appl. Cryst.* **2009**, *42*, 339.

[125] C.F. Macrae, I.J. Bruno, J.A. Chisholm, P.R. Edgington, P. McCabe, E. Pidcock, L. Rodriguez-Monge, R. Taylor, J. van de Streek and P.A. Wood, *J. Appl. Cryst*. **2008**, *41*, 466.

[126] Diamond - Crystal and Molecular Structure Visualization Crystal Impact - Dr. H. Putz & Dr. K. Brandenburg GbR, Kreuzherrenstr. 102, 53227 Bonn, Germany at http://www.crystalimpact.com/diamond

[127] K. Hasegawa, *Introduction to single crystal X-ray analysis, part I*, *The Rigaku Journal*, **2012**, *28*(1), 14-18.

[128] P. Marcon, K. Bartusek, M. Budrkova and Z. Dokoupil, *Measurement Science and Technology*, **2011**, *22*.

[129] C.J. Ballhausen, *Introduction to ligand field theory.* McGraw-Hill Book Company, New York, **1962,** Chapter 6.

[130] P. Marcon and K. Ostanina, *Overview of Methods for Magnetic Susceptibility Measurement*, PIERS Proceeding, Kuala Lumpur, Malysia, March 27-30 **2012**, 420-424.

[131] T. Owen*, Fundamentals of UV-Visible spectroscopy primer*, Agilent Technologies, **2000**.

[132] H. Willard, L. Merritt and J. Dean, *Instrumental Methods of Analysis*, D. Van Nostrand Company (5th ed): New York, **1974**.

[133] F.C. Strong, *Anal. Chem.* **1952**, *24*(2), 338.

[134] D.C. Harris, *Quantitative Chemical Analysis*, W.H. Freeman and Company, 6th Ed., New York, **2000**.

[135] M.F. L'Annuziata, *Handbook of Radioactivity Analysis*, Academic press, 3rd Ed., San Diego, **2012**.

[136] http://www.cornerstonelab.com/EPA-Methods/100-400/345_1.PDF and http://www.epa.gov/region1/info/testmethods/index.html

[137] M. Dunlap and J.E. Adaskaveg, *Introduction to the Scanning Electron Microscope Theory, Practice & Procedure*, **1997**.

[138] J. Goldestein, D. Newbury, D. Joy, C. Lyman, P. Echlin, E. Lifshin, L. Sawyer and J. Michael, *Scanning Electron Microscopy and X-Ray Microanalysis*, Kluwer Academic/Plenum Publishers, 3rd ed, Springer, **2003**.

[139] D. Ferrer, D.A. Bloom, L.F. Allard, S. Mejia, E. Perez-Tijerina and M. Jose-Yacaman, *J. Mater. Chem.* **2008**, *18*, 2442.

[140] G.W.C. Silva, Evaluation of Low-Temperature Fluoride Routes to synthesize Actinide Nitrides and Oxides Solid Solutions, *Thesis from University of Nevada Las Vegas*, **2009**.

[141] M. Newville, Consortium for Advanced Radiation Sources, University of Chicago, **2004**.

[142] M.A. Denecke, *Coord. Chem. Rev.* **2006**, *250*, 730.

[143] S. Bare, EXAFS Data Collection and Analysis Course, **2005**.

[144] M. Newville, P. Livins, Y. Yacoby, E.A. Stern and J.J. Rehr, *Phys. Rev. B Condensed Matter and Materials Physics* **1993**, *47*(21), 14126.

[145] B. Ravel, *J. Synchrotron Radiat.* **2001**, *8*, 314.

[146] J.J. Rehr and R.C. Albers, *Rev. Mod. Phys.* **2000**, *72*, 621.

[147] T. Ressler, *J. Synchrotron Radiat.* **1998**, *5*(2), 118.

[148] J. Skowronek and W. Preetz, *Z. Naturforsch.* **1992**, *47B*, 482.

[149] A. Rezvov, L. Zaitseva, A. Kotel'nikova and A. Shtemenko, U.S.S.R Patent, SU 819116 A1 19810407, **1981**.

[150] W. Preetz, G. Peters and D. Bublitz, *J. Clust. Sci.* **1994**, *5*, 83.

[151] F.A. Cotton, N.F. Curtis, B.F.G. Johnson and W.R. Robinson, *Inorg. Chem.* **1965**, *4*, 326.

[152] F. Poineau, A.P. Sattelberger and K.R. Czerwinski, *J. Coord. Chem.* **2008**, *61*, 2356.

[153] N.A. Baturin, K.E. German, M.S. Grigor'ev and S.V. Kryuchkov, *Koordinats. Khim.* **1991**, *17*, 1375.

[154] P. Koz'min, M. Surazhskaya, T. Larina, A. Kotel'nikova and T. Misailova, *Koordinats. Khim.* **1980**, *6*, 1256.

[155] D.M. Collins, F.A. Cotton and L.D. Gage, *Inorg. Chem.*, **1979**, *18*, 1712.

[156] P.A. Koz'min, M.D. Surazhskaya, T.B. Larina, Sh.A. Bagirov, N.S. Osmanov, *Sov. J. Coord. Chem.*, **1979**, *5*, 1229.

[157] F.A. Cotton, L.D. Gage and C.E. Rice, *Inorg. Chem.*, **1979**, *18*, 1138.

[158] J.P. Collin, A. Jouaiti, J.-P. Sauvage, W.C. Kaska, M.A. McLoughlin, N.L. Keder, W.T.A. Harrison and G.D. Stucky, *Inorg. Chem.* **1990**, *29*, 2238.

[159] M.A.S. Aquino, Coordination Chemistry Reviews 2004, 248, 1025-1045.

[160] M.C. Barral, R. Jimenez-Aparicio, J.L. Priego, E.C. Royer, F.A. Urbanos, U. Amador, *Inorg. Chem.* **1998**, *37*, 1413.

[161] M.C. Barral, R. Gonzalez-Prieto, R. Jimenez-Aparicio, L.L. Priego, M.R. Torres and F.A. Urbanos, *Eur. J. Inorg. Chem*. **2006**, 4229-4232.

[162] W.M. Kerlin, F. Poineau, P.M. Forster, K.R. Czerwinski, A.P. Sattelberger, *Inorg. Chim. Acta.* **2015**, *424*, 329.

[163] Environmental Protection Agency Environmental Monitoring and Support Laboratory Office of Research and Development, USA EPA method 345.1. Methods for chemical analysis of water and wastes, Environmental Protection Agency, Cincinnati, Ohio, 1979. http://www.epa.gov/region1/info/testmethods/index.html
http://www.cornerstonelab.com/EPA-Methods/100-400/345_1.PDF

[164] V.I. Spitsyn, B. Baierl, S.V. Kryuchkov, A.F. Kuzina and M.Varen, *Dokl. Akad. Nauk*., **1981**, *256*, 608.

[165] S.V. Kryuchkov, A.F. Kuzina and V.I. Spitsyn, *Dokl. Chem.*, **1982**, *266*, 304.

[166] T. Kimura, T. Sakurai, M. Shima, T. Togano, M. Mukaida and T. Nomura, *Bull. Chem. Soc. Jpn.*, **1982**, *55*, 3927.

[167] F.A. Cotton, K.R. Dunbar, L.R. Falvello, M. Thomas and R.A. Walton, *J. Am. Chem.*, **1983**, *105*, 4950.

[168] F.A. Cotton, M. Matusz and Bianxiao, *Inorg. Chem.* **1988**, *27*, 4368.

[169] M. Sphon, J. Strahle and W. Hiller, *Z. Naturforsch*. **1986**, *41b*, 541.

[170] B. Ravel and M.J. Newville, *Synchrotron Rad.* **2005**, *12*, 537-541.

[171] Y.V. Rakitin, S.V. Kryuchkov, A.I Aleksandrov, A.F. Kuzina, N.V. Nemtsev, B.G. Ershov and V.I. Spitsyn, *Dokl. Akad. Nauk. SSSR*, **1983**, *269*, 1123.

[172] M. Mukaida, T. Nomera and T. Ishimori, *Bull. Chem. Soc. Jpn.* **1972**, 45, 2143.

[173] M. Ferrier, W.M. Kerlin, F. Poineau, A.P. Sattelberger and K.R. Czerwinski, *Dalton Trans.*, **2013**, *42*, 15540.

[174] S.V. Kryuchkov, A.F. Kuzina and V.I. Spitzin, *Z. anorg. allg. Chem.* **1988**, *563*, 153.

[175] R.A. Wheeler and R. Hoffman, *J. Am. Chem. Soc*. **1986**, *108*, 6605.

[176] F.A. Cotton, *Multiple Bonds between Metal Atoms*, 3rd Ed., F.A. Cotton, C.A. Murillo, R.A. Walton (eds.), Springer, NY, **2005**, chap. 7, p. 267, Fig. 7.9.

[177] F.A. Cotton, *Multiple Bonds between Metal Atoms*, 3rd Ed., F.A. Cotton, C.A. Murillo, R.A. Walton (eds.), Springer, NY, **2005**, chap. 7, p. 266, Fig. 7.8.

[178] K. Jödden, H.G. Schnering and H. Schäfer, *Angew. Chem., Int. Ed. Engl*. **1975**, 14, 570.

[179] J.D. Franolic, J.R. Long and R.H. Holm, *J. Am. Chem. Soc.* **1995**, 117, 8139-8153.

[180] S.V. Kryuchkov, A.F. Kuzina and V.I. Spitsyn, *Dokl. Chem.* **1982**, *266*, 127.

[181] P. Pyykko and M. Atsumi, *Chem. Eur. J*. **2009**, *15*, 12770.

[182] S.S. Batsanov, *Inorg. Mat.*, **2001**, *37*, 871.

[183] S.V. Kryuchkov, A.F. Kuzina and V.I. Spitsyn, *Dokl. Chem*. **1986**, *287*, 1400.

[184] N.J. Taylor, *Chem. Soc. Chem. Comm.* **1985**, *8*, 478-479.

VITA

WILLIAM KERLIN

CONTACT INFORMATION:

75 N. Valle Verde Dr. #113, Henderson, NV 89074
Email: kerlinw@unlv.nevada.edu

DEGREES:

Bachelor of Science, Chemistry, **2004**
California State University of Sacramento

SPECIAL HONORS AND AWARDS

Margaret Etter Student Lecturer Award, American Crystallographic Association **2014**
Certificate of APSORC13 Student Oral Presentation, JNRS, Japan **2013**
Innovations in Fuel Cycle Research Award, U.S DOE-NE Office of Fuel Cycle R&D **2013**
Graduate Student Teaching Award in Chemistry **2012**
Chemistry Departmental Award for Outstanding Student **2004**
Graduation with Honors **2004**

PUBLICATIONS

William M. Kerlin, Frederic Poineau, Paul M. Forster, Kenneth R. Czerwinski, Alfred P. Sattelberger. "Hydrothermal Synthesis and Solid-state Structures for Polynuclear Technetium Iodide Compounds" Inorganica Chimica Acta 2015.

Frederic Poineau, Paul M. Forster, Tanya K. Todorova, Erik V. Johnstone, William M. Kerlin, Laura Gagliardi, Kenneth R. Czerwinski, Alfred P. Sattelberger. "A Decade of Dinuclear Technetium Complexes with Multiple Metal-Metal Bonds" Eur. J. Inorg. Chem. 2014. 4484-4495.

William M. Kerlin, Frederic Poineau, Kenneth R. Czerwinski, Paul M. Forster, Alfred P. Sattelberger. "Hydrothermal Synthesis and solid-state structure of $Tc_2(\mu\text{-}O_2CCH_3)_4Cl_2$" Polyhedron 2013. 58. 115-119.

Maryline Ferrier, William M. Kerlin, Frederic Poineau, Alfred P. Sattelberger, Kenneth R. Czerwinski. "Recent developments in the synthetic chemistry of technetium disulfide" Dalton Trans., 2013. 42, 15540-15543.

Frederic Poineau, Philippe F. Weck, Benjamin P. Burton-Pye, Ibthihel Denden, Eunja Kim, William Kerlin, Konstantin E. German, Massoud Fattahi, Lynn C. Francesconi, Alfred P. Sattelberger, Kenneth R. Czerwinski. "Reactivity of $HTcO_4$ with methanol in Sulfuric

acid: Tc-sulfate complexes reealed by XAFS spectroscopy and first principles calculations" Dalton Trans., 2013. 42, 4348.

Brian Currier, Michael Werlinich, Dr. John Johnston, William Kerlin. CIWMB Used Oil Demonstration Grant: Laboratory Evaluation of Four Strom Drain Inlet Filters for Oil Removal. Report to California Integrated Waste Management Board (CIWMB), 2005 Sacramento, CA.

DISSERTATION TITLE:
Hydrothermal Routes to Technetium Cluster Compounds

DISSERTATION EXAMINATION COMMITTEE:

Chairperson, Kenneth R. Czerwinski, Ph.D.
Committee Member, Paul Foster, Ph.D.
Committee Member, Frederic Poineau, Ph.D.
Committee Member, Alfred P. Sattelberger, Ph.D.
Graduate Faculty Representative, Ralf Sudowe, Ph.D.